

University of Southampton Research Repository ePrints Soton

Copyright © and Moral Rights for this thesis are retained by the author and/or other copyright owners. A copy can be downloaded for personal non-commercial research or study, without prior permission or charge. This thesis cannot be reproduced or quoted extensively from without first obtaining permission in writing from the copyright holder/s. The content must not be changed in any way or sold commercially in any format or medium without the formal permission of the copyright holders.

When referring to this work, full bibliographic details including the author, title, awarding institution and date of the thesis must be given e.g.

AUTHOR (year of submission) "Full thesis title", University of Southampton, name of the University School or Department, PhD Thesis, pagination

UNIVERSITY OF SOUTHAMPTON

Faculty of Engineering, Science and Mathematics
School of Civil Engineering and the Environment

**3D modelling of bored pile installation effects and long
term monitoring of a propped retaining wall**

Luca Montalti

Thesis for the degree of Doctor of Philosophy

April 2015

UNIVERSITY OF SOUTHAMPTON

ABSTRACT

FACULTY OF ENGINEERING, SCIENCE AND MATHEMATICS
SCHOOL OF CIVIL ENGINEERING AND THE ENVIRONMENT

Doctor of Philosophy

3D MODELLING OF BORED PILE INSTALLATION EFFECTS AND LONG TERM
MONITORING OF A PROPPED RETAINING WALL

Luca Montalti

In the last few decades much effort has been spent to investigate the installation effects of diaphragm wall panels in an overconsolidated deposit. Conversely, in the literature there is relatively little focus on the effects of bored pile construction. In this thesis a number of three dimensional finite difference analyses using *FLAC^{3D}* have been carried out to investigate the stress changes and consequent movements due to bored pile and diaphragm wall installation in stiff clay. The three-dimensional numerical models developed to carry out these analyses were used to analyse, interpret and explain the instrumented data of ground stress changes during bored pile wall installation in an overconsolidated clay deposit in connection with the Channel Tunnel Rail Link (CTRL; now HS1) at Ashford. Two different soil models were implemented in the three dimensional finite difference analyses, having linear and non-linear stress strain characteristic. It was found that both analyses could capture the observed pattern of changes in stresses. Furthermore, it was found that the difference in stress changes and ground movements after a single pile or panel installation were primarily a consequence of the different geometry between pile and panel.

In the literature, only limited research has been carried out to quantify the three dimensional effects of diaphragm wall installation. For this thesis a number of three dimensional finite difference analyses, using *FLAC^{3D}*, were carried out, to investigate the installation effects of a group of panels in an overconsolidated clay deposit.

One of the key uncertainties associated with the design of in situ embedded retaining walls in an overconsolidated deposit concerns the long-term horizontal stress acting on the wall. There is some concern that the high in situ horizontal stresses in an overconsolidated deposit may become re-established in the long-term, despite the reductions that occur during retaining wall installation and subsequent excavation in front of the wall. This thesis also presents long term case record from an embedded retaining wall that forms part of the Channel Tunnel Rail Link at Ashford, Kent, and a retaining wall at Coventry are also presented. Approximately 13 years of lateral stress monitoring around the embedded retaining wall at Ashford are presented and discussed. The long term field data shows that the in situ total horizontal stresses in the ground close to a retaining wall in an overconsolidated clay deposit did not re-establish in the long term.

LIST OF CONTENTS

<u>CHAPTER 1: INTRODUCTION</u>	1
1.1 Introduction	1
1.2 Aim and Objectives	4
<u>CHAPTER 2: PREVIOUS WORK</u>	5
2.1 Introduction	5
2.2 Case Histories	6
2.3 Laboratory investigations	12
2.4 2D and 3D numerical analysis	14
2.5 Long term monitoring	27
2.6 Summary	27
<u>CHAPTER 3: 3D MODELLING OF BORED PILE WALL INSTALLATION EFFECTS</u>	30
3.1 Introduction	30
3.2 Field Monitoring	31
3.2.1 Instrumentations	32
3.2.2 Wall installation sequence	34
3.3 Numerical Model	37
3.4 Numerical Results	43
3.4.1 Horizontal deformations	62
3.4.2 Investigation of the effect of the in situ stress state on the horizontal stress variation behind the bored pile wall	66
3.5 Summary	69
<u>CHAPTER 4: 3D MODELLING OF BORED PILE WALL INSTALLATION EFFECTS USING A NON-LINEAR STRESS-STRAIN MODEL</u>	72
4.1 Introduction	72
4.2 Ground model	73
4.3 Results and discussion	78
4.3.1 Calculated and observed horizontal stresses on the position of the spade cells	78
4.3.2 Total horizontal stress profile on section A-A and B-B	92
4.3.3 Total horizontal stress distribution normal to the centre of the wall following the completion of the bored piles wall	98
4.3.4 Horizontal displacement	102
4.4 Summary	109

<u>CHAPTER 5: COMPARISON OF THE 3D INSTALLATION EFFECTS FOR A DIAPHRAGM WALL CONSIDERING DIFFERENT CONSTRUCTION SEQUENCES</u>	111
5.1 Introduction	111
5.2 Numerical models	112
5.2.1 Soil model and parameters	114
5.2.2 In situ stresses	115
5.2.3 Installation procedure	115
5.3 Results and analysis	119
5.3.1 Stress distributions for a single panel excavation	119
5.3.2 Comparison of 3D installation effects for fifth different panel installation sequences	126
5.3.3 Comparison of the vertical shear stress (τ_{zy}) after the five sequences of the diaphragm wall installation	132
5.3.4 Comparison of the horizontal shear stress (τ_{xy}) after the five sequences of diaphragm wall installation	135
5.3.5 Stress distribution behind the wall at 0.3, 5, 10, and 15 m far from the wall	161
5.3.6 Horizontal displacement along the excavation after all the sequences modelled	165
5.4 Summary	171
<u>CHAPTER 6: LONG TERM MONITORING</u>	174
6.1 Introduction	174
6.2 Total horizontal stress and pore water pressure measurements at the site in Ashford	175
6.2.1 Geology	175
6.2.2 Instrumented section of the retaining wall at Ashford	176
6.3 Long term pore water pressure variation	176
6.3.1 Pore water pressure variation behind the retaining wall	177
6.3.2 Pore water pressure distribution in front of the retaining wall	181
6.3.3 Pore pressure at various depth below ground level	184
6.3.4 Comparison between the total horizontal stress with the pore water pressure variation and impact of pile gaps on lateral loads on the retaining wall	190
6.3.5 Comparison between the short and long term horizontal total stress and pore pressure	195
6.3.6 Total horizontal stress measurements behind the retaining wall	198
6.3.7 Total horizontal stress distribution in front of the retaining wall	202
6.3.8 Total horizontal stresses at various depth below ground level	203
6.4 Coventry long term data recording	211
6.4.1 Introduction	211
6.4.2 The study site	211
6.4.3 Ground conditions	212
6.4.4 Instrumentation	214
6.4.4.1 Wall bending moments and vertical stress beneath the stabilising base	215
6.5 Summary	223

<u>CHAPTER 7: CONCLUSIONS AND FURTHER WORK</u>	224
7.1 Conclusions	224
7.2 Further work	233
<u>LIST OF REFERENCES</u>	234

LIST OF TABLES

Table 3.1. Sequence of pile installation.	35
Table 3.2. Parameters used in the model.	39
Table 4.1.	76
Table 4.2.	76
Table 6.1 Main stages of construction at the instrumented cross section (Hayward, 2000)	214

LIST OF FIGURES

- Figure 2.1. Section showing the instrumentation layout and the instrumentation details (Tedd *et al.*, 1984). 7
- Figure 2.2. (a) Change in total horizontal stress with time and (b) distribution of the total horizontal stress in the soil 0.6 m from the wall at various stages of excavation (Tedd *et al.*, 1984). 8
- Figure 2.3. Stresses measured before and after diaphragm wall installation (Carder *et al.*, 1991). 9
- Figure 2.4. Stress changes at 1.1 m from the wall during its installation (Carswell *et al.*, 1993). 10
- Figure 2.5. Lateral stresses distribution before and after pile wall installation (Bennet *et al.*, 1996). 11
- Figure 2.6. Total lateral pressures during and after construction in Gault Clay at Lion Yard, Cambridge (Ng and Yan, 1998). 12
- Figure 2.7. General view of the centrifuge model used by Powrie and Kantartzi (1996). 12
- Figure 2.8. Comparison of edge and centre-line soil surface profiles following excavation under bentonite slurry, 10 m and 5 m panels Powrie and Kantartzi (1996). 13
- Figure 2.9. Finite element mesh used in the axi-symmetric analysis by Pantelidou (1994). 16
- Figure 2.10. Change in the horizontal effective stress profile in the vicinity of the wall at different stages of wall installation for axi-symmetric conditions (Pantelidou, 1994). 16
- Figure 2.11. Change in the horizontal effective stress distribution with distance from the side of the excavation (a) for axi-symmetric conditions and (b) for plane strain conditions (Pantelidou, 1994). 17
- Figure 2.12. Section used in the analysis by De Moor *et al.* (1994). 18
- Figure 2.13. Finite element mesh for HPA (horizontal plan analysis); Ng *et al.* (1995). 19
- Figure 2.14. Finite element mesh for VSA (Vertical section analysis); Ng *et al.* (1995). 20
- Figure 2.15. Finite-Difference Mesh used by Ng and Yan (1998). 21
- Figure 2.16. Total Horizontal Stresses arching on the central area behind of the panel, Ng and Yan (1998). 21
- Figure 2.17. Total Horizontal Stresses arching on the edges behind of the panel, Ng and Yan (1998). 22

Figure 2.18. Horizontal displacement behind trench during construction of panel, Ng and Yan (1998).	23
Figure 2.19. Three-dimensional finite-element mesh, Gourvenec and Powrie (1999).	24
Figure 2.20. Horizontal displacements along the wall/soil interface at the centre of the primary panel: effect of panel length, Gourvenec and Powrie (1999).	25
Figure 2.21. Horizontal crest displacements at the centre of the primary panel as a percentage of the plane strain crest displacement: comparison of different panel lengths, Gourvenec and Powrie (1999).	26
Figure 3.1. Plan of the north wall in the instrumented section showing locations of instrumented piles, spade cell, sand drains and sequence of pile installation.	33
Figure 3.2. Spade cell locations (elevation).	33
Figure 3.3. Total horizontal stress measurements during the period of wall installation (1.275 m from the wall); Clark <i>et al.</i> (2006).	36
Figure 3.4. Total horizontal stress measurements during the period of wall installation (2.375 m from the wall); Clark <i>et al.</i> (2006).	36
Figure 3.5. Total horizontal stress measurements during the period of wall installation (3.475 m from the wall); Clark <i>et al.</i> (2006).	37
Figure 3.6. Geometry of <i>FLAC</i> ^{3D} model.	38
Figure 3.7. Pile installation sequence.	40
Figure 3.8. Sequence of construction stages. (a) In situ stress. (b) Slurry trenching. (c) Concreting. (d) Hardening of concrete.	42
Figure 3.9. 3D Stress state.	42
Figure 3.10. Calculated horizontal stress (σ_{yy}) 0.3 m behind the wall after hardening of pile 'A' at a depth of 15.3 m.	43
Figure 3.11. Calculated horizontal stress (σ_{yy}) 0.3 m behind the wall after hardening of pile 'A' at a depth of 3.3 m.	44
Figure 3.12. Plan view of sections A-A, B-B, C-C, D-D and E-E 0.3 m behind the wall.	45
Figure 3.13. Variation of the calculated total horizontal stress (σ_{yy}) acting on section A-A and B-B, with depth down the wall at the end of construction of piles 'A'. At a normal distance from the wall of 0.3 m.	47

Figure 3.14. Variation of calculated shear stress (τ_{zy}) acting on section A-A and B-B, with depth down the wall at the end of construction of piles 'A'. At a normal distance from the wall of 0.3 m. 50

Figure 3.15. Variation of the calculated shear stress (τ_{zy}) acting on section A-A and B-B, with depth down the wall at the end of construction of piles 'A'. At a normal distance from the wall of 0.3 m. 51

Figure 3.16. Variation of the calculated total horizontal stress (σ_{yy}) acting on section D-D, with depth down the wall at the end of construction of piles 'E'. At a normal distance from the wall of 0.3 m. 52

Figure 3.17. Variation of the calculated total horizontal stress (σ_{yy}) acting on section B-B, with depth down the wall at the end of construction of piles 'A', 'E' and 'I'. At a normal distance from the wall of 0.3 m. 53

Figure 3.18. Variation of the calculated total horizontal stress (τ_{zy}) acting on section B-B, with depth down the wall at the end of construction of piles 'A', 'E' and 'I'. At a normal distance from the wall of 0.3 m. 55

Figure 3.19. Generation of negative values of the shear stress (τ_{zy}) above the toe of the wall allow (σ_{yy}) to reduce. 56

Figure 3.20. Variation of the calculated shear stress (τ_{zy}) acting on section B-B, with depth down to wall at the end of construction of piles 'A', 'E' and 'I'. At a normal distance from the wall of 0.3 m. 56

Figure 3.21 Calculated horizontal stress (σ_{yy}) 0.3 m behind the wall after hardening of pile 'I' at a depth of 15.3 m. 57

Figure 3.22 Calculated horizontal stress (σ_{yy}) 0.3 m behind the wall after hardening of pile 'I' at a depth of 3.3 m. 58

Figure 3.23. Total horizontal stresses (σ_{yy}) measured during wall installation compared with those calculated by the *FLAC*^{3D} model (Spade Cell 2). 59

Figure 3.24. Total horizontal stresses (σ_{yy}) measured during wall installation compared with those calculated by the *FLAC*^{3D} model (Spade Cell 4). 59

Figure 3.25. Total horizontal stresses (σ_{yy}) measured during wall installation compared with those calculated by the *FLAC*^{3D} model (Spade Cell 5). 60

Figure 3.26 Total horizontal stresses (σ_{yy}) measured during wall installation compared with those calculated by the *FLAC*^{3D} model (Spade Cell 16). 60

- Figure 3.27. Calculated horizontal displacement along the section B-B calculated in the 3D analysis of installation of the bored pile wall. At a normal distance from the wall of 0.3 m. 62
- Figure 3.28. Distribution of the calculated horizontal displacement 0.4 m behind the wall along the wall after the hardening of the concrete in piles ‘A’ at a depth of 3.3 m. 63
- Figure 3.29. Distribution of the calculated horizontal displacement 0.4 m behind the wall along the wall after the hardening of the concrete in piles ‘I’ at a depth of 3.3 m. 64
- Figure 3.30. Distribution of the calculated horizontal displacement 0.4 m behind the wall along the wall after the hardening of the concrete in piles ‘A’ at a depth of 15.3 m. 65
- Figure 3.31. Distribution of the calculated horizontal displacement 0.4 m behind the wall along the wall after the hardening of the concrete in piles ‘I’ at a depth of 15.3 m. 66
- Figure 3.32. In situ earth pressure coefficient $K_0 = 1$ (Richards et al., 2006) compared K_0 with the profile used by Gourvenect and Powrie (1999). 67
- Figure 3.33. Comparison of the total horizontal stresses (σ_{yy}) calculated by the $FLAC^{3D}$ model using different in situ stress states (Spade Cell 5). 68
- Figure 3.34. Comparison of the total horizontal stresses (σ_{yy}) calculated by the $FLAC^{3D}$ model using different in situ stress state, (Spade Cell 5). 68
- Figure 3.35. Comparison of the total horizontal stresses (σ_{yy}) calculated by the $FLAC^{3D}$ model using different in situ stress state, (Spade Cell 5). 69
- Figure 4.1. Soil stiffness (Young’s modulus E) used in Chapter 3 and 4. (E=constant with the depth, Chapter 3; E=increasing with the depth, initial Young’s modulus for the linear and non-linear stress strain model, Chapter 4). 77
- Figure 4.2. Curve fitting to stiffness-strain data (Jardine et al., 1986). 78
- Figure 4.3. Total horizontal stresses (σ_{yy}) measured during wall installation compared with those calculated by the $FLAC^{3D}$ model (Spade Cell 1). 79
- Figure 4.4. Total horizontal stresses (σ_{yy}) measured during wall installation compared with those calculated by the $FLAC^{3D}$ model (Spade Cell 2). 80
- Figure 4.5. Total horizontal stresses (σ_{yy}) measured during wall installation compared with those calculated by the $FLAC^{3D}$ model (Spade Cell 3). 81
- Figure 4.6. Total horizontal stresses (σ_{yy}) measured during wall installation compared with those calculated by the $FLAC^{3D}$ model (Spade Cell 4). 82

Figure 4.7. Total horizontal stresses (σ_{yy}) measured during wall installation compared with those calculated by the <i>FLAC^{3D}</i> model (Spade Cell 5).	83
Figure 4.8. Total horizontal stresses (σ_{yy}) measured during wall installation compared with those calculated by the <i>FLAC^{3D}</i> model (Spade Cell 6).	84
Figure 4.9. Total horizontal stresses (σ_{yy}) measured during wall installation compared with those calculated by the <i>FLAC^{3D}</i> model (Spade Cell 7).	85
Figure 4.10. Total horizontal stresses (σ_{yy}) measured during wall installation compared with those calculated by the <i>FLAC^{3D}</i> model (Spade Cell 8).	86
Figure 4.11. Total horizontal stresses (σ_{yy}) measured during wall installation compared with those calculated by the <i>FLAC^{3D}</i> model (Spade Cell 9).	87
Figure 4.12. Total horizontal stresses (σ_{yy}) measured during wall installation compared with those calculated by the <i>FLAC^{3D}</i> model (Spade Cell 12).	88
Figure 4.13. Total horizontal stresses (σ_{yy}) measured during wall installation compared with those calculated by the <i>FLAC^{3D}</i> model (Spade Cell 13).	89
Figure 4.14. Total horizontal stresses (σ_{yy}) measured during wall installation compared with those calculated by the <i>FLAC^{3D}</i> model (Spade Cell 15).	90
Figure 4.15. Total horizontal stresses (σ_{yy}) measured during wall installation compared with those calculated by the <i>FLAC^{3D}</i> model (Spade Cell 16).	90
Figure 4.16. Total horizontal stresses (σ_{yy}) measured during wall installation compared with those calculated by the <i>FLAC^{3D}</i> model (Spade Cell 17).	91
Figure 4.17. Horizontal stress (σ_{yy}) 0.3 m behind the wall after hardening of piles ‘A’ at a depth of 3.3 m.	92
Figure 4.18. Horizontal stress (σ_{yy}) 0.3 m behind the wall after hardening of piles ‘I’ at a depth of 3.3 m.	93
Figure 4.19. Horizontal stress (σ_{yy}) 0.3 m behind the wall after hardening of piles ‘A’ at a depth of 15.3 m.	93
Figure 4.20. Horizontal stress (σ_{yy}) 0.3 m behind the wall after hardening of piles ‘I’ at a depth of 15.3 m.	94

Figure 4.21. Variation of the total horizontal stress (σ_{yy}) acting on section A-A, with depth down to the wall at the end of construction of piles A, E and I.	95
Figure 4.22. Variation of the total horizontal stress (σ_{yy}) acting on section B-B, with depth down to the wall at the end of construction of piles A, E and I.	96
Figure 4.23. Variation of the total horizontal stress (τ_{xy}) acting on section B-B, with depth down to the wall at the end of construction of piles A, E and I.	97
Figure 4.24. Variation of the total horizontal stress (τ_{xy}) acting on section B-B, with depth down to the wall at the end of construction of piles A, E and I.	98
Figure 4.25. Computed horizontal total stress (σ_{yy}) 0.5 m behind the wall on section B-B.	99
Figure 4.26. Computed horizontal total stress (σ_{yy}) 1 m behind the wall on section B-B.	100
Figure 4.27. Computed horizontal total stress (σ_{yy}) 4 m behind the wall on section B-B.	100
Figure 4.28. Computed horizontal total stress (σ_{yy}) 10 m behind the wall on section B-B.	101
Figure 4.29. Computed horizontal total stress (σ_{yy}) 20 m behind the wall on section B-B.	101
Figure 4.30. Horizontal displacement along the section B-B calculated in the 3D analysis of installation of the diaphragm wall.	103
Figure 4.31. Horizontal displacement along the section B-B and A-A calculated in the 3D analysis after the hardening of the concrete in the piles A.	105
Figure 4.32. Horizontal displacement along the section B-B and A-A calculated in the 3D analysis after the hardening of the concrete in the piles I.	106
Figure 4.33. Distribution of the horizontal displacement 0.4 m behind the wall along the wall after the hardening of the concrete in piles 'A' at a depth of 3.3 m.	107
Figure 4.34. Distribution of the horizontal displacement 0.4 m behind the wall along the wall after the hardening of the concrete in piles 'I' at a depth of 3.3 m.	108
Figure 4.35. Distribution of the horizontal displacement 0.4 m behind the wall along the wall after the hardening of the concrete in piles 'A' at a depth of 15.3 m.	108
Figure 4.36. Distribution of the horizontal displacement 0.4 m behind the wall along the wall after the hardening of the concrete in piles 'A' at a depth of 15.3 m.	109

Figure 5.1. Finite-Difference mesh	113
Figure 5.2. Different sequences of panel installation. (a) Construction sequence 1, (b) Construction sequence 2, (c) Construction sequence 3, (d) Construction sequence 4, (a) Construction sequence 5.	114
Figure 5.3. In situ earth pressure coefficient profiles.	115
Figure 5.4. Wall Geometry.	116
Figure 5.5. Sequence of construction stages. (a) In situ stress (b) Slurry trenching, (c) Concreting, (d) Hardening of concrete and (e) excavation in front of the wall.	118
Figure 5.6. Modelling sequence for Construction Diaphragm Wall Panel.	118
Figure 5.7. 3D Stress state.	119
Figure 5.8. Plan view.	120
Figure 5.9. Distribution of total horizontal stresses (σ_{yy}) along the length of the wall after concreting of the central panel.	121
Figure 5.10. Distribution of total horizontal stresses (σ_{yy}) along the length of the wall after concreting of the central panel.	122
Figure 5.11. Variation with depth of the total horizontal stress (σ_{yy}) acting on section B-B, at a normal distance from the wall of 0.3 m.	123
Figure 5.12. Variation with depth of the total horizontal stress (σ_{yy}) acting on section A-A, at a normal distance from the wall of 0.3 m.	125
Figure 5.13. Variation with depth of the total horizontal stress (σ_{yy}) acting on section A-A, at a normal distance from the wall of 0.3 m. Sequences 1, 2, 3, 4 and 5.	130
Figure 5.14. Variation with depth of the total horizontal stress (σ_{yy}) acting on section B-B, at a normal distance from the wall of 0.3 m. Sequences 1, 2, 3, 4 and 5.	131
Figure 5.15. Variation with depth of the total horizontal stress (σ_{yy}) acting on section C-C, at a normal distance from the wall of 0.3 m. Sequences 1, 2, 3, 4 and 5.	132
Figure 5.16. Variation with depth of the shear stress (τ_{zy}) acting on section A-A, at a normal distance from the wall of 0.3 m. Sequences 1, 2, 3, 4 and 5.	133
Figure 5.17. Variation with depth of the shear stress (τ_{zy}) acting on section B-B, at a normal distance from the wall of 0.3 m. Sequences 1, 2, 3, 4 and 5.	134

Figure 5.18. Variation with depth of the shear stress (τ_{xy}) acting on section C-C, at a normal distance from the wall of 0.3 m. Sequences 1, 2, 3, 4 and 5.	135
Figure 5.19. Variation with depth of the shear stress (τ_{xy}) acting on section A-A, at a normal distance from the wall of 0.3 m. Sequences 1, 2, 3, 4 and 5.	137
Figure 5.20. Variation with depth of the shear stress (τ_{xy}) acting on section B-B, at a normal distance from the wall of 0.3 (m). Sequences 1, 2, 3, 4 and 5.	138
Figure 5.21. Variation with depth of the shear stress (τ_{xy}) acting on section C-C, at a normal distance from the wall of 0.3 m. Sequences 1, 2, 3, 4 and 5.	139
Figure 5.22. Variation with depth of the total horizontal stress (σ_{yy}) acting on section A-A, at a normal distance from the wall of 0.3 m. Sequence 1.	142
Figure 5.23. Variation with depth of the total horizontal stress (σ_{yy}) acting on section B-B, at a normal distance from the wall of 0.3 m. Sequence 1.	143
Figure 5.24. Variation with depth of the total horizontal stress (σ_{yy}) acting on section C-C, at a normal distance from the wall of 0.3 m. Sequence 1.	144
Figure 5.25. Variation with depth of the shear stress (τ_{xy}) acting on section A-A, at a normal distance from the wall of 0.3 m. Sequence 1.	145
Figure 5.26. Variation with depth of the shear stress (τ_{xy}) acting on section C-C, at a normal distance from the wall of 0.3 m. Sequence 1.	146
Figure 5.27. Variation with depth of the shear stress (τ_{xy}) acting on section B-B, at a normal distance from the wall of 0.3 m. Sequence 1.	147
Figure 5.28. Variation with depth of the shear stress (τ_{xy}) acting on section A-A, at a normal distance from the wall of 0.3 m. Sequence 1.	148
Figure 5.29. Variation with depth of the shear stress (τ_{xy}) acting on section C-C, at a normal distance from the wall of 0.3 m. Sequences 1.	149
Figure 5.30. Variation of the shear stress (τ_{xy}) acting on section B-B, at a normal distance from the wall of 0.3 m. Sequence 1.	150
Figure 5.31 Variation with depth of the total horizontal stress (σ_{yy}) acting on section B-B, at a normal distance from the wall of 0.3 m. Sequence 1.	153

Figure 5.32. Variation with depth of the total horizontal stress (σ_{yy}) acting on section C-C, at a normal distance from the wall of 0.3 m. Sequence 4.	154
Figure 5.33. Variation with depth of the total horizontal stress (σ_{yy}) acting on section B-B, at a normal distance from the wall of 0.3 m. Sequence 4.	155
Figure 5.34. Variation with depth of the shear stress (τ_{zy}) acting on section A-A, at a normal distance from the wall of 0.3 m. Sequence 4.	156
Figure 5.35. Variation with depth of the shear stress (τ_{zy}) acting on section C-C, at a normal distance from the wall of 0.3 m. Sequence 4.	157
Figure 5.36. Variation with depth of the shear stress (τ_{zy}) acting on section B-B, at a normal distance from the wall of 0.3 m. Sequence 4.	158
Figure 5.37. Variation with depth of the shear stress (τ_{zy}) acting on section A-A, at a normal distance from the wall of 0.3 m. Sequence 4.	159
Figure 5.38. Variation with depth of the shear stress (τ_{zy}) acting on section C-C, at a normal distance from the wall of 0.3 m. Sequence 4.	160
Figure 5.39. Variation with depth of the shear stress (τ_{zy}) acting on section B-B, at a normal distance from the wall of 0.3 m. Sequence 4.	161
Figure 5.40. Total horizontal stress (σ_{yy}) profiles 5 m from the wall, normal to the centre of panel 3, for all installation sequences.	162
Figure 5.41. Total horizontal stress (σ_{yy}) profiles 10 m from the wall, normal to the centre of panel 3, for all installation sequences.	163
Figure 5.42. Total horizontal stress (σ_{yy}) profiles 15 m from the wall, normal to the centre of panel 3, for all installation sequences.	164
Figure 5.43. Total horizontal stress (σ_{yy}) profiles at various normal distances from the centre of panel 3 (sequence 1).	165
Figure 5.44. Comparison of the horizontal displacements behind the wall at sections B-B with those calculated by Ng and Yan (1998) and Gourvenec and Powrie (1999).	167
Figure 5.45. Horizontal displacements behind the wall at sections A-A, B-B and C-C, after the installation of all panels. Sequences 1.	168
Figure 5.46. Horizontal displacements behind the wall at section A-A after the installation of all panels. Sequences 1, 2, 3, 4 and 5.	169

Figure 5.47. Horizontal displacements behind the wall at section B-B after the installation of all panels. Sequences 1, 2, 3, 4 and 5.	170
Figure 5.48. Horizontal displacements behind the wall at section C-C after the installation of all panels. Sequences 1, 2, 3, 4 and 5.	171
Figure 6.1. Pore water pressures measured before, during and over 13 years after wall installation (Spade Cells 1, 2, 3, 4 and 5) (Wiggan, 2013).	178
Figure 6.2. Pore water pressures measured before, during and over 13 years after wall installation (Spade Cells 15 and 16) (Wiggan, 2013).	178
Figure 6.3. Pore water pressures measured before, during and over 13 years after wall installation (Spade Cells 6, 7, 8 and 10) (Wiggan, 2013).	179
Figure 6.4. Pore water pressure profile taken at different times at a distance of 1.275 m behind the retaining wall (Wiggan, 2013).	180
Figure 6.5. Pore water pressure profile 3.475 m behind the retaining wall (Wiggan, 2013).	180
Figure 6.6. Long term pore water pressures 1.275 m in front of the retaining wall (Wiggan, 2013).	183
Figure 6.7. Long term pore water pressures 3.475 m in front of the retaining wall (Wiggan, 2013).	183
Figure 6.8. Long term pore water pressures in front of the retaining wall (Wiggan, 2013).	184
Figure 6.9. Long term pore water pressures at a depth of 3.3 m below ground level (Wiggan, 2013).	185
Figure 6.10. Long term pore water pressures measured at a depth of 3.3 m below ground level (Wiggan, 2013).	186
Figure 6.11. Long term pore water pressures at a depth of 8.3 m below ground level (Wiggan, 2013).	187
Figure 6.12. Long term pore water pressures measured at a depth of 11.3 m below ground level (Wiggan, 2013).	188
Figure 6.13. Long term pore water pressures measured at a depth of 15.3 m below ground level (Wiggan, 2013).	189
Figure 6.14. Normalised (a) horizontal total stresses and (b) pore water pressures 1.275 m behind the contiguous pile retaining wall.	191
Figure 6.15. Normalised horizontal total stresses and pore water pressures 3.475 m behind the contiguous pile retaining wall.	193

Figure 6.16. Normalised (a) horizontal total stresses and (b) pore water pressures 1.275 m in front of the contiguous pile retaining wall.	194
Figure 6.17. Comparison of the pore water pressure and horizontal stress profiles for short term and long term conditions at a distance of 1.275 m behind the retaining wall.	195
Figure 6.18. Comparison of the pore water pressure and horizontal stress profiles for short term and long term conditions at a distance of 2.375 m behind the retaining wall.	196
Figure 6.19. Comparison of the pore water pressure and horizontal stress profiles for short term and long term conditions at a distance of 3.475 m behind the retaining wall.	196
Figure 6.20. Changes in the total horizontal stresses ($\sigma_{h0} - \Delta\sigma_h$) and pore pressures ($u_0 - u$) normalised with respect to in situ values at distances of 1.275 m and 3.475 m behind the retaining wall.	198
Figure 6.21. Total horizontal stress measured before, during and over 13 years after wall installation, (Spade Cells 1, 2, 3, 4, 5).	200
Figure 6.22. Total horizontal stresses measured before, during and over 13 years after wall installation (Spade Cells 15, 16).	201
Figure 6.23. Total horizontal stress measured before, during and 13 years after wall installation. (Spade Cell 6, 7, 8, 9).	201
Figure 6.24. Total horizontal stresses measured before, during and over 13 years after wall installation (Spade Cells 11, 12).	202
Figure 6.25. Total horizontal stresses measured before, during and over 13 years after wall installation (Spade Cells 13, 17).	203
Figure 6.26. Total horizontal stresses measured before, during and over 13 years after wall installation (Spade Cells 1, 6).	204
Figure 6.27. Total horizontal stress measured before, during and 13 years after wall installation. (Spade Cell 2, 7, 15).	205
Figure 6.28. Total horizontal stresses measured before, during and over 13 years after wall installation (Spade Cells 3, 8, 16).	206
Figure 6.29. Total horizontal stresses measured before, during and over 13 years after wall installation (Spade Cells 4, 9, 11, 13).	207
Figure 6.30. Total horizontal stresses measured before, during and over 13 years after wall installation (Spade Cells 5, 12, 17).	208
Figure 6.31. Total horizontal stresses measured before, during and over 13 years after wall installation (Spade Cells 1, 2, 3, 4, 5, 6, 7, 8, 9, 11, 12, 13, 15, 16, 17).	209

Figure 6.32. Total horizontal stresses behind the wall before and after wall installation, construction, excavation and long term (13 years).	210
Figure 6.33. Cross section through monitored section of road (Hayward, 2000).	212
Figure 6.34. Ground condition at the instrumented cross section (Hayward, 2000).	212
Figure 6.35. Cross section through monitored cross section, showing location of instrumentation (Hayward, 2000).	215
Figure 6.36. Development of wall bending moments at 1.73 m below top of wall.	217
Figure 6.37. Development of wall bending moments at 2.73 m below top of wall.	217
Figure 6.38. Development of wall bending moments at 3.73 m below top of wall.	218
Figure 6.39. Development of wall bending moments at 5.03 m below top of wall.	218
Figure 6.40. Development of wall bending moments at 6.33 m below top of wall.	219
Figure 6.41. Development of wall bending moments at 7.63 m below top of wall.	219
Figure 6.42. Development of wall bending moments at 9.43 m below top of wall.	220
Figure 6.43. Development of wall bending moments at 10.23 m below top of wall.	220
Figure 6.44. Development of wall bending moments at 12.03 m below top of wall.	221
Figure 6.45. Development of wall bending moments at 13.33 m below top of wall.	221
Figure 6.46. Stresses beneath the base adjacent to pile 3.	222

DECLARATION OF AUTHORSHIP

I, Luca Montalti declare that the thesis entitled “**3D modelling of bored pile installation effects and long term monitoring of a propped retaining wall**” and the work presented in the thesis are both my own, and have been generated by me as the result of my own original research. I confirm that:

- this work was done wholly or mainly while in candidature for a research degree at this University;
- where any part of this thesis has previously been submitted for a degree or any other qualification at this University or any other institution, this has been clearly stated;
- where I have consulted the published work of others, this is always clearly attributed;
- where I have quoted from the work of others, the source is always given. With the exception of such quotations, this thesis is entirely my own work;
- I have acknowledged all main sources of help;
- where the thesis is based on work done by myself jointly with others, I have made clear exactly what was done by others and what I have contributed myself;

ACKNOWLEDGEMENTS

I am extremely grateful to my supervisors, Professor William Powrie and Professor David Richards, for their invaluable guidance and support. Many thanks to Dr Joel Smethurst for his helpful remarks as the examiner for my MPhil to PhD transfer report.

This work would not have been possible without the support of my best friend, Dr Eduardo Mangieri.

I also would like to express my gratitude to my friends, Dr Antonio Penta, Dr Giorgio Ponti, Dr Lorenzo Capretto, Marco Giovannelli, Niuvia Johansson, Stefan Johansson and Jelena Bavrina.

Finally, I am forever indebted to my parents and sister for their understanding, endless patience and encouragement when it was most required. Words cannot express how grateful I am for your unconditional love and support.

NOTATION

Roman Symbols

A	Non-linear soil parameter (Scott <i>et al.</i> 2003)
B	Non-linear soil parameter (Scott <i>et al.</i> 2003)
C	Non-linear soil parameter (Scott <i>et al.</i> 2003)
c_u	Undrained shear strength of the soil
d	Pile diameter
E	Young's modulus
$FLAC^{3D}$	Fast Lagrangian Analysis of Continua in 3 dimensions
G	Elastic shear modulus
G_{tan}	Tangent shear modulus
H	Panel depth
K_0	Earth pressure coefficient
K_f	Fluid bulk modulus
K_{tan}	Elastic shear modulus
L	Panel length
LT	Long term
p'	Mean effective stress
R	Non-linear soil parameter (Scott <i>et al.</i> 2003)
S	Non-linear soil parameter (Scott <i>et al.</i> 2003)
ST	Short term
T	Non-linear soil parameter (Scott <i>et al.</i> 2003)
u	Pore water pressure
X	Non-linear soil parameter (Scott <i>et al.</i> 2003)
x	Co-ordinate direction
y	Co-ordinate direction
Y	Non-linear soil parameter (Scott <i>et al.</i> 2003)
z'	Depth below the head of the pile
z	Co-ordinate direction
$2D$	Two-dimensional

3D Three-dimensional

Greek Symbols

α	Non-linear soil parameter (Scott <i>et al.</i> 2003)
β	Non-linear soil parameter (Scott <i>et al.</i> 2003)
λ	Non-linear soil parameter (Scott <i>et al.</i> 2003)
μ	Non-linear soil parameter (Scott <i>et al.</i> 2003)
ν	Poisson's ratio
ν_u	Undrained Poisson's ratio
ϕ	Frictional soil resistance
γ	Unit weight of soil
γ_{oct}	Engineering octahedral shear strain
ρ	Density
σ	Normal stress
σ'_h	Horizontal effective stress
σ'_v	Vertical effective stress
τ	Shear stress
ε_a	Axial strain
ε_v	Volumetric strain

CHAPTER 1

INTRODUCTION

1.1 Introduction

There is no need to emphasise that diaphragm wall and bored pile walls are nowadays used in many engineering projects, especially in urban areas. A diaphragm wall or bored pile wall is a popular solution to the problem of earth retention on sites in congested urban areas, where disturbance to the adjoining ground must be kept to a minimum. There are many applications where these structures can be implemented. Diaphragm walls and bored pile walls may be used as temporary support systems or as a part of the permanent structure.

From the viewpoint of wall performance, installation effects are important because they can significantly alter the horizontal total stresses applied to the retained side of the wall and can be

expected to influence the actual values of prop and anchor forces, and of maximum bending moment within to the wall (Gunn and Clayton, 1992).

Despite the fact that the finite element method permits modelling of the whole sequence of operations occurring during construction of deep excavations, the installation of diaphragm walls and bored piles is still often ignored in analyses. It is now commonly accepted that the effects associated with slurry trenching and concreting can cause significant displacements of the surrounding ground, of the same order of magnitude as those caused by subsequent excavation in front of the wall, and influence the behaviour of the retaining structure during the main excavation stage.

In the last few decades much effort has been spent to investigate the installation effects of diaphragm wall panels in an overconsolidated deposit. Conversely, in literature there is relatively little focus of the installation effects of bored pile construction. Therefore, the main aim of this research is to investigate the stress changes and ground movements due to bored pile wall installation in an overconsolidated deposit. Pile-soil interaction is a complex three dimensional problem in nature, therefore all the analyses presented in this research were carried out using three dimensional finite difference computer code *FLAC^{3D}* (Itasca, 2006).

Only limited research has been carried out to quantify the three dimensional effects of diaphragm wall installation. Even though Ng and Yan (1998) carried out a three-dimensional finite-difference analysis of the installation of a single diaphragm wall panel, they did not model the installation of subsequent panels. Gourvenec and Powrie (1999) also carried out a series of finite-element analyses to investigate the impact of three-dimensional effects in lateral stress during the sequential installation of a number of diaphragm wall panels; they only considered one sequence of panel installation.

Thus, in this thesis, a comprehensive numerical analysis is also presented to investigate if different sequences of panel installation could lead to different pre-arching stress distributions behind the wall. As in the case of bored pile installation effects, several analysis were carried out using the three dimensional finite difference computer code *FLAC^{3D}* (Itasca, 2006).

Finally, there is some concern that the high horizontal stresses in an overconsolidated deposit may become re-established in the long-term, despite the reductions that occur during retaining wall installation and subsequent excavation in front of the wall. This is thought not to occur because of shear stresses maintaining the difference between near field and far field horizontal stresses (Clark, 2006). As pointed out by Simpson and Powrie (2000) it seems unlikely, particularly in the design lifetime of the wall, that if the horizontal shear stresses break down then the vertical shear stresses necessary to produce a K_0 of more than 1 will exist either. Therefore, the long-term value of K_0 can be no more than 1.

To investigate the long-term stress state of the soil around a retaining wall, studies have been undertaken on walls that have been in service for a number of years. Analysis of the long term behaviour of the Bell Common Tunnel was carried out by Symons *et al.* (1989). They found insignificant changes in earth pressure behind the wall and small decreases in earth pressure in front of the wall in the four years after construction. Furthermore, they found very small changes in pore water pressure, which was measured on both sides of the wall.

Several years of instrumentation data from a cantilever retaining wall and a wall propped just below the carriageway were investigated by Symons *et al.* (1990). Measurements taken 150 m and 1.5 m from the cantilever wall showed that significant stress relief had occurred due to construction/installation. However, for the propped wall, measurements taken at 16 m and 1.5 m from the wall suggested no stress relief had occurred in this case.

Despite this, as reported previously, there is considerable uncertainty regarding the long term soil behaviour behind retaining walls in overconsolidated deposits. For example Design Standard BD 42/00 (Highways Agency, 2000) requires that in situ retaining walls are designed to withstand a long term lateral earth pressure coefficient of up to 1.5.

At the serviceability limit state, Report/CP/96 (Gaba *et al.*, 2002) suggests that the greatest pressures and loads are likely to act on the structure during its design life in which any long term changes in pore water pressures are taken into account. Long-term field measurements behind embedded retaining walls in London Clay at Walthamstow, Hackney, Reading and Malden generally indicate a slight reduction in the measured lateral stresses near the wall over a duration of up to eight years following construction (Carder and Darley, 1998). Then, Report/CP/96

(Gaba *et al.*, 2002) states that for walls embedded in stiff overconsolidated clay, the long term total lateral earth pressure remains largely unchanged from that at the end of the construction period.

In this thesis, thanks to high-quality long term case records from a section of contiguous bored pile retaining wall in overconsolidated clay in Kent, England, and a retaining wall in weak rock in Coventry, the potential for the re-establishment of the total horizontal stress behind diaphragm wall and bored pile wall in overconsolidated clay deposit was also investigated. More than 13 years of high-quality long term data have been collected from the retaining wall in Kent. A better understanding of the changes in stress that occur in the long term behind retaining wall in overconsolidated deposit has been drawn out from these results.

1.2 Aim and objectives

The objectives of the research were to:

- 1) Gain an improved understanding of bored pile installation effects in an overconsolidated deposit.
- 2) Back analyse the observed performance of a bored pile wall installation in Ashford, Kent.
- 3) Gain and improve understanding of the 3D effects of bored pile and diaphragm wall panel installation in overconsolidated clay deposits and stress transfer during bored pile wall installation.
- 4) Investigate the influence of a non-linear stress-strain characteristic on a 3D numerical model of bore pile installation.
- 5) Understand whether different sequences of panel installation could affect the post-installation stress state conditions.
- 6) Analyse the state of research into the effect of long-term total horizontal stress changes around retaining structures in an overconsolidated deposits.
- 7) Investigate the potential for the re-establishment of the total horizontal stresses behind diaphragm and bored pile walls in an overconsolidated deposit.

CHAPTER 2

PREVIOUS WORK

2.1 Introduction

The construction of diaphragm walls and bored piles may cause considerable stress changes in heavily overconsolidated soils and can induce substantial ground deformation (Burland & Hancock, 1977; Symons & Carder, 1993). The sequence of diaphragm wall and bored pile construction in stiff clay results in a complex soil behaviour which needs to be carefully investigated.

The main aim of this research was to investigate the stress changes and consequent movements in a stiff clay due to bored pile and diaphragm wall installation. Thus, this chapter synthesises the results collected during previous research studies which explored the problems associated with diaphragm wall and bored pile installation in overconsolidated deposits.

This chapter contains also a general review of the long-term change in soil pressure behind diaphragm wall and bored pile wall in overconsolidated deposit.

2.2 Case Histories

In the last few decades, several diaphragm and bored pile walls have been monitored. There is an abundance of information on wall and soil displacements from different sites in different soil conditions. Nevertheless, stress measurements in situ are much more complex to perform. Therefore, there is a limited amount of stress data from sites. Thus, the mechanisms of stress transfer and their influence on ground movements have been investigated by only a few researchers in the field. Furthermore, these data were collected in most cases from diaphragm walls and in only a few cases were bored pile wall sections monitored.

Farmer and Attewell (1973) investigated the horizontal stress variation and deformation of a diaphragm panel excavation supported by bentonite slurry. The trench excavation was 6.1 m long, 0.8 m wide and 15 m deep. They found that the maximum horizontal deformation occurred at about one-third of the panel depth below ground level. Behind a distance of about two-fifths of panel depth from the trench the horizontal movements at the surface were negligible.

Reductions in total horizontal stress during the wall installation have been measured at various sites in the U.K.; Tedd *et al.* (1984) installed spade shaped cells in London Clay at various depths and distances from the secant pile wall constructed at Bell Common Tunnel, Figure 2.1, and measured the changes in total lateral stress at different stages of construction. The reductions in effective lateral stresses measured during wall installation at Bell Common Tunnel were of the order of 70 kPa. They reported that the construction of the secant pile wall caused horizontal movement of the ground toward the wall and significant reductions in total horizontal stress, Figure 2.2, stage I (construction of the secant pile). About 30% of the total surface ground movements during construction took place within the period of installing the secant pile wall.

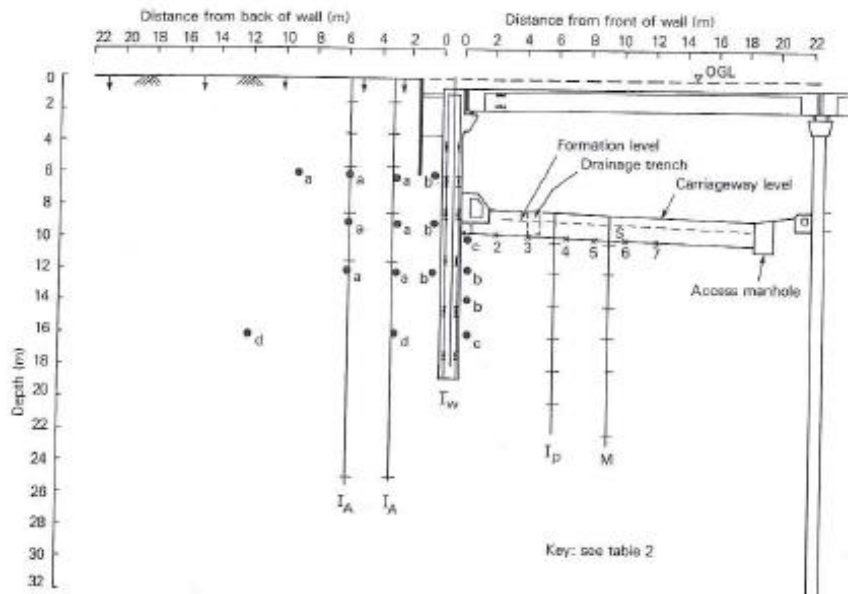


Fig. 5. Section showing the instrumentation layout

Table 2. Instrumentation details

Instrument symbol in Fig. 5	Instrument description	Date observations began	Measurement technique reference
● _a	Pressure cell/piezometer	Jan. 1981	Tedd & Charles (1981, 1983)
I _N	Combined inclinometer & vertical magnet extensometer	Mar. 1981	Chard & Symons (1982)
— ↓	Position of magnets 600 mm length ground anchor surface movement station	Aug. 1981	Chard & Symons (1982)
I _W	Inclinometer tube attached to web of I beam in wall	1 May 1982	
⊕	Vibrating-wire strain gauges attached to flanges of I beam in wall	1 May 1982	Thomas (1966), Tyler (1968)
● _N	Pressure cell/piezometer	12 May 1982	
S	Levelling station	15 Aug. 1982	Barratt & Tyler (1976)
●	Vibrating-wire strain gauges fixed to roof beams	19 Aug. 1982	
—x—x—x— 1 2 3	Horizontal plate gauge magnet extensometer & hydraulic settlement cell	18 Nov. 1982	Penman & Charles (1982) Penman, Charles, Nash & Humphreys (1975)
I _D	Combined inclinometer & vertical magnet extensometer	9 Dec. 1982	
M	Vertical magnet extensometer	9 Dec. 1982	McCaul, Morgan & Boden (1976)
● _c	Pressure cell/piezometer	15 Nov. 1982	
● _d	Pressure cell/piezometer	Aug. 1983	

Figure 2.1. Section showing the instrumentation layout and the instrumentation details (Tedd *et al.*, 1984).

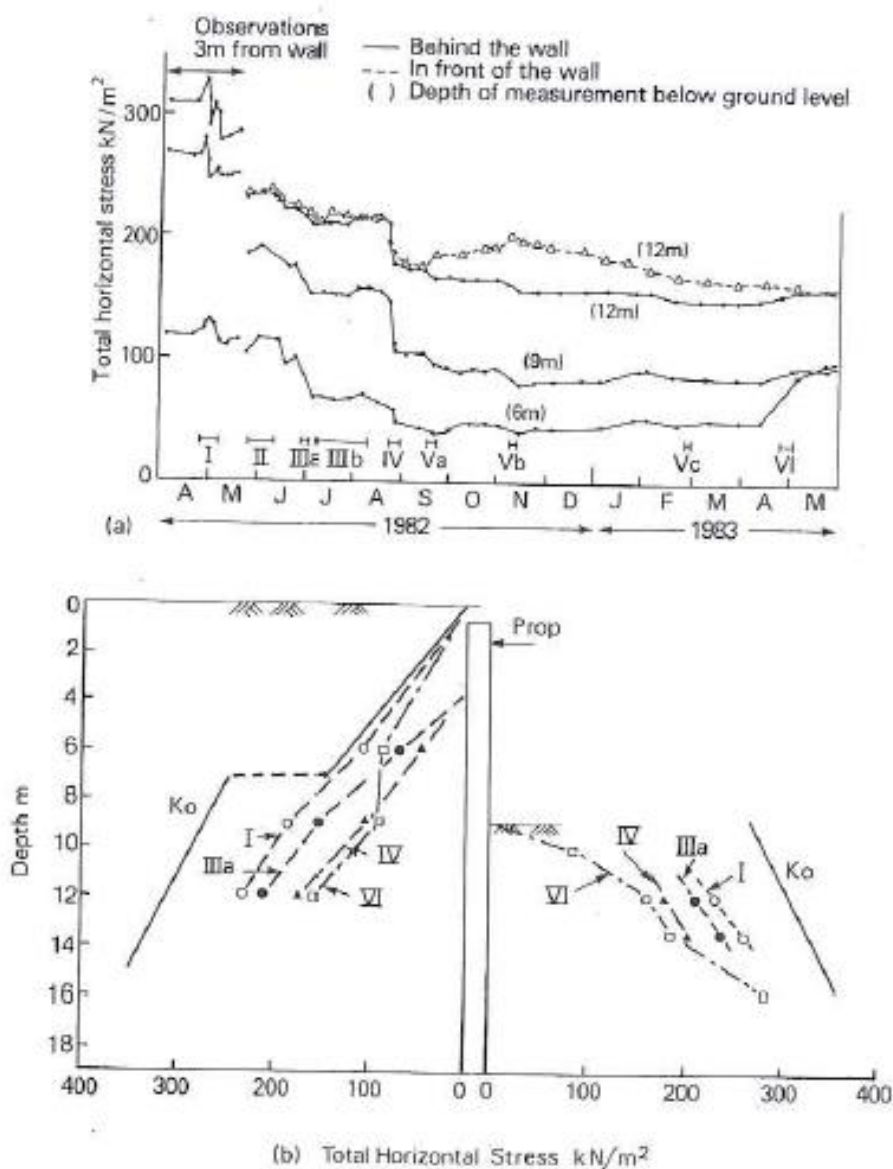


Figure 2.2. (a) Change in total horizontal stress with time and (b) distribution of the total horizontal stress in the soil 0.6 m from the wall at various stages of excavation (Tedd *et al.*, 1984).

Lings *et al.* (1991) reported a marked reduction in lateral stress during the construction of a diaphragm wall in stiff fissured Gault Clay at Lion Yard, Cambridge. The in-situ K_0 value at a depth of about 10 m was initially measured to be close to $K_0 = 3$. The earth pressure coefficient fell to less than unity after the wall installation.

Carder *et al.* (1991) monitored a diaphragm retaining wall formed of T-panels founded in over-consolidated clay, during and immediately after its construction as part of the A406 North Circular Road, Great Cambridge Road Junction Improvement Scheme in North London. The

construction sequence involved installation of the wall under bentonite followed by excavation below temporary props and casting of a permanent reinforced concrete prop slab below the final carriageway level. Spade cells were installed at different depths and locations around the wall. Figure 2.3 shows the magnitude of the effective lateral stress change measured by the cells in front of and behind the T-panels.

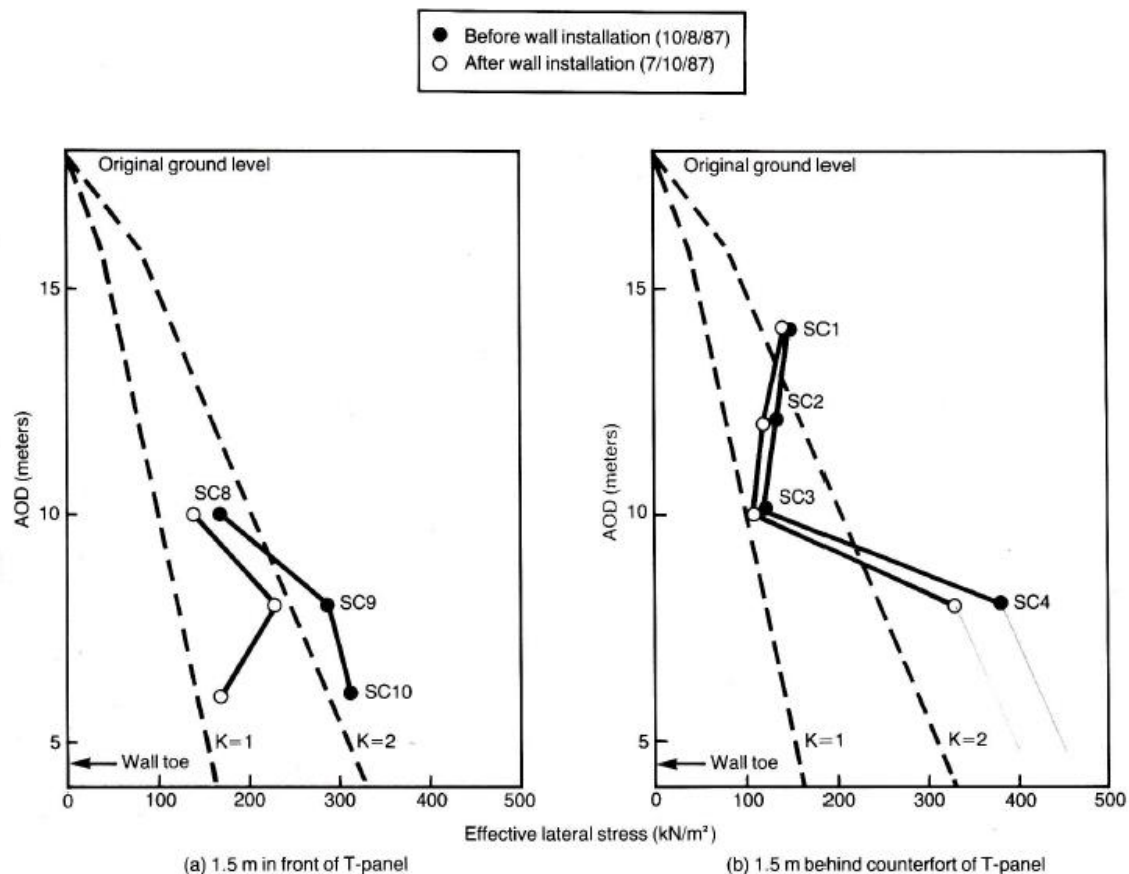


Figure 2.3. Stresses measured before and after diaphragm wall installation (Carder *et al.*, 1991).

Carder *et al.* (1991) observed that during the installation of the diaphragm wall the reduction in the initial lateral stress ranged from 50 kN/m^2 and 160 kN/m^2 . A maximum lateral movement towards the excavation of 7 mm was measured at 5 m behind the wall face.

Field data from two further sites are reported by Symons *et al.* (1992). They found that the decrease in the total lateral stresses at a depth of 10 to 12 m in the vicinity of the wall was similar to that observed at the Bell Common Tunnel. They found that the change in earth pressure coefficient of the wall installation is quite small, representing on average a 20% reduction of the recorded at rest value.

Symons *et al.* (1992) found that during pile installation, lateral movements at the surface away from the pile were measured with a maximum of about 7 mm being recorded at 1 m distance. They explained this by saying that the behaviour was probably caused by a ‘displacement effect’ in the 5.8 m surficial sandy gravel as a consequence of using a heavy oscillator to drive full depth casing for installation of the male piles.

Carswell *et al.* (1993) monitored a contiguous bored pile retaining wall in an over-consolidated deposit during and after its construction as part of the A406 North Circular Road Improvement Scheme in Walthamstow. Push-in spade shaped pressure cells (SC) were installed in the ground both in front of and behind the line of the retaining wall. The profiles of total lateral stresses measured in the ground at 1.1 m from the face of the wall before and after its installation as shown in Figure 2.4.

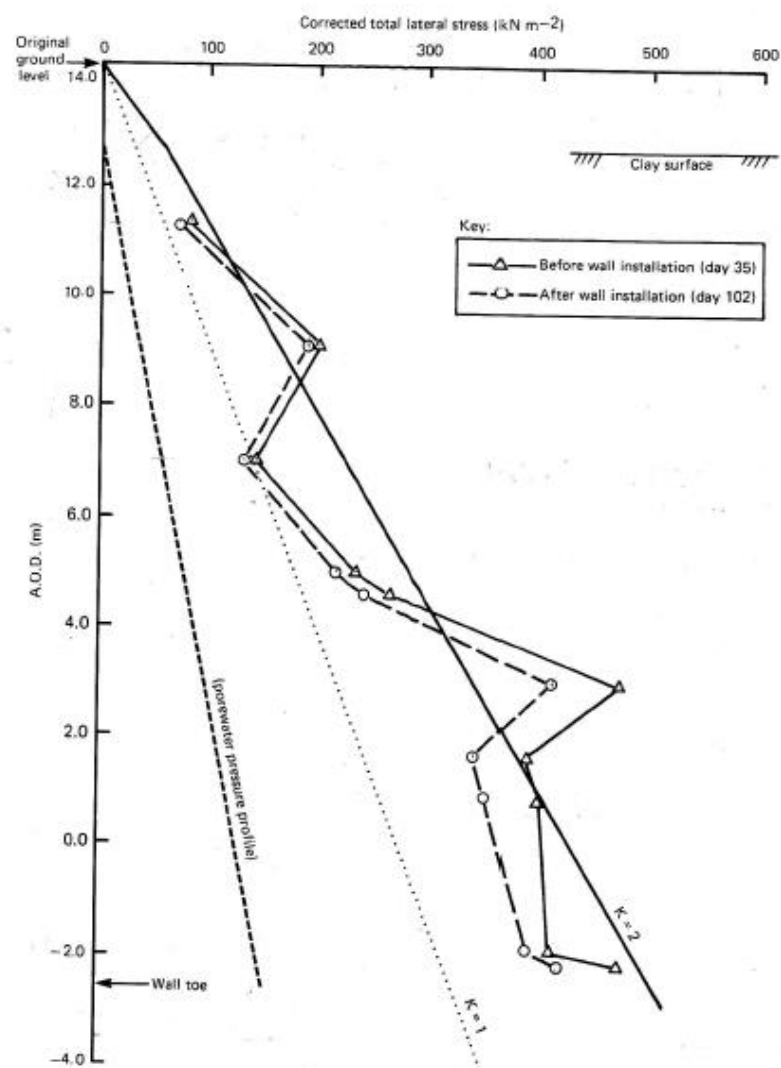


Figure 2.4. Stress changes at 1.1 m from the wall during its installation (Carswell *et al.*, 1993).

The net effect of the wall installation was to reduce the total lateral stress by between 9 kN/m^2 and 62 kN/m^2 . They reported that in general the large reductions occurred at the greater depths.

Bennett *et al.* (1996) monitored the behaviour of a propped secant bored pile wall at Hackney. Nine spade shaped pressure cells (SC) were installed to monitor total lateral stresses and pore water pressures in the ground. They monitored the lateral stress change during pile installation. Figure 2.5 shows the overall change in lateral total stress caused by wall installation.

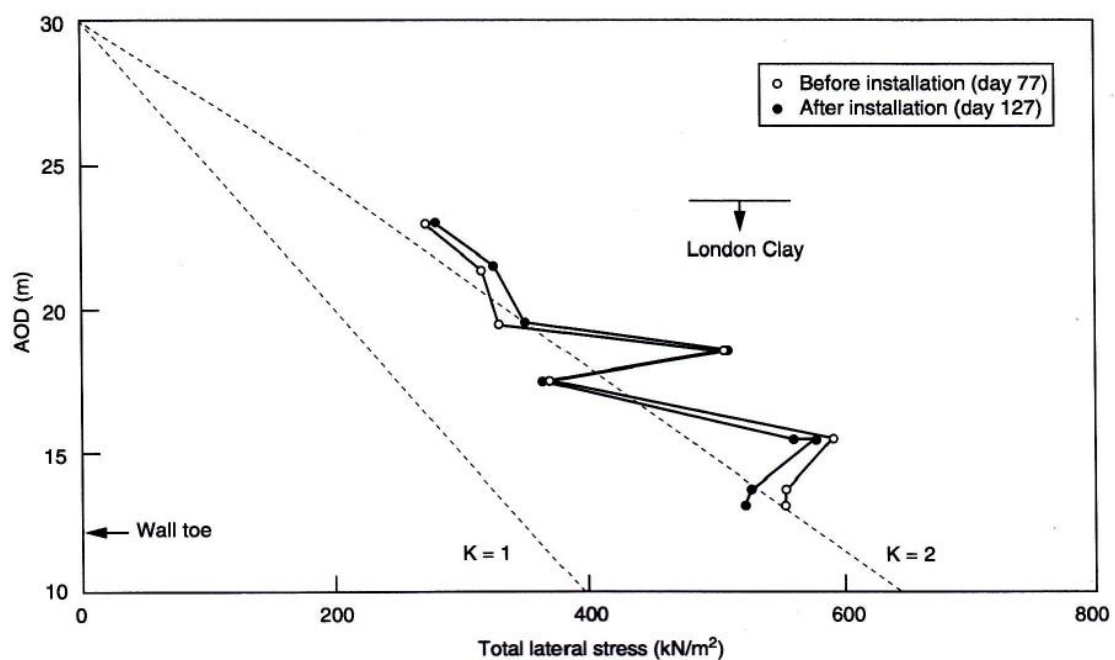


Figure 2.5. Lateral stresses distribution before and after pile wall installation (Bennet *et al.*, 1996).

Bennett *et al.* (1996) found that the largest reductions of 120 kN/m^2 and 80 kN/m^2 were measured behind and in front of the wall respectively at 14.5 m depth. Interestingly, they found that the effect of pile installation on the stresses was such that a small amount of stress relief was recorded on the deep spade cells, while stresses on the shallow spade cells generally returned to values similar to those measured before construction.

A 10-m -deep multipropped excavation in overconsolidated, stiff fissured Gault Clay was monitored by Ng and Yan (1998). They observed a marked reduction in total lateral stresses at the soil/wall interface due to diaphragm wall construction. The reduction in the total horizontal

stress was substantially larger at the wall installation stage than during the main excavation period, Figure 2.6.

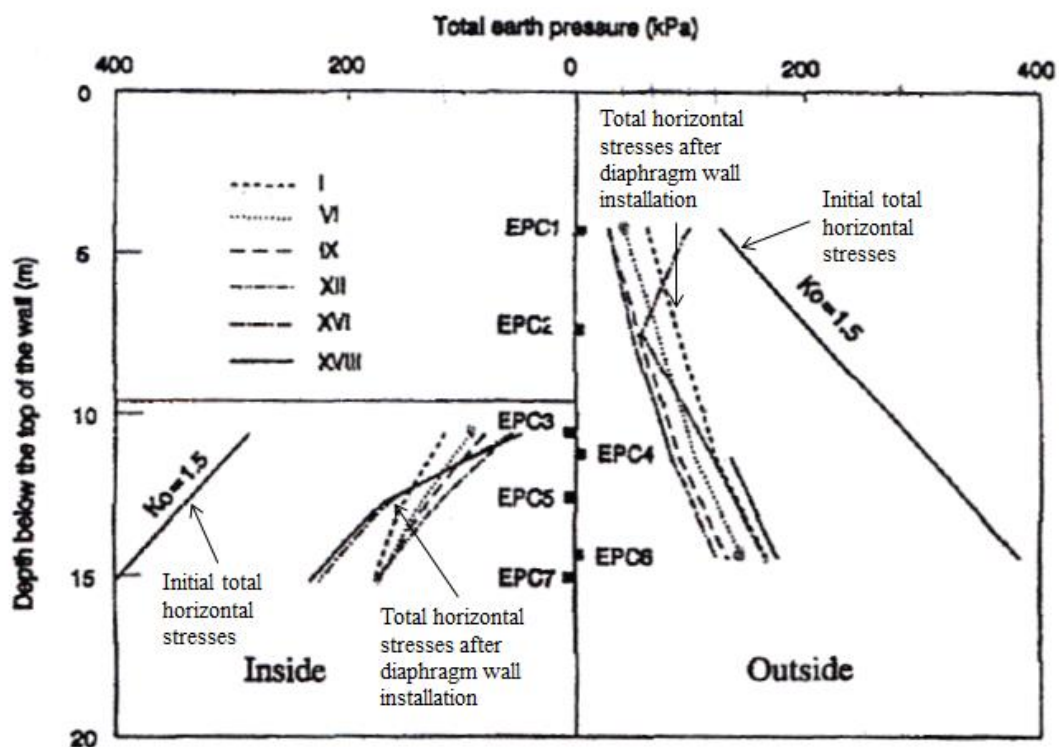


Figure 2.6. Total lateral pressures during and after construction in Gault Clay at Lion Yard, Cambridge (Ng and Yan, 1998).

2.3 Laboratory investigations

The effects of diaphragm wall installation were investigated using a centrifuge model by Powrie and Kantartzi (1996), Figure 2.7.

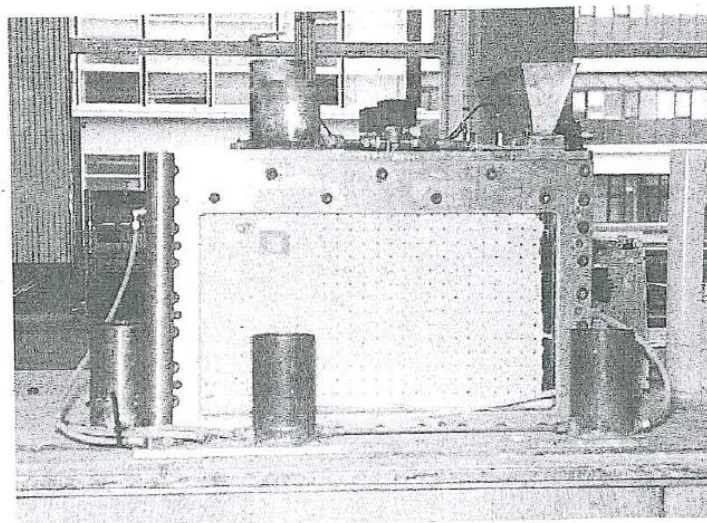


Figure 2.7. General view of the centrifuge model used by Powrie and Kantartzi (1996).

They reported that the deformation associated with a trench excavation of finite length was less than for a plane strain excavation. Ground movements were found to depend on a number of factors, including the initial ground water level and the geometry (length/depth ratio) of the panel. They observed that the soil surface settlement was reduced by a factor of 10 when a plane strain excavation was carried out with the water-table 10 m below ground level rather than at the soil surface. For a diaphragm wall trench 18.5 m deep and 1 m wide, three-dimensional effects were found to reduce the displacement at the centre-line of a single panel by a factor of 3 (compared with the plane strain case) for a panel 5 m long, but the benefit for a panel 10 m long was much smaller (Figure 2.8).

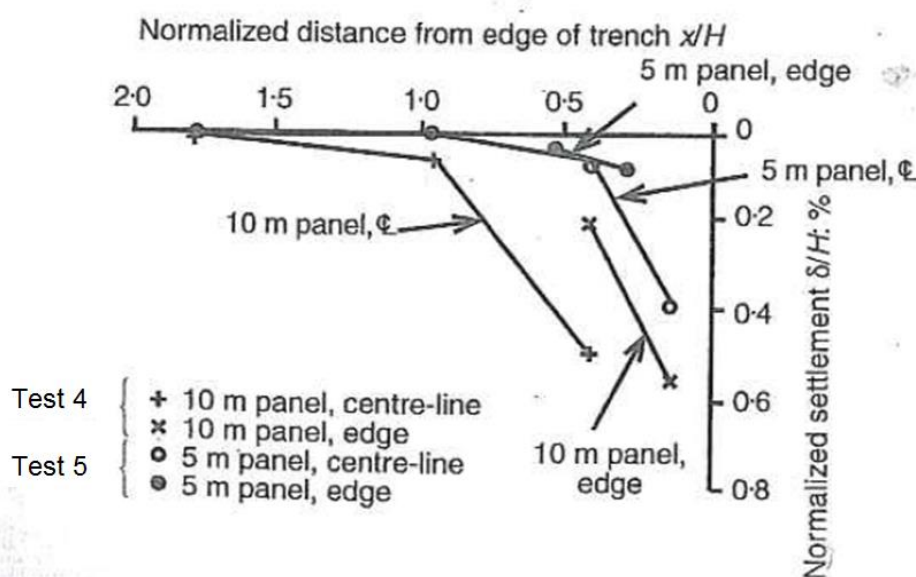


Figure 2.8. Comparison of edge and centre-line soil surface profiles following excavation under bentonite slurry, 10 m and 5 m panels Powrie and Kantartzi (1996).

They found that the vertical settlement was negligible at a distance greater than 1-1.8 panel depths away from the panel.

The stress changes and consequent movements in a stiff clay due to diaphragm wall installation and subsequent excavation in front of the wall were the focus of the research carried out by Pantelidou (1994). The problem was investigated experimentally using soil elements tested in a computer controlled triaxial stress path cell. The effects of wall installation were investigated both as a series of stress changes on a soil element in the vicinity of the wall, simulated in the triaxial cell, and as a whole by means of finite element modelling. It was found that the wall installation process had a major influence on the soil stiffness and on the mobilised strength

during excavation of the soil from in front of the wall. A reduction in lateral effective stress during wall installation was calculated. A general reduction of total horizontal stress took place, with only a temporary reduction in the pore water pressures. It was found that the initial pore water pressures were substantially re-established soon after wall installation had been completed. After wall installation, the lateral effective stresses remained close to the passive stress state prior to excavation. Inconsistencies were found between the design predictions and the computed results, and explained that with reference to the role of wall installation, which was not considered or was highly idealised at that time. Finally, it was found that the movements occurring during wall installation were very important and consisted of a large percentage of the total deformation at the end of excavation.

Richards *et al.* (1998) investigated the effects of retaining wall installation using centrifuge modelling techniques. They found that ground movements due to the installation of a diaphragm wall in panels of finite length are reduced by three dimensional effects, particularly if the panel length:depth ratio is less than 0.27. The reduction in ground movements associated with a low ground-water level is even more significant.

Another effect of the wall installation process is that it modifies the recent stress history of the soil. The effects of this on the stress-strain behaviour of the soil was investigated by Powrie *et al.* (1998). They carried out a series of triaxial tests on speswhite kaolin to investigate the stress-strain relations during the different stages of construction of a diaphragm wall in clay. They confirmed that in an overconsolidated clay deposit, the in-situ lateral effective stress is likely to be closer to the passive than the active limit, because of the geological stress history (Skempton, 1961; Burland *et al.*, 1979). The stress path describing wall installation resulted in different mobilized soil strengths at the beginning of the bentonite stage. From the triaxial tests, they investigated the relation between ϕ'_{mob} and K_0 and found that high value K_0 samples shear much more during the trench excavation than samples with low K_0 .

2.4. 2D and 3D numerical analysis

Two approaches are generally used to model diaphragm wall installation effects. The first involves simply reducing the lateral earth coefficient with the wall already in place. Powrie and Li (1991) used this approach. They modelled the effects of wall installation by reducing K_0 to 1

in the soil above the toe of the wall, with the finite element analysis starting with the wall already in place. Thus, the initial in situ lateral stresses were modified to take into account the stress reduction which installation of the wall might cause.

The second approach is to consider the full construction sequence from the excavation to bentonite slurry, followed by concreting and hardening. This approach was modelled in 2-D by Gunn *et al.* (1993). They used the finite element method with a plane strain assumption in the vertical plane to demonstrate the effects of wall installation. They used fully hydrostatic concrete pressure rather than the more appropriate bilinear concrete pressure (Ng 1992, Lings *et al.* 1994). Reduction in lateral stress associated with wall installation was found to be significant for the proposed retaining wall. They did not give details of any ground deformations, but unrealistically large ground deformation would be expected in a plane-strain analysis.

Pantelidou (1994) used 2D finite element analysis to investigate the stress change and consequent movements due to diaphragm wall installation in stiff clay and subsequent excavation in front of the wall. She used plane strain and axi-symmetric conditions to take into consideration the upper and lower bounds of what is happening in reality. An in situ wall can be constructed as a sequence of panels or bored piles. Wall panels are normally of limited length. Bored piles nominally correspond to axi-symmetric conditions, although Higgins *et al.* (1989) pointed out that an axi-symmetric analysis would underestimate the stress changes and displacements that would happen in reality, while the plane strain analysis would over-estimate them. Pantelidou (1994) used the assumption of axi-symmetric conditions to simulate the installation of a bored pile, Figure 2.9.

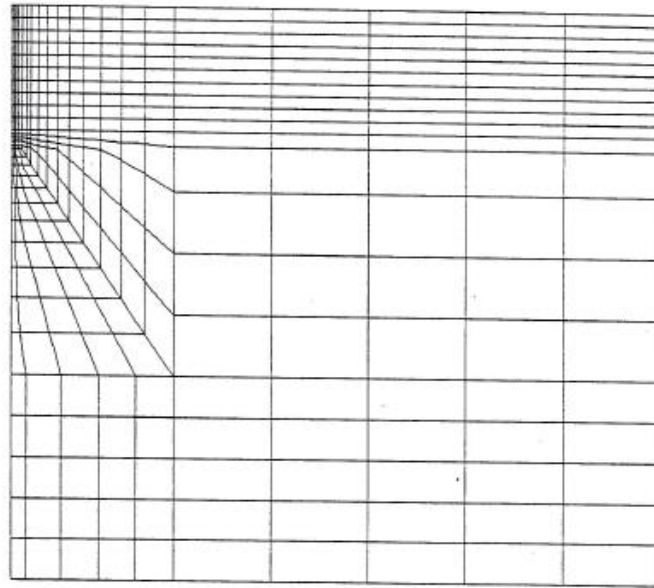


Figure 2.9. Finite element mesh used in the axi-symmetric analysis by Pantelidou (1994).

The horizontal effective stress distributions with depth at different wall installation stages are shown in Figure 2.10.

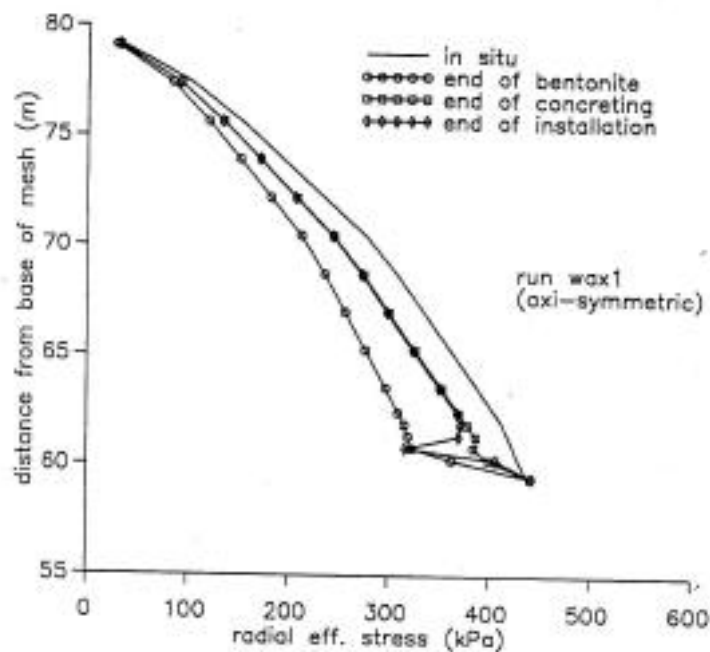


Figure 2.10. Change in the horizontal effective stress profile in the vicinity of the wall at different stages of wall installation for axi-symmetric conditions (Pantelidou, 1994).

Stress reductions during the excavation of the hole, did not exhibit any abrupt reduction at the lower part of the pile. During the consequent concreting and hardening the stress increased but

remained smaller than the in-situ values. Pantelidou (1994) explained that due to arching (Terzaghi and Peck, 1967), most of the change in the stress is redistributed in the circumference of the pile hole so that a large part of the horizontal stress change during installation is taken by the out-of-plane stress at the periphery of the hole. The reduction in horizontal effective stress was generally similar to that calculated in the plane strain analysis, but the change in magnitude was much smaller and the change with distance from the trench is more dramatic. Figure 2.11 reproduces the horizontal effective stress distribution with depth at the end of wall installation, in plane strain and axi-symmetric conditions. Pantelidou (1994) found that in contrast with the plane strain analysis, the in-situ horizontal effective stress profile was re-established by 3 m from the trench in the axisymmetric case.

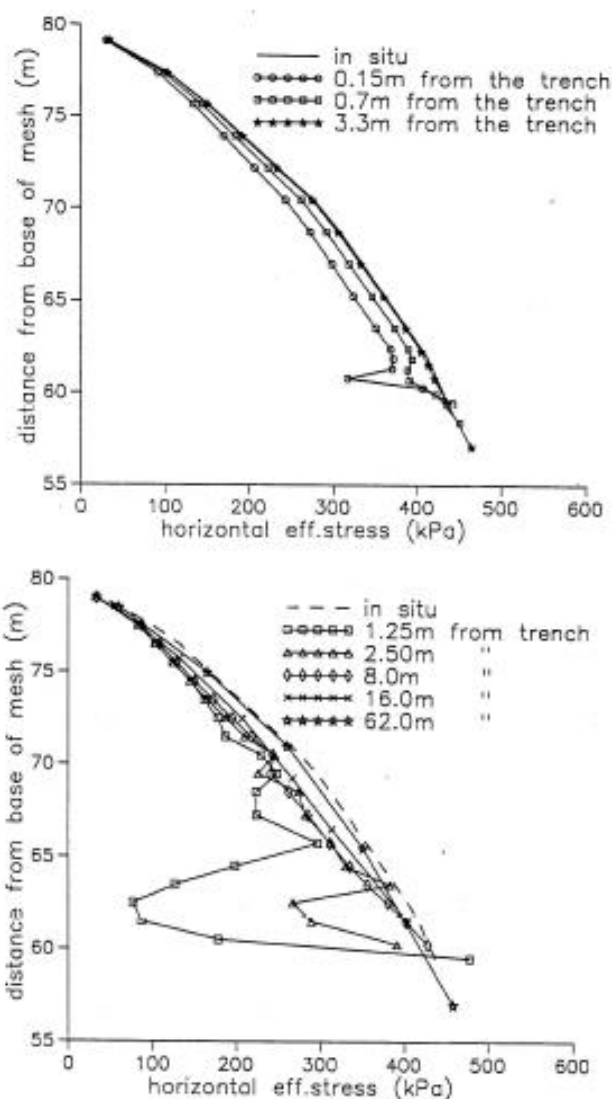


Figure 2.11. Change in the horizontal effective stress distribution with distance from the side of the excavation (a) for axi-symmetric conditions and (b) for plane strain conditions (Pantelidou, 1994).

vertical direction. It was assumed that the depth of the wall was significantly greater than the panel width. Any arching that may occur vertically between the soil strata was neglected. Finally, the wet concrete pressure was not implemented as it was assumed that the concrete pressure did not increase below a depth of 6-7 m, and was less than the bentonite pressure at the assumed depth of 15 m. Results of the analyses suggest that a K_0 of 1.5 could be reduced to K_0 of 1.1 for the purposes of a subsequent plane strain analysis. These values were determined for relatively short-term conditions after panel construction.

Ng *et al.* (1995) investigated the three-dimensional effects of diaphragm wall installation in stiff clay using two simple perpendicular plane sections. They explored the horizontal arching effects using a plane strain analysis with plane stress assumption (Figure 2.13). The average displacement from the first analysis was used as a boundary condition for the vertical section analysis, Figure 2.14.

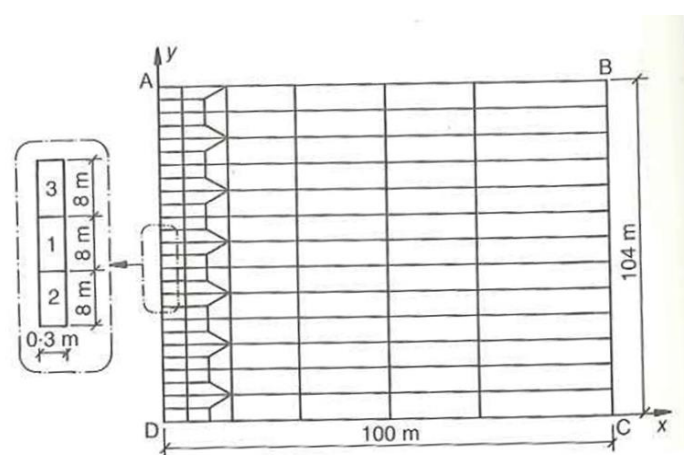


Figure 2.13. Finite element mesh for HPA (horizontal plan analysis); Ng *et al.* (1995).

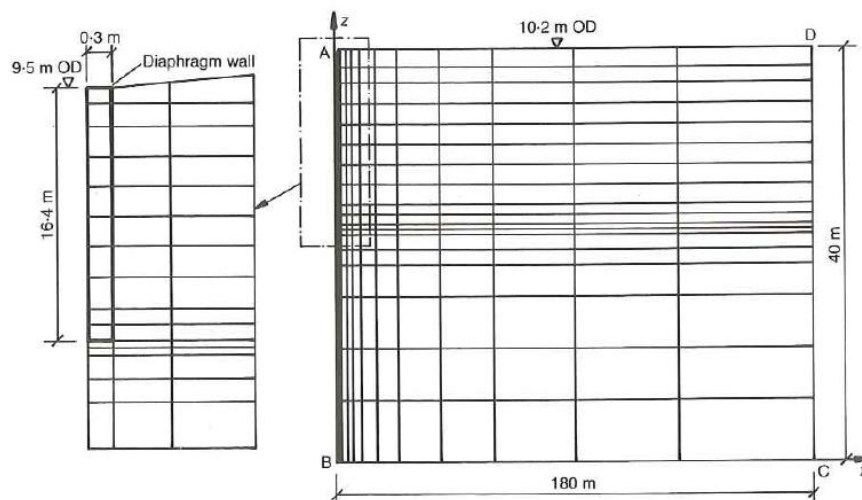


Figure 2.14. Finite element mesh for VSA (Vertical section analysis); Ng *et al.* (1995).

Ng *et al.* (1995) analyses were used to explain the complex stress transfer mechanism that results in large lateral stress reductions. However, their approximate analysis had some limitations. First, stresses cannot be redistributed simultaneously in both vertical and horizontal directions. Second, the deformation profile down the depth of the panel could not be computed because a wall displacement shape with depth was assumed during the vertical section analysis with the plane strain assumption.

The construction sequence of a typical diaphragm wall panel in stiff clay was simulated fully by Ng and Yan (1998) using a three-dimensional finite difference program. A typical diaphragm wall panel, 8 m long, 0.6 m wide, and 15 m deep, constructed in Gault Clay at Lion Yard Cambridge was adopted for the numerical simulation. The Finite-Difference mesh used is shown in Figure 2.15.

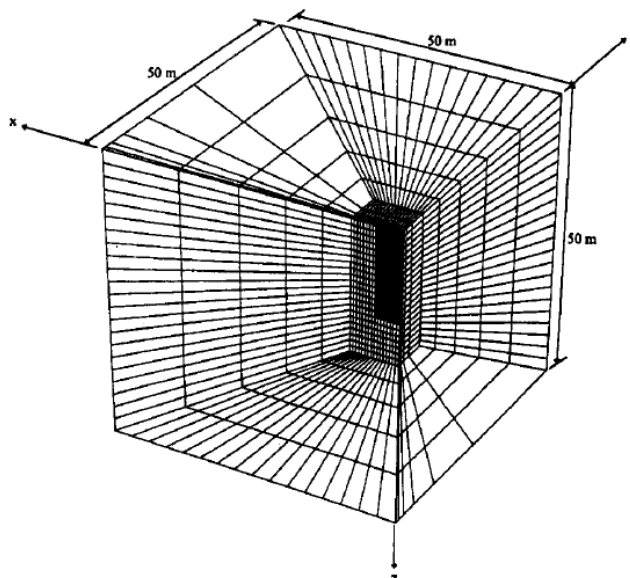


Figure 2.15. Finite-Difference Mesh used by Ng and Yan (1998).

Ng and Yan (1998) found significant stress reductions at the centre and above the toe of the panel caused by the installation process, which was attributed to both downward load transfer and horizontal arching. These two mechanisms act simultaneously and result in only a gentle increase in horizontal stress below the toe. The horizontal stress distributions with depth behind the wall calculated by Ng and Yan (1998) are shown in Figure 2.16 and Figure 2.17.

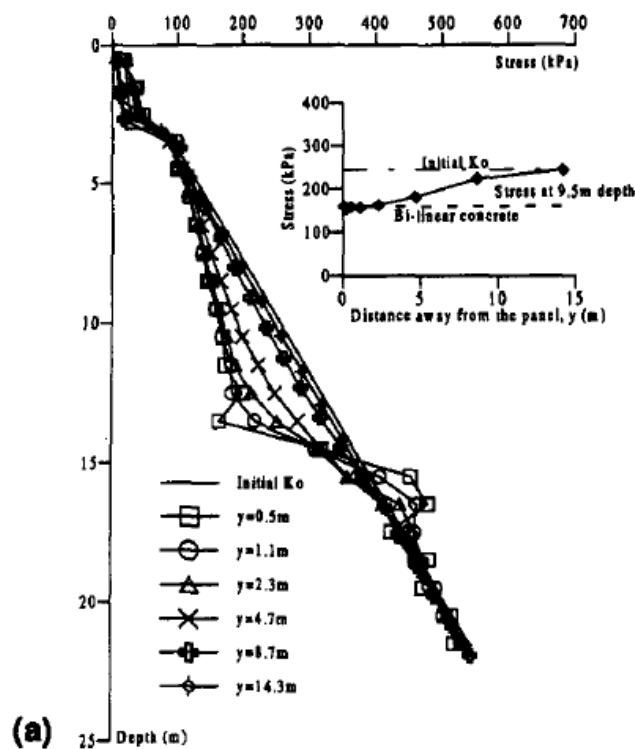


Figure 2.16. Total Horizontal Stresses arching on the central area behind of the panel, Ng and Yan (1998).

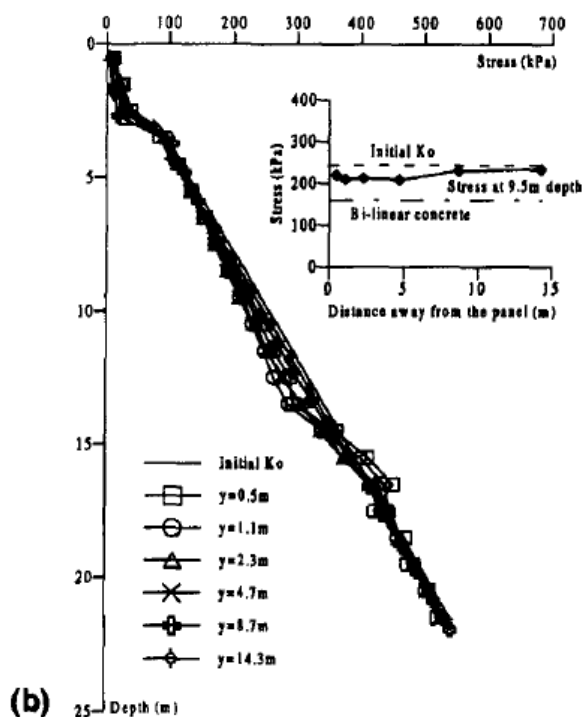


Figure 2.17. Total Horizontal Stresses arching on the corner behind of the panel, Ng and Yan (1998).

Ng and Yan (1998) compared the areas of stress reduction and the increases above and below the toe of the wall, Figure 2.16, respectively, and they deduced that about one-third of the stress reduction above the toe of the panel could be attributed to the downward load transfer mechanism, while the rest of the stress is redistributed laterally via the horizontal arching mechanism. Furthermore, it was observed that at the edge of the panel, the horizontal arching mechanism appeared to dominate, limiting substantial horizontal stress reductions and ground deformations (Figure 2.17). It was found that the zone of influence due to the diaphragm wall panel installation falls within a normal distance of approximately one panel depth, D , from the face of the panel, $D/3$ below from the toe and $L/3$ from the edge and along the length of the panel (L).

Ng and Yan (1998) also found that the horizontal ground deformation with depth behind the trench was largest at the centre of the panel during the bentonite stage, Figure 2.18. The deformation at the centre was about five times that at the edge. The distribution of horizontal deformations along the panel length was not uniform. However, Ng and Yan (1998) observed that the horizontal deformations were surprisingly uniform down the depth of the trench during

this phase of construction. Finally, they explained that the installation process of a diaphragm wall in stiff clays could result in a significant reduction in horizontal stresses above the toe and at the centre of the wall, with only small induced ground movements.

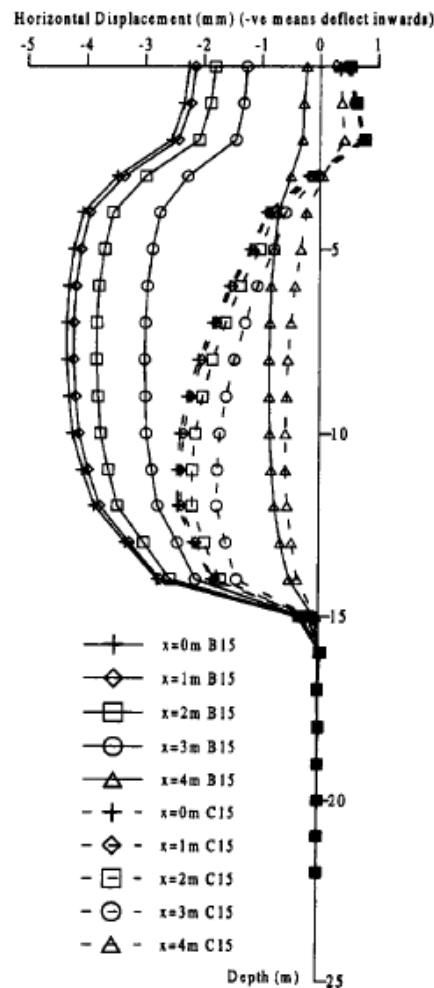


Figure 2.18. Horizontal displacement behind trench during construction of panel, Ng and Yan (1998).

Gourvenec and Powrie (1999) carried out a series of finite-element analyses to investigate the impact of three-dimensional effects in lateral stress during the sequential installation of a number of diaphragm wall panels. The finite- element mesh used is shown in Figure 2.19.

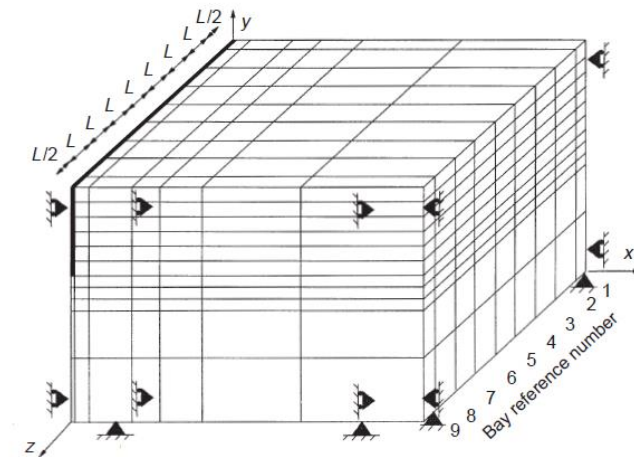


Figure 2.19. Three-dimensional finite-element mesh, Gourvenec and Powrie (1999).

They found that the magnitude and extent of lateral stress reduction in the vicinity of a diaphragm wall depended on the panel length, and were over predicted in the analysis assuming conditions of plane strain. They reported that as the panel length increased, the degree of reduction in the earth pressure coefficient during installation of the primary panel also increased, while the increase in earth pressure coefficient during installation of the subsequent panel was reduced.

Figure 2.20 shows the horizontal displacements calculated along the centre line of the central (primary) panel at the wall/soil interface after completion of the wall in each of the analyses carried out by Gourvenec and Powrie (1999). It is clear from Figure 2.20 that the maximum displacement increased with panel length, being greatest in the plane strain analysis.

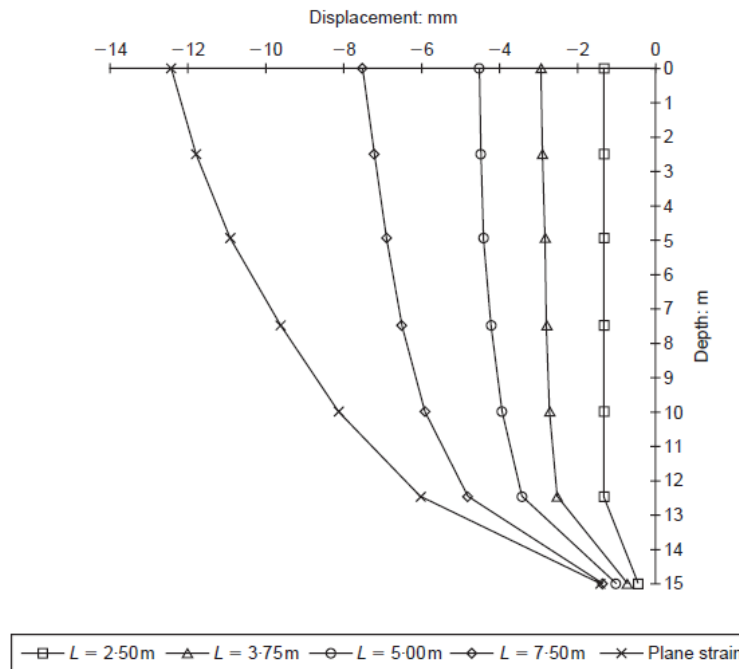


Figure 2.20. Horizontal displacements along the wall/soil interface at the centre of the primary panel: effect of panel length, Gourvenec and Powrie (1999).

Figure 2.21 shows the horizontal displacement at the crest of the primary panel (normalized with respect to the horizontal displacement at the crest calculated in the plane strain analysis) as a function of the panel depth : length ratio H/L . Gourvenec and Powrie (1999) found that as the panel length was increased (and H/L reduced), the crest displacements increased at a gradually accelerating rate until a depth : length ratio of 3 was reached. As H/L was reduced below 3, the displacements increased in proportion to the reduction in H/L . This suggests that in practice, panel aspect ratios H/L should be 3 or more to take full advantage of three-dimensional effects so as to minimize ground movements. This is slightly more onerous than, but of the same order as, the criterion of $H/L \geq 2$ suggested by Powrie & Kantartzi (1996) on the basis of soil settlements measured in centrifuge model tests.

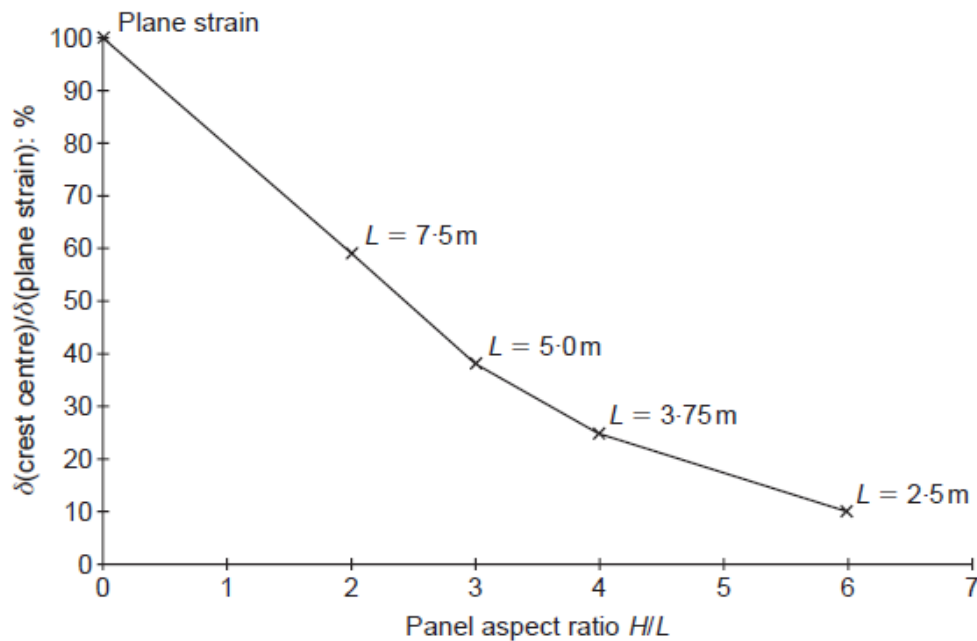


Figure 2.21. Horizontal crest displacements at the centre of the primary panel as a percentage of the plane strain crest displacement: comparison of different panel lengths, Gourvenec and Powrie (1999).

Powrie and Batten (2000) carried out a series of parametric finite-element analyses, assuming plane strain condition, using the program CRISP (Britto & Gunn, 1987). Prop loads and wall movements measured during the construction of the London Underground Jubilee Line Extension (JLE) station at Canada Water were compared with the results from their finite-element analyses. Powrie and Batten (2000) investigated the effects of wall installation at Canada Water with an axisymmetric finite-element analysis simulating the installation of a single pile. The earth pressure coefficients at the end of the axisymmetric analysis were specified as the pre-excavation values at the start of the plane strain analysis of the main excavation sequence. Although an axisymmetric analysis may underestimate the stress changes due to the installation of a complete wall, it has shown to give results closer to the actual stress changes measured in the field than those of a plane strain analysis, which tends to overestimate wall installation effects (Higgins *et al.*, 1989).

2.5. Long term monitoring

To investigate the long-term stress state of the soil around a retaining wall, studies have been undertaken on walls that have been in service for a number of years. Analysis of the long term behaviour of the Bell Common Tunnel (Symons and Tedd, 1989) showed insignificant changes in earth pressure behind the wall and small decreases in earth pressure in front of the wall in the four years after construction. Very small changes in pore water pressure were measured on both sides of the wall.

Symons & Carder (1990) describe data obtained at two retaining wall sites: a cantilever wall and a wall propped just below the carriageway, several years after construction was completed. Measurements of total pressure and pore water pressure were taken in order to determine whether equilibrium conditions had been reached. Measurements taken 150 m and 1.5 m from the cantilever wall showed that significant stress relief had occurred due to construction/installation. However, for the propped wall, measurements taken at 16 m and 1.5 m from the wall suggested that the total horizontal stress did not re-establishment.

Long-term field data are reported by Clark (2006) Richards et al. (2007). The long-term spade cell measurements were showing constant total horizontal stresses and pore water pressures over the years following construction of the cutting, and in a few cases overall reductions being recorded. They observed some seasonal and daily variations in the readings, occurring more in the shallower spade cells than the deeper ones, which were probably due to temperature.

2.5 Summary

This chapter has presented a review of the literature of the main research that has explored the problems associated with diaphragm wall and bored pile installation in overconsolidated deposits.

The mechanisms of load transfer and ground deformation during the construction of diaphragm wall have been investigated by many researches in the field (Farmer and Attewell, 1973; Lings *et al.*, 1991; Carder *et al.*, 1991; Ng and Yan, 1998). Similar results were found by all of them, in that all observed a marked reduction in total lateral stress at the soil/wall interface due to

diaphragm wall construction. However, the mechanisms of load transfer and ground deformation during the construction of bored pile wall has been investigated by relatively few researchers in the field (Bennett *et al.*, 1996; Symons *et al.*, 1992; Carswell *et al.*, 1993). They reported that in general, a large reduction in the lateral stress behind the wall occurred only at depth. The overall average decrease of the total lateral stress during bored pile installation was less than that during diaphragm wall construction.

Powrie *et al.* (1996) and Richards *et al.* (1998) investigated the effects of diaphragm wall installation using a centrifuge model. Analysis of ground movements of diaphragm wall installations were carried out in both studies. In their analysis, they found that ground movement depends on a number of factors, including the initial ground water level and the geometry (length/depth ratio) of the panel. Powrie *et al.* (1996) found that three-dimensional effects can reduce the displacement at the centre-line of a single panel by a factor of 3. Centrifuge model tests to investigate the effects of bored pile installation were not found in the literature.

Numerical modelling is quite economical compared to field monitoring and laboratory testing. Various researches have been carried out using finite element and finite difference analysis to investigate the effects of diaphragm wall installation.

2D finite element analyses were carried out by Gunn *et al.* (1993) to investigate the stress changes due to wall installation. They found lateral stress reductions due to wall installation. Pantelidou (1994) used 2D finite element analysis with an axi-symmetric condition to simulate the installation of a bored pile. She found stress reductions during the excavation of the hole without any abrupt reduction on the lower part of the pile. A similar analysis was carried out by Powrie and Batten (2000). They investigated the effects of wall installation at Canada Water with an axisymmetric finite-element analysis simulating the installation of a single pile.

De Moor *et al.* (1994) presented an analysis of a plan (horizontal) section through a series of wall panels using 2D finite elements. Their technical note describes a form of analysis that allows lateral total stress redistribution or arching around a single diaphragm wall panel excavation to be evaluated. A similar analysis was carried out by Ng *et al.* (1995) in which they used two simple perpendicular plane sections to investigate the three-dimensional effects of diaphragm wall installation. However, their approximate analysis had some limitations. For

example, the stresses could not be redistributed simultaneously in both vertical and horizontal directions.

The construction sequence of a typical diaphragm wall panel in stiff clay was fully simulated by Ng and Yan (1998) using a three-dimensional finite difference program. They attributed significant stress reduction at the centre and above the toe of the panel caused by the installation process to both downward load transfer and horizontal arching. These two mechanisms act simultaneously and result in only a gentle increase in horizontal stress below the toe. Moreover, it was observed that at the edge of the panel, the horizontal arching mechanism appears to dominate, which limits substantial horizontal stress reductions and ground deformations.

Finally, Gourvenec and Powrie (1999) carried out a series of 3D finite-difference analysis to investigate the impact of three-dimensional effects in lateral stress during the sequential installation of a number of diaphragm wall panels. They found that as the panel length increased, the degree of reduction in the earth pressure coefficient during installation of the primary panel also increased, while the increase in earth pressure coefficient during installation of the subsequent panel was reduced.

Ng and Yan (1998) and Gourvenec and Powrie (1999) only considered one sequence of panel installation. Thus further investigations are needed to investigate the effects of different sequences of panel installation on the stresses of the soil near the wall. Furthermore, in the literature there is a lack of understanding of the installation effects due to bored pile construction. Further investigations are therefore needed to investigate the stress changes and consequently ground movements due to bored pile wall installation in overconsolidated clay deposits. Thus, the main objective of this thesis is to gain some fundamental understanding of, and new insight into, the stress transfer mechanisms and ground deformations during bored pile wall installation. 3D finite-difference analyses were also carried out to investigate the effects of different sequences of panel installation in the stress of the soil near the wall.

CHAPTER 3

3D MODELLING OF BORED PILE WALL INSTALLATION EFFECTS

3.1 Introduction

This chapter describes the use of a three-dimensional model to analyse, interpret and explain the real data of ground stress changes during bored pile wall installation in an overconsolidated clay deposit in connection with the Channel Tunnel Rail Link (CTRL; now HS1) at Ashford. The limited space available in modern cities and the need to minimize damage to adjacent buildings during construction have led to the increased use of cast-in-situ concrete diaphragm and bored pile walls as permanent retaining structures. It is generally accepted that the process of installing such a wall may influence the stress state of the soil and hence the post construction displacements, wall bending moment and prop loads. Wall installation is a complicated, three-dimensional soil-structure interaction problem in which the induced ground

movements may be affected by a number of factors, and despite considerable recent research its effects are not yet fully understood.

The mechanisms of load transfer and ground deformation during the construction of diaphragm wall and bored piles have been investigated by many researchers in the field (Farmer *et al.*, 1973; Tedd *et al.*, 1984; Lings *et al.*, 1991; Carder *et al.*, 1991; Symons *et al.*, 1992; Carswell *et al.*, 1993 and Bennett *et al.*, 1996) and using a geotechnical centrifuge (Powrie *et al.*, 1996; Richards *et al.* 1998). An improved numerical method for investigation of the three-dimensional (3D) effects of diaphragm wall installation was developed using two simple perpendicular plane sections (Ng *et al.* 1995) to model stress transfer mechanisms and ground deformations. The construction sequence of a typical diaphragm wall panel in stiff clay was fully simulated by Ng and Yan (1998) using a three-dimensional finite difference program. The mechanical response of the ground during diaphragm wall construction was also investigated by Gourvenec and Powrie (1999) using a three-dimensional finite difference program.

Most of the publications analysed three dimensional effects during construction of a diaphragm wall panel; innovatively in this Chapter an investigation of the changes in total stress associated with the installation of 21 bored piles excavated in eleven different construction sequences is presented. The main aim of the analyses presented in this chapter is to show how numerical modelling can be used to explore and investigate the stress changes and consequent ground movements due to bored pile installation in an overconsolidated clay deposit.

3.2 Field Monitoring

The study of pile wall installation effects was carried out on a section of retaining wall forming a part of a propped cutting on the Channel Tunnel Rail Link (CTRL, now HS1) at Ashford, Kent. The main geological deposits at the site are from the Lower Cretaceous Hythe Beds, Atherfield Clay from the Lower Greensand, and Weald Clay from the Wealden formation. The top of the Weald Clay formation is approximately 15 m below the ground surface; it is generally a stiff to very stiff clay. The upper part of the deposit contains many silt laminations and occasional bands of siltstone 100-200 mm thick. The lower Atherfield Clay is a very stiff, brown clay, about 4.5 m thick, with a plasticity index of 20–30%. It is delineated by a distinctive band of light brown material, 400–500 mm thick, at the top. The upper Atherfield

Clay is very stiff to stiff, fissured, closely to extremely closely bedded, grey, sandy, and about 8 m thick with a plasticity index of approximately 50%. It contains zones with thin silt partings, which become more frequent towards the bottom of the layer (Richards *et al.*, 2006).

The Hythe Beds overlying the Atherfield Clay outcrop over much of the HS1 Ashford site and are approximately 1.5 m thick at the main instrumented section. They comprise a firm to stiff yellow/brown/light grey mottled sandy clay with alternating layers of Ragstone (a hard, sandy limestone) and Hassock (a grey to brownish grey, glauconitic, calcareous sand or soft sandstone), (Richards *et al.*, 2006).

The junction between the Hythe Beds and the Atherfield Clay is not distinct, with the base of the Hythe Beds being generally clayey sand and the top of the Atherfield Clay being sandy and glauconitic (Gallois, 1965; Skempton & Weeks, 1976). The Hythe Beds are overlain by about 2 m of made ground, which comprises firm mottled dark brown/grey organic sandy clay with rootlets, pottery tile and rotten wood fragments.

The moisture content is generally at or near the plastic limit (range between 20-30%, Richards *et al.*, 2006), and there is a clear change in plasticity within the upper Atherfield Clay. The bulk density of the Atherfield and Weald Clays was determined from undisturbed block samples taken during the main site investigation for the CTRL, and from samples taken from the excavation, as 21 kN/m³.

3.2.1 Instrumentations

The instrumentation consisted of 17 vibrating-wire spade cells with integral vibrating-wire piezometers to measure the total horizontal stresses and pore water pressure near the retaining wall, as indicated in Figure 3.1 and Figure 3.2.

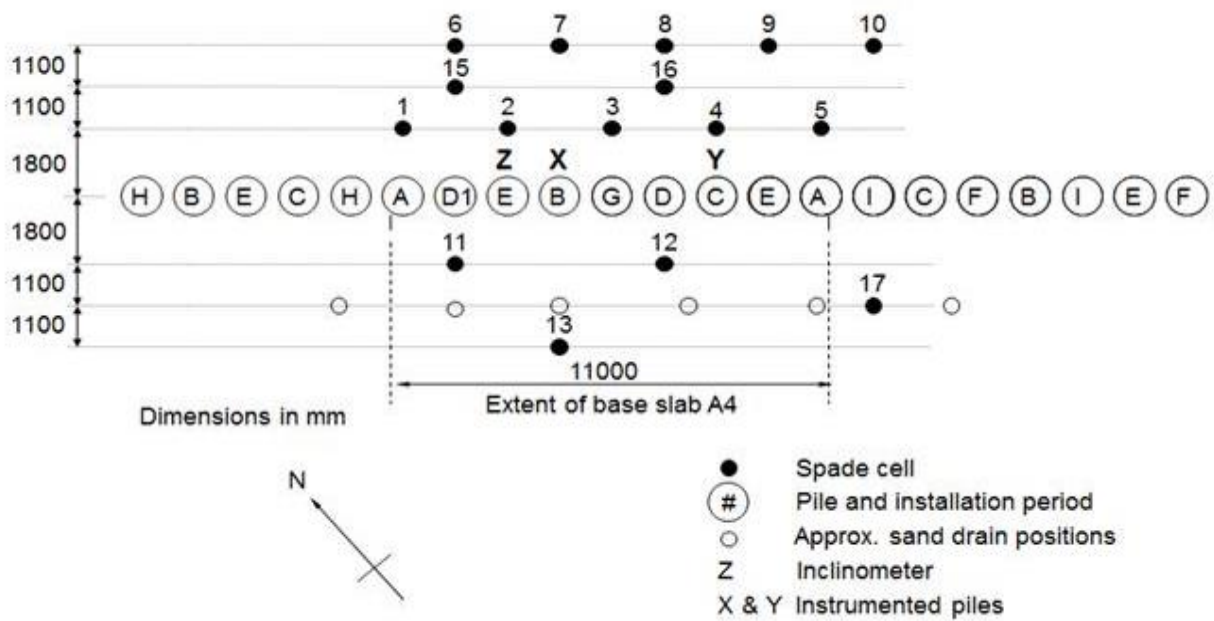


Figure 3.1. Plan of the north wall in the instrumented section showing locations of instrumented piles, spade cell, sand drains and sequence of pile installation.

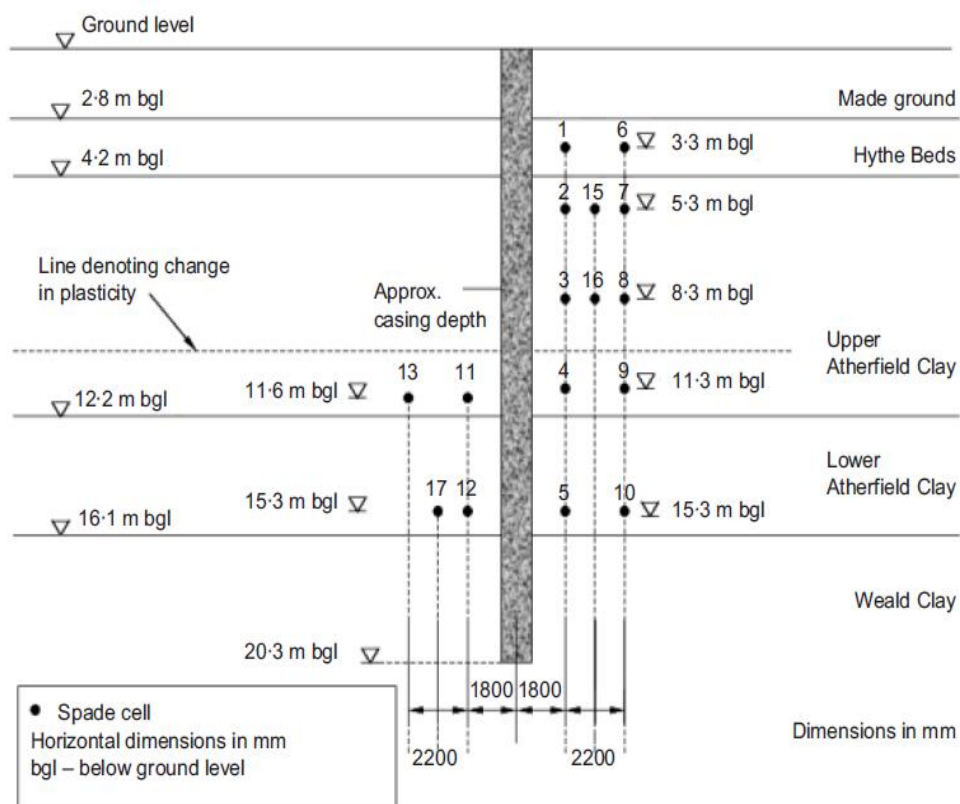


Figure 3.2. Spade cell locations (elevation).

Each spade cell was installed by drilling a vertical borehole to approximately 0.5 m above the final installation depth and then pushing the spade cell into the ground, taking great care to ensure that it was aligned to measure the horizontal stress perpendicular to the wall (Richards *et al.*, 2005).

Spade cells installed in stiff overconsolidated clays overestimate the magnitude of the in situ horizontal stress because of the complex local stress field created in the ground during installation (Tedd & Charles, 1981). Tedd & Charles (1983) compared readings from spade cells installed to measure vertical stress in stiff clay with the overburden acting on them calculated from the bulk density of the soil, and concluded that the amount by which a spade cell will over-read is dependent on the soil stiffness. Owing to the difficulties in determining the appropriate soil stiffness, a correlation between the spade cell over-read and the undrained shear strength (c_u) of the soil was proposed. This was considered reasonable as the undrained shear strength of a stiff clay is related to its stiffness, and it is a commonly determined soil parameter and therefore widely available. A simple empirical correction of $0.5c_u$ was suggested, although Tedd & Charles noted that where possible a direct site specific determination of the spade cell over-reading in stiff clay, for example by comparison with self-boring pressuremeter tests or calculation of overburden on a vertically aligned cell, is advisable. In this study, the raw spade cell data has been corrected for over-read due to installation effects by subtracting $0.35c_u$, as determined in a calibration exercise in the Atherfield Clay at the HS1 Ashford site (Richards *et al.*, 2006).

3.2.2 Wall installation sequence

The multi propped retaining wall at Ashford was made up of circular piles 20 m long and 1.05 m in diameter, with a centre spacing of 1.35 m. Installation commenced in November 1999 and finished in December 1999. In most cases, the upper part of the pile was excavated and a casing installed to approximately 8 m depth to support it over the first excavation. The remainder of the pile was excavated the next day, and bentonite support slurry introduced up to ground level. As a last step, the reinforcement cage was lowered into the hole and concrete was tremied in from the base to the top of the excavation as the bentonite was removed.

The pile installation sequence is summarized in Table 3.1. The instrumented zone modelled comprised 21 piles and was constructed in 10 different steps labelled A to I (Table 3.1). Pile installation time is identified by means of day numbers, with Day 1 being the date of excavation of the first pile which was 8 October 1999.

A different sequence of installation was used for one particular pile in period D1, with excavation and concreting being carried out within one afternoon, immediately after period D.

Installation period*	Boring started		Casing depth reached, casing inserted	Boring restarted		Pile completed, bentonite added	Concreting started	Concreting ended
	Day	Time	Time	Day	Time	Time	Time	Time
A	47	1510-1550	1540-1620	48	1155-1255	1235-1330	1420-1550	1453-1638
B	49	1440-1720	1600-1740	50	0805-0916	0845-1001	0916-1225	1002-1311
C	53	1459-1625	1520-1646	54	0800-0934	0835-1000	0955-1227	1032-1315
D	55	1518	1542	56	0910	1000	1109	1150
D1	56	1220	1255	56	1255	1350	1626	1724
E	57	1150-1435	1218-1500	60	0906-1310	0941-1335	1112-1540	1156-1627
F	64	1040-1108	1130-1200	67	0810-0842	0842-0905	0950-1114	1036-1201
G	67	1715	1746	68	0848	0908	1058	1145
H	69	1631-1659	1657-1721	70	0810-0841	0840-0905	0933-1040	1006-1117
I	71	1135-1203	1200-1225	74	1120-1148	1146-1210	1430-1605	1545-1705

* The lettering on the piles in Figure 3.1 indicates the sequence in which the piles were installed and is detailed in Table 3.1 (e.g. piles 'A' were both installed on day 47).

Table 3.1. Sequence of pile installation.

The sequence of pile installation did not follow a geometric pattern, other than to avoid excavating adjacent piles simultaneously. Figures 3.3, 3.4 and 3.5 (after Clark *et al.*, 2006) show the real data from the spade cell during the period of pile installation.

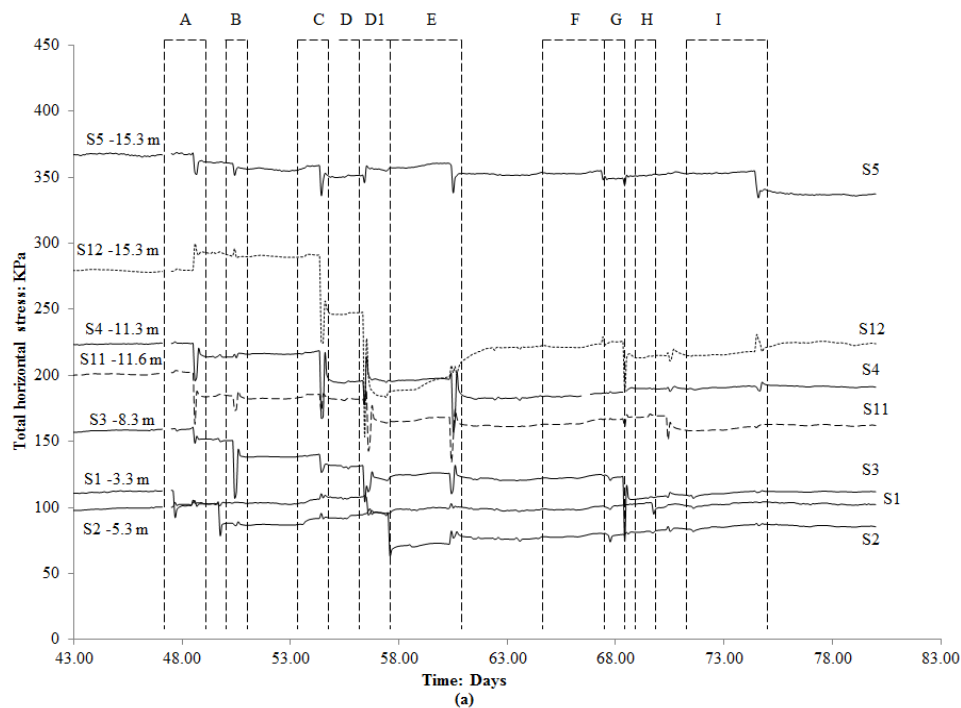


Figure 3.3. Total horizontal stress measurements during the period of wall installation (1.275 m from the wall); Clark *et al.* (2006).

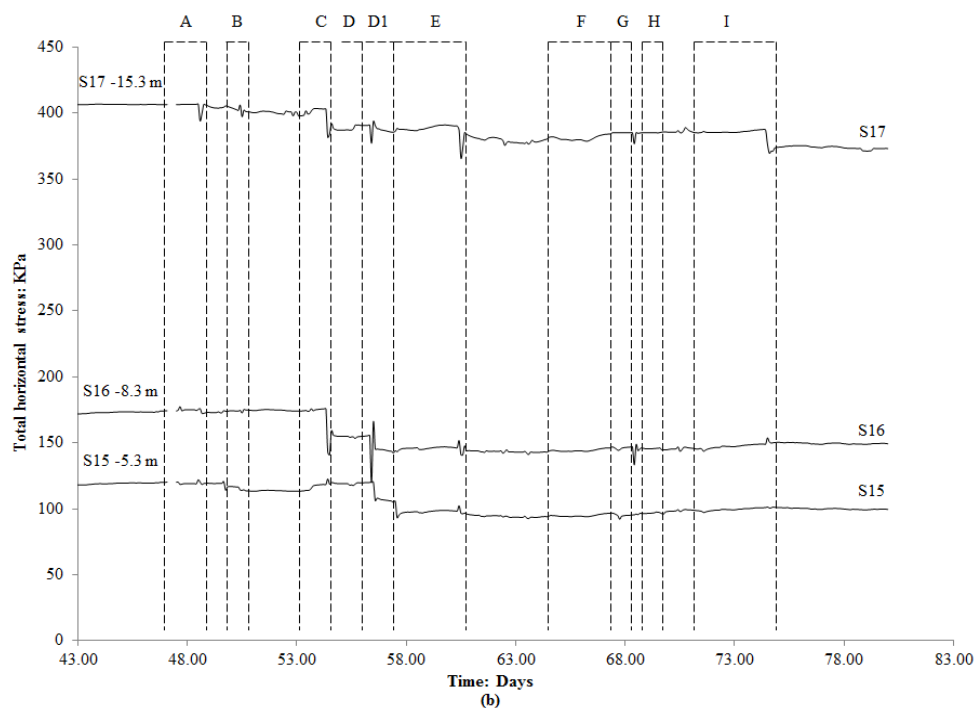


Figure 3.4. Total horizontal stress measurements during the period of wall installation (2.375 m from the wall); Clark *et al.* (2006).

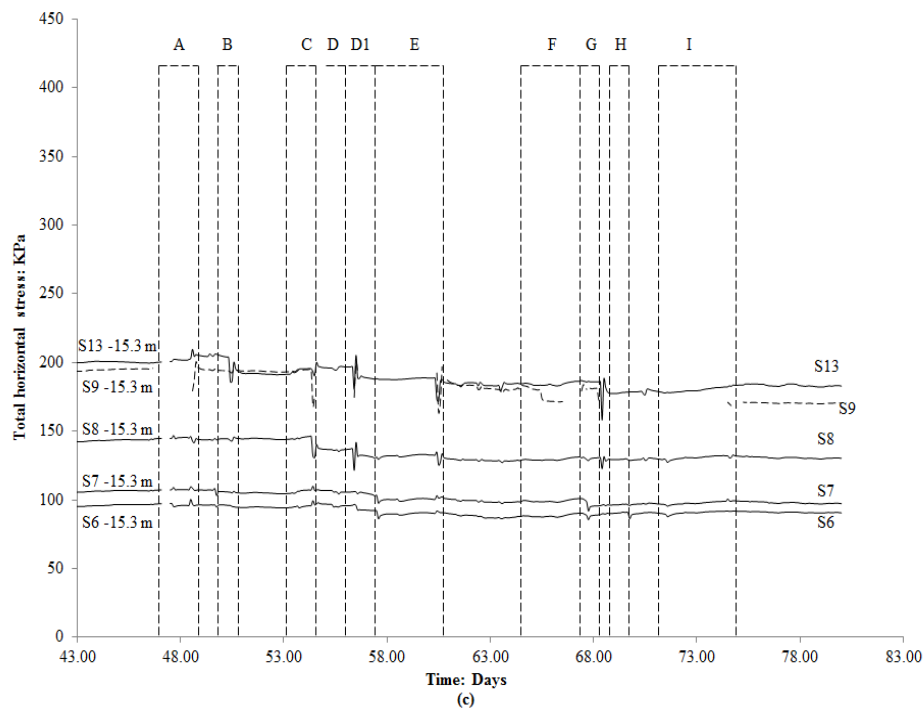


Figure 3.5. Total horizontal stress measurements during the period of wall installation (3.475 m from the wall); Clark *et al.* (2006).

3.3 Numerical Model

Installation of the bored pile wall was modelled using the three-dimensional explicit finite-difference program *FLAC^{3D}* 4.0 (Fast Lagrangian Analysis of Continua in 3 Dimension, Version 4.0, Manual 2009). The global model of propped embedded contiguous pile wall installation consisted of a rectangular parallelepiped 35 m high, 35 m deep and 35 m in length, Figure 3.6. Particular attention was paid to defining the finite element mesh. The density of the mesh was increased significantly around the wall and the pile excavation zones were modelled with 21 different semi cylindrical-shaped meshes (Figure 3.6).

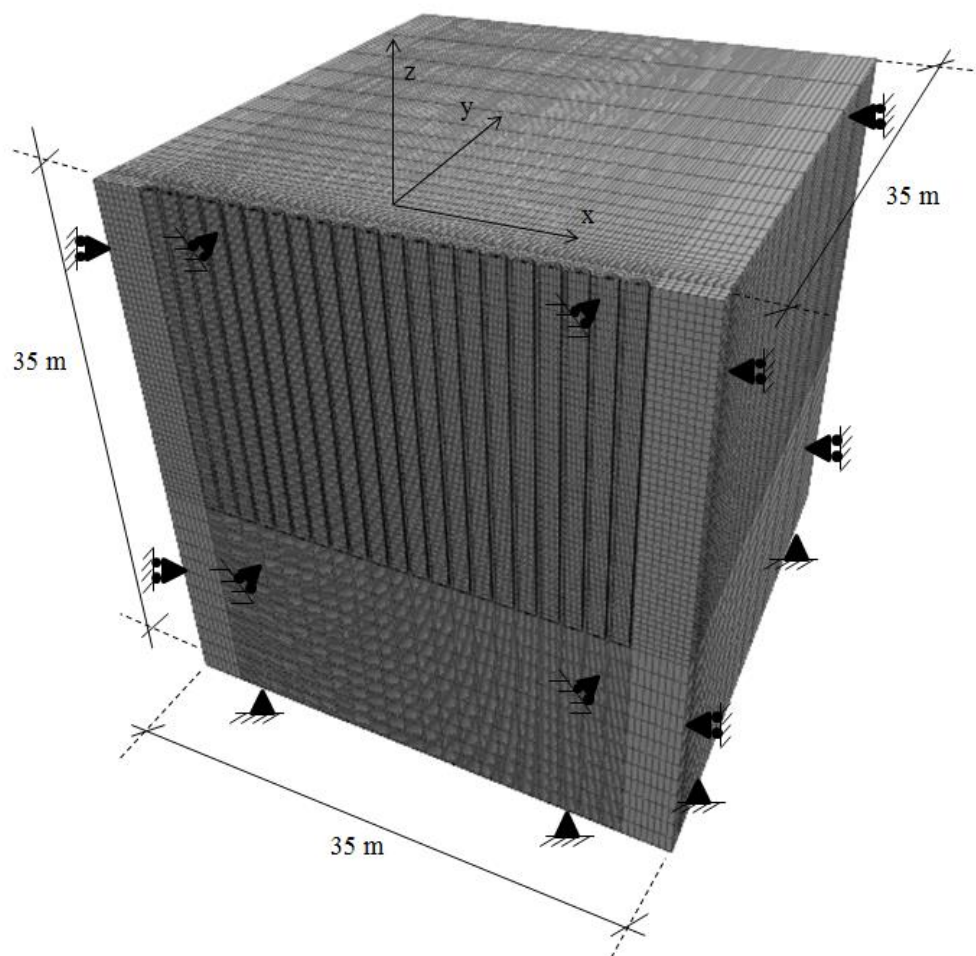


Figure 3.6. Geometry of $FLAC^{3D}$ model.

The soil was divided into more than 300,000 elements to give a high quality of computed output. All soils were modelled as simple linear elastic perfectly plastic isotropic materials with a Mohr-Coulomb yield surface. Because the 3D soil-structure interaction of bored pile installation is rather complex, it was decided to choose this relatively simple soil model for ease of computation and interpretation of the results. Notwithstanding, in Chapter 4 a non-linear stress-strain characteristic was implemented in the 3D finite-difference model, to investigate the possible benefit. The main model parameters that are summarized in Table 3.2 were reported by Loveridge (2001) who investigated the prop loads data from the Channel Tunnel Rail Link at Ashford tunnels.

Soil Type	Young's Modulus E_u [MPa]	ν_u	γ_d [kN/ m ³]	ϕ_u
Made Ground	20	0.487	17.56	0
Hythe Beds	18	0.487	15.00	0
Upper Atherfield Clay	36	0.487	15.80	0
Lower Atherfield Clay	36	0.487	17.20	0
Weald Clay	182	0.487	17.40	0

Table 3.2. Parameters used in the model.

Undrained conditions were chosen for the analysis, as reported by Clark *et al.* (2006). Undrained behaviour during diaphragm wall and bored pile installation process has been observed by many researchers in the field (Carder *et al.*, 1991; Carswell *et al.*, 1993; Bennett *et al.*, 1996; Clark, 2006). The undrained shear strength was characterized by the following equation, (Clark *et al.*, 2006):

$$c_u = 22 + 7z' \text{ kPa} \quad \text{Equation 3.1}$$

where z' is the depth below the ground surface. The in situ stress state initialized at the beginning of the analysis is reported in terms of the earth pressure coefficient $K_0 (= \sigma'_h / \sigma'_v) = 1$ (Richards *et al.*, 2006).

The mesh was 35 m deep and 35 m wide, Figure 3.6. Ng and Yan (1998), and Gourvenec and Powrie (1999) used an idealised geometry to investigate the diaphragm wall installation effects and modelled the soil as an elasto-plastic material that yields according to the Mohr-Coulomb failure criterion. In these analyses a geometry similar to that used by Ng and Yan (1998) and Gourvenec and Powrie (1999) was used.

One plane of symmetry, $y = 0$ m, was used in generating the finite different mesh. The vertical planes $x = 17.5$ m and $x = -17.5$ m were allowed to move freely in the y -direction and the z -direction but not in the x -direction. The vertical planes $y = 0$ m and $y = 35$ m were free to move in the x -direction and the z -direction but not in the y -direction. Finally, on the boundary horizontal plane, $z = -35$ m, all movements were restrained.

Figure 3.7 illustrates the sequence of bored wall installation modelled.

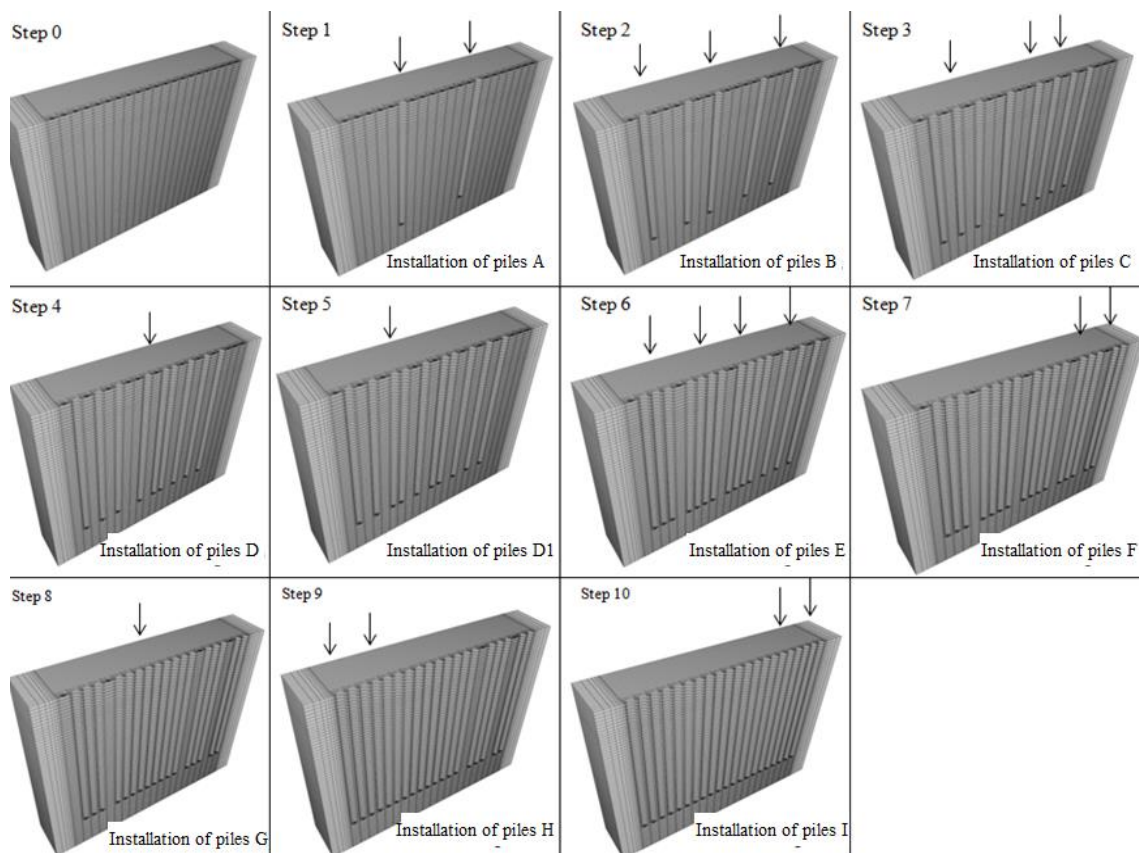


Figure 3.7. Pile installation sequence.

Wall construction started with the excavation of piles 'A' and finished with the excavation of piles 'I'. The modelling procedure for each pile is shown in Figure 3.8 and is summarized as follows:

1. Excavate the pile using the NULL command and apply normal hydrostatic bentonite pressure (i.e., the normal pressure is a function of the unit weight, 10.1 kN/m^3 , and the depth of the bentonite) on the excavated face using the APPLY NSTRESS command as shown in Fig.3.8. As reported previously, in most cases the uppermost 8 m of the pile

bore was excavated on one working day following which a casing was inserted to support the sides. The presence of the casing was modelled by fixing and applying null lateral pressure on the excavated face where the casing was lowered.

2. Cast the concrete pile by increasing the lateral pressure inside the excavated zone from the bottom using the empirical bilinear wet concrete pressure proposed by Ng (1992) and Lings *et al.* (1994), developed on the basis of a number of case histories in various sites and ground conditions. The bilinear envelope adopted for the analysis was as follows:

$$\sigma_h \text{ (kPa)} = \left\{ \begin{array}{l} 24z \rightarrow z' \leq 7.5m \\ 64 + 10.1z \rightarrow z' \leq 7.5m \end{array} \right\} \quad \text{Equation 3.2}$$

where z' = depth below the head of the pile. As reported by Ng and Yan (1998) this equation suggests that lateral pressure exerted by concrete placed under bentonite in a bored pile wall follows a bilinear pressure envelope, in which full fluid concrete pressures apply above a critical depth (in this case, 7.5 m). Below this depth, pressures increase with depth following the slope of the hydrostatic bentonite line. This envelope might be viewed as approximating the effects of concrete set on lateral pressure during concreting.

3. Hardening of the concrete by placing elastic concrete elements in and simultaneously removing the applied bilinear concrete pressure from the pile bores.

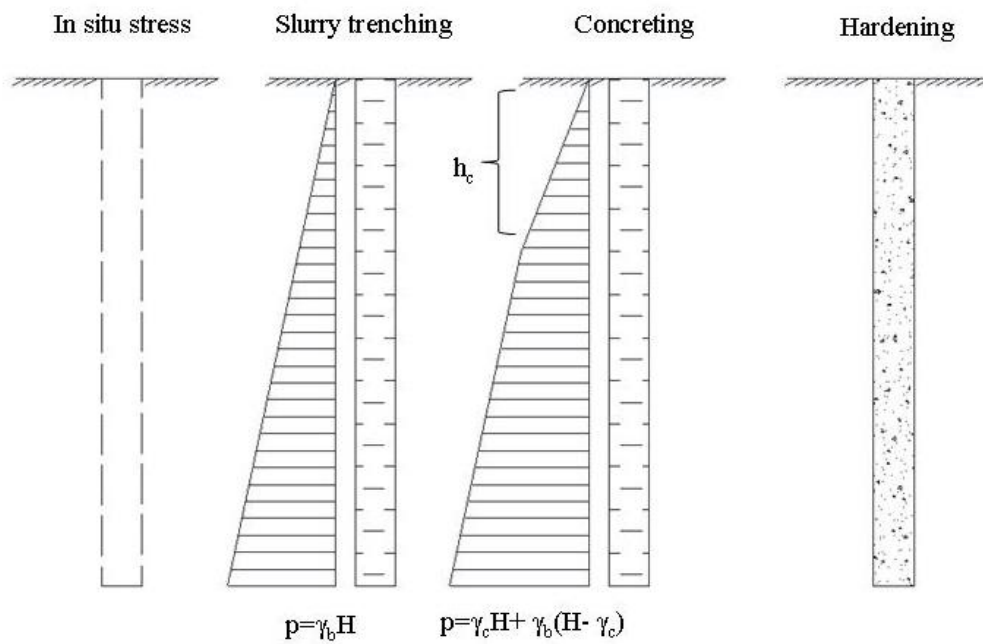


Figure 3.8. Sequence of construction stages. (a) In situ stress. (b) Slurry trenching. (c) Concreting. (d) Hardening of concrete.

Figure 3.9 shows the notation used in describing the 3D stress adopted in this paper. The total horizontal stresses (σ_{yy}) are redistributed via the horizontal shear stresses (τ_{xy}) and the vertical shear stresses (τ_{zy}).

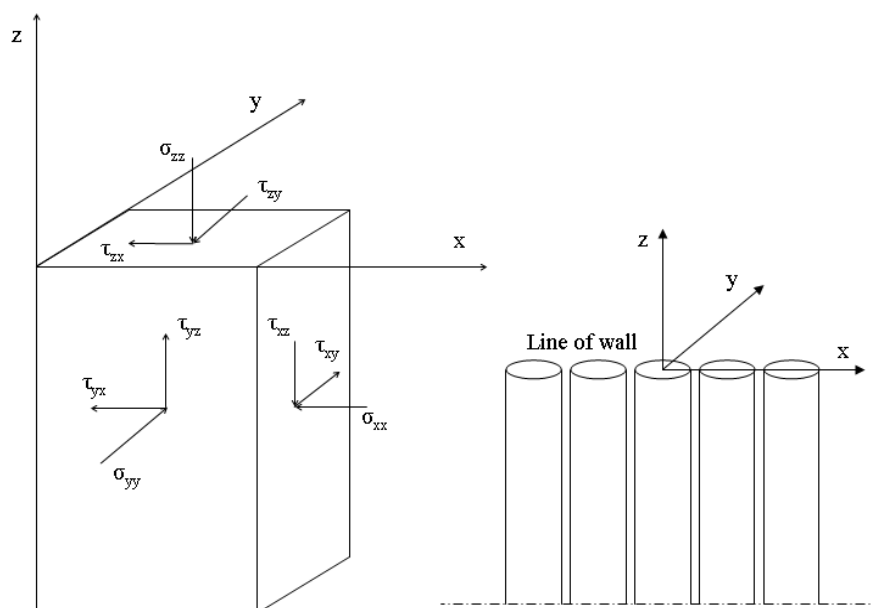


Figure 3.9. 3D Stress state.

3.4 Numerical Results

The computed horizontal stress (σ_{yy}) at a distance of 0.3 m behind the piles along the length of the wall after the hardening of concrete of piles 'A' is shown in Figures 3.10 and 3.11.

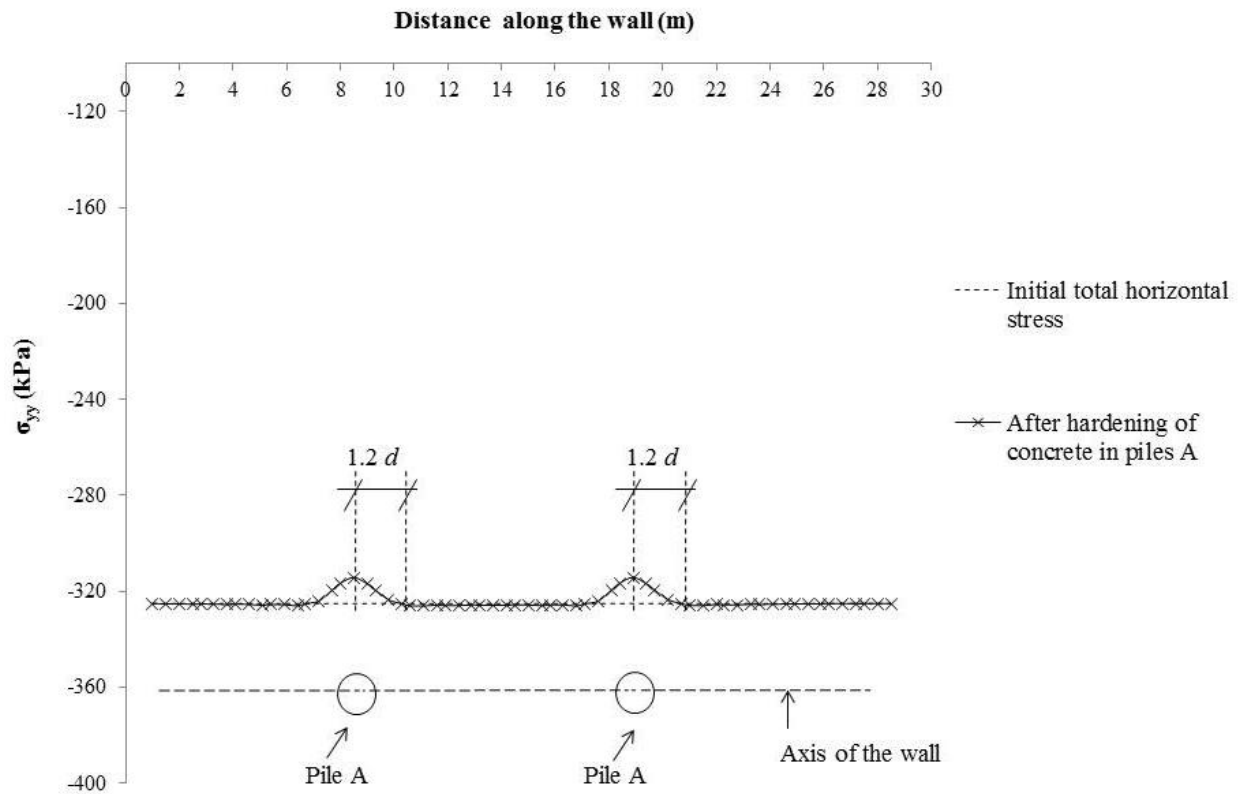


Figure 3.10. Calculated horizontal stress (σ_{yy}) 0.3 m behind the wall after hardening of pile 'A' at a depth of 15.3 m.

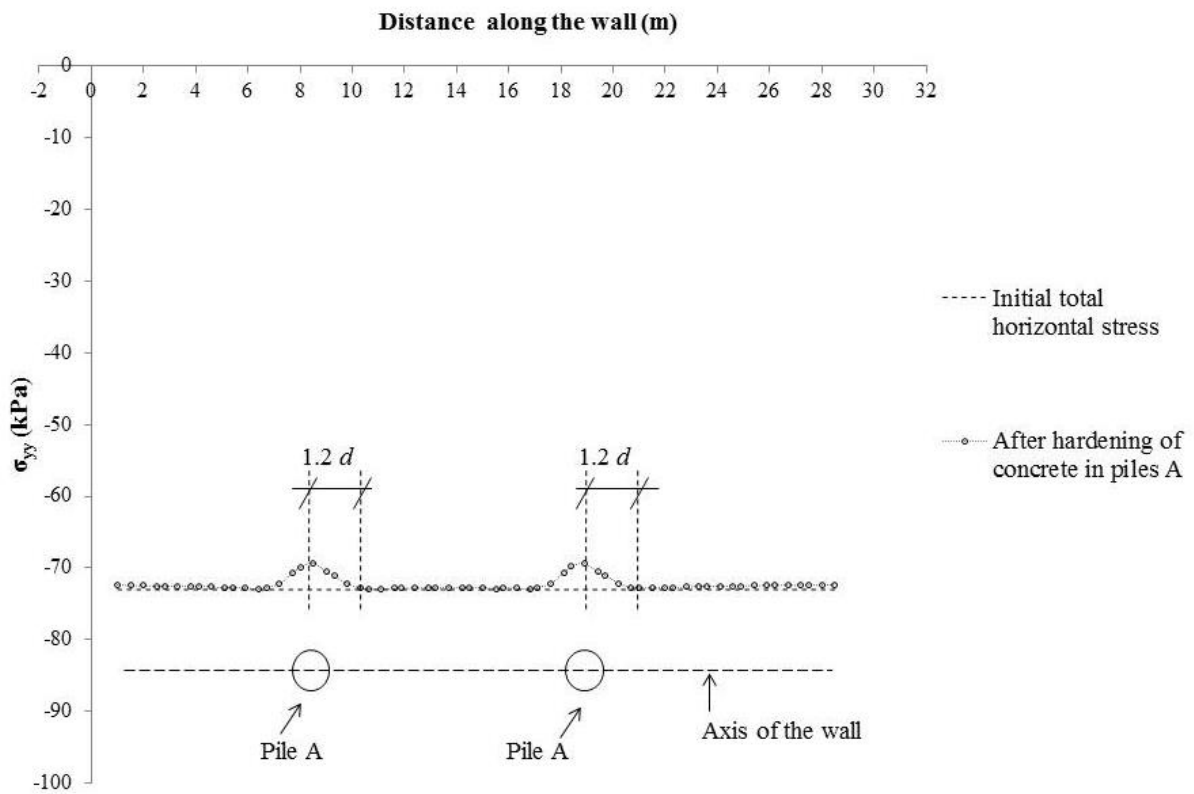


Figure 3.11. Calculated horizontal stress (σ_{yy}) 0.3 m behind the wall after hardening of pile 'A' at a depth of 3.3 m.

It can be seen that the horizontal stresses are reduced from the initial values. The maximum distance affecting the installation of one pile is approximately 1.2 m from the centre of the pile. Then the influence of the pile installation became insignificant beyond a distance of $1.2d$ (where d is the diameter of the pile, $d = 1\text{m}$) from the centre of the pile installed.

Therefore, considering the section B-B, Figure 3.12, the stress variations in that area are result only from the installation of the piles 'A', 'E' and 'I'.

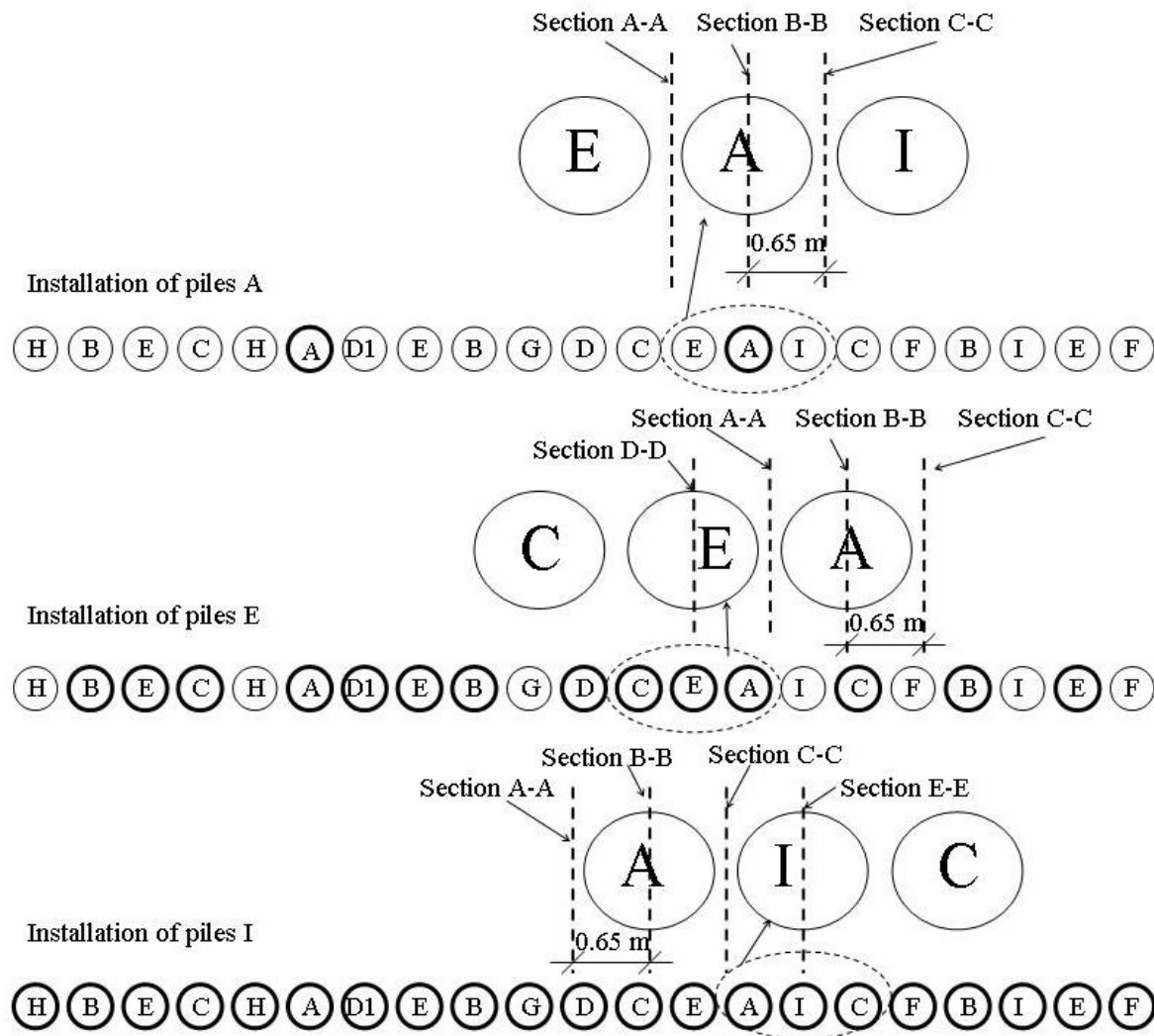


Figure 3.12. Plan view of sections A-A, B-B, C-C, D-D and E-E 0.3 m behind the wall.

Furthermore, the horizontal stresses in the region of the sections A-A and C-C at the edges of the pile 'A' did not change after the excavation of pile 'A'. These results are quite different from those found by Gourvenec and Powrie (1999) and Ng and Yan (1998), who for a diaphragm wall panel both reported an increase in the total horizontal stress at the edges of a single panel after the installation stage.

Ng and Yan (1998) explained the increase in the horizontal stresses near the edges of the panel as being the result of the redistribution of the horizontal stress from the centre of the panel to

the edge via the shear stress component (τ_{xy}). Gourvenec and Powrie (1999) explained the increase in total horizontal stress at the edges of a single panel installed by arguing that the horizontal displacement along both the vertical and the horizontal edges of the trench are restricted by end effects, and this kinematic restraint results in an increase in lateral stresses on either side and below the trench to above their *in situ* values. Moreover, Ng and Yan (1998) suggest that an increase in lateral stress of the order of 20% of the *in situ* value would be expected within 0.1 L of the edge of the panel, with a return to the *in situ* value within 0.15 L (where L is the length of the panel).

The results calculated after a single pile installation would be expected to be different from those found for a diaphragm wall because the geometry is different. Lower values of the shear stress (τ_{xy}) that do not redistribute the total horizontal stress from the centre of the pile to the edges could be the main reason for this. In fact, the total horizontal stress in the region of the sections A-A and C-C, and the edges of the pile 'A', after the excavation of pile 'A', did not change at depths of 3.3 m and 15.3 m respectively. This is also consistent with the values of the shear stress (τ_{xy}) shown later. In fact, low values of the shear stress (τ_{xy}) were calculated at the edges of the piles A installed.

Figure 3.13 shows the calculated total horizontal stresses at two different locations 0.3 m behind the wall, section A-A and section B-B in Figure 3.13, after the installation of piles 'A'.

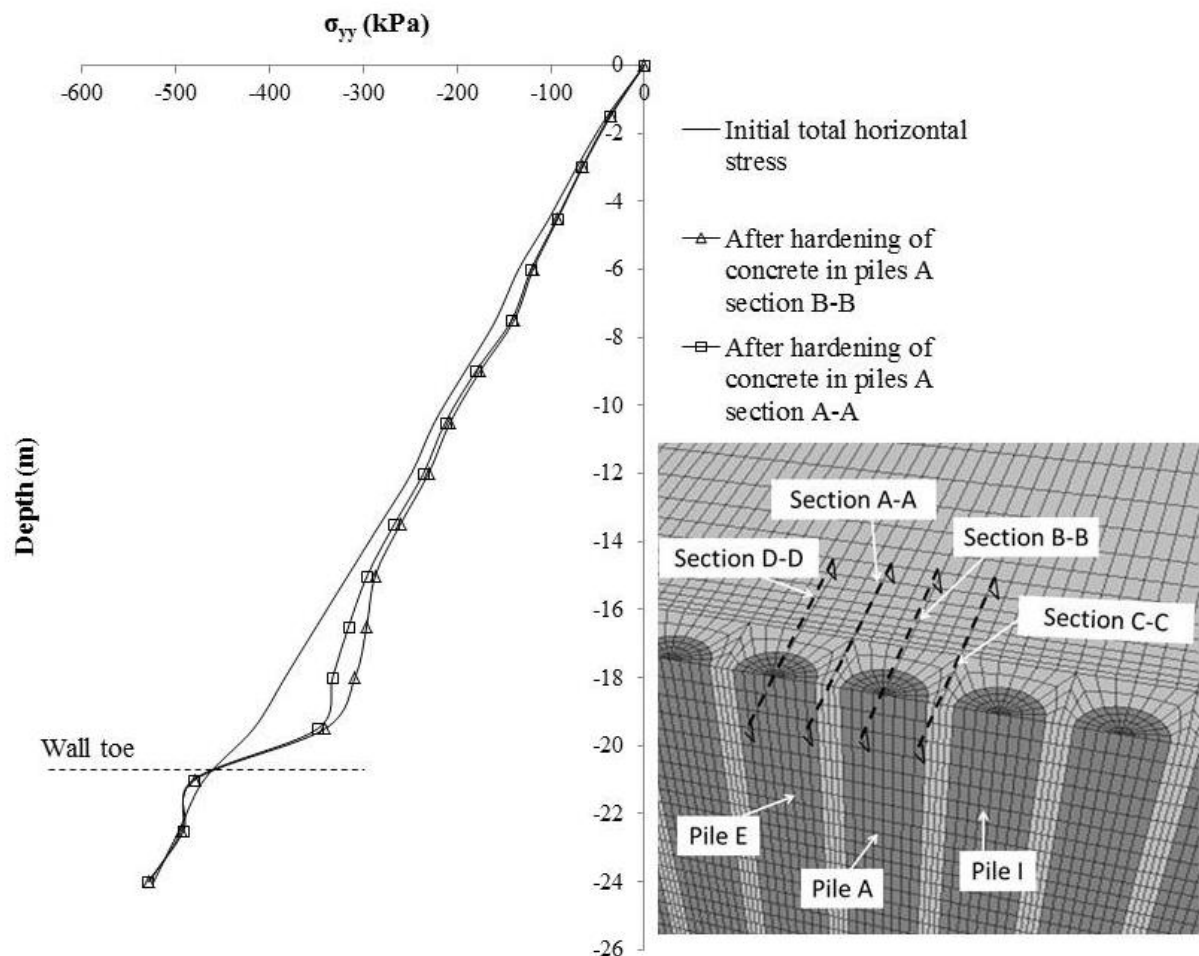


Figure 3.13. Variation of the calculated total horizontal stress (σ_{yy}) acting on section A-A and B-B, with depth down the wall at the end of construction of piles 'A'. At a normal distance from the wall of 0.3 m.

From the head of the pile down to 15 m depth, at a distance of 0.3 m behind the pile, only a minimal decrease of the total horizontal stresses was calculated. These results are different from those found by Gourvenec and Powrie (1999) and Ng and Yan (1998) both of whom calculated a significant reduction in the initial horizontal stress after a single panel installation.

Geometric effects could be the main reason for the differences between the stress changes calculated after a single pile excavation in the current analysis and those found by both Ng and Yan (1998) and Gourvenec and Powrie (1999). The pile geometry is very different from the geometry of a single panel. A pile can be seen as a panel where the aspect ratio H/L is maximum (considering the diameter of the pile equivalent to the panel length). Gourvenec and Powrie (1999) carried out three dimensional analyses to investigate the influence of panel

length on three-dimensional effects. They found that the degree of lateral stress reduction behind the wall, represented by the decrease in earth pressure coefficient, increased with the panel length, with the plane strain condition giving the largest reduction in lateral stress. Then, the decrease of stress reduction will be minimal after a single pile installation compared with the stress decrease after a single panel installation. This is consistent with the results found in this chapter. Furthermore, they found that the extent of the lateral stress reduction, indicated by earth pressure coefficient profiles, calculated following completion of each wall panel at various distances from the wall, reduced as panel length reduced.

Richards *et al.* (2006) compared the changes in stress measured due to the installation of a single pile with the values calculated using an elastic analysis. In their simplified elastic analysis, they assumed as an upper limit that the change in stress at the pile bore is from the in situ stress to zero. They considered that the installation of any piles affects the stress state of the ground at the positions where further piles are to be installed. They reported that at the centres of the piles yet to be installed, the stress in the direction perpendicular to the wall increases. However, from Figure 3.10 and 3.11 it can be seen that the stress in the area close to the pile in the direction to the wall do not increase.

Richards *et al.* (2006) found that the measured reduction in stress due to pile installation was generally larger than that calculated using the simple elastic analysis. Similar results were also found from the analyses presented in this chapter. Richards *et al.* (2006) stated that this could be a result of shrinkage of the concrete (possibly due to thermal effects) as it sets, and/or vertical arching and stress transfer below the bottom of the bore, which is not taken into account in the simple analysis. In this analysis it was found that the stress reduction behind the wall is concentrated especially in the area above the toe of the wall, Figure 3.13.

Figure 3.13 shows that the stress changes in the area near the toe of a single pile are quite different from those calculated after a panel installation by Gourvenec and Powrie (1999) and Ng and Yan (1998). It can be noted that only a minimal stress increase occurs under the toe of the wall. Gourvenec and Powrie (1999) and Ng and Yan (1998) calculated a more significant increase in the total horizontal stresses below the toe of the wall after the excavation of a single panel. This means that the horizontal stresses above the toe of the pile are only minimally redistributed via the vertical shear stress (τ_{zy}) below the toe of the wall. In the case of a bored

pile, in fact, the area of stress reduction above the toe would be equal to the area of stress increase below the toe if the stress reduction were solely attributed to the downward load transfer mechanism via the vertical shear stress (τ_{zy}), as suggested by Ng and Yan (1998). By comparing the area of stress reduction above the toe of the pile with the area of the stress increase below the toe it can be deduced that only a minimal percentage of the horizontal stress reduction above the toe is due to horizontal stress redistribution via the vertical shear stress (τ_{zy}). The distribution of the shear stress is presented and discussed later.

Figure 3.14 shows the shear stress distribution (τ_{zy}) at two different locations, sections A-A and B-B, Figure 3.12, after the excavation of the piles 'A'. These stresses are concentrated near the toe of the pile, consistent with the results of Ng and Yan (1998). Ng and Yan (1998) calculated a maximum shear stress (τ_{zy}) of 100 kPa above the toe of the diaphragm wall installed and 40 kPa below the toe of the wall at the centre of the panel. These values are large compared with the values of the shear stress (τ_{zy}) shown in Figure 3.14. This means that only a minimal part of the horizontal stress (σ_{yy}) is redistributed progressively downward beneath the toe via the shear stress (τ_{zy}) after the installation of piles 'A'.

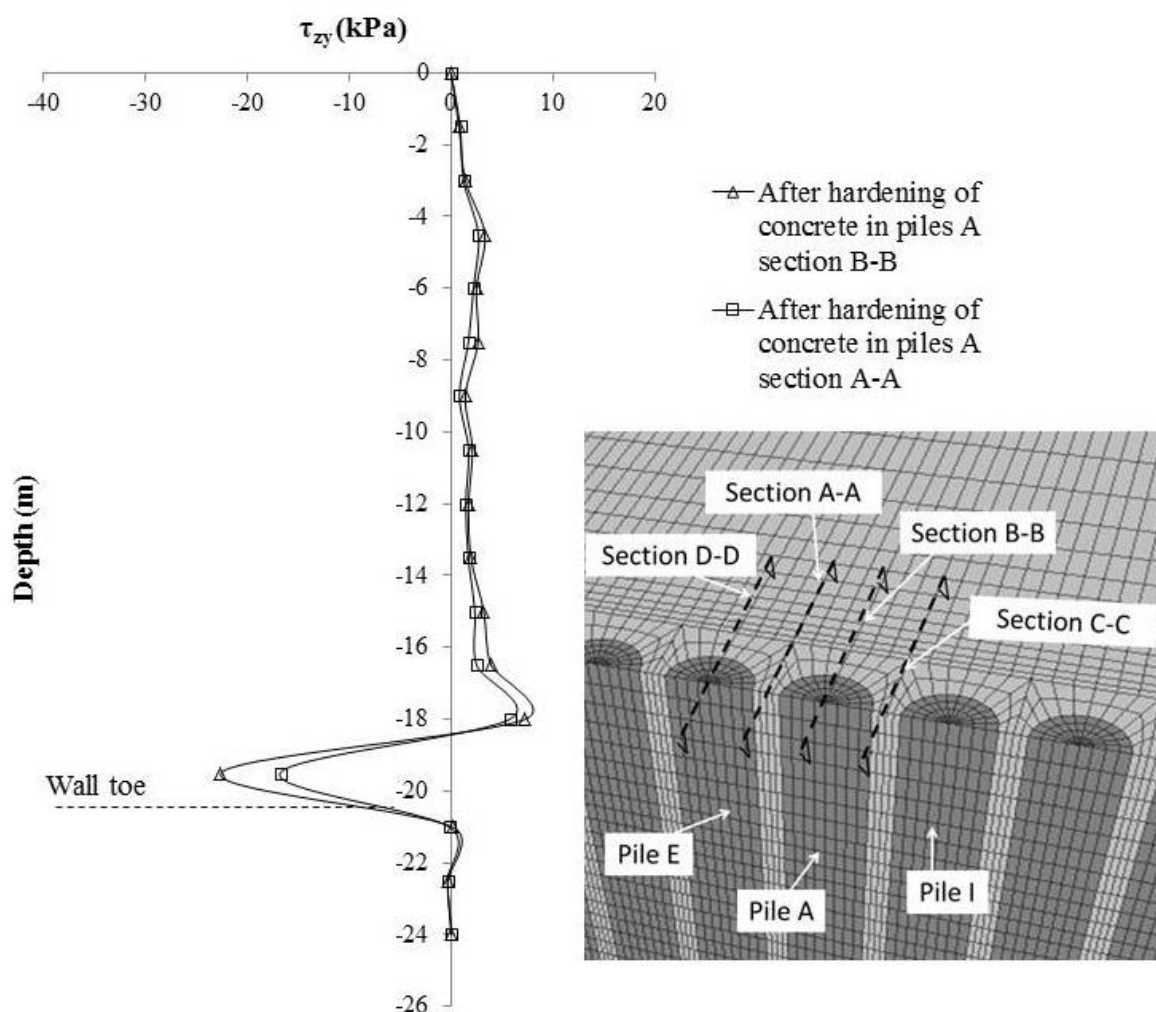


Figure 3.14. Variation of calculated shear stress (τ_{zy}) acting on section A-A and B-B, with depth down the wall at the end of construction of piles 'A'. At a normal distance from the wall of 0.3 m.

Figure 3.15 shows the variation of the shear stress (τ_{xy}) with the depth at two different locations, section A-A and section B-B in Figure 3.13, after the excavation of the piles 'A'.

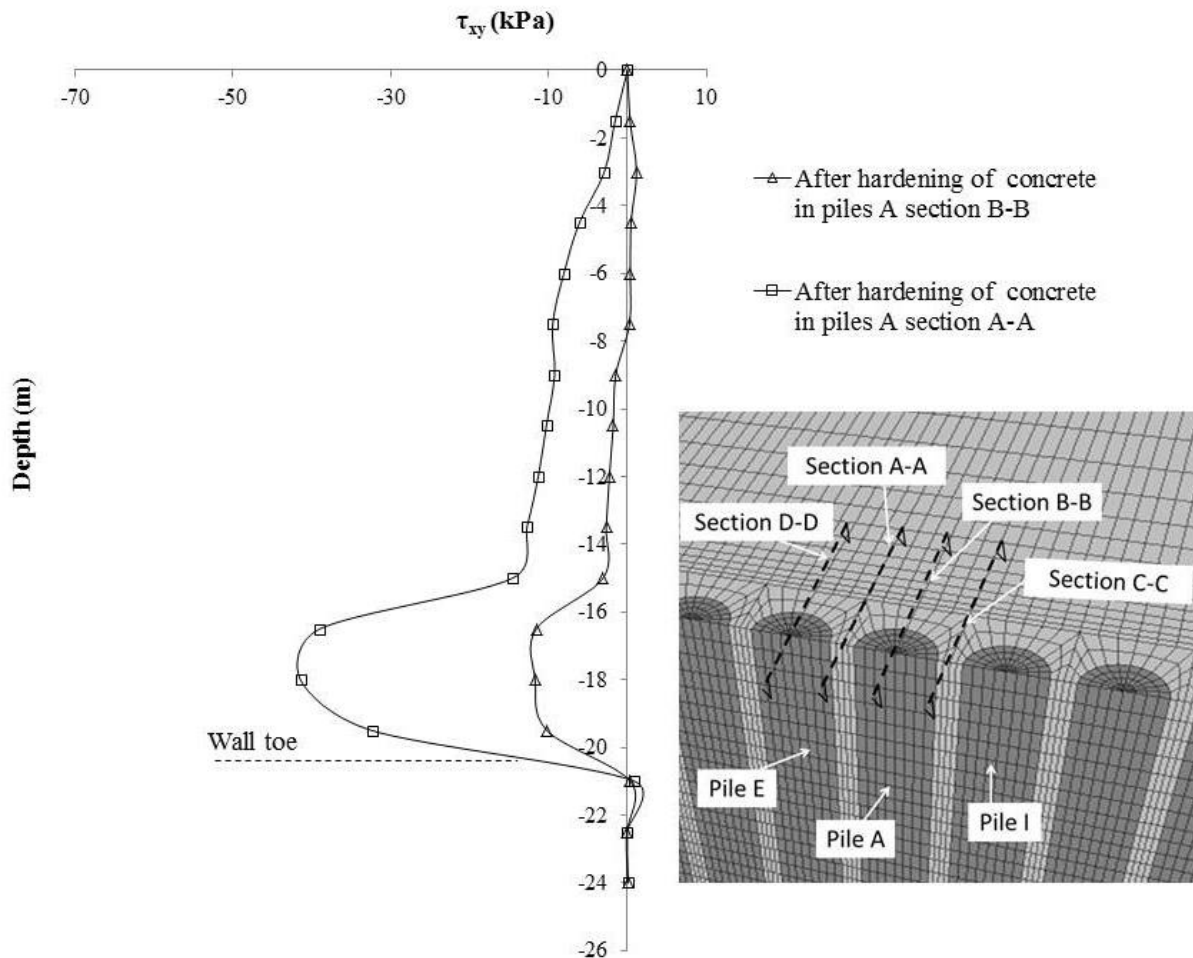


Figure 3.15. Variation of the calculated shear stress (τ_{xy}) acting on section A-A and B-B, with depth down the wall at the end of construction of piles 'A'. At a normal distance from the wall of 0.3 m.

The shear stress (τ_{xy}) increases linearly from the head of the pile to 15 m depth. Above the toe of the pile these values increase, especially at section B-B. The horizontal shear stresses (τ_{xy}) calculated by Ng and Yan (1998) after a single panel installation, were concentrated especially in the central area of the panel below the wall above the toe of the panel.

Furthermore from Figure 3.15 it can be noted that the shear stress (τ_{xy}) increases slightly on the edge of the pile, section A-A, and above the wall toe. The maximum value of the shear stress (τ_{xy}) found by Ng and Yan (1998) at the edge of the panel installed was approximately

100 kPa, which is large compared with the value found at the edge of a single pile. However the slight increase in the shear stress (τ_{xy}) in the area above the toe of the wall and at the edge of the pile, section A-A, led to a redistribution of the horizontal stress from the centre of the pile to the edge and limited the reduction of the horizontal stress on section A-A.

From Figure 3.15 it can be observed that the shear stress (τ_{xy}) changed markedly below 16 m depth. This could be mainly due to the presence of the Weald Clay. In fact, the elastic properties of this soil are substantially different from the other ground modelled in this analysis.

The horizontal stress distributions (σ_{yy}) with depth at section D-D, Figure 3.12, after the excavation of the pile 'E', are shown in Figure 3.16.

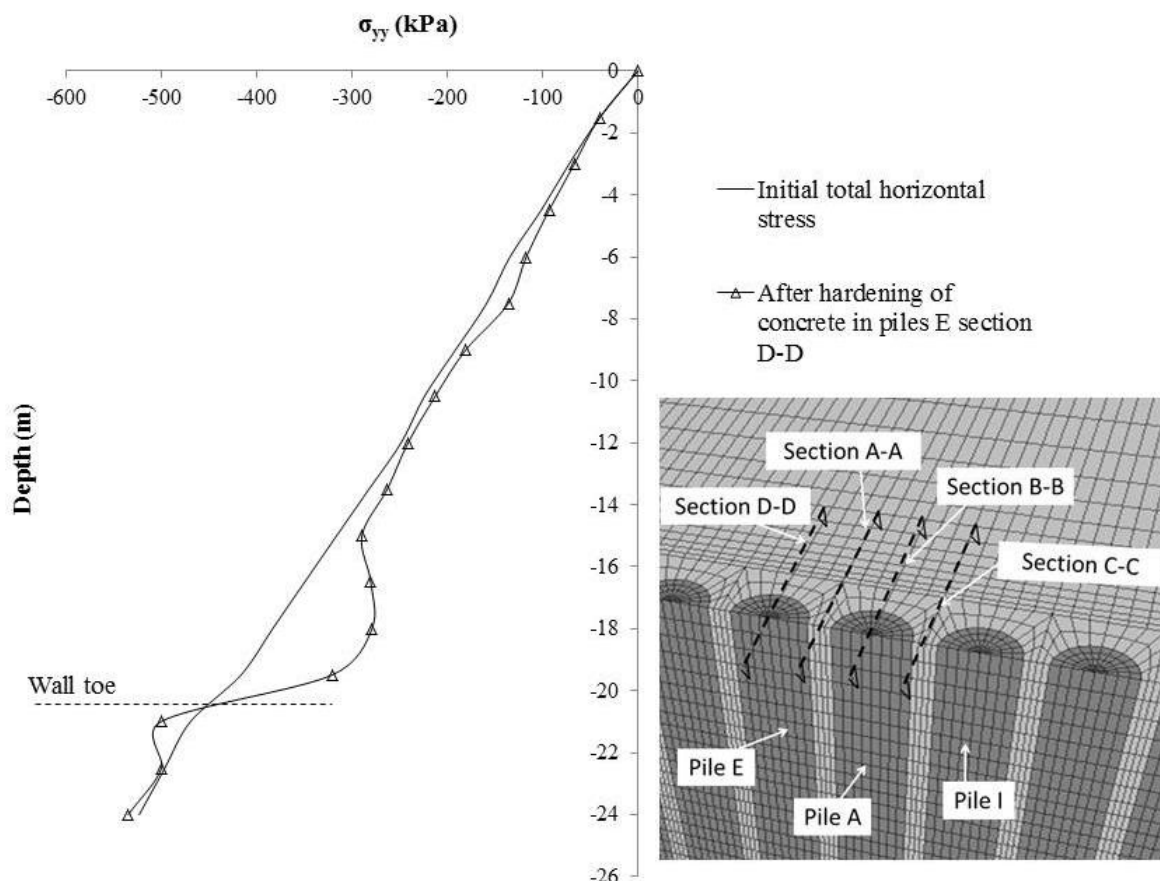


Figure 3.16. Variation of the calculated total horizontal stress (σ_{yy}) acting on section D-D, with depth down the wall at the end of construction of piles 'E'. At a normal distance from the wall of 0.3 m.

A small, approximately linear with depth decrease in the horizontal stress is apparent from the surface until a depth of 16.5 m is reached. The major horizontal stress decreases are concentrated above the toe of the pile. These results are quite different from those found by Pantelidou (1994). She used 2D finite element analysis to investigate the stress change and consequent movements in stiff clay due to diaphragm wall and bored pile installation. She found stress reductions during the excavation of the hole, without the abrupt reduction at the lower part of the pile.

Figure 3.17 shows the computed horizontal stress distribution with depth in section B-B after the installation of piles 'A', 'E' and 'I'.

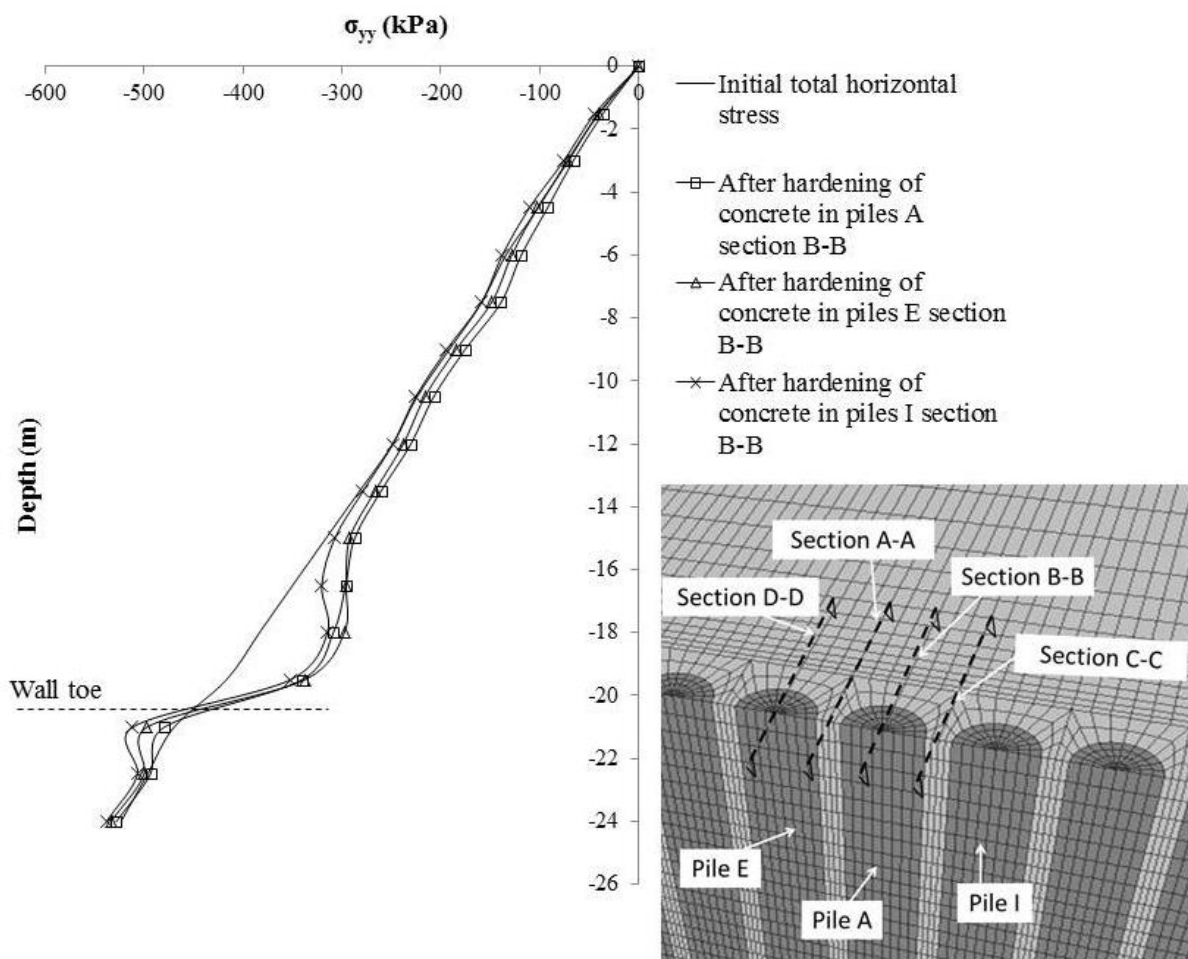


Figure 3.17. Variation of the calculated total horizontal stress (σ_{yy}) acting on section B-B, with depth down the wall at the end of construction of piles 'A', 'E' and 'I'. At a normal distance from the wall of 0.3 m.

The total horizontal stresses reduced after the excavation of the pile 'A'. During the subsequent installation of piles 'E' and 'I' the horizontal stresses increased slightly. Similar results were observed by Bennett *et al.* (1996). They had been monitoring the behaviour of a propped secant bored pile wall at Hackney using nine spade shaped pressure cells to monitor the total lateral stresses and pore water pressures in the ground. Interestingly, they found that the effect of pile installation was such that a small amount of overall stress relief was recorded on the deep spade cells, while stresses on the shallow spade cells generally returned to values similar to those measured before construction. These results are similar to those calculated in this chapter and also in Chapter 4.

The slight increase in total horizontal stress in the area from the surface down to 15 m depth, section B-B, could be due to horizontal stress redistribution via the horizontal shear stress (τ_{xy}) from the centre of the piles E and I to the section B-B. In fact, Figure 3.18 shows a variation of the shear stress (τ_{xy}) during the installation of the piles A, E and I, acting on the section B-B. Instead, the shear stress (τ_{yz}) remains constant and almost zero in the area from the surface down to 15 m depth on section B-B, after the installation of the piles A, E and I. Furthermore it was calculated that the shear stress (τ_{xy}), on section B-B, shown in Figure 3.15, in the area from the surface down to 14 m depth, remain almost minimal compare to the shear stress (τ_{xy}) found during the installation of Piles I, Figure 3.18.

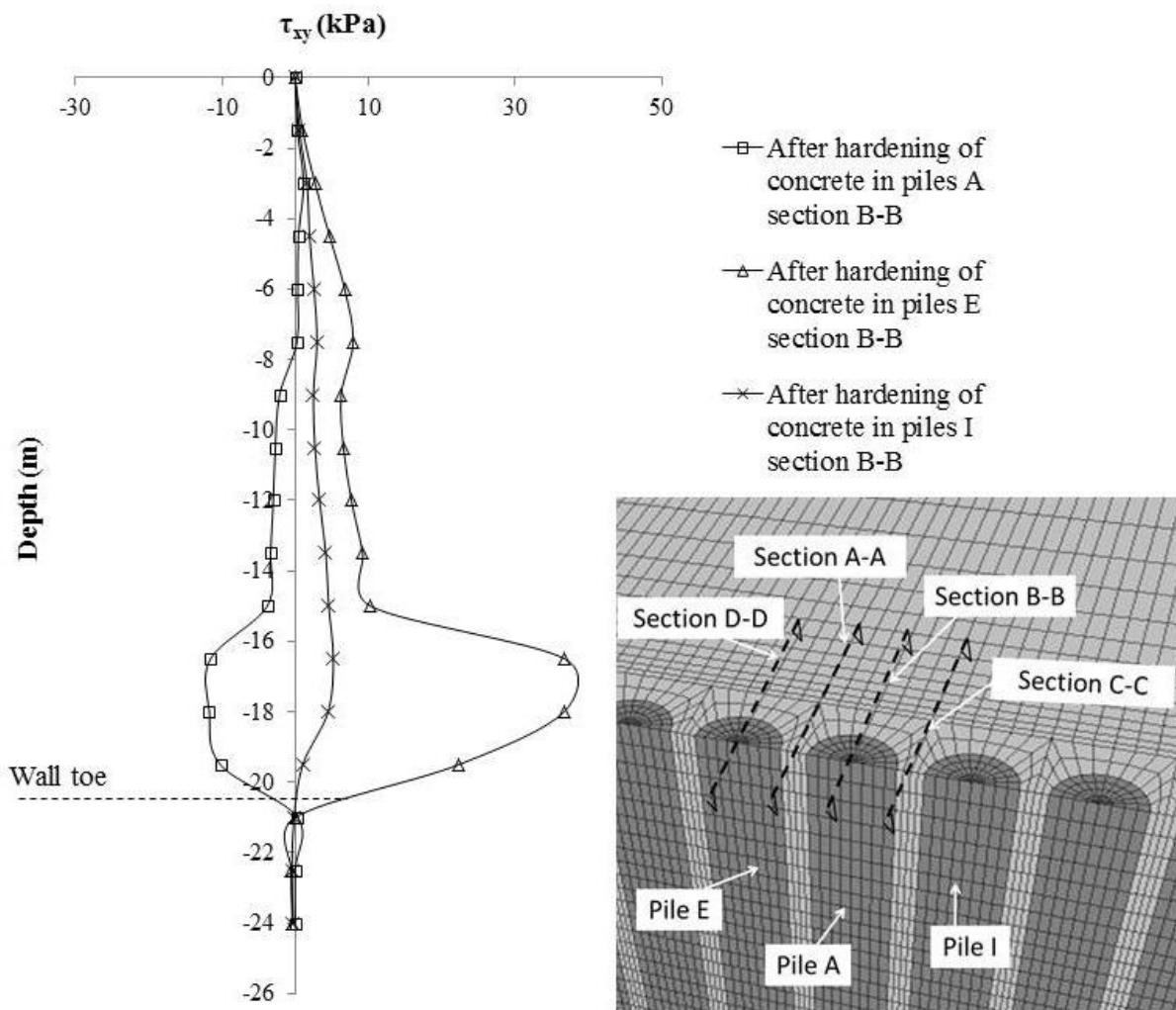


Figure 3.18. Variation of the calculated total horizontal stress (τ_{xy}) acting on section B-B, with depth down the wall at the end of construction of piles 'A', 'E' and 'I'. At a normal distance from the wall of 0.3 m.

Furthermore, Figure 3.17 shows that the horizontal stresses below the toe of the wall increased slightly after the excavation of piles E and I. This was mainly due to horizontal stress redistribution via the vertical shear stress (τ_{zy}). This mechanism can be simply explained as shown in Figure 3.19. The generation of negative values of vertical shear stress (τ_{zy}) above the toe of the wall allows the total horizontal stress (σ_{yy}) to reduce. This mechanism is consistent with the results plotted in Figure 3.20, where an increase in the vertical shear stress (τ_{zy}) after the installation of the piles E and I can be seen.

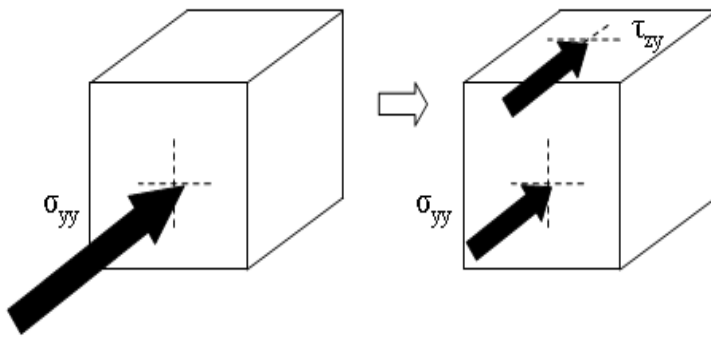


Figure 3.19. Generation of negative values of the shear stress (τ_{zy}) above the toe of the wall allow (σ_{yy}) to reduce.

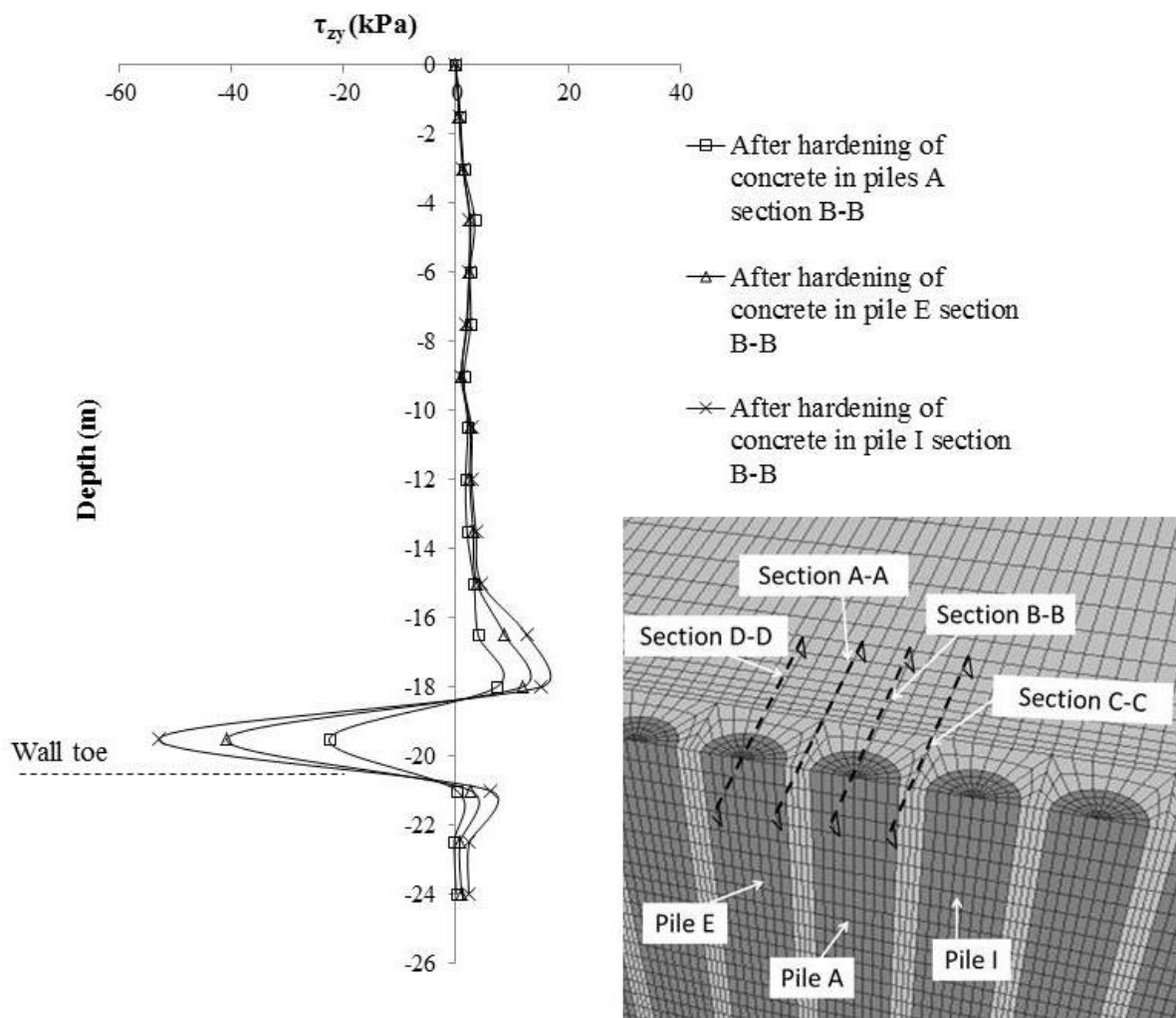


Figure 3.20. Variation of the calculated shear stress (τ_{zy}) acting on section B-B, with depth down to wall at the end of construction of piles 'A', 'E' and 'I'. At a normal distance from the wall of 0.3 m.

The computed horizontal stress (σ_{yy}) at 0.3 m behind the wall after the hardening of concrete of piles I is shown in Figures 3.21 and 3.22.

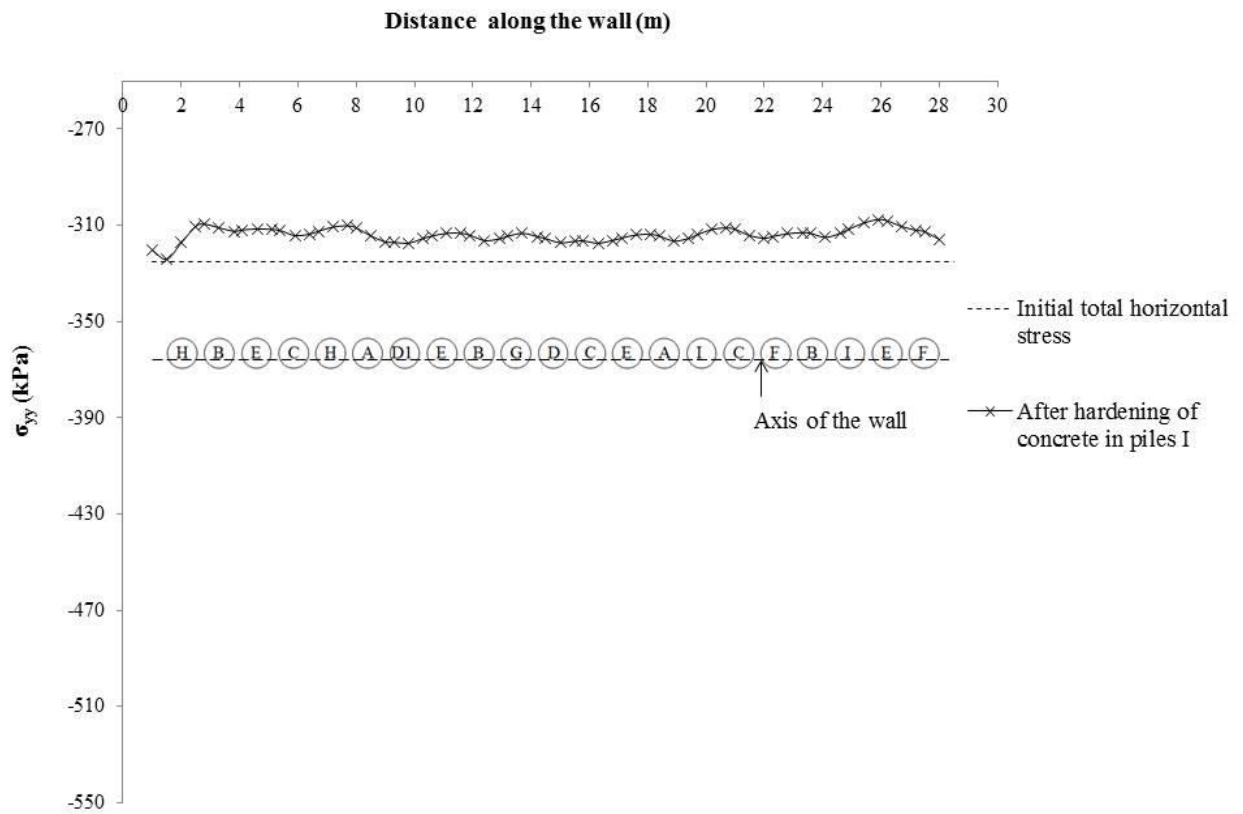


Figure 3.21. Calculated horizontal stress (σ_{yy}) 0.3 m behind the wall after hardening of pile 'I' at a depth of 15.3 m.

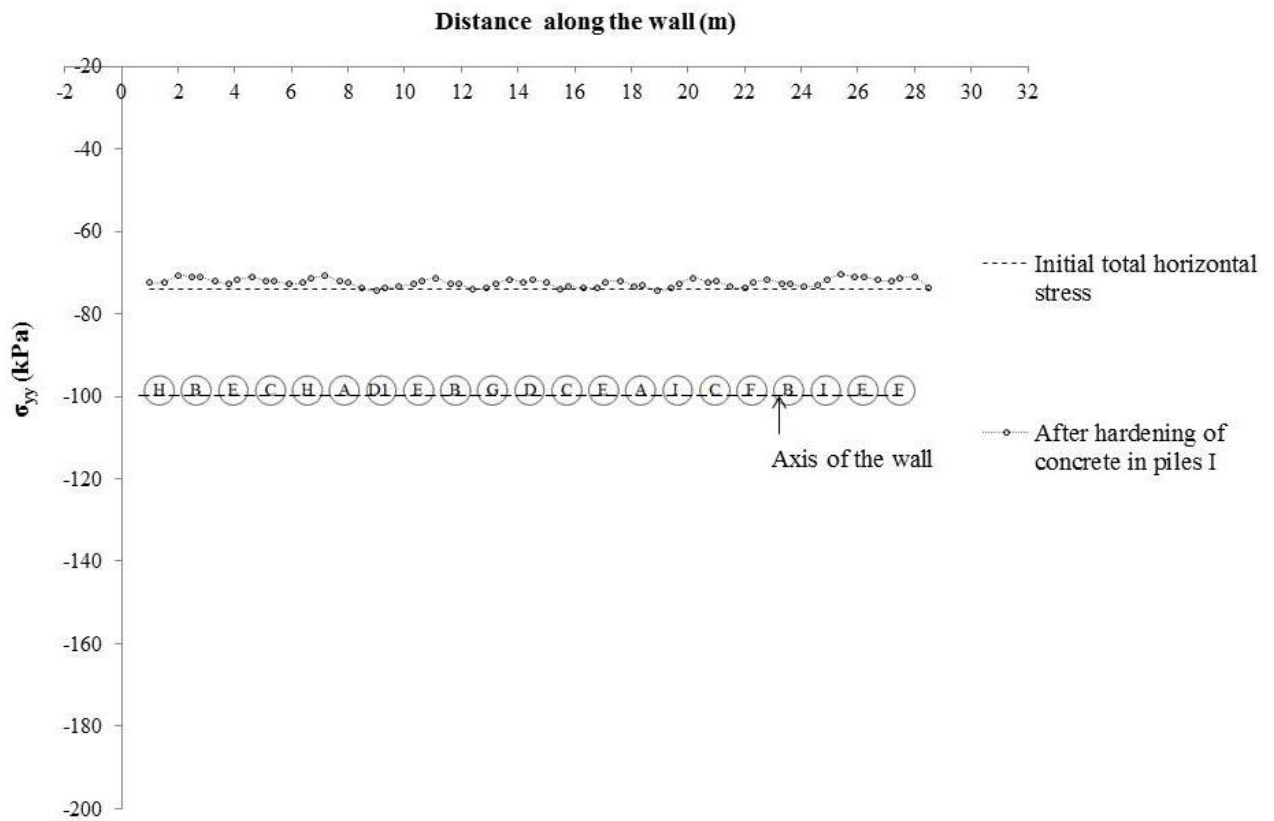


Figure 3.22. Calculated horizontal stress (σ_{yy}) 0.3 m behind the wall after hardening of pile 'I' at a depth of 3.3 m.

Figures 3.23, 3.24, 3.25 and 3.26 compare the total horizontal stresses measured during the installation of the wall by spade cells 2, 4, 5 and 16 with those calculated by the 3D model.

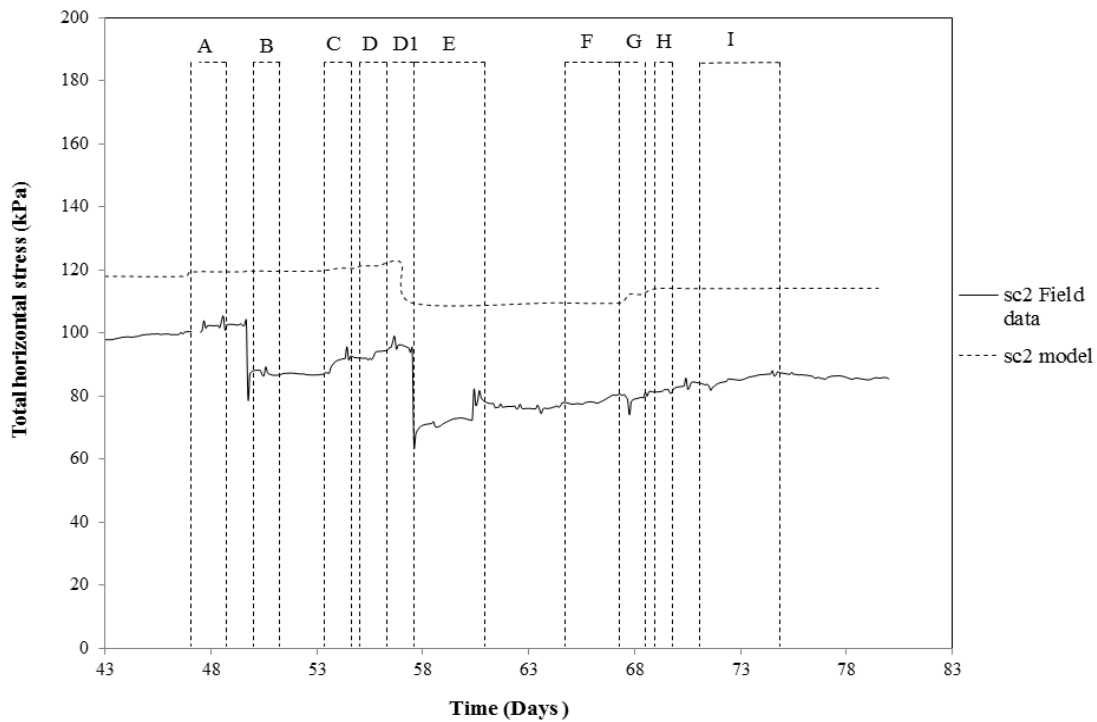


Figure 3.23. Total horizontal stresses (σ_{yy}) measured during wall installation compared with those calculated by the $FLAC^{3D}$ model (Spade Cell 2).

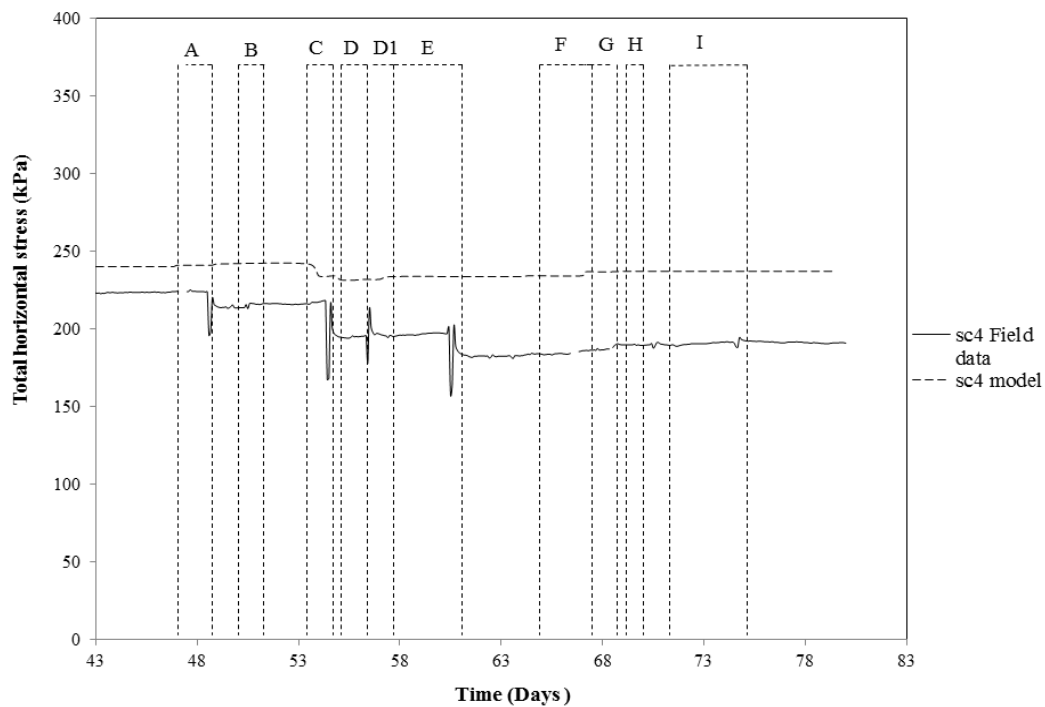


Figure 3.24. Total horizontal stresses (σ_{yy}) measured during wall installation compared with those calculated by the $FLAC^{3D}$ model (Spade Cell 4).

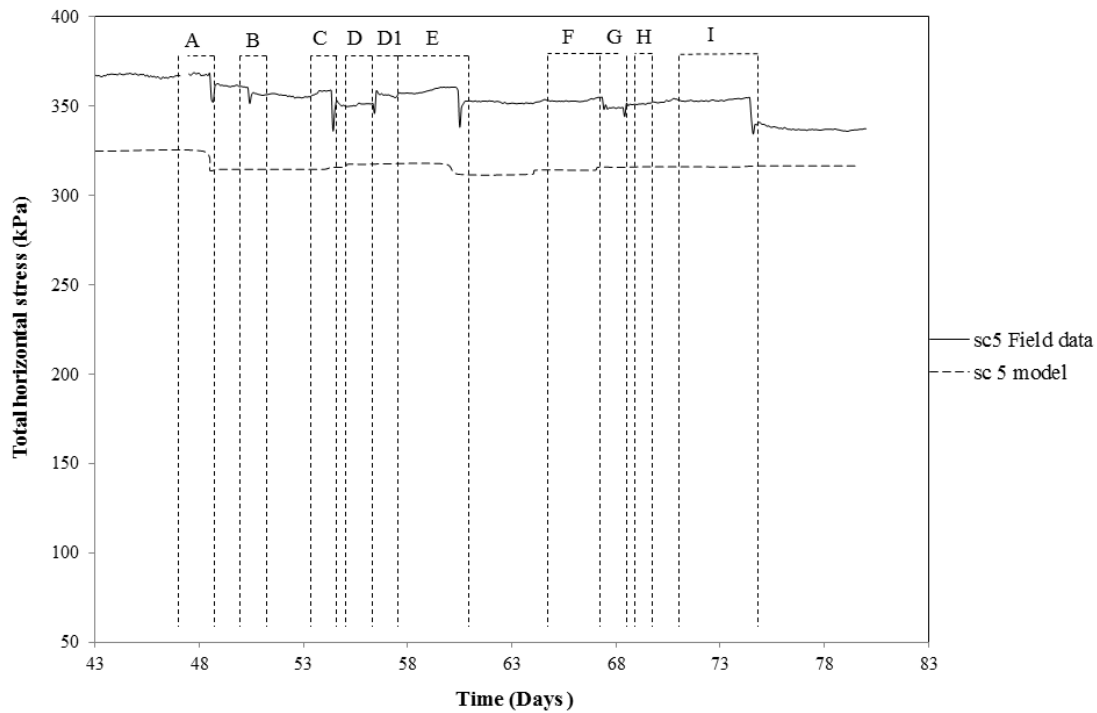


Figure 3.25. Total horizontal stresses (σ_{yy}) measured during wall installation compared with those calculated by the $FLAC^{3D}$ model (Spade Cell 5).

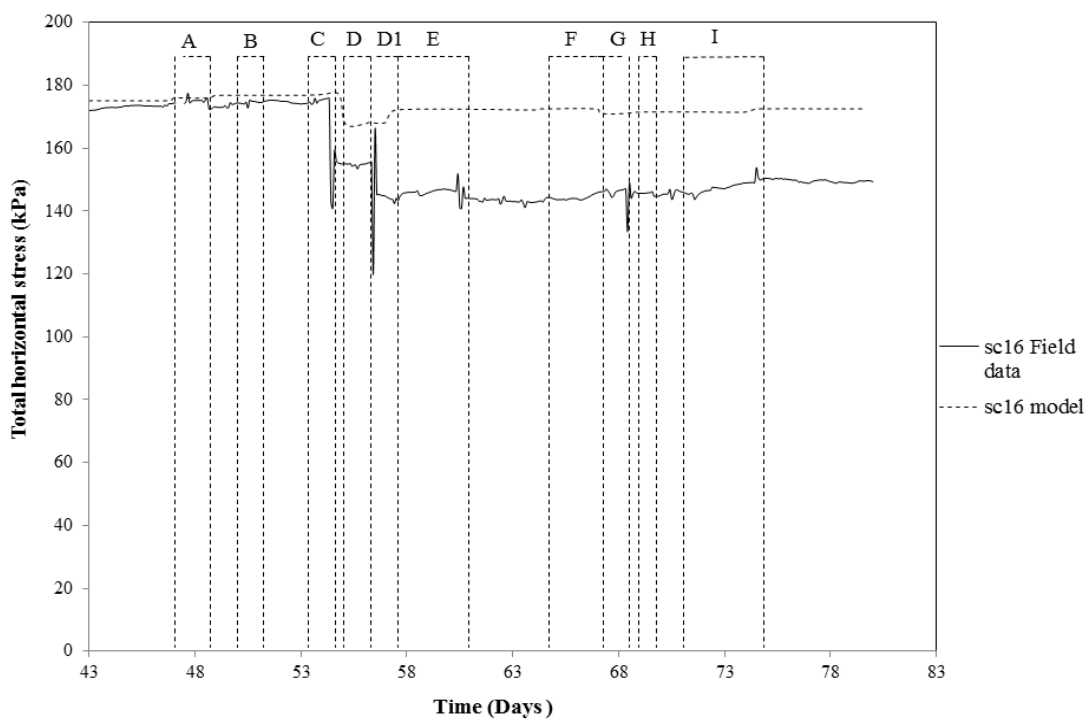


Figure 3.26. Total horizontal stresses (σ_{yy}) measured during wall installation compared with those calculated by the $FLAC^{3D}$ model (Spade Cell 16).

The initial stresses in the analyses are not perfectly coincident with those from the observed data (spade cells). This is because it was decided to use the idealized earth pressure coefficient $K_0 = 1$ reported by Richards *et al.* (2006) from their investigation of the site at Kent. Nevertheless, Figures 3.23-3.26 show that the total horizontal stress variation during wall installation is reasonably well represented by the *FLAC*^{3D} model. In particular, in Figure 3.27 the slight total horizontal stress increase after the excavation of pile G is captured by the analysis. This phenomenon is due to the redistribution of the horizontal stress change via the shear stress (τ_{xy}), as discussed previously. The model cannot capture the stress decrease measured in spade cell 2. Thus, in Chapter 4, the soil model was improved by the implementation of non-linear stress strain properties in the *FLAC*^{3D} simulation to represent the non-linear behaviour of soils at small strains.

3.4.1 Horizontal deformations

Changes in stress during the construction of a bored pile wall will inevitably result in ground deformation. In most cases the investigation and prediction of ground movements are important to assess possible damage to neighbouring structures. Elastic analyses are the simplest to use for the calculation of deformation. However, an elastic model, even with a realistic variation of the Young's modulus E with depth, cannot predict accurately the deformation of soils that behaves elasto-plastically, even at small strain. In Chapter 4, a non-linear stress-strain constitutive model is implemented to improve the calculation of soil deformations during pile installation.

Figure 3.27 shows the variation in horizontal displacement with depth at section A-A, 0.3 m behind the bored pile wall after the installation of the piles 'A' calculated using the linear elastic soil model.

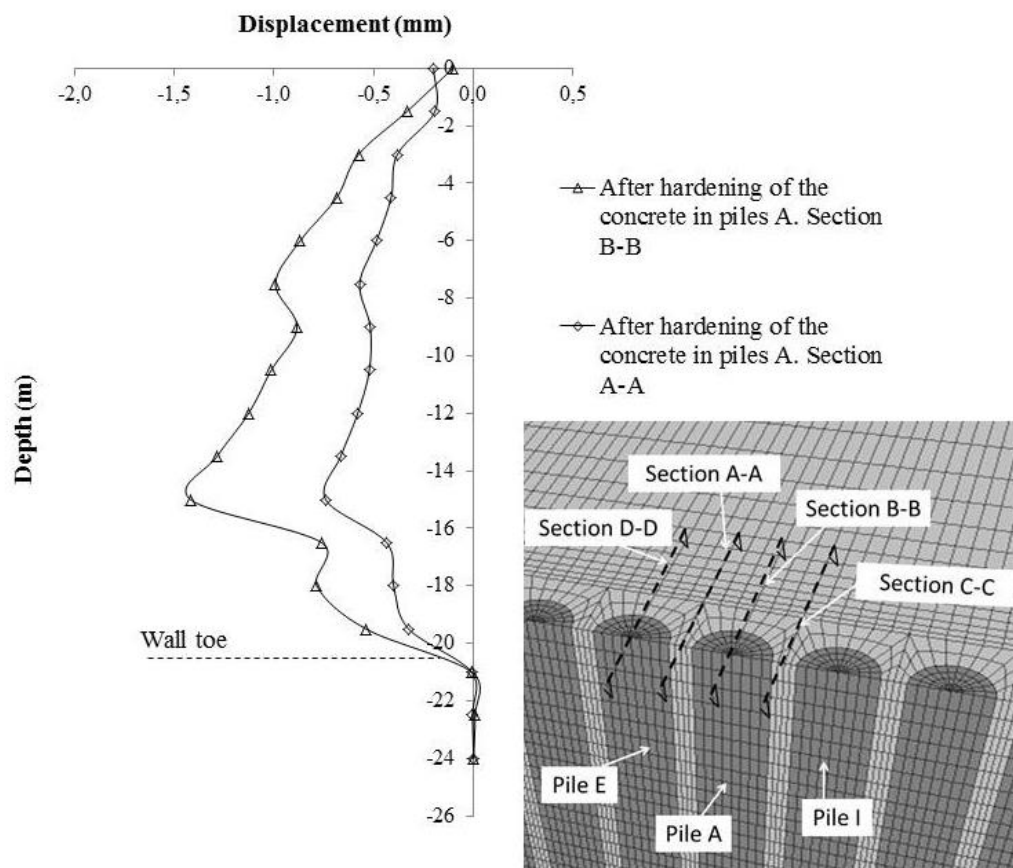


Figure 3.27. Calculated horizontal displacement along the section A-A and B-B calculated in the 3D analysis of installation of the bored pile wall. At a normal distance from the wall of 0.3 m.

Horizontal ground deformations are larger near the toe of the pile. These results are different from those of Ng and Yan (1998) who found that deformations were largest in the centre of the panel installed. Again this is mainly due to the geometry effects. Also, it can be seen that the deformations at the centre of the pile are twice as large as at the edge. The horizontal deformations along the pile length are clearly not uniform. Furthermore, the horizontal deformations are minimal compared with those calculated by Ng and Yan (1998). However, a close correlation between the computed stresses variations and the observed values from the spade cells was found.

Figures 3.28 and 3.30 show the horizontal displacement profile along the wall 0.4 m behind the piles at 3.3 m and 15.3 m depth after the excavation of the primary piles 'A'. The displacements became negligible at a distance of $1.2 d$ from the centres of both the piles 'A'.

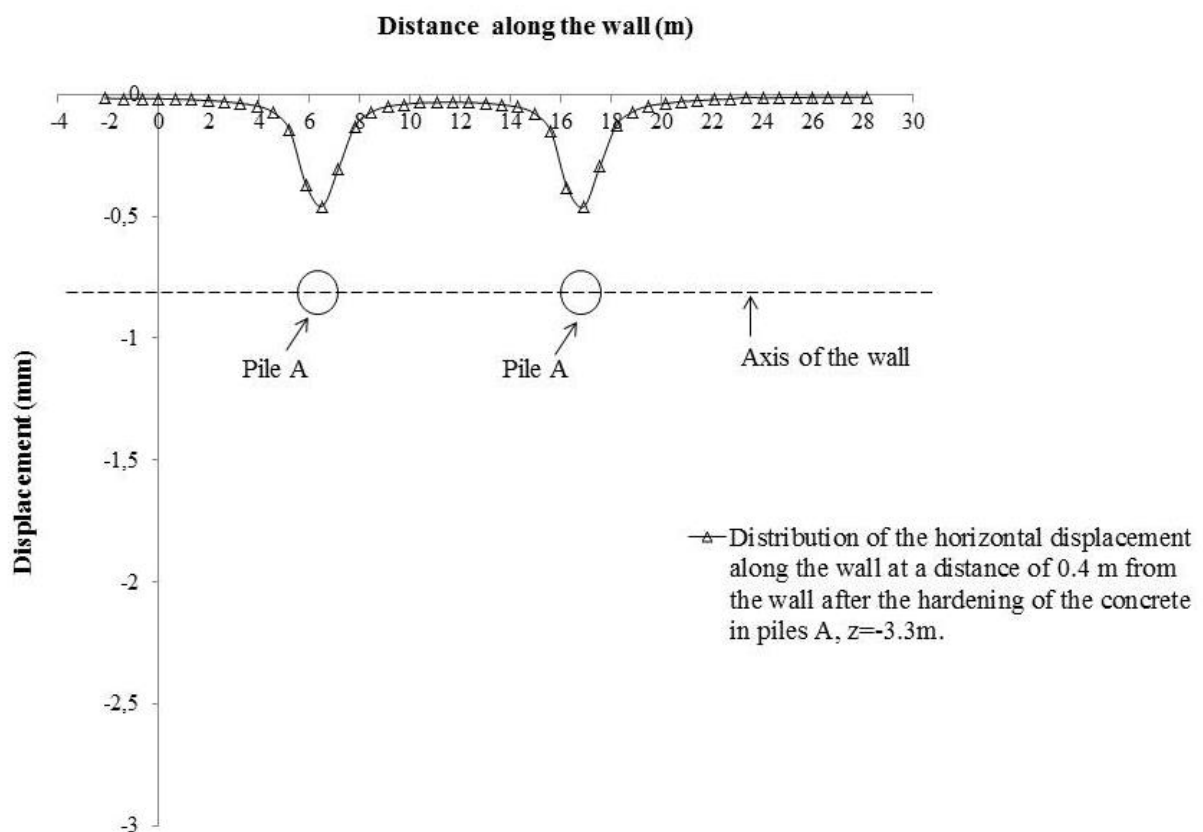


Figure 3.28. Distribution of the calculated horizontal displacement 0.4 m behind the wall along the wall after the hardening of the concrete in piles 'A' at a depth of 3.3 m.

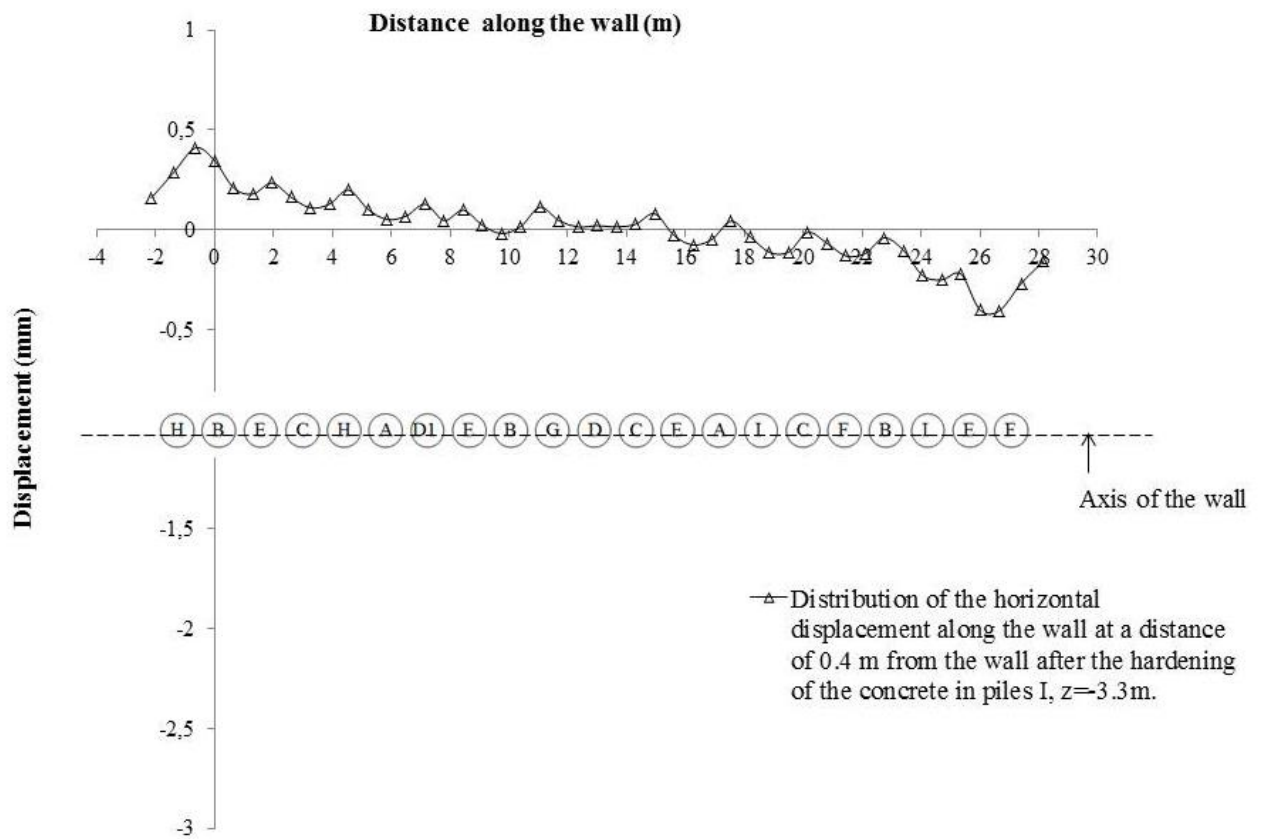


Figure 3.29. Distribution of the calculated horizontal displacement 0.4 m behind the wall along the wall after the hardening of the concrete in piles 'I' at a depth of 3.3 m.

Figure 3.30 and 3.31 show the horizontal displacement profile along the wall 0.4 m behind the piles at 3.3 and 15.3 m depth at the end of the wall construction after the installation of piles I. The displacements behind the wall after pile installation are minimal.

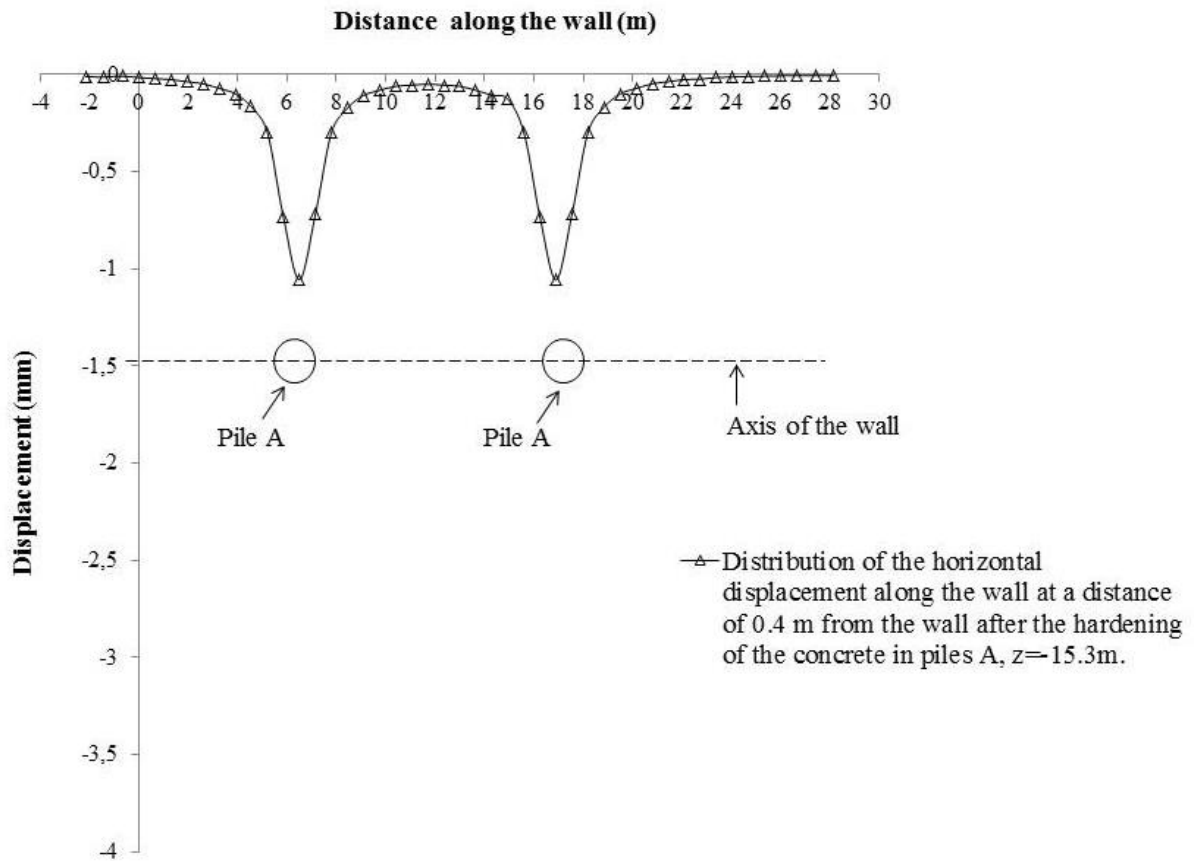


Figure 3.30. Distribution of the calculated horizontal displacement 0.4 m behind the wall along the wall after the hardening of the concrete in piles 'A' at a depth of 15.3 m.

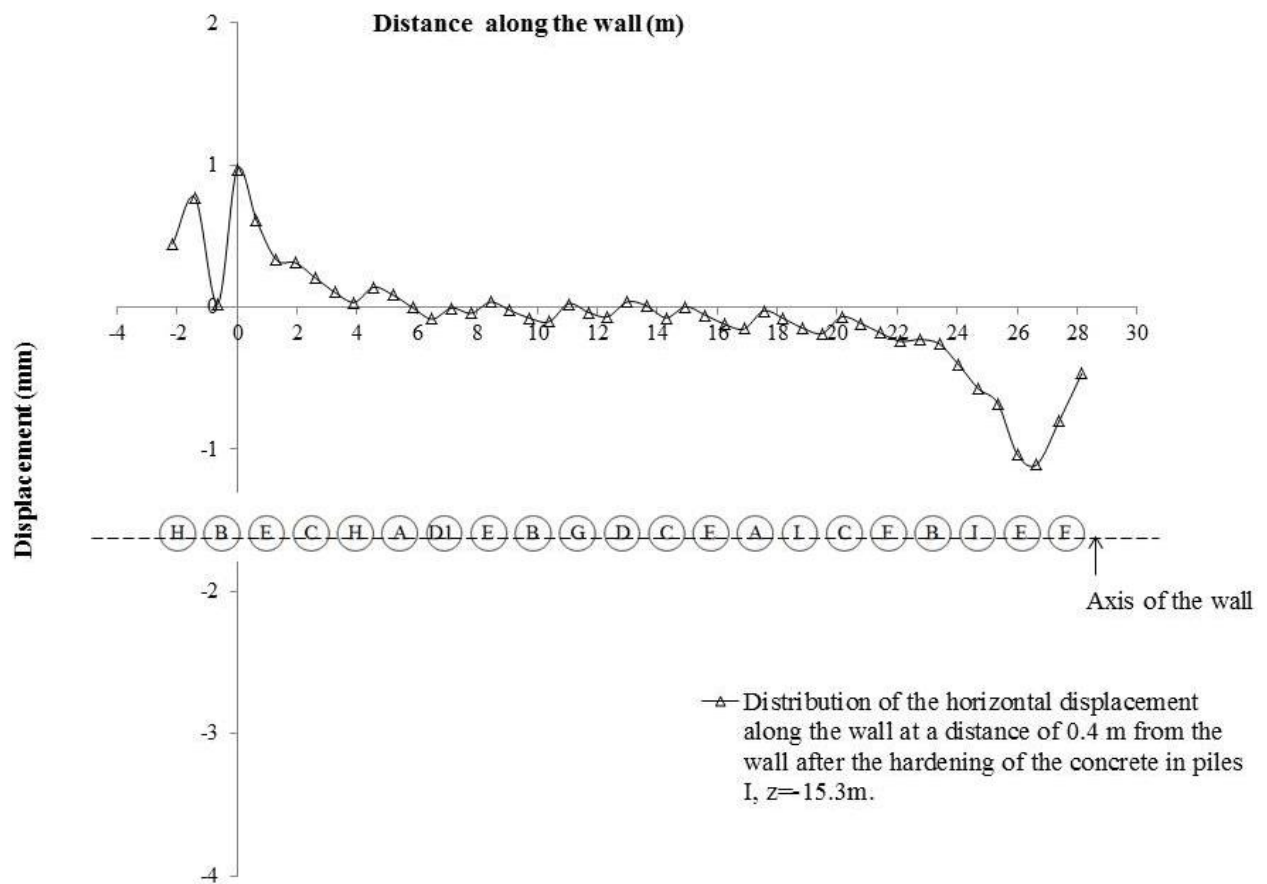


Figure 3.31. Distribution of the calculated horizontal displacement 0.4 m behind the wall along the wall after the hardening of the concrete in piles ‘I’ at a depth of 15.3 m.

3.4.2 Investigation of the effect of the in situ stress state on the horizontal stress variation behind the bored pile wall

The stress changes in the area of the spade cells 2, 4 and 5 calculated using an initial earth pressure coefficient $K_0 (= \sigma'_h / \sigma'_v) = 1$ as proposed by Richards *et al.* (2006) were compared with those from a different K_0 , as used by Gourvenec and Powrie (1999) (Figure 3.32).

From Figures 3.33, 3.34 and 3.35 it can be seen that the total horizontal stress variation for $K_0 (= \sigma'_h / \sigma'_v) = 1$. (Richards *et al.*, 2006), are similar to those found using the K_0 profile proposed by Gourvenec and Powrie (1999). This means that the stress change is relatively insensitive to K_0 and matches the measured changes reasonably closely.

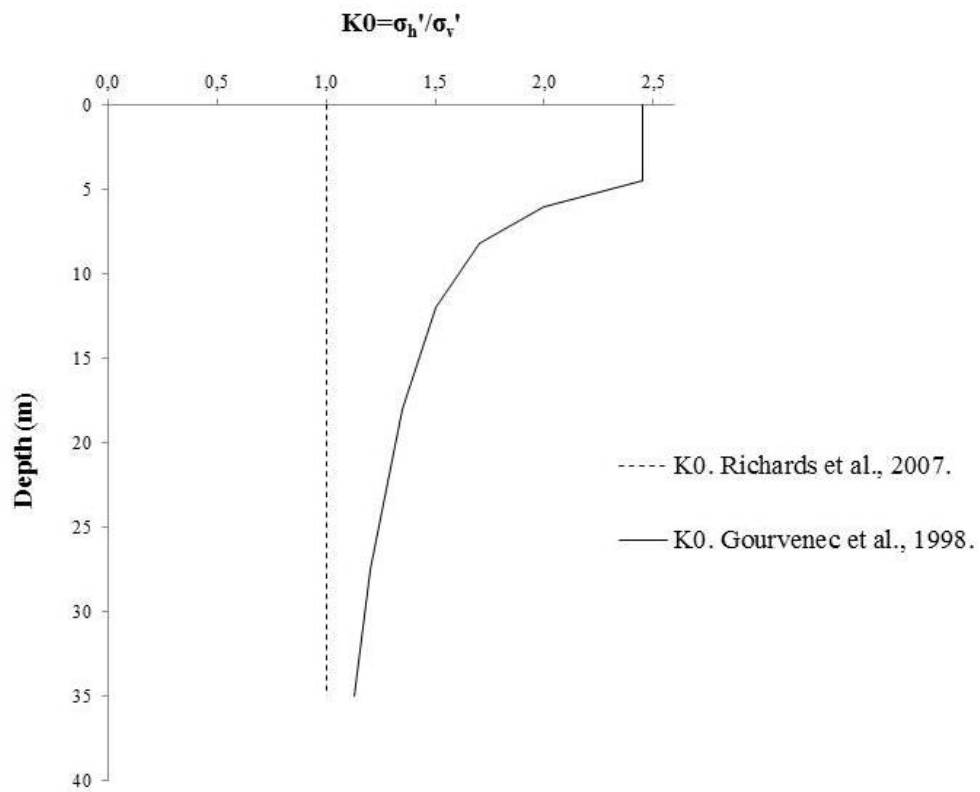


Figure 3.32. In situ earth pressure coefficient $K_0 = 1$ (Richards *et al.*, 2006) compared K_0 with the profile used by Gourvenec and Powrie (1999).

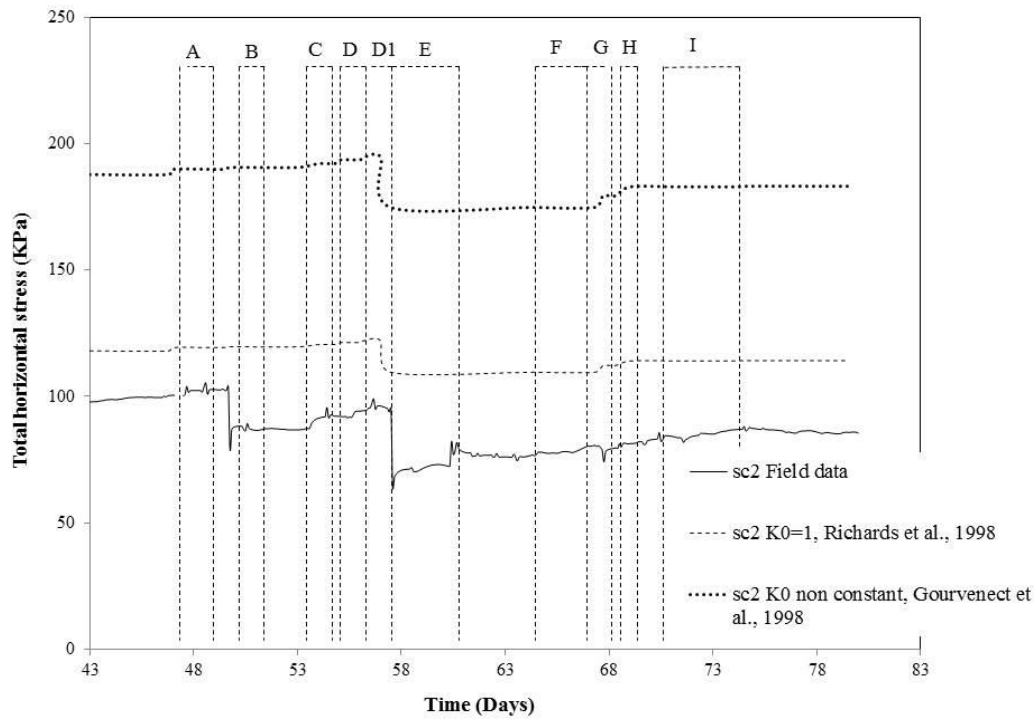


Figure 3.33. Comparison of the total horizontal stresses (σ_{yy}) calculated by the $FLAC^{3D}$ model using different in situ stress states (Spade Cell 5).

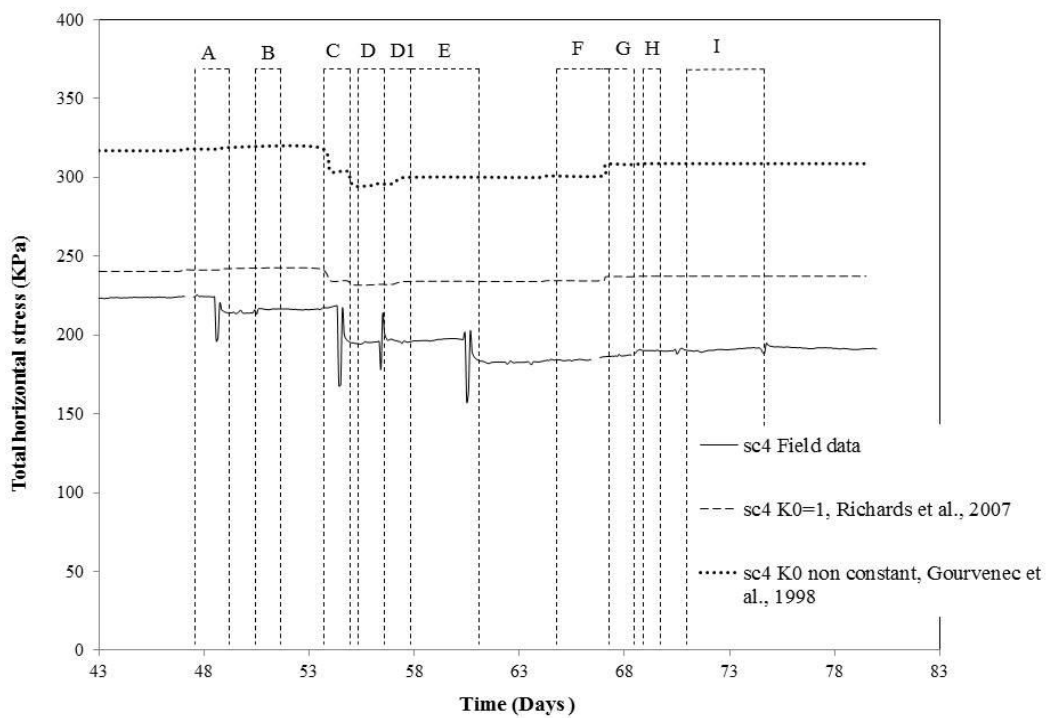


Figure 3.34. Comparison of the total horizontal stresses (σ_{yy}) calculated by the $FLAC^{3D}$ model using different in situ stress state, (Spade Cell 5).

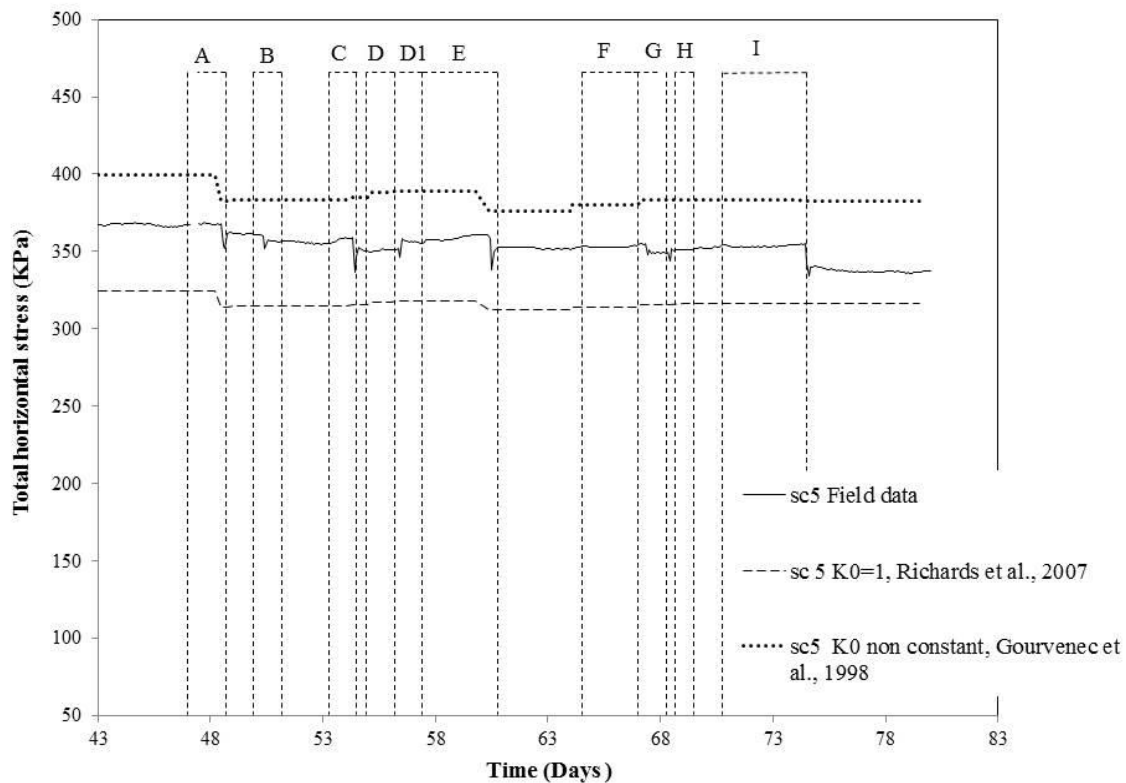


Figure 3.35. Comparison of the total horizontal stresses (σ_{yy}) calculated by the $FLAC^{3D}$ model using different in situ stress state, (Spade Cell 5).

3.5 Summary

In the last few decades much effort has been spent to investigate the effects of diaphragm wall panel installation in an overconsolidated deposit. Conversely, there is a relative lack of understanding of the installation effects of bored pile construction. Therefore, in this chapter a 3D analysis of the construction sequence of a bored pile wall installed in stiff clay has been carried out using a three-dimensional explicit finite-difference program. The stiff clay has been assumed to behave as an isotropic, linear elastic perfectly plastic material in the analysis. The analyses have clarified the stress changes during the installation of a single pile and a sequence of piles. The following conclusions were made from these first analyses:

- It has been found that the influence of the pile installation became insignificant at a distance of $1.2 d$ along the line of the wall from the centre of the pile installed. Furthermore, it was observed that the horizontal stress in the area on the edges of the pile installed does not change after the pile construction. These results are different

from those of Gourvenec and Powrie (1999), and Ng and Yan (1998), both of whom found an increase of the total horizontal stress in the soil on the edges of a single diaphragm wall installed.

- Again, it has been found that the horizontal stresses in the ground close to the edges of the pile 'A' did not change after the excavation of that pile. These results are different from those found by Gourvenec and Powrie (1999) and Ng and Yan (1998). The main reason could be the different geometry between the panel and the pile that lead to different stress states during the wall construction.
- A minimal decrease in the horizontal stresses was observed in the soil behind the pile, in the area from the head of the pile down to 15 m depth. A similar result was found by Bennett *et al.* (1996). Furthermore, only a minimal total horizontal stress increase was observed below the pile installed.
- After a single pile had been installed it was observed that the horizontal stress decreases were mainly concentrated above the toe of the pile. These results were quite different from those observed by Pantiledou (1994). This was because she used a simplified 2D analysis with the assumption of axy-symmetric condition that cannot take into consideration the horizontal stress transfer below the toe of the wall via the horizontal and vertical shear stress.
- Only a minimal stress increment occurs under the toe of the wall during bored pile construction. Again this was different from the results calculated by Gourvenec and Powrie (1999) and Ng and Yan (1998) for the case of panel installation. Again this is mainly due to the geometry effects.
- There was a slight increase in the total horizontal stress behind the wall after the installation of piles 'E' and 'I'. This was attributed to the horizontal stress redistribution via the horizontal shear stress (τ_{xy}). Similar results found observed by Bennet *et al.* (1996).
- Richards *et al.* (2006) compared the changes in stress measured due to the installation of a single pile with the values calculated using a simplified elastic analysis. They found that the reduction in stress due to pile installation from the instrumentation was generally larger than that calculated using the simple elastic analysis. Similar results were also found from the analyses presented in this Chapter.

- Good correlations were found between the computed stress change from the 3D model and the real data from the instrumented section of the bored pile wall at Ashford, Kent.
- The displacements after a single pile installation became negligible at a distance of $1.2d$ from the centre of the pile.
- It has been found that the total horizontal stress variation from $K_0 (= \sigma'_h / \sigma'_v) = 1$, (Richards *et al.*, 2006) are quite similar to those found from a different K_0 , proposed by Gourvenec and Powrie (1998). This means that the stress change is relatively insensitive to K_0 and matches measured changes reasonably closely.

CHAPTER 4**3D MODELLING OF BORED PILE WALL INSTALLATION EFFECTS
USING A NON-LINEAR STRESS-STRAIN MODEL****4.1 Introduction**

The aim of the finite difference simulations described in this chapter was to represent more realistically the effects of installing a bored pile wall in over-consolidated clay by using a non-linear soil stress-strain model. The results are compared with the real data of ground stress changes during bored pile wall installation in an overconsolidated clay deposit in connection with the Channel Tunnel Rail Link (CTRL; now HS1) at Ashford.

Field and laboratory studies have shown that, even at very small strain, many soils exhibit non-linear stress-strain behaviour (e.g. Jardine *et al.*, 1986). Many laboratory investigations show the non-linearity of soil behaviour under working conditions (Daramola, 1978; Costa-Filho, 1980; Burland *et al.*, 1982). Detailed experimental investigations into the stress-strain

response of overconsolidated soil have also shown the effects of the most recent loading paths (Stallebrass *et al.*, 1997) and loading history (for example Smith *et al.*, 1992; and other researchers).

In this chapter, non-linear stress-strain properties were implemented in the *FLAC^{3D}* model used in Chapter 3 to represent non-linear soil behaviour even at small strain. The results of the analyses are presented in terms of computed stress changes at various positions around the wall, and ground movements during wall installation. The results from the non-linear stress-strain model are compared with those from the analyses using a linear stress-strain law.

4.2 Ground Model

As reported in Chapter 3, the soils were assumed to behave in an undrained manner during pile installation. Undrained behaviour during diaphragm wall and bored pile installation process has been observed or demonstrated by many researchers in the field (Carder *et al.*, 1991; Carswell *et al.*, 1993; Bennett *et al.*, 1996; Clark, 2006). The same value of undrained Poisson's ratio was used as in Chapter 3, Table 3.2. The undrained shear strength was characterized by the equation $c_u = 22 + 7z'$ kPa (Clark, 2006). The in situ stress state initialized at the beginning of the analysis is reported in terms of the earth pressure coefficient as follows, (Clark *et al.*, 2006).

$$K_0 = \left(\frac{\sigma'_h}{\sigma'_v} \right) = 1 \quad \text{Equation 4.1}$$

On the basis of the pressuremeter data studied by Richards *et al.* (2007) for the Ashford site, a value of $K_0 = 1$, was adopted for the design of the retaining structures.

One of the most important idealisations in modelling boundary value problems is the choice of an appropriate constitutive model. Numerical analysis, in which linear elastic/plastic behaviour is generally assumed, fails to predict the observed pattern of ground movement around excavations (Burland *et al.*, 1997). The ground model used in this case was isotropic nonlinear elastic-perfectly plastic. The tangent shear and bulk moduli varied with strain using the relationship proposed by Jardine *et al.* (1986). These relationships were adapted to work

in 3 dimensions for application in $FLAC^{3D}$. The model's equations are as follows (Jardine *et al.*, 1986):

$$G_{\tan} = \frac{p}{3} \left[A + B \cos(\alpha X^\beta) - \frac{B\beta\alpha X^{\beta-1}}{\ln 10} \sin(\alpha X^\beta) \right] \quad \text{Equation 4.2}$$

$$\text{where } X = \log\left(\frac{\varepsilon_a}{3}\right) \quad \text{Equation 4.3}$$

$$K_{\tan} = \frac{p}{3} \left[R + S \cos(\lambda Y^{\mu-1}) - \frac{S\lambda\mu Y^{\mu-1}}{\ln 10} \sin(\lambda Y^\mu) \right] \quad \text{Equation 4.4}$$

$$\text{where } Y = \log\left(\frac{\varepsilon_v}{T}\right) \quad \text{Equation 4.5}$$

The Jardine *et al.* (1986) equation that describes the relation between strain and stiffness is based on the axial strain in an undrained triaxial test, and is basically an hyperbolic function. It is therefore necessary to find how this relates to 3D stresses. In an undrained triaxial test the following relationships are valid:

$$\varepsilon_1 = \varepsilon_a \quad \text{Equation 4.6}$$

And

$$\varepsilon_2 = \varepsilon_3 = -0.5\varepsilon_a \quad \text{Equation 4.7}$$

Now,

$$\gamma_{oct} = \frac{2}{3} \left[(\varepsilon_1 - \varepsilon_2)^2 + (\varepsilon_2 - \varepsilon_3)^2 + (\varepsilon_3 - \varepsilon_1)^2 \right]^{1/2} \quad \text{Equation 4.8}$$

Substituting Equation 4.6 and Equation 4.7 into Equation 4.8:

$$\gamma_{oct} = \frac{2}{3} \left[(\varepsilon_a + 0.5\varepsilon_a)^2 + (-0.5\varepsilon_a + 0.5\varepsilon_a)^2 + (-0.5\varepsilon_a - \varepsilon_a)^2 \right]^{1/2} \quad \text{Equation 4.9}$$

$$\gamma_{oct} = \sqrt{2} \cdot \varepsilon_a \quad \text{Equation 4.10}$$

The tensorial octahedral shear strain, ε_{soct} , is required instead of the engineering octahedral shear strain γ_{oct} . Therefore:

$$\varepsilon_{soct} = \frac{\gamma_{oct}}{2} = \frac{1}{\sqrt{2}} \varepsilon_a \Rightarrow \varepsilon_a = \sqrt{2} \cdot \varepsilon_{soct} \quad \text{Equation 4.11}$$

Now in a Cartesian coordinate system, the formulation of Equation 4.8 is:

$$\varepsilon_{soct} = \frac{1}{3} \left[(\varepsilon_x - \varepsilon_y)^2 + (\varepsilon_y + \varepsilon_z)^2 + (\varepsilon_z - \varepsilon_x)^2 + 6(\varepsilon_{xy}^2 + \varepsilon_{yz}^2 + \varepsilon_{zx}^2) \right]^{1/2} \quad \text{Equation 4.12}$$

Combining Equation 4.11 and Equation 4.12 gives Equation 4.13:

$$\varepsilon_a = \frac{\sqrt{2}}{3} \left[(\varepsilon_x - \varepsilon_y)^2 + (\varepsilon_y - \varepsilon_z)^2 + (\varepsilon_z - \varepsilon_x)^2 + 6(\varepsilon_{xy}^2 + \varepsilon_{yz}^2 + \varepsilon_{zx}^2) \right]^{1/2} \quad \text{Equation 4.13}$$

The full strain increment vector is available in *FLAC*^{3D} using the command `z_fsi(pnt,array)`. This command contains all the required strain components for the equations above. Equation 4.4 is used as a FISH function to apply the nonlinearity to the model. Every 10 calculation steps these vectors (`z_fsi` and the mean effective stress, p') are determined for each zone and the stiffness is updated.

Made Ground	A	B	C	α	β	ε_{amin}	ε_{amax}
	1100	1050	9e-6	1.22	0.3	5e-5	2.2e-3

Table 4.1

Over-consolidated clay	A	B	C	α	β	ε_{amin}	ε_{amax}
	1022	980	4e-6	1.35	0.28	5e-5	2.2e-3

Table 4.2

It was not possible to determine the empirical constants A, B, C, α and β through laboratory experiments using samples from the site at Ashford. Thus, it was decided to use the values of the stiffness parameters suggested by Scott *et al.* (2003), Tables 4.1 and 4.2, on the basis of back analysis of the Heathrow ART (Airside Road Tunnel) Eastern Portal contiguous piled walls.

Two different stress-strain models were investigated in this chapter, non-linear and linear. The initial stiffness profile used in the non-linear stress strain model was chosen to match the stiffness profile of the linear stress strain analysis. The stiffness profile used in this chapter, $E = 10 + 3.5z'$ MPa, (where z' is the depth below the soil surface), was chosen as the best fit of the stiffness profile used in Chapter 3, Table 3.2. Figure 4.1 shows the soil stiffness profile (Young's modulus E) used in the analysis carried out in this chapter and in Chapter 3.

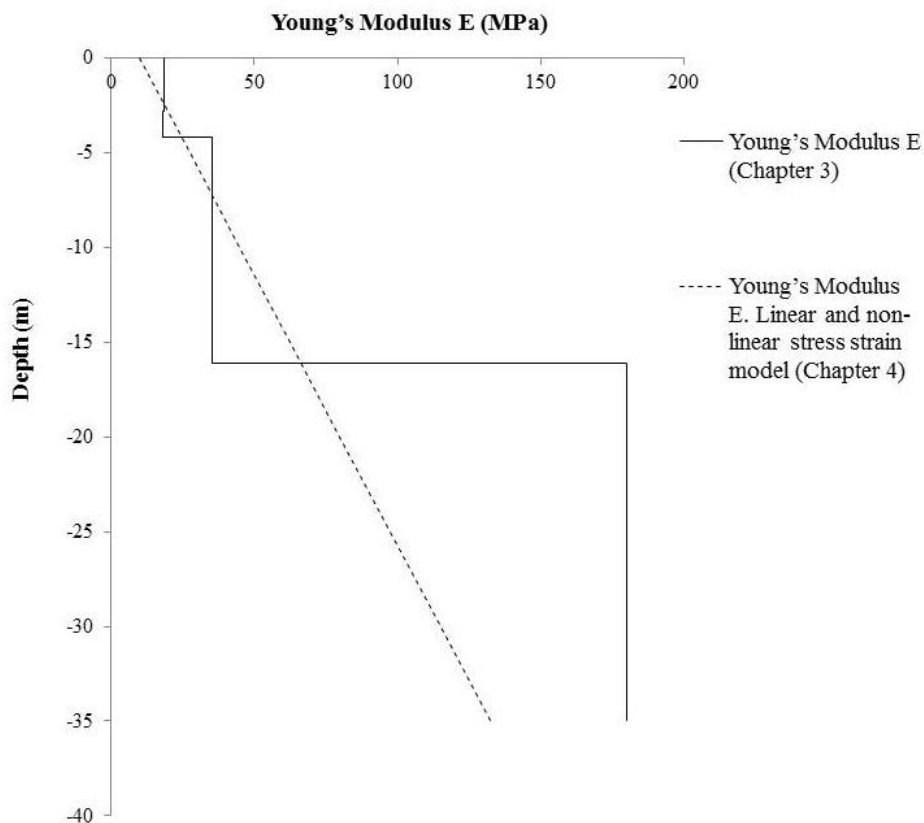


Figure 4.1. Soil stiffness (Young's modulus E) used in Chapter 3 and 4. (E =constant with depth, Chapter 3; E =increasing with depth, initial Young's modulus for the linear and non-linear stress strain model, Chapter 4).

Then, in this chapter it has chosen to use an initial Young's modulus, E , that increase with depth (Figure 4.1). This property was implemented in both the linear and non-linear models. Differently, in Chapter 3, it was chosen to use a Young's modulus, E , constant with depth, Table 3.2.

In the non-linear stress strain model the soil stiffness varies with strain. A typical variation of stiffness with strain used in this Chapter is shown in Figure 4.2.

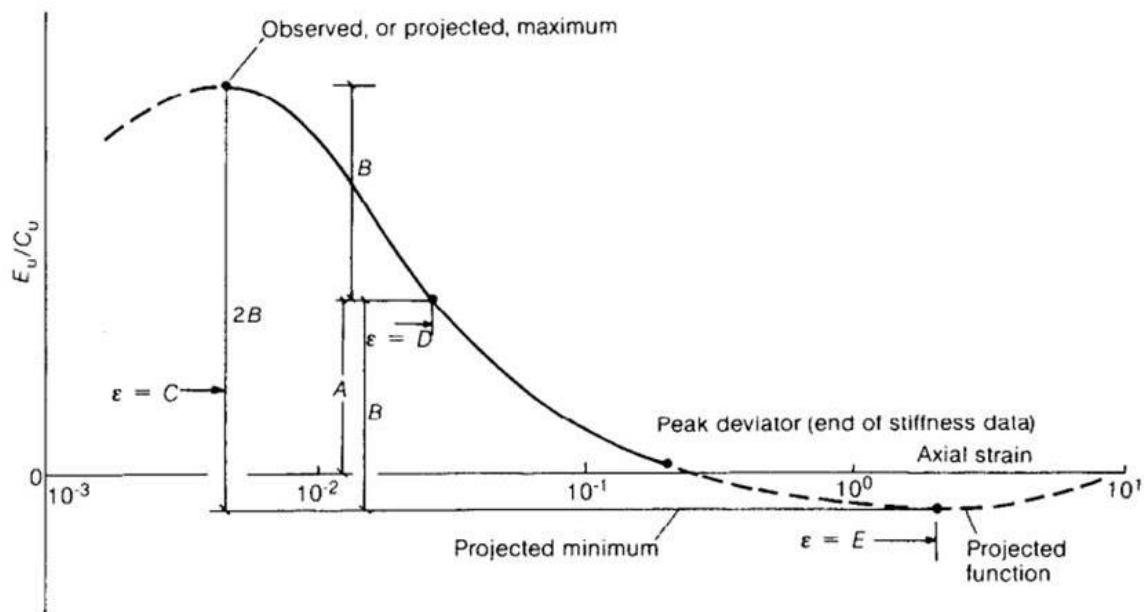


Figure 4.2. Curve fitting to stiffness-strain data (Jardine *et al.*, 1986).

4.3 Results and discussion

4.3.1 Calculated and observed horizontal stresses on the position of the spade cells

Figures 4.3-4.16 compare the computed profiles of the total horizontal stress with those measured by the instruments at Ashford, Kent. It can be seen that the non-linear stress-strain characteristic has given slightly better overall results than the linear-stress-strain model.

Figure 4.3 compares the computed profile of the horizontal stress with those measured by the spade cell 1. A slight decrease of the total horizontal stress after the installation of piles A is captured by both models. This corresponds to the result found in the previous chapter and to those presented later in this chapter.

Total horizontal stress increases are seen in the computed profile and were also measured by the instrumentation after the installation of the pile H, which is positioned at the edge of the spade cell 1. As shown in Chapter 3, Figure 3.17, and later in this chapter, the slight increase in the horizontal stress after the excavation of the pile H is due mainly to horizontal stress

redistribution via the shear stress (τ_{yx}) from the area close to the edge of the pile to the soil near to the spade cell 3.

During the installation of pile C, positioned on the edge of spade cell 1, a minimal increase of the total horizontal stress was observed and calculated.

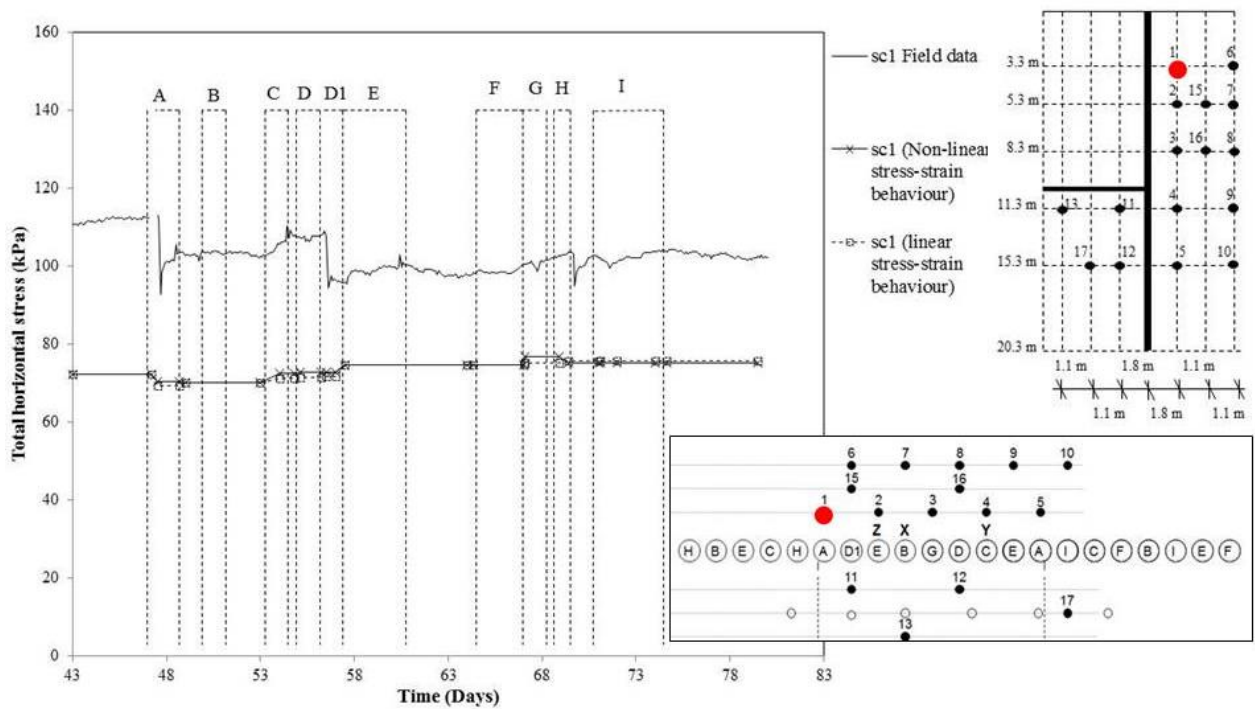


Figure 4.3. Total horizontal stresses (σ_{yy}) measured during wall installation compared with those calculated by the *FLAC^{3D}* model (Spade Cell 1).

Again, from Figure 4.4 it can be seen that the slight total horizontal stress increase during the final installation is captured by both models.

The horizontal stress decrease during the installation of the pile E (positioned in front of the spade cell 2) that was measured by spade cell 2 was also calculated by both the models. A small (few kPa) increase in total horizontal stress after the installation of piles G was registered by spade cell 2 and was also calculated by the models. As explained previously, this is due to the horizontal stress distribution from the soil at the edges of the pile E to the area close to the centre of the pile E, and close to spade cell 2.

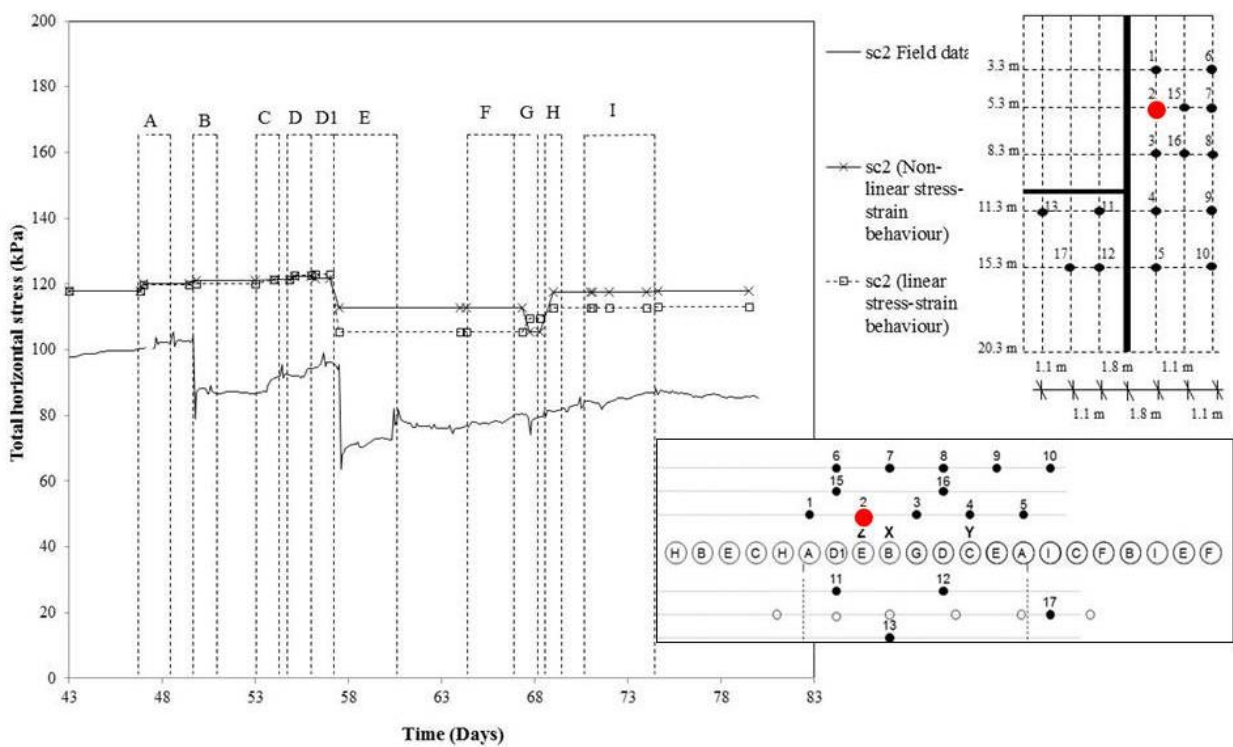


Figure 4.4. Total horizontal stresses (σ_{yy}) measured during wall installation compared with those calculated by the *FLAC^{3D}* model (Spade Cell 2).

From Figure 4.5 it can be noted that both the models (linear and non-linear stress-strain model) can capture efficiently the stress decrease after the excavation of the pile G, in front of spade cell 3. In contrast to the computed results, total horizontal stress decrease was measured by the instrumentation during the installation of the piles B and D. Similar results were found by Richards *et al.* (2006). They observed that the effect of pile installation in the area of the soil at the middle depth of the wall close to the piles was generally larger than that calculated using the simple elastic analysis even assuming zero pressure (rather than the pressure of the bentonite or wet concrete). They reported that this could be the result of shrinkage of the concrete (possibly due to thermal effects) as it sets.

Carswell *et al.* (1993) monitored a contiguous bored pile retaining wall in an over-consolidated deposit immediately and after its construction as part of the A406 North Circular Road Improvement Scheme in Walthamstow. The net effect of the wall installation was to reduce the total lateral stress by between 9 kN/m² and 62 kN/m². They reported that in general, a larger reduction occurred at greater depths.

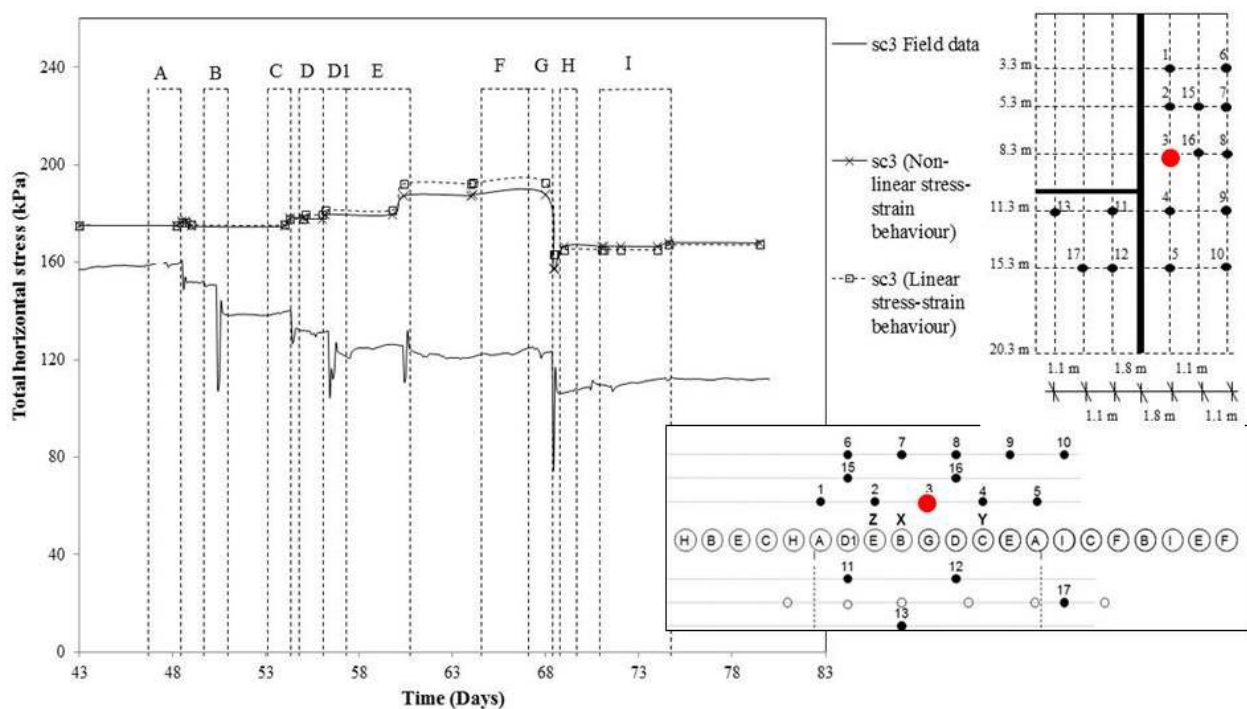


Figure 4.5. Total horizontal stresses (σ_{yy}) measured during wall installation compared with those calculated by the $FLAC^{3D}$ model (Spade Cell 3).

Figure 4.6 compares the total horizontal stresses (σ_{yy}) measured during wall installation with those calculated by the $FLAC^{3D}$ model in the area of spade cell 4, Figure 3.2. It can be seen that the data from the instruments are well represented by the computed results. Both the linear and non-linear stress-strain models are able to describe the stress variations during the installation of the piles C, D, and G, Figure 4.6.

An apparent decrease of the total horizontal stress of approximately 20 kPa was measured by the spade cell during the installation of pile C that takes position in front of the spade cell. A decrease of 15 kPa was also measured during the installation of the pile E. Instead, total horizontal stresses were detected by both models during the installation of the piles C and D. This discrepancy, between the computed and measured data, suggest that the spade cell 4 was not installed perfectly in front of the pile C but instead was positioned more close to the pile E.

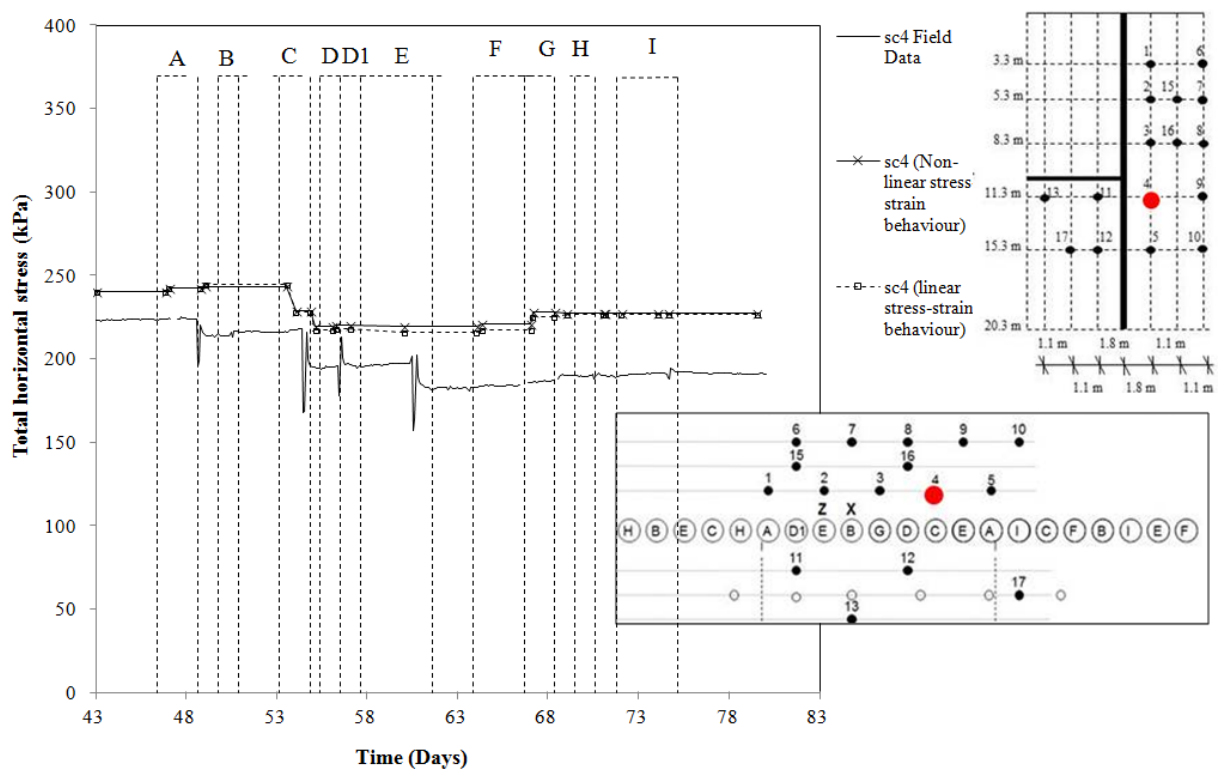


Figure 4.6. Total horizontal stresses (σ_{yy}) measured during wall installation compared with those calculated by the $FLAC^{3D}$ model (Spade Cell 4).

Figure 4.7 compares the horizontal stress changes in the area of spade cell 5, Figure 3.2, during pile installation with those calculated in the analyses. The trend of the horizontal stress changes is well represented by the non-linear stress strain model. The analyses represent the horizontal stress changes reasonably well, especially during the installation of the piles ‘A’ ‘E’ and ‘I’. Decreases of the total horizontal stresses were calculated by both the models and measured by the spade cell 5 after the installation of the piles more close to the instrumentation, piles A, E and I.

A slight increase in the total horizontal stress at a distance of 0.3 m from the wall at a depth of 15.3 m during the installation of a subsequent pile is shown in Chapter 3 and later in this chapter. Instead, stress decreases were calculated and measured during the installation of a subsequent pile in the zone of the soil at a distance of 1.8 m from the wall at a depth of 15.3 m (that is the position of the spade cell 5). This indicates that the shear stresses are mainly concentrated in the soil close to the wall and the effects of redistribution of the horizontal stress via the shear stress (τ_{xy}) are minimal in the area away from the wall.

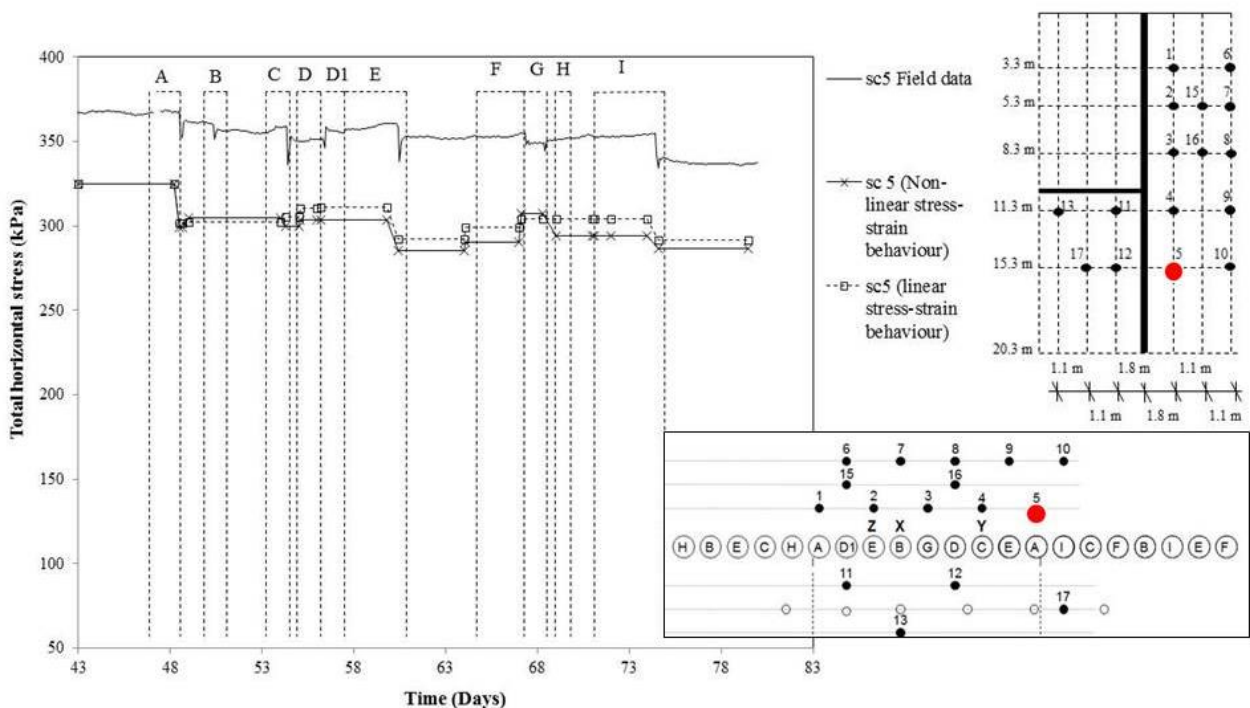


Figure 4.7. Total horizontal stresses (σ_{yy}) measured during wall installation compared with those calculated by the $FLAC^{3D}$ model (Spade Cell 5).

The horizontal stress changes are minimal at spade cell 6, Figure 4.8. The wall construction does not influence the total horizontal stress change in the area close to spade cell 6. This result is similar to the results shown later in this chapter. In fact, no changes in the total horizontal stress on the soil at a distance of 4 m from the wall and near the surface was calculated by both the models.

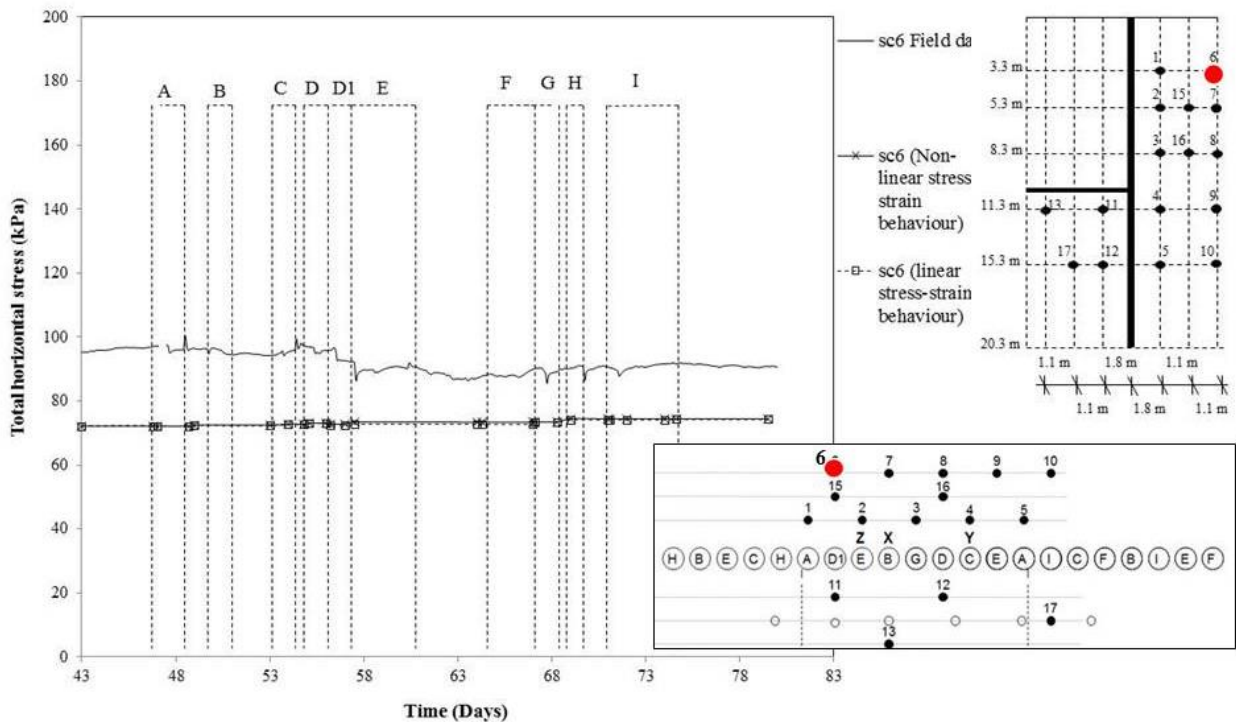


Figure 4.8. Total horizontal stresses (σ_{yy}) measured during wall installation compared with those calculated by the $FLAC^{3D}$ model (Spade Cell 6).

Figure 4.9 compares the horizontal stress changes measured at spade cell 7 with those calculated using both numerical models. The results are similar to those shown in Figure 4.8. The horizontal stress changes are minimal because the spade cell is positioned at a distance of 4 m from the wall and the instrument is relatively close to the surface.

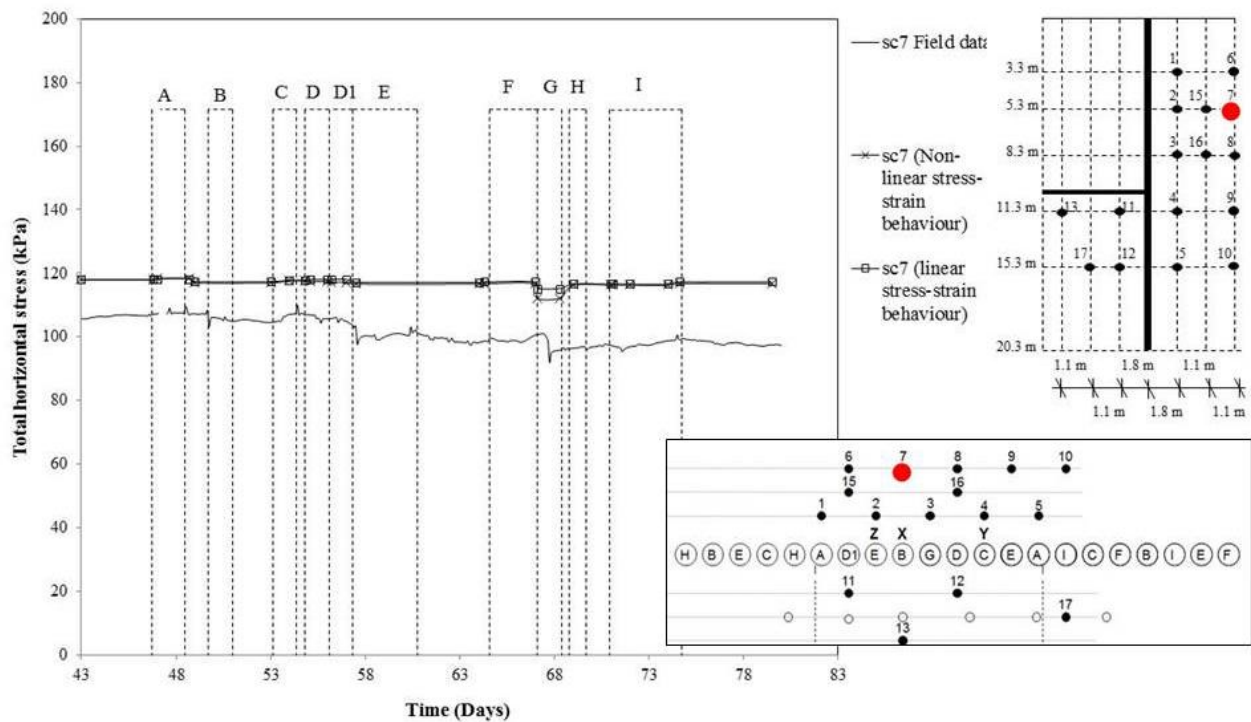


Figure 4.9. Total horizontal stresses (σ_{yy}) measured during wall installation compared with those calculated by the *FLAC^{3D}* model (Spade Cell 7).

The total horizontal stress decreases slightly in the area of spade cell 8 after wall installation as shown in Figure 4.10. This is different from the results measured and computed in the area of spade cells 6 and 7 where the total horizontal stresses remain almost constant during the wall installation. In fact, as shown later in this chapter (Figure 4.27) at a distance of 4 m from the wall the horizontal stress changes are mainly distributed in the area of the soil close to the toe of the wall.

A small total horizontal stress decrease was computed and measured by the instrumentation after the excavation of the piles G, D and C; these piles are the three closest to the spade cells, Figure 4.10. Furthermore, there was no measured or calculated increase in horizontal stress during the excavation of the piles.

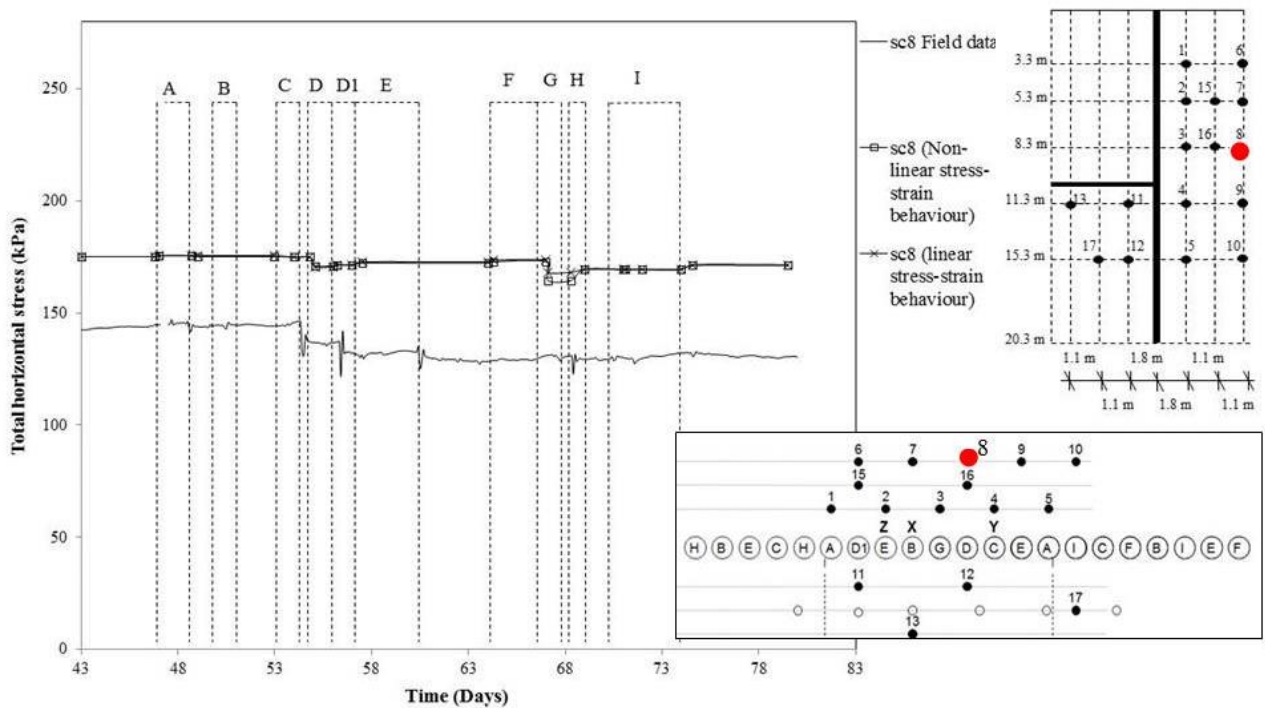


Figure 4.10. Total horizontal stresses (σ_{yy}) measured during wall installation compared with those calculated by the *FLAC^{3D}* model (Spade Cell 8).

Figure 4.11 shows the total horizontal stress change computed from both the linear and non-linear model and measured by the instrumentation in the area of spade cell 9. The results are similar to those calculated and measured in the area of spade cell 8. The total horizontal stress changes occur after the installation of three of the closest piles to the spade cell 9, piles 'E', 'C' and 'A'. At a distance of 4 m from the wall and a depth of 11.3 m below the surface, the total horizontal stress decreases only slightly. A few data points are missing but it is possible to distinguish the trend of the total horizontal stress changes measured in the area of the spade cell 9.

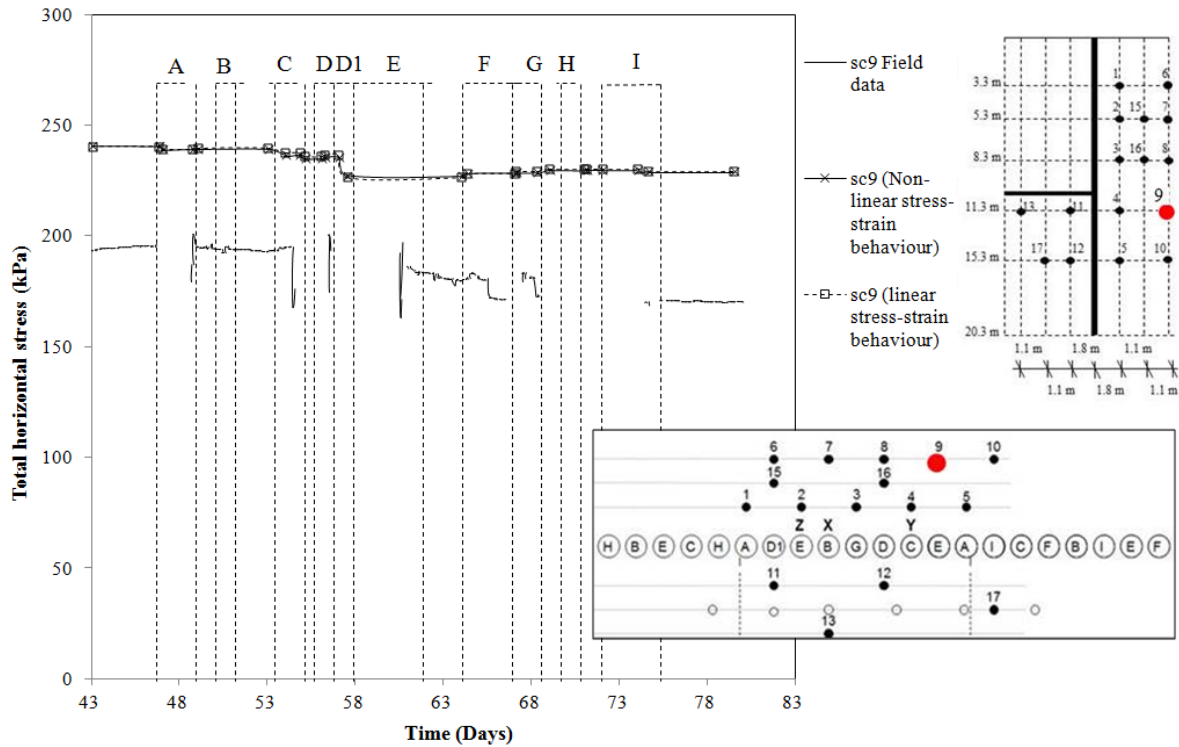


Figure 4.11. Total horizontal stresses (σ_{yy}) measured during wall installation compared with those calculated by the $FLAC^{3D}$ model (Spade Cell 9).

Figure 4.12 shows the total horizontal stress changes of spade cell 12. The non-linear model can describe slightly better the horizontal stress variation during the piles installation. The total horizontal stress decrease is caused mainly by the installation of the piles 'E' and by the construction of the piles 'C'. Further minor changes were calculated and measured after the installation of the piles 'G'.

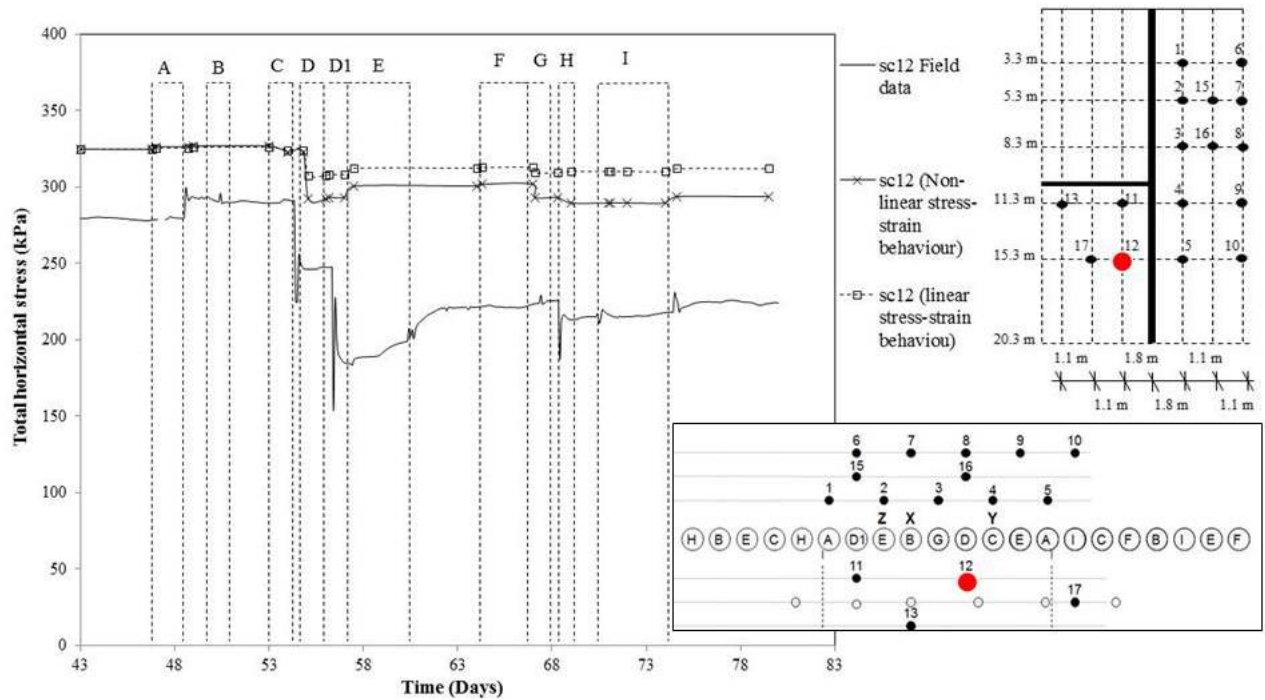


Figure 4.12. Total horizontal stresses (σ_{yy}) measured during wall installation compared with those calculated by the $FLAC^{3D}$ model (Spade Cell 12).

Spade cell 13 was positioned at a distance of 4 m from the wall and at 11.3 m depth from the surface. A decrease in horizontal stress was measured in the zone of spade cell 13 during the installation of the piles B and C although the spade cell 13 takes position quite far from the wall (4 m from the centre of the head of the pile). This result is consistent with the total horizontal stress changes calculated in the zone of the spade cell 13. The stress decreases were mainly measured and computed after the installation of the piles ‘B’ ‘E’ and ‘G’ which are the closest three piles to spade cell 13.

The same observations are valid for the computed horizontal stress changes in the vicinity of spade cell 16. From Figure 4.14, it is clear that the models can reproduce the stress changes well in the soil close to spade cell 16. Furthermore, good correspondence was found between the computed and the measured data after the excavation of the piles D and D1, Figure 4.14.

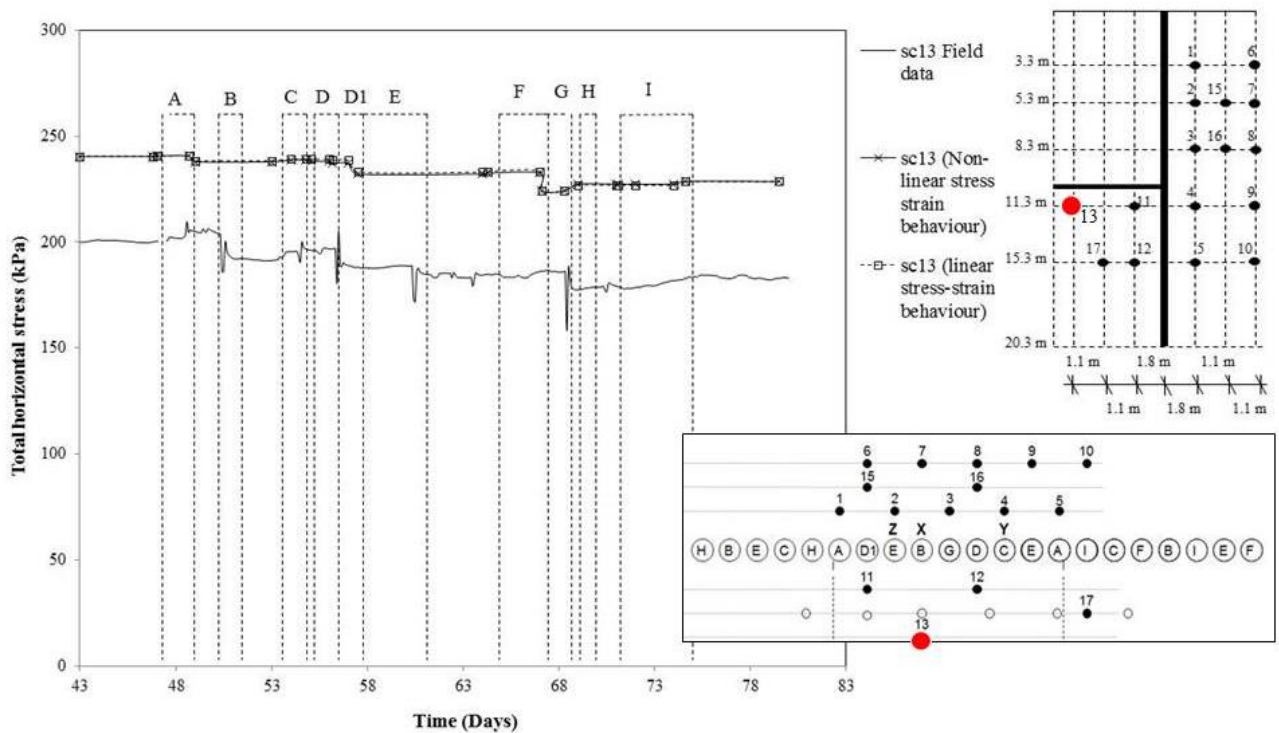


Figure 4.13. Total horizontal stresses (σ_{yy}) measured during wall installation compared with those calculated by the $FLAC^{3D}$ model (Spade Cell 13).

Figure 4.14 and 4.15 show the stress changes in the area of spade cell 15 and 16. During the installation of the subsequent piles E the stresses recorded by spade cell 15 and 16 were slightly larger than those calculated. As discussed previously for the spade cell 3, the difference between the data from the spade cells 15 and 16 and those from the models could be the result of shrinkage of the concrete (possibly due to thermal effects) as it sets (Richards *et al.*, 2006).

A small increment of the total horizontal stress during the installation of piles H was measured by spade cell 15 and was also detected by the models. Again, this could be due to the redistribution of the total horizontal stress from the area close to the edge of spade cell 15 to the soil in front of the pile D1.

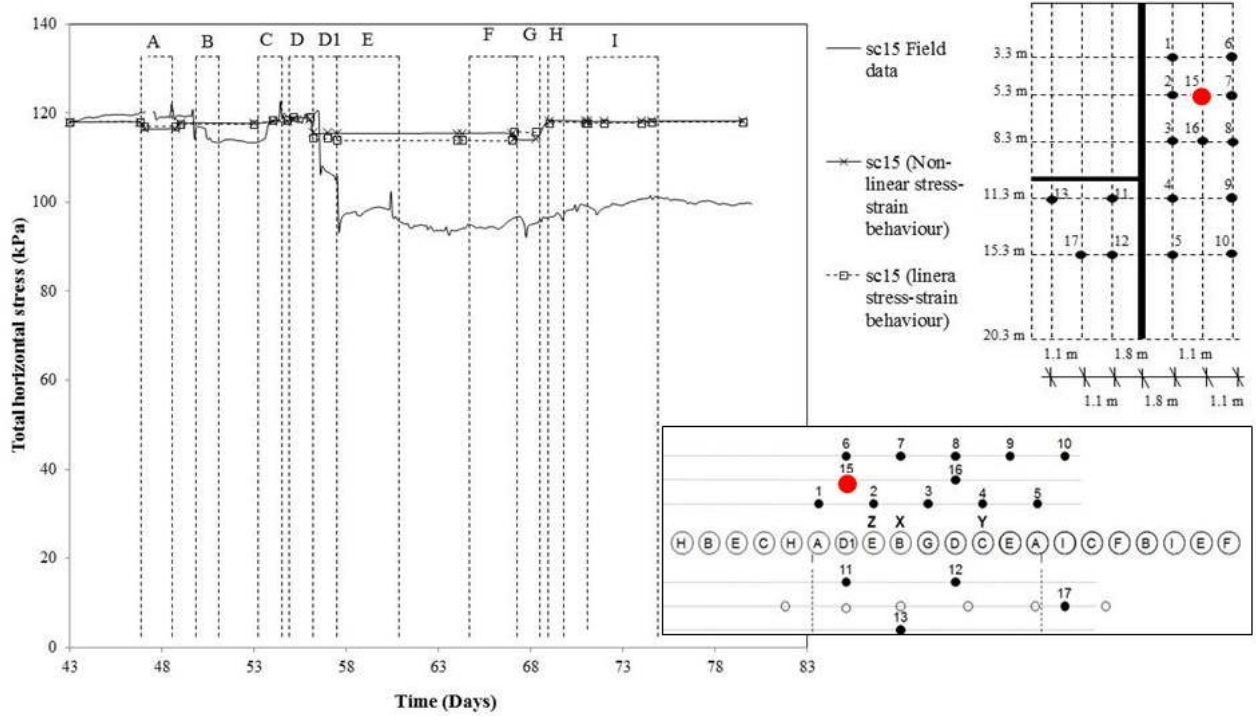


Figure 4.14. Total horizontal stresses (σ_{yy}) measured during wall installation compared with those calculated by the *FLAC^{3D}* model (Spade Cell 15).

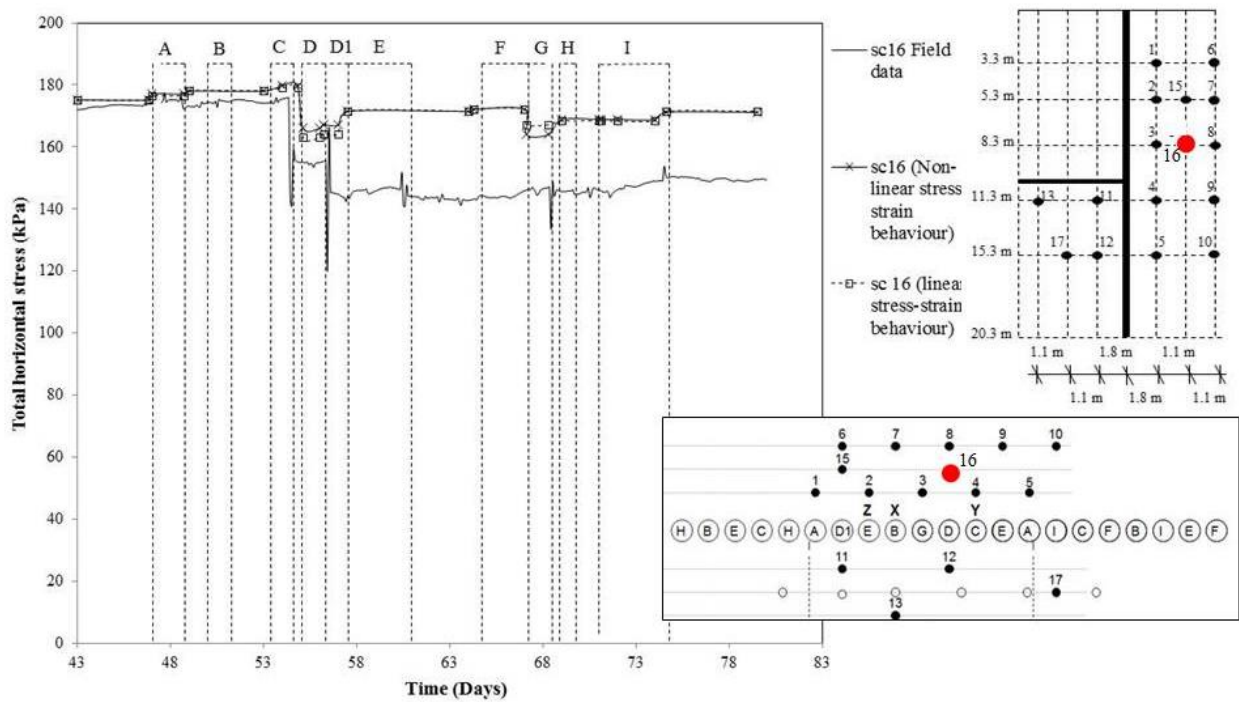


Figure 4.15. Total horizontal stresses (σ_{yy}) measured during wall installation compared with those calculated by the *FLAC^{3D}* model (Spade Cell 16).

Finally, good agreement between the results from the $FLAC^{3D}$ analyses and the measured data are apparent in Figure 4.16. It can be observed how the stress variation after the construction of the piles 'I' are well represented by the $FLAC^{3D}$ analyses.

As it was shown in Chapter 3 and reported later in this chapter, the horizontal stress decreases are mostly concentrated in the area above the toe of the wall. This is consistent with the results show in Figure 4.16 where the stress decreases were measured after the installation of piles A, C and I.

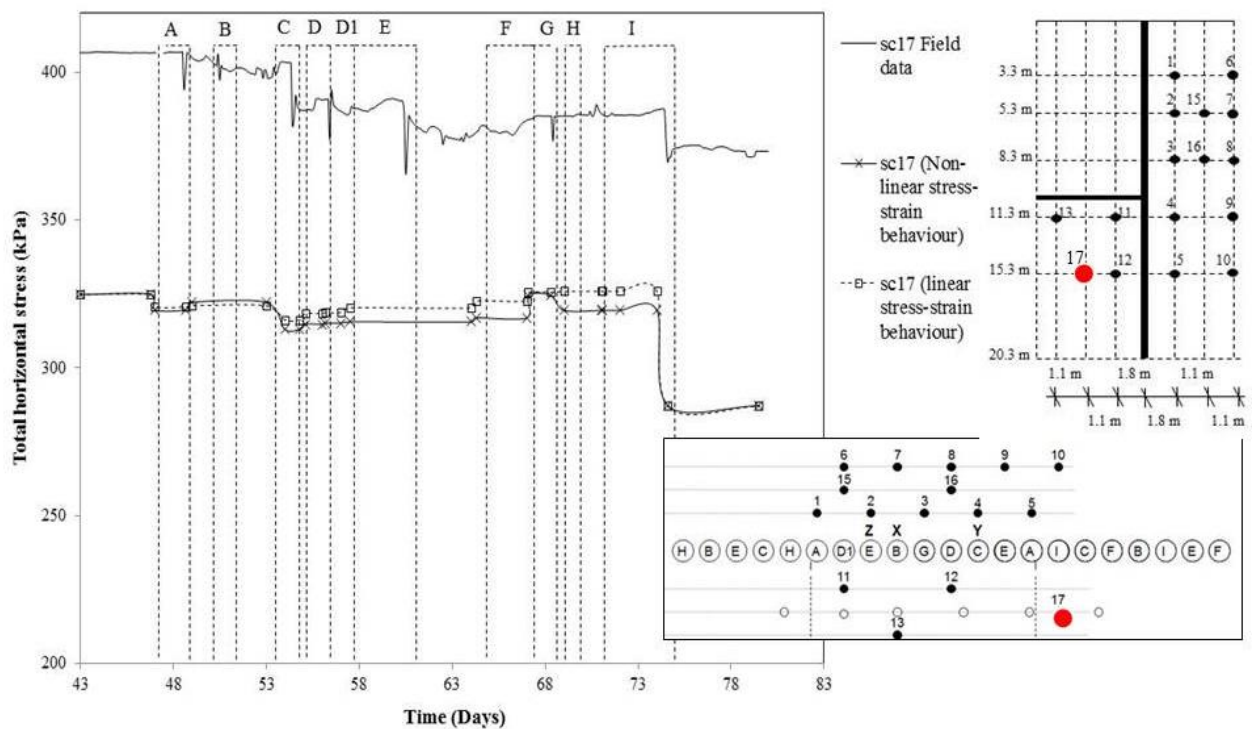


Figure 4.16. Total horizontal stresses (σ_{yy}) measured during wall installation compared with those calculated by the $FLAC^{3D}$ model (Spade Cell 17).

Overall, it can be observed, especially from Figures 4.4, 4.6, 4.7, 4.14 and 4.16 that the results from the non-linear stress-strain model are very slightly closer to the real data from the instrumented section of the bored pile wall at Ashford than those from the linear stress-strain model. However, the differences between the two models are small, and both the models capture the observed pattern of changes in stress in general.

4.3.2 Total horizontal stress profile on section A-A and B-B

As in Chapter 3, where the Young's modulus, E , was constant with the depth, the installation of the piles 'A' does not affect the soil further than $1.2d$ (where d is the diameter of the pile, $d = 1m$) from the centre of each installed pile, Figure 4.17 and 4.19, measured along the line of the wall. Thus, the stress state on sections A-A and B-B, Figure 3.13, is mainly influenced by the installation of the piles 'E' and 'I', Figure 3.13. Furthermore, it can be noted that (as reported in Chapter 3) the horizontal stresses in the area of the section A-A and B-B and the edges of the pile 'A' after the excavation of piles 'A' do not change.

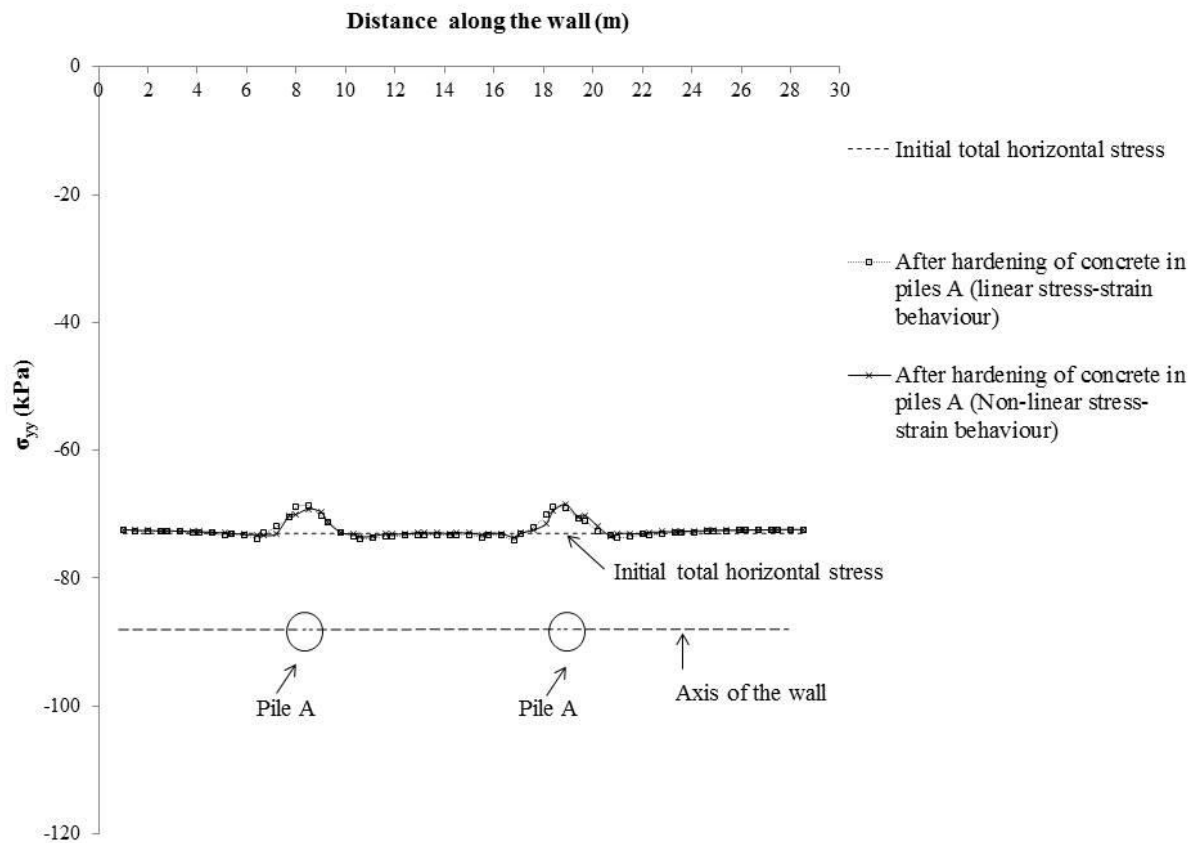


Figure 4.17. Horizontal stress (σ_{yy}) 0.3 m behind the wall after hardening of piles 'A' at a depth of 3.3 m.

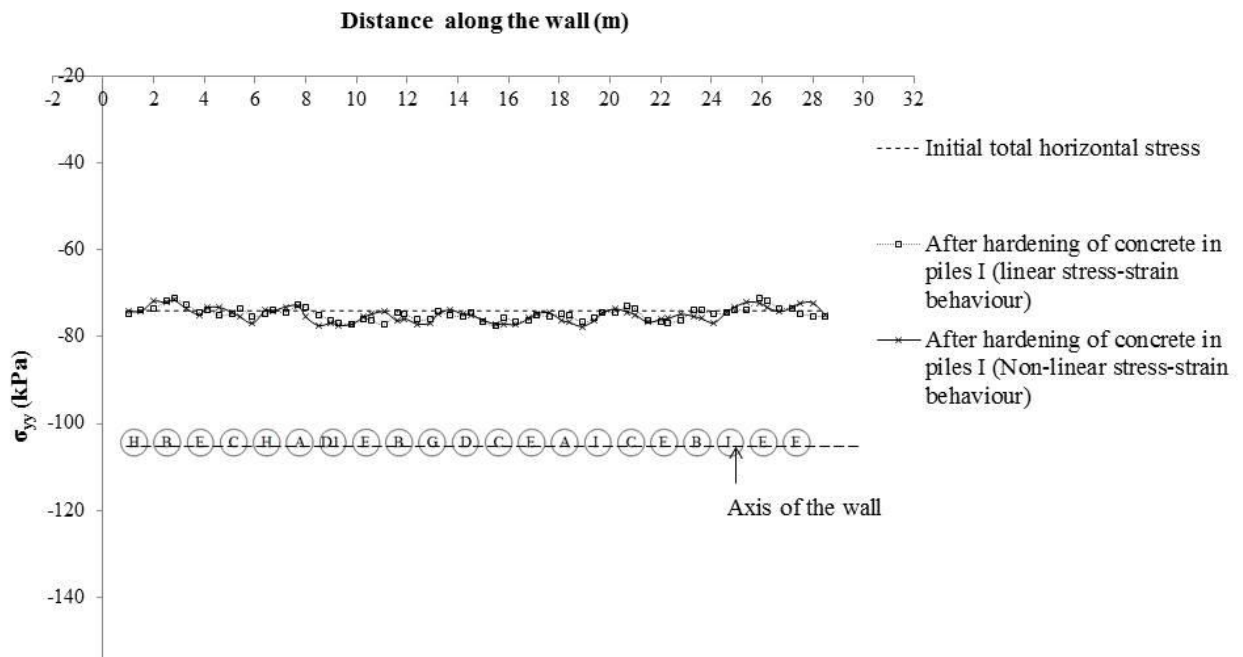


Figure 4.18. Horizontal stress (σ_{yy}) 0.3 m behind the wall after hardening of piles 'I' at a depth of 3.3 m.

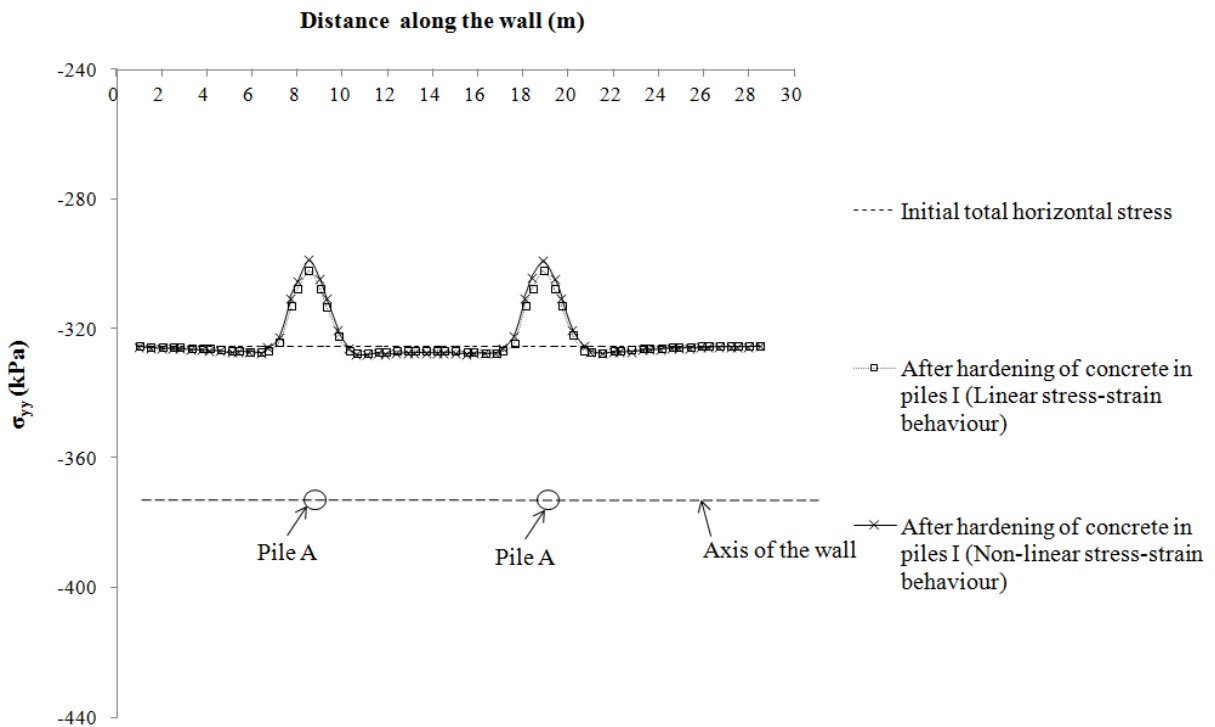


Figure 4.19. Horizontal stress (σ_{yy}) 0.3 m behind the wall after hardening of piles 'A' at a depth of 15.3 m.

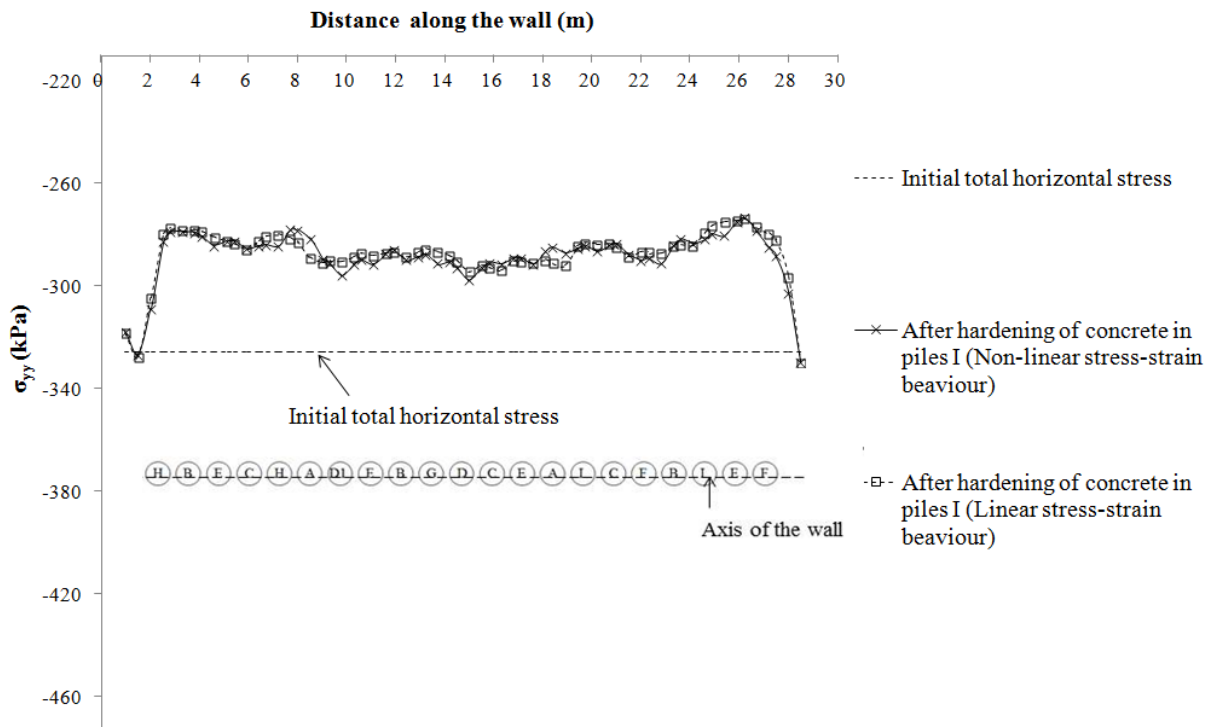


Figure 4.20. Horizontal stress (σ_{yy}) 0.3 m behind the wall after hardening of piles ‘I’ at a depth of 15.3 m.

Figure 4.21 shows the profiles of horizontal stress computed at section A-A, in Figure 3.13, in the modelling of wall installation after the hardening of the concrete of piles ‘A’, in Figure 3.13. On the whole, the stress changes computed with the non-linear stress-strain model are similar to those calculated using a linear stress-strain characteristic analysis. Furthermore, the major part of the horizontal stress relief is concentrated in the area above the toe of the pile, Figure 4.21. Compared to the results in Chapter 3, (Figure 3.14), a slight decrease in the total horizontal stress in the area from the head of the pile down to 14 m depth is apparent. However, as found in Chapter 3, from the head of the pile down to 15 m depth at a distance of 0.3 m behind the pile, only a minimal decrease in the total horizontal stresses is seen.

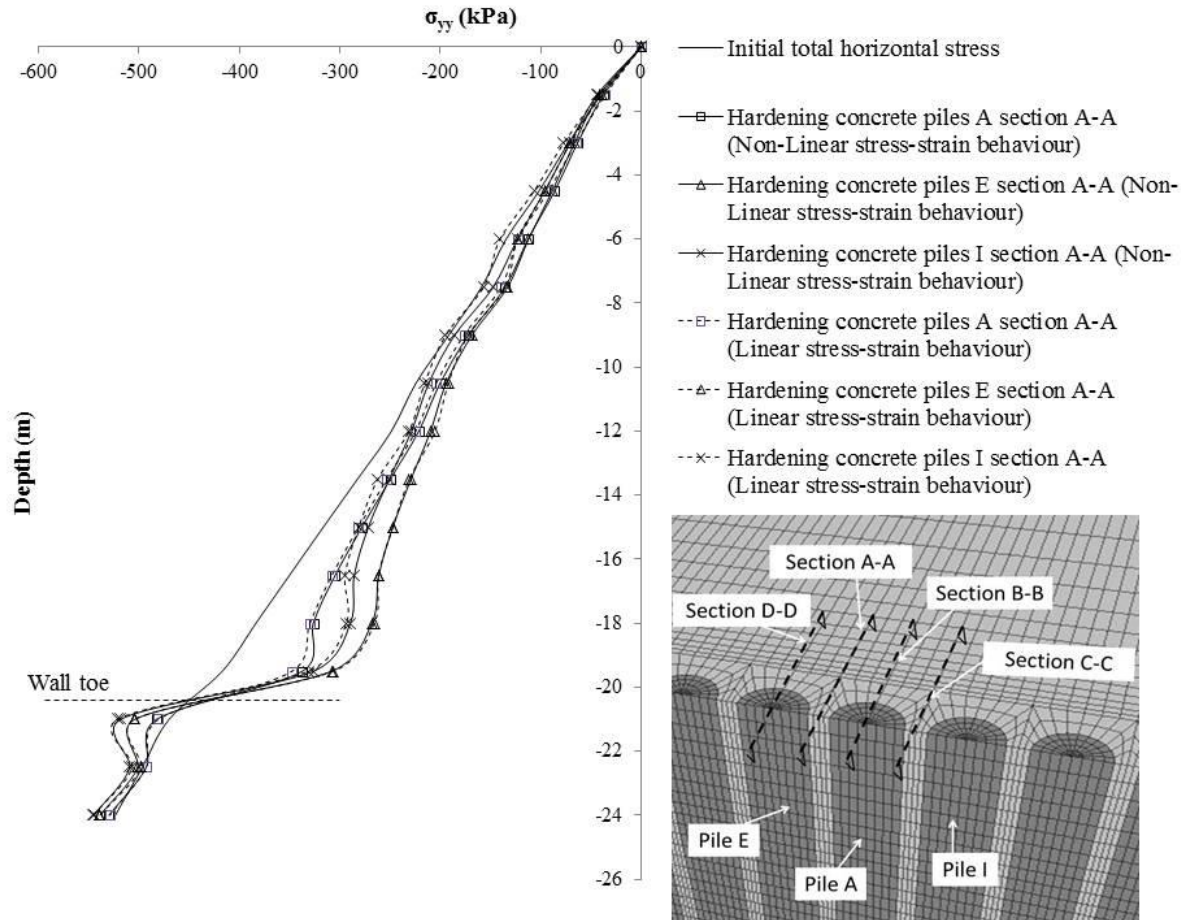


Figure 4.21. Variation of the total horizontal stress (σ_{yy}) acting on section A-A, with depth down to the wall at the end of construction of piles A, E and I. At a normal distance from the wall of 0.3 m.

Figure 4.21 shows that during the subsequent installation of piles ‘I’, the horizontal total stress behind the wall slightly increases in the area above the toe of the wall. However, after pile installation the total horizontal decreases are mainly concentrated in the area above the toe of the wall. This was observed in both analyses, with linear and non-linear stress behaviour. Moreover, a small increase of the total horizontal stress in the area below the toe of the pile was observed during the piles installation. As explained in Chapter 3, this is due to the redistribution of the horizontal stress via the shear stress (τ_{yz}), Figure 4.24, under the toe of the wall.

Figure 4.22 shows the horizontal stress change behind the wall at section B-B, Figure 3.13. It can be seen that the stress variations at section A-A and B-B are similar.

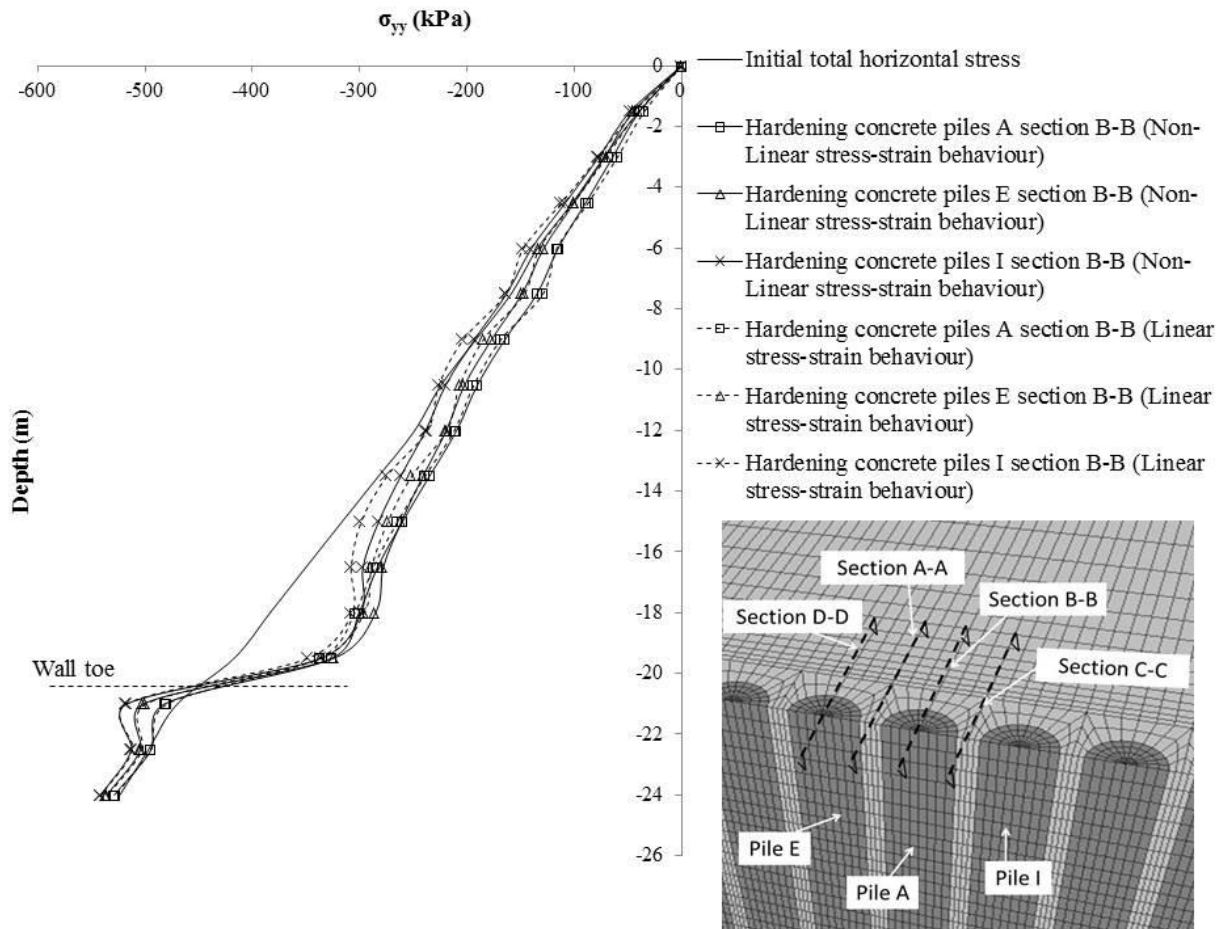


Figure 4.22. Variation of the total horizontal stress (σ_{yy}) acting on section B-B, with depth down to the wall at the end of construction of piles A, E and I. At a normal distance from the wall of 0.3 m.

Figure 4.23 shows the computed shear stress distribution on section B-B, Figure 3.13. Similar to the horizontal stress, the values of horizontal shear stress calculated using the non-linear model are close to those found in the linear stress-strain analyses. The shear stress (τ_{xy}) is more concentrated in the area from 12 m to 18 m depth.

After the excavation of piles 'I' and 'B', the horizontal shear stress (τ_{xy}) does not change substantially and these values remain less than 10 kPa. In contrast, after the excavation of pile 'E', a slight increase in the horizontal shear stress (τ_{xy}) especially near the toe of the wall was calculated, Figure 4.23.

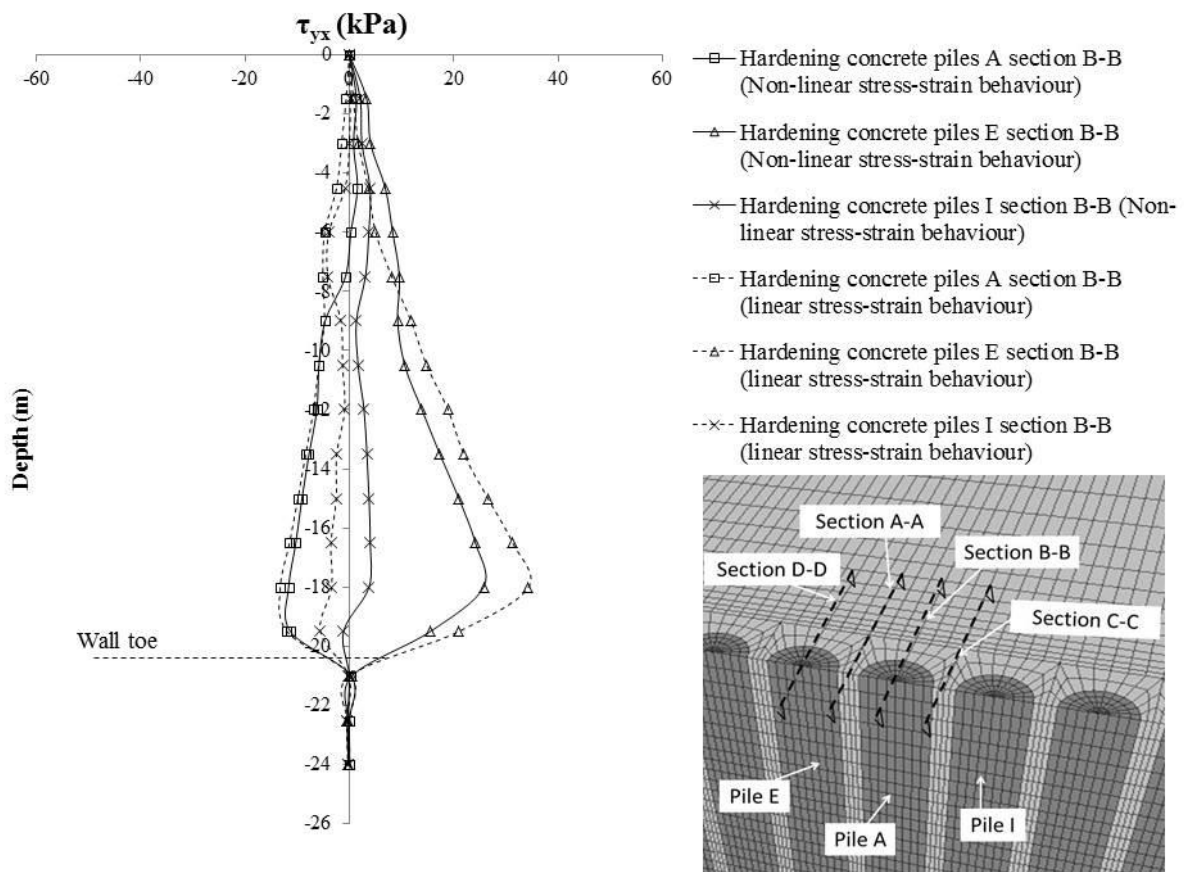


Figure 4.23. Variation of the total horizontal stress (τ_{yx}) acting on section B-B, with depth down to the wall at the end of construction of piles A, E and I. At a normal distance from the wall of 0.3 m.

Figure 4.24 shows the computed vertical shear stress (τ_{yz}) on section BB. These stresses are similar to those found by Ng and Yan (1998) who found a large variation in the vertical shear stress (τ_{yz}) near the toe. However, Ng and Yan (1998) calculated a large variation in the shear stress (τ_{yz}) in the area below the toe of the wall. Instead, for a bored pile wall, the shear stresses (τ_{yz}) during wall installation are mainly concentrated in the soil above the toe of the pile. Furthermore, it can be seen that after the excavation of the piles 'I' there is a slight difference between the vertical shear stresses (τ_{yz}) found using the non-linear and the linear stress-strain models. However, on the whole, the vertical shear stresses (τ_{yz}) are similar in both of the analyses.

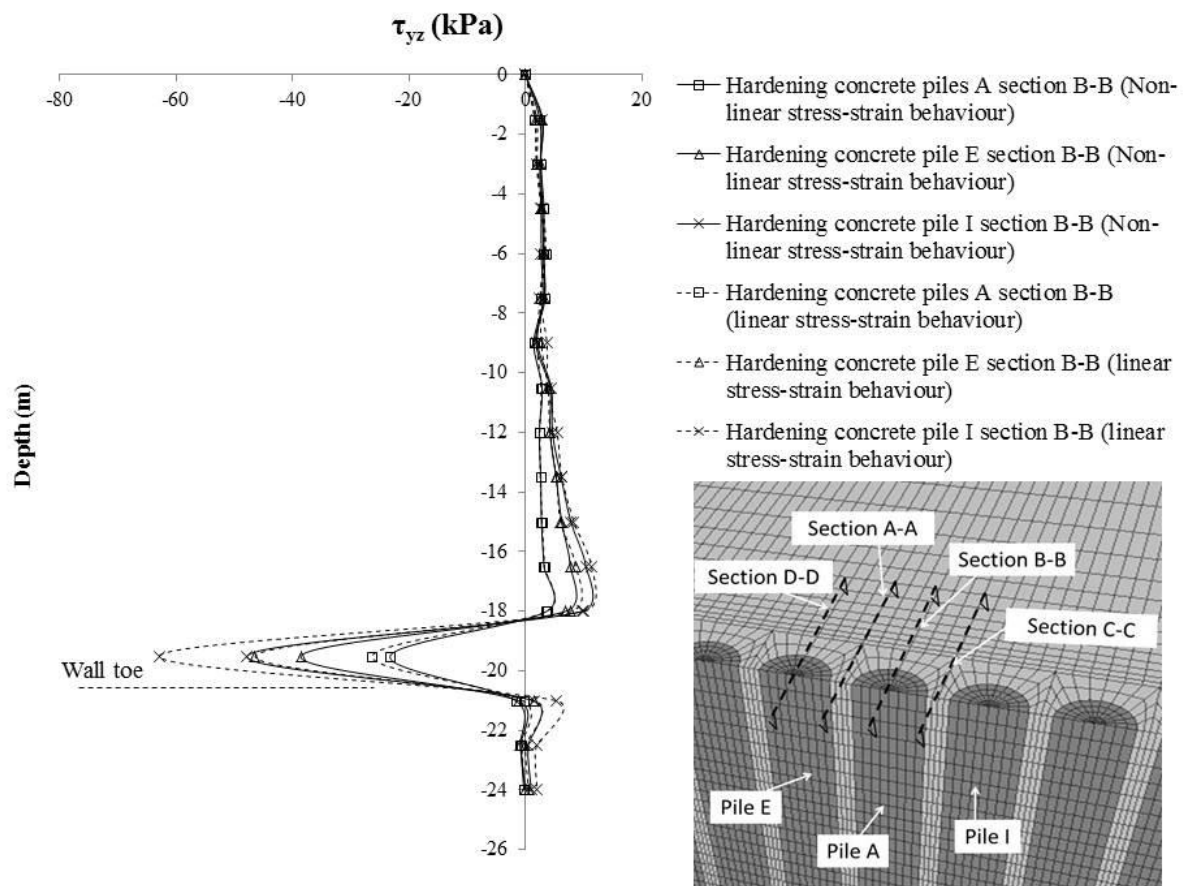


Figure 4.24. Variation of the total horizontal stress (τ_{yz}) acting on section B-B, with depth down to the wall at the end of construction of piles A, E and I. At a normal distance from the wall of 0.3 m.

4.3.3 Total horizontal stress distribution normal to the centre of the wall following the completion of the bored piles wall

Figures 4.25, 4.26, 4.27 and 4.28 show the variation of the computed horizontal total stress, σ_{yy} , with distance perpendicular to the centre of the wall after the completion of the wall. Again, it can be noted that the results obtained from the non-linear stress-strain model are almost identical to those from the linear stress-strain analyses. At 1 m distance from the wall, Figure 4.26, the stress state is similar to that 0.5 m from the wall, Figure 4.25. However, at 1 m behind the wall, Figure 4.26, the horizontal stress relief above the toe of the wall is slightly less than at 0.5 m behind the wall, Figure 4.25. The horizontal stress relief 0.5 m and 1 m behind the wall is minimal from the head of the wall down to 12 m depth.

Figure 4.27 shows the computed horizontal stress distribution with depth 4 m behind the wall. Above the toe of the wall the horizontal stress relief becomes minimal and below the toe of the wall the total horizontal stress increases only slightly.

The influence of wall construction on the initial stress condition became minimal at a distance of 10 m from the wall, Figure 4.28.

The measured results from spade cells 6 and 7, Figures 4.8 and 4.9, are similar to the computed data shown in Figure 4.27. The horizontal stresses do not change in the region of soil between the surface and 8 m depth. On the contrary, a slight decrease in the horizontal total stress was calculated in the area 4 m from the wall for a depth of 8 m down to the toe of the wall, Figure 4.27. As a matter of fact, decreases in the total horizontal stresses were measured from spade cells 8 and 9, Figures 4.10 and 4.11. These spade cells are 4 m from the wall, at depths of 8.3 m and 11.3 m respectively below from the surface of the wall.

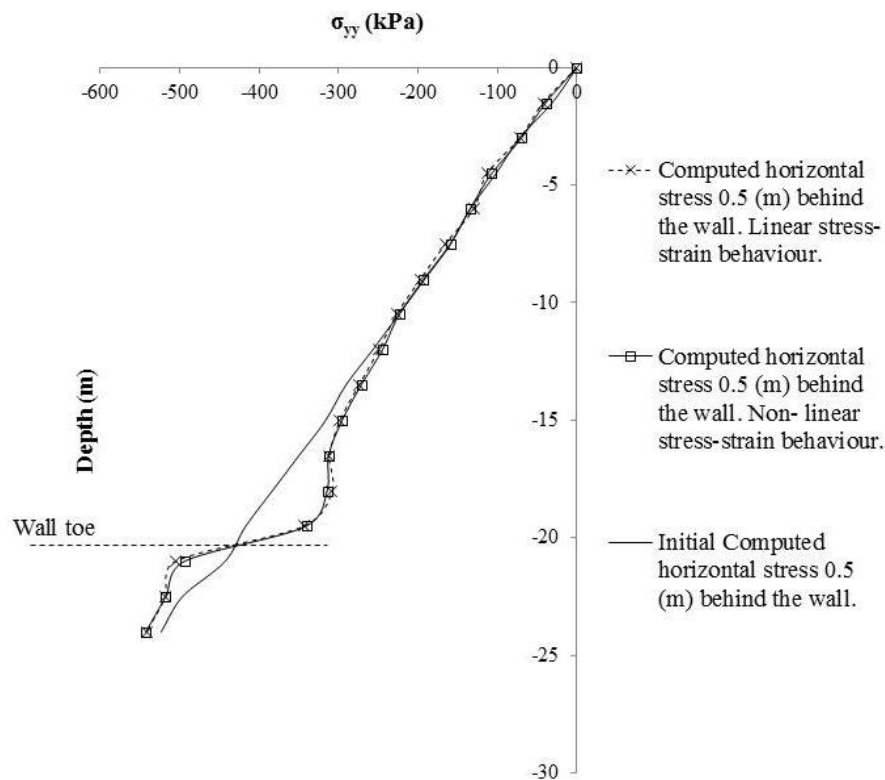


Figure 4.25. Computed horizontal total stress (σ_{yy}) 0.5 m behind the wall on section B-B.

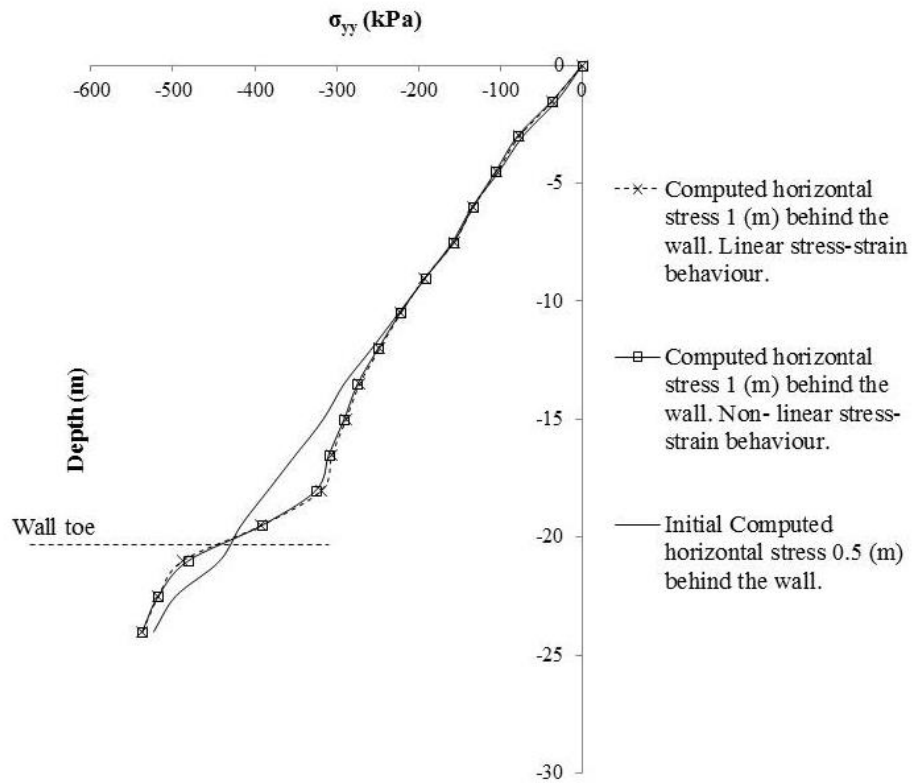


Figure 4.26. Computed horizontal total stress (σ_{yy}) 1 m behind the wall on section B-B.

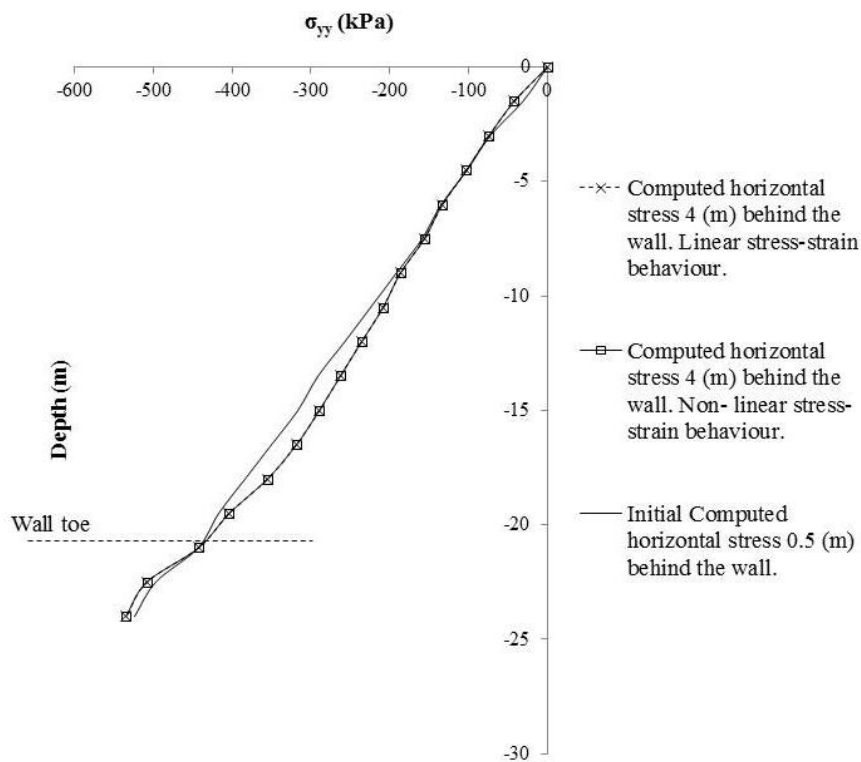


Figure 4.27. Computed horizontal total stress (σ_{yy}) 4 m behind the wall on section B-B.

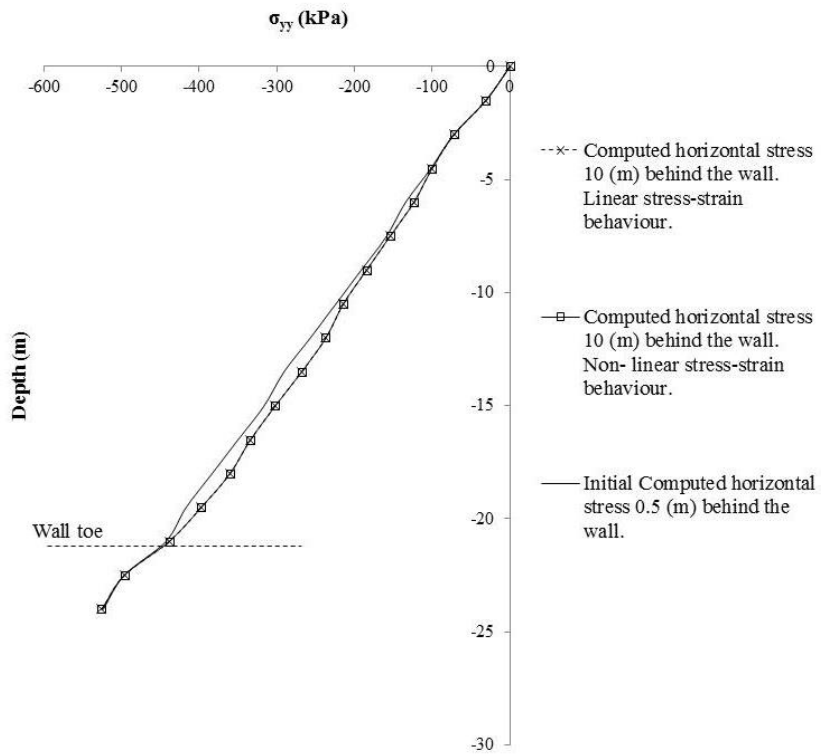


Figure 4.28. Computed horizontal total stress (σ_{yy}) 10 m behind the wall on section B-B.

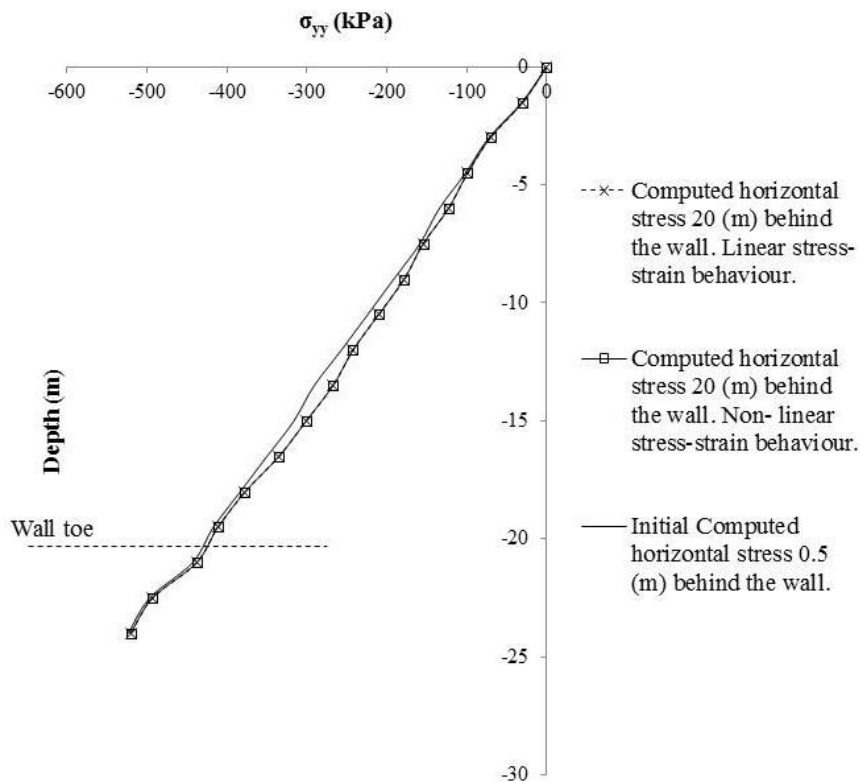


Figure 4.29. Computed horizontal total stress (σ_{yy}) 20 m behind the wall on section B-B

4.3.4 Horizontal displacement

The prediction of ground movements is of primary importance to assess possible damage to neighbouring structures. Pantelidou (1994) found that the displacements calculated during excavation in a finite element analysis in which wall installation was modelled, were much smaller than those in an analysis starting with the wall already in place. The reason was that some relaxation of lateral stress had already taken place during wall installation. Therefore, the stress relief during excavation is not as dramatic as it is when the analysis starts with high in-situ stress conditions.

Gunn *et al.* (1992) concluded that the effect of wall installation is more important in the case of a wall propped at the top. They explained this as the propping action “locking in” the reduction in lateral stresses associated with wall installation. This is not obvious from the results of the finite element analyses in the present work.

Figure 4.30 shows the horizontal displacement profile on section B-B, Figure 3.13, calculated using two different models, with non-linear and linear stress-strain characteristics.

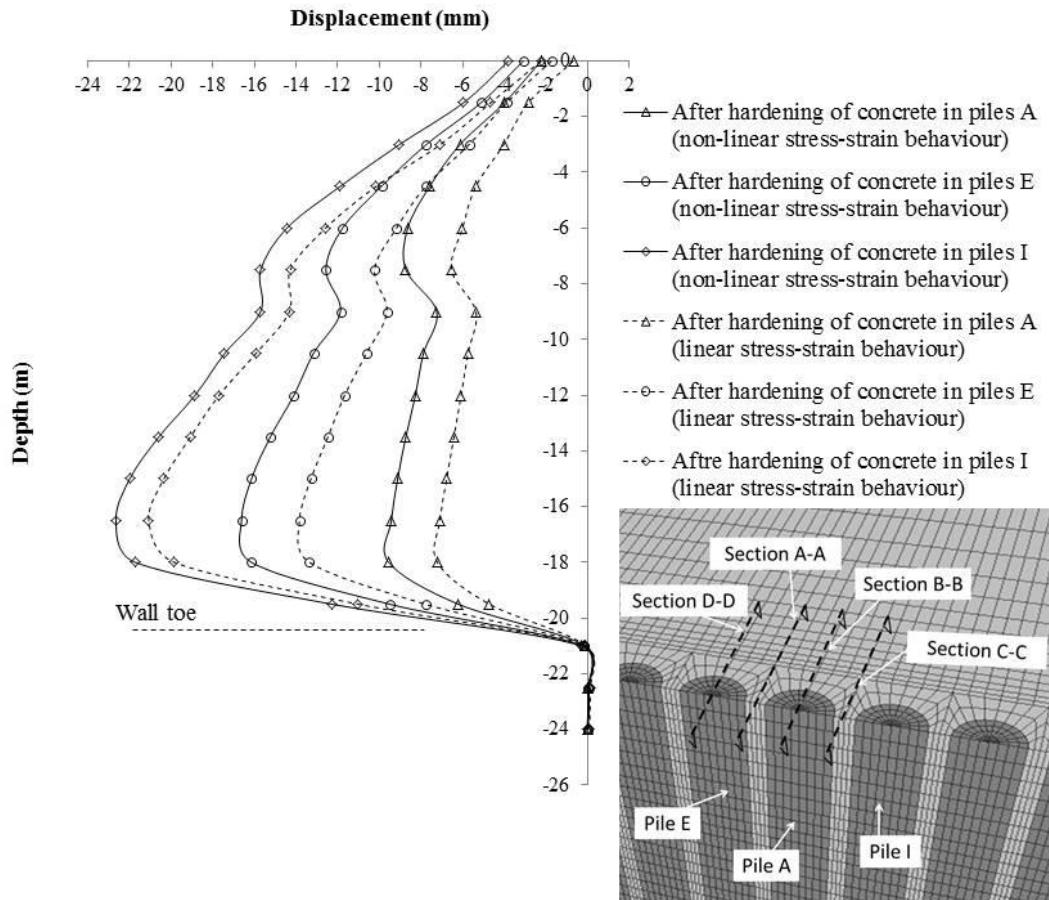


Figure 4.30. Horizontal displacement along the section B-B calculated in the 3D analysis of installation of the diaphragm wall. At a normal distance from the wall of 0.3 m.

The horizontal displacements were calculated after the excavation of piles ‘A’, ‘E’ and ‘I’. Figure 4.30 shows that the computed horizontal displacements assuming non-linear stress-strain behaviour at section B-B are larger than those calculated assuming a linear stress-strain soil model, even if the initial stiffness was similar in both models (Figure 4.1). The horizontal deformations along the panel length are clearly not uniform.

Again, in Figure 4.30 it can be seen that the horizontal displacements, after the installation of a row of piles, are largest at 18 m depth from the surface. This is different from the finding of Gourvenec and Powrie (1999) that after the installation of a diaphragm wall the horizontal displacements were larger in the soil close to the surface. Figure 4.30 indicates that the maximum horizontal displacements calculated with non-linear and linear stress-strain characteristics were 23 mm and 20 mm respectively. Furthermore, the horizontal displacements found in Chapter 3, which were calculated using constant soil properties with depth, are distinctly different from those found in Chapter 4. In Figure 3.30, the maximum

horizontal displacement is 3.5 mm while in Figure 4.30 the maximum horizontal displacements 0.3 m behind the wall on section B-B are 24 mm and 22 mm respectively for the non-linear and linear stress-strain characteristics.

Powrie *et al.* (1999) carried out a series of parametric finite element analyses to investigate the behaviour of an embedded retaining wall in London Clay supported by a stabilizing base slab. Three different soil models were used: the Brick model, the Schofield model, and an elastic/Mohr-Coulomb plastic model. They found that the wall movements calculated in the finite element analyses depend more on the soil stiffness than on the soil model. They reported that the lateral stresses and wall bending moments calculated depend on both the soil model and the soil stiffness, while the calculated ground movements depend on both the soil model and soil stiffness. The comparison between Figure 3.27 with the results from the linear stress strain model in 4.30 shows that the differences in soil displacement are mainly due to the implementation of different values of Young's modulus, Figure 4.1.

The large discrepancy between the displacements calculated in the non-linear and linear stress strain models, Figure 4.30, and the results found in Chapter 3 using a constant value of the Young's modulus, Figure 3.30, seem to suggest that the calculated ground movements are mainly affected by the soil stiffness. This was also observed by Powrie *et al.* (1999).

Figure 4.31 shows the horizontal displacement along section A-A (excavation boundary of the first pile installed) and section B-B (midside nodes) calculated after the installation of piles 'A'.

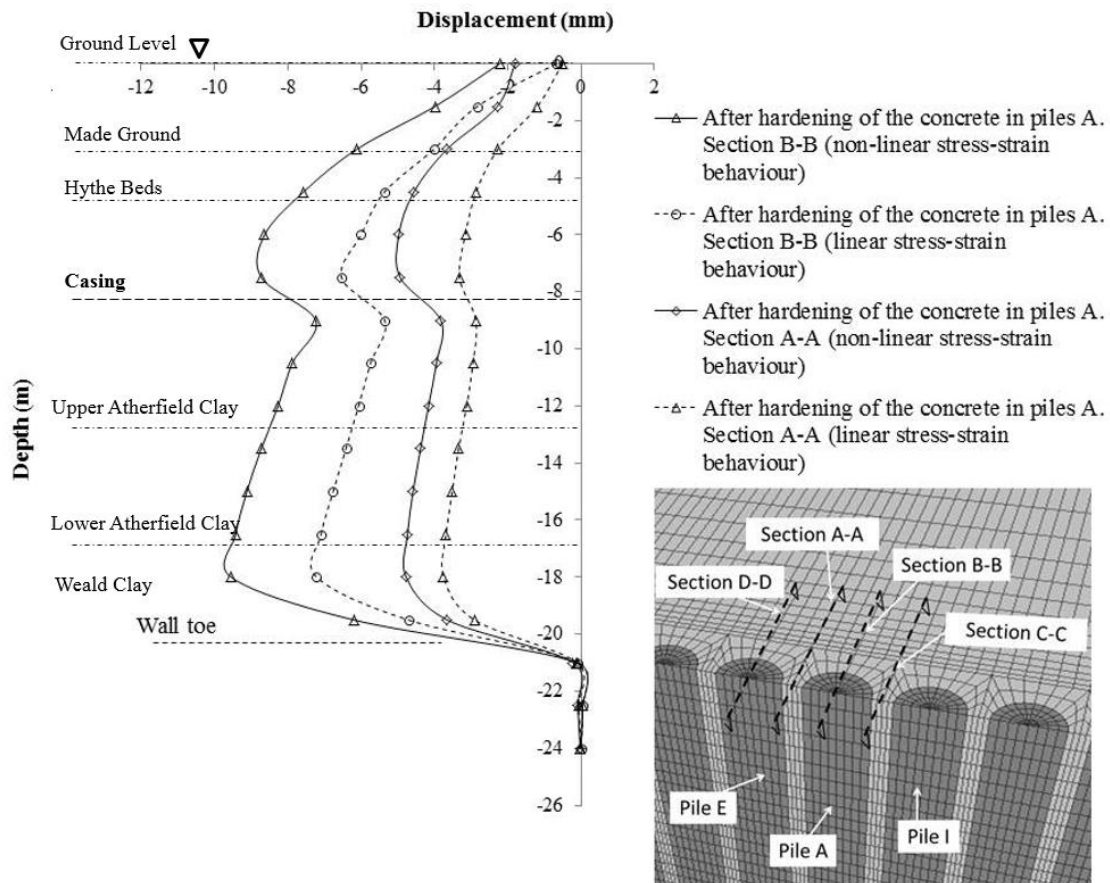


Figure 4.31. Horizontal displacement along the section B-B and A-A calculated in the 3D analysis after the hardening of the concrete in the piles A. At a normal distance from the wall of 0.3 m.

Displacements along the edge of the pile were quite small compared to the displacements along the centre line. Gourvenec and Powrie (1999) observed that the displacements along the edges of diaphragm wall panel were negligible, while displacements were largest at the centre of the panel.

In Figure 4.31 it can be noted that the horizontal displacements have a different distribution from the surface to 8 m depth, owing to the presence of the casing. In fact, as reported in Chapter 3, the presence of the casing was modelled by fixing and applying null lateral pressure on the excavated face were the casing was lowered.

For a typical diaphragm wall panel, 8 m long, 0.6 m wide and 15 m deep constructed in Gault clay, Ng and Yan (1998) found that the horizontal ground deformation at the centre of the panel was 5 times larger than that at the edge, which agrees with Gourvenec and Powrie (1999). Nevertheless, for a single pile excavation it was found that the horizontal

displacement at the centre of the pile, section B-B, was twice that at the edge, Figure 4.31. After a single pile installation, Figure 4.31, the horizontal displacements were smaller than those calculated by Gourvenec and Powrie (1999), Ng and Yan (1998) and Conti *et al.* (2012) during the installation of a single panel. As discussed in Chapter 3, this is mainly due to the effects of differences in geometry between a pile and a panel wall.

Figure 4.32 represents the horizontal displacement along the sections B-B (centre line of the pile) and A-A (edge of the pile), Figure 3.13.

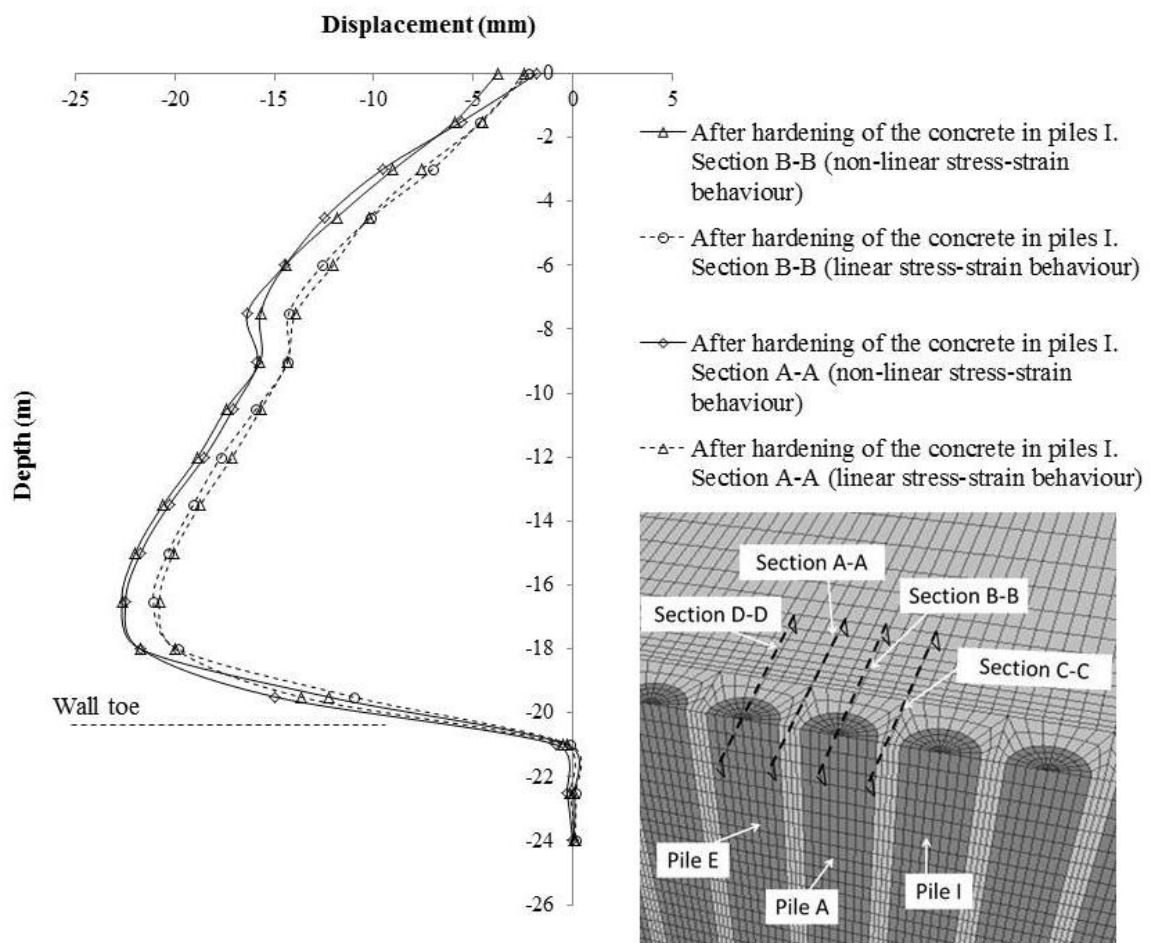


Figure 4.32. Horizontal displacement along the section B-B and A-A calculated in the 3D analysis after the hardening of the concrete in the piles I. At a normal distance from the wall of 0.3 m.

It can be noted that after wall construction, the horizontal stresses in the zone near the centre line of the pile, section B-B and near the edge of the pile, section AA, are similar with both the non-linear and linear stress strain models.

Figures 4.33 and 4.35 show the distribution of total horizontal displacement 0.4 m behind the piles, along the wall, after the installation of piles 'A', at depths of 3.3 m and 15.3 m respectively. The horizontal displacements are concentrated in the centre of the piles and become negligible at a distance of $1.2d$ (where d is the diameter of the pile, $d = 1\text{m}$) far from the centre of the pile, measured along the line of the wall.

Figures 4.34 and 4.36 show the distribution of the horizontal displacement 0.4 m behind the piles along the wall at the end of the whole installation. The stresses vary slightly along the wall.

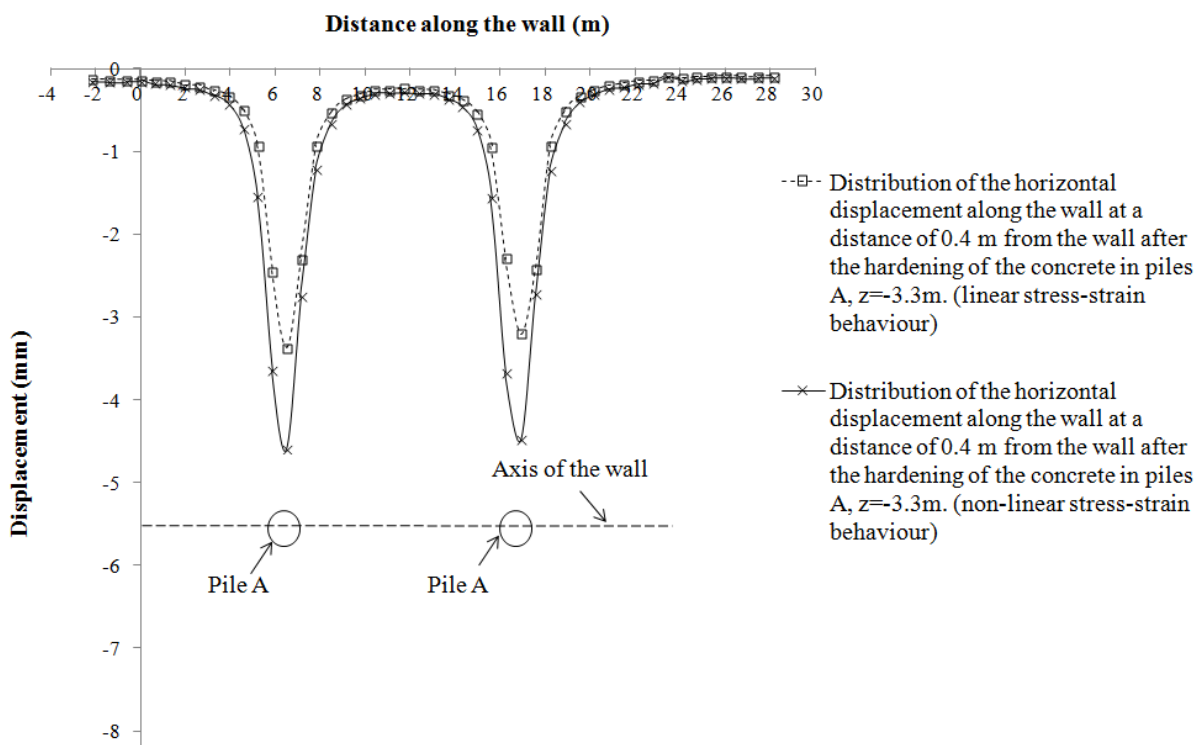


Figure 4.33. Distribution of the horizontal displacement 0.4 m behind the wall along the wall after the hardening of the concrete in piles 'A' at a depth of 3.3 m.

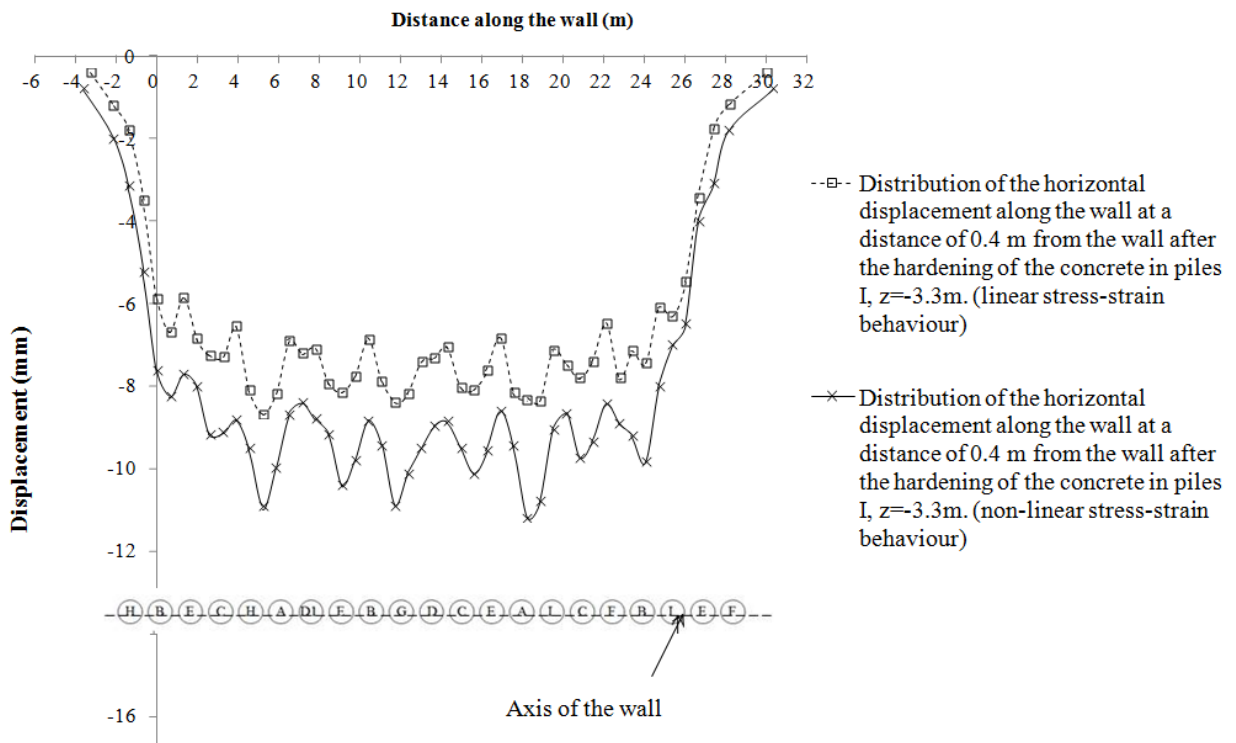


Figure 4.34. Distribution of the horizontal displacement 0.4 m behind the wall along the wall after the hardening of the concrete in piles 'I' at a depth of 3.3 m.

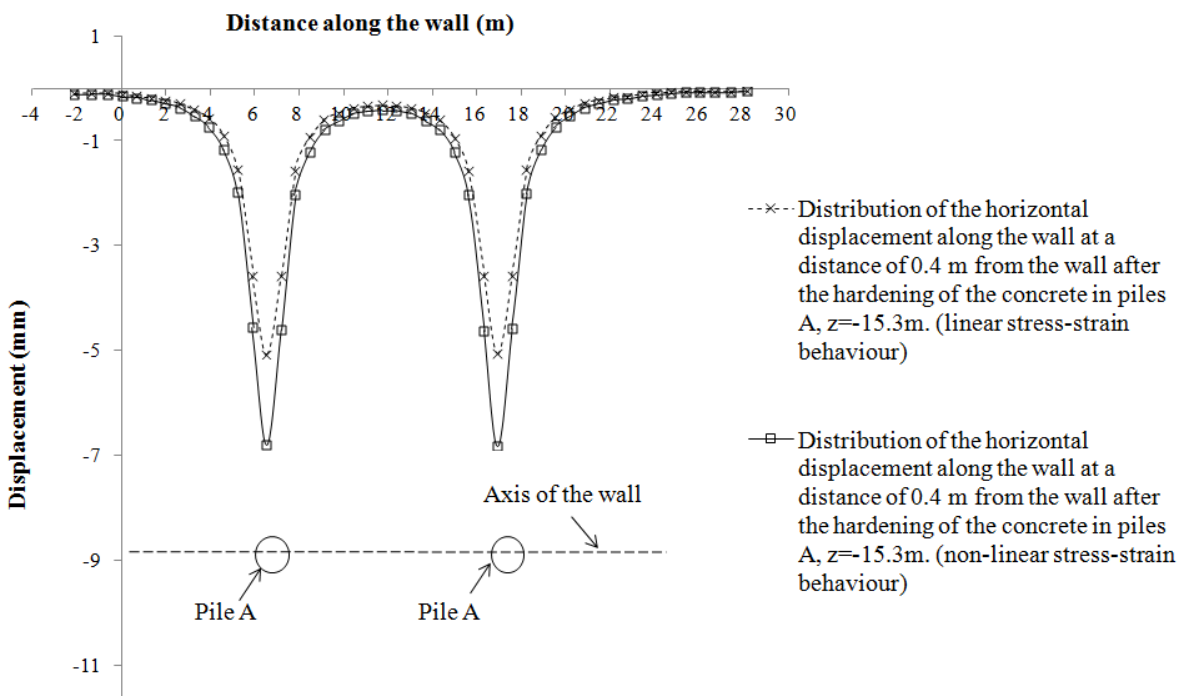


Figure 4.35. Distribution of the horizontal displacement 0.4 m behind the wall along the wall after the hardening of the concrete in piles 'A' at a depth of 15.3 m.

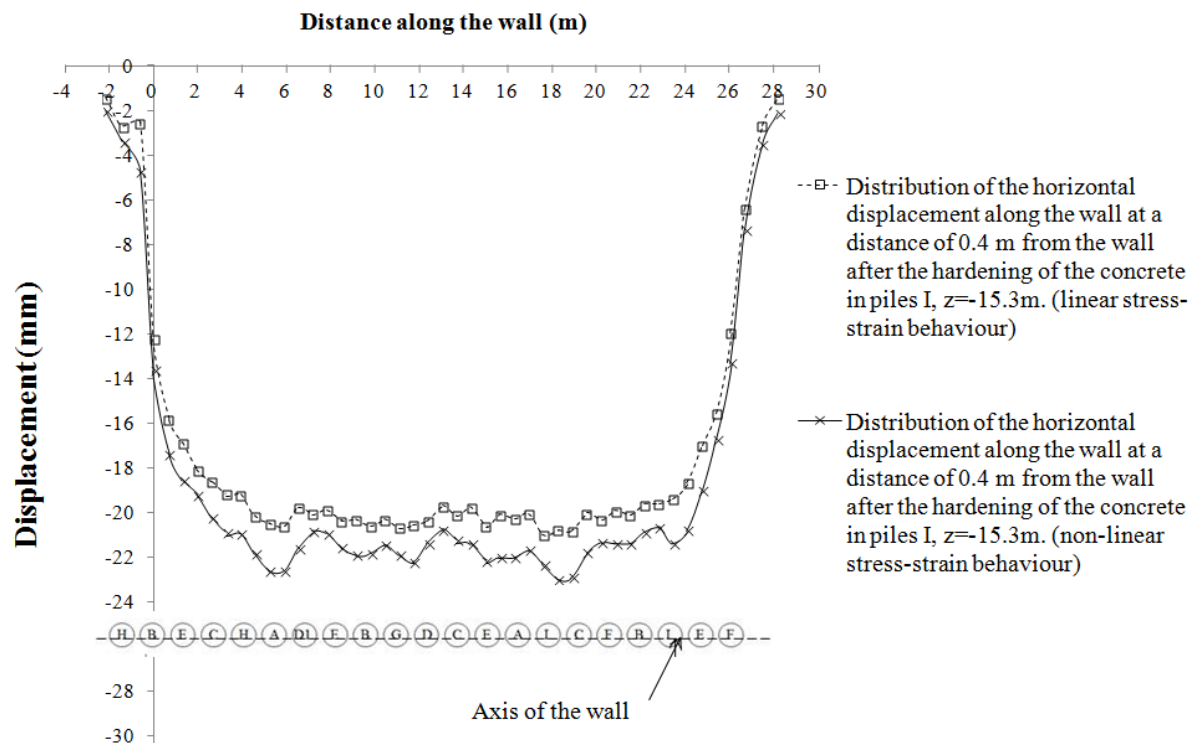


Figure 4.36. Distribution of the horizontal displacement 0.4 m behind the wall along the wall after the hardening of the concrete in piles ‘I’ at a depth of 15.3 m.

4.4 Summary

In this Chapter two $FLAC^{3D}$ analyses of the construction sequence of a bored pile wall in stiff clay have been conducted. Linear and non-linear stress-strain characteristics were implemented in the 3D model. The results from these analyses were also compared to those found in Chapter 3. The non-linear stiffness parameters suggested by Scott *et al.* (2003) were used for the Hythe Beds, Upper Atherfield Clay, Lower Atherfield Clay and Weald Clay. The following conclusions were made:

- Figures 4.2-4.16 compared the computed profiles of the total horizontal stress with those measured by the instrumentation at Ashford, Kent. The non-linear stress-strain characteristic gave overall slightly better results than the linear-stress-strain behaviour, but there was little difference between the two.
- Both of the analyses (non-linear stress strain and linear stress-strain characteristics) gave better results than those found in Chapter 3. This is mainly due to the fact that in the previous model in Chapter 3 a constant value of Young’s modulus, E , with depth, Table 3.2, was used.

- However, as in Chapter 3, where the Young's modulus, E , was constant with depth, the installation of a single pile did not affect the soil further than $1.2 d$ (where d is the diameter of the pile, $d = 1$ m) along the wall from the centre of the installed pile, Figure 4.17, 4.19.
- The major part of the horizontal stress relief is concentrated in the area above the toe of the pile, Figure 4.21. Compared with results in Chapter 3, Figure 3.13, a slight decrease of the total horizontal stress in the area from the head of the pile down to 14 m depth was observed.
- At distances of 0.5 m and 1 m from the wall, Figure 4.26, the final stress state was similar to that 0.4 m from the wall. At 4 m from the wall, the horizontal stress relief above the toe of the wall became minimal. Below the toe of the wall, only minor increases in the total horizontal stresses were apparent. The influence of wall construction on the initial stress condition became minimal at a distance of 20 m from the wall, Figure 4.29.
- Comparing the displacements calculated in Chapter 3 and Chapter 4 it was found that the differences on soil displacements are mainly due to the implementation of different values of Young's modulus, Figure 4.1. In Figure 4.28 it can be observed that the maximum horizontal displacement calculated with the non-linear stress-strain relationship was 23 mm. This is substantially different from the results in Chapter 3. In fact, in Figure 3.30, the maximum horizontal displacement was 3.5 mm.
- For a typical diaphragm wall panel, 8 m long, 0.6 m wide and 15 m deep constructed in Gault clay, Ng and Yan (1998) found horizontal ground deformations at the centre of the panel are 5 times larger than that at the edge. In contrast, for a single pile excavation it was found that the horizontal displacement at the centre of the pile is less than twice that at the edges, Figure 4.29. Again this implies that the different geometries between pile and panel lead to a different stress change and soil displacements in the ground close to the wall. This is similar to the results found by Gourvenec and Powrie (1999) who investigated the effect of panel aspect ratio on the response of the soil to the panel installation.

CHAPTER 5**COMPARISON OF THE 3D INSTALLATION EFFECTS FOR A DIAPHRAGM WALL CONSIDERING DIFFERENT CONSTRUCTION SEQUENCES****5.1 Introduction**

The effects of diaphragm wall installation are potentially significant (both in reality and in an analysis) because the associated changes in soil stress will cause ground movements during installation and influence the behaviour of the wall during the main excavation process (Gunn *et al.*, 1993; Symons *et al.*, 1993, Powrie *et al.*, 1996). The installation of a sequence of diaphragm wall panels in the ground, involving in each case excavation under a bentonite support slurry followed by placing, and subsequent hardening of the concrete, is, in reality, a complex three-dimensional event (Gourvenec and Powrie, 1999). This chapter includes a comprehensive numerical analysis of the 3D installation effects of a group of panels in an overconsolidated clay deposit. Several analyses were carried out to compare the final stress variations for five different installation sequences for a group of five panels installed in an

overconsolidated soil deposit. Based on previous research, this study investigates whether different sequences of panel installation could lead to pre-excavation stress distributions behind the wall. Changes in stress variation as a consequence of different wall construction sequences have not been investigated before, although Ng and Yan (1998) considered the construction sequence of single panels in stiff clay. Gourvenec and Powrie (1999) carried out a series of three-dimensional analysis to investigate the impact of panel length and three-dimensional effects on horizontal ground movement and changes in lateral stress, again using a single sequence of panel installation.

In this chapter, the stress changes after five different sequences of diaphragm wall installation were investigated and compared. The stress changes and horizontal soil displacement during the installation of a single panel and subsequently the installation of a group of panels are presented and compared to the most relevant works in the literature.

5.2 Numerical models

The numerical simulation of diaphragm wall construction was carried out using a finite difference programme *FLAC^{3D}* 4.0. The global model for the installation of the diaphragm wall panels consisted of a rectangular parallelepiped, of dimensions 25 m high, 20 m deep and 45 m longitudinally, Figure 5.1. Particular attention was paid to the choice of the finite element mesh. The density of the mesh was significantly increased around the wall, Figure 5.1.

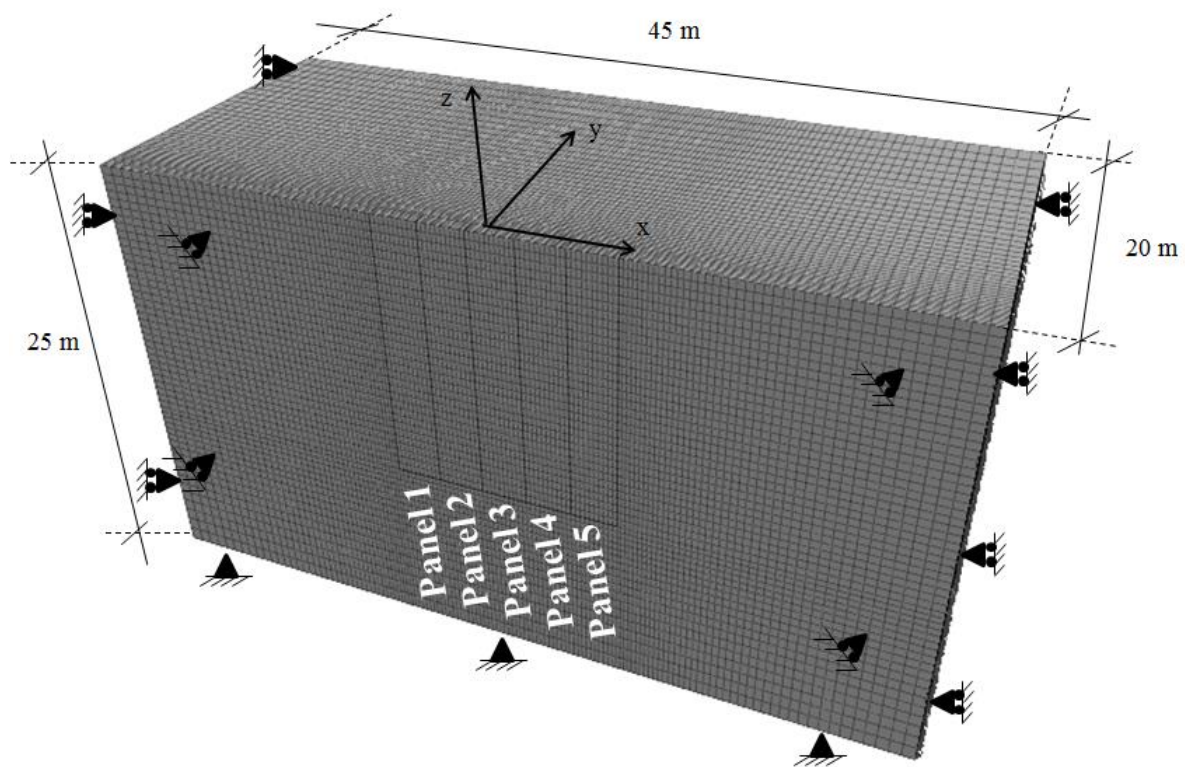


Figure 5.1. Finite-Difference mesh.

In these analyses the geometries were similar to those used by Gourvenec and Powrie (1999). One plane of symmetry, $y = 0$ m, was used in generating the finite difference mesh. The vertical planes, $x = 22.5$ m, and, $x = -22.5$ m, were allowed to move freely in the y -direction and the z -direction but not in the x -direction. The vertical planes, $y = 0$ m, and $y = 25$ m, were free to move in the x -direction and z -direction but not in the y -direction. Finally on the boundary horizontal plane, $z = -25$ m, all movements were restrained.

Five different diaphragm wall installation sequences were investigated and the soil stress changes close to the wall were investigated after each sequence, Figure 5.2.

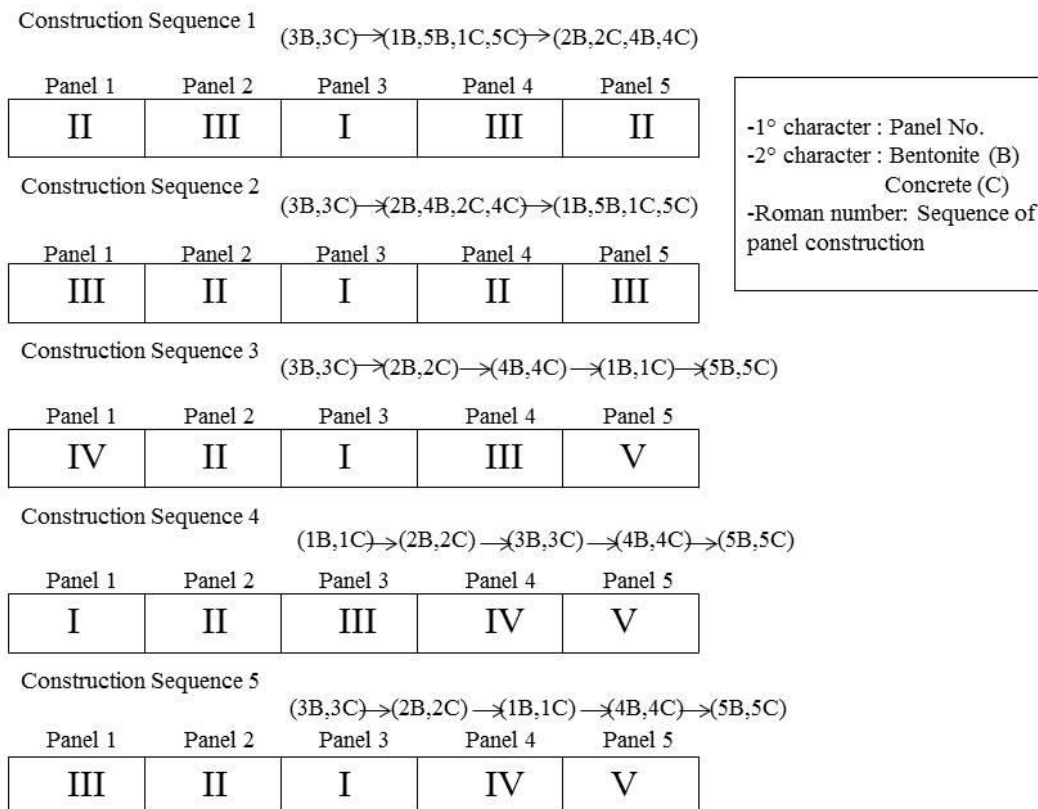


Figure 5.2. Different sequences of panel installation. (a) Construction sequence 1, (b) Construction sequence 2, (c) Construction sequence 3, (d) Construction sequence 4, (e) Construction sequence 5.

5.2.1 Soil model and parameters

The soil models chosen for these analyses were the same as those used by Gourvenec and Powrie (1999). The soil has been modelled as an undrained linear elastic, perfectly plastic isotropic materials with a Mohr-Coulomb yield surface and a Young's Modulus increasing with depth. The ground conditions were representative of a uniform stratum of stiff, overconsolidated, saturated clay. The geotechnical parameters were unit weight, $\gamma = 20 \text{ kN/m}^3$, effective internal friction angle $\phi_u = 0$, shear strength $c_u = 60 + 10z'$ kPa, undrained Young's Modulus $E_u = 21.6 + 7.2z'$ MPa, Gourvenec and Powrie (1999), where, z' , is the depth below the ground surface. Soils were assumed to be undrained during the construction stages of the diaphragm wall panels. Undrained conditions were assumed by Ng and Yan (1998). The concrete diaphragm wall was modelled as an isotropic elastic material (Gourvenec and Powrie, 1999; and Ng and Yan, 1998).

5.2.2 In situ stresses

The in situ stress state initialized at the beginning of the analysis is reported in terms of the earth pressure coefficient (K_0) in Figure 5.3. The *in situ* earth pressure coefficient profile was the same as that used by Gourvenec and Powrie (1999).

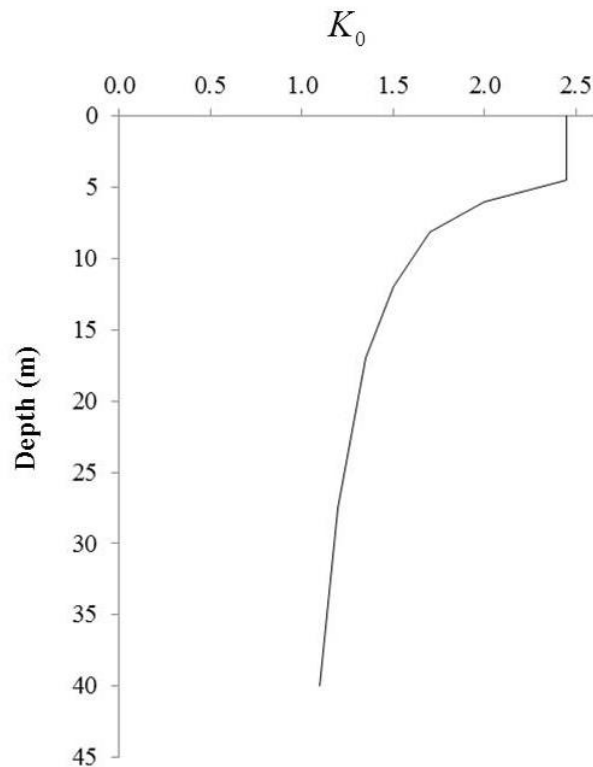


Figure 5.3. In situ earth pressure coefficient profiles.

The vertical effective stresses were determined by considering the pore water pressures to be hydrostatic with depth below a water table at ground level. The initial conditions of horizontal stress were based on the pressuremeter data from the Batheaston bypass (Mackinson, 1998; Gourvenec and Powrie, 1999).

5.2.3 Installation procedure

The dimensions of each diaphragm wall panel were 2.5 m long, 0.7 m thick and 15 m deep as shown in Figure 5.4.

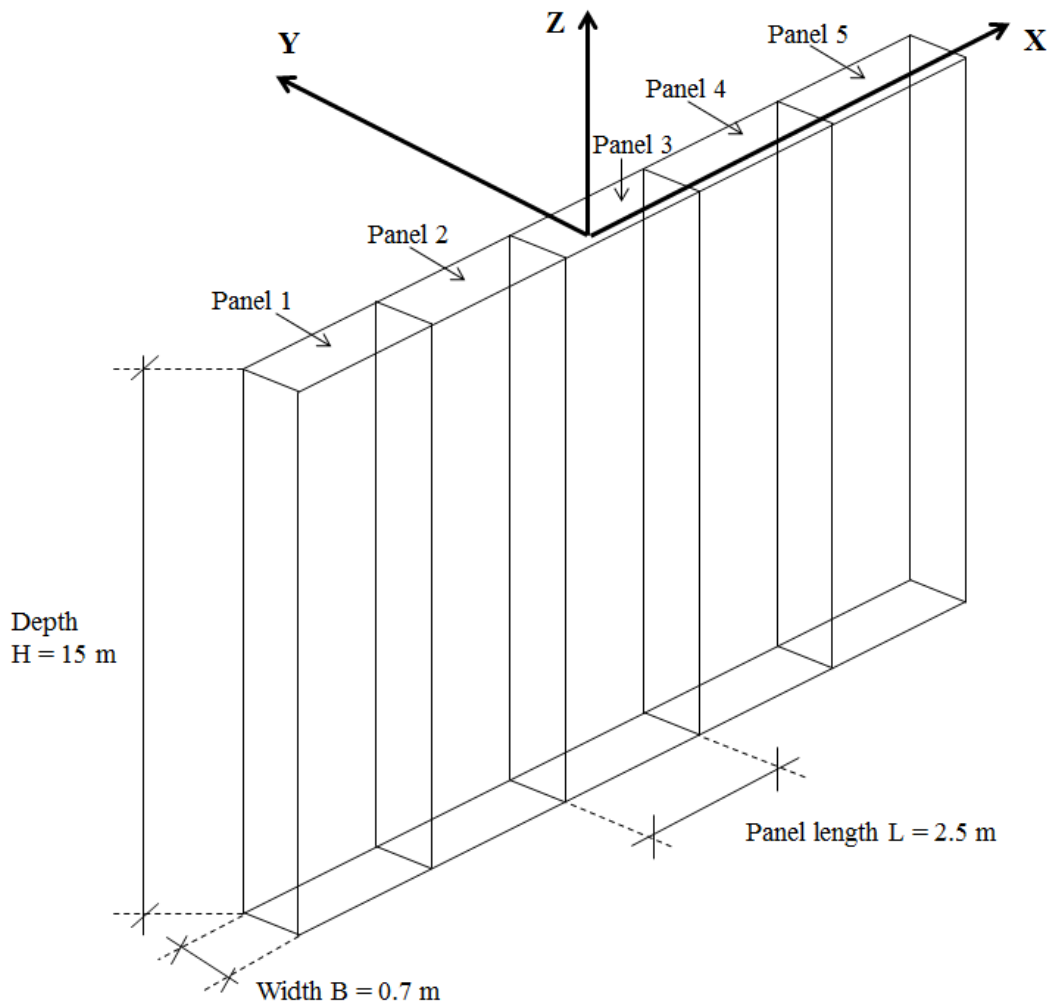


Figure 5.4. Wall Geometry.

The construction steps for each of the five analyses are similar to the work presented by Ng and Yan (1998) and Gourvenec and Powrie (1999) and they are described as follow:

1. The installation of the first panel was carried out by excavating a 3 m deep trench and applying normal hydrostatic bentonite pressure on the face of the excavation. This procedure was repeated until 15 m depth was reached, Figure 5.6. The excavation of the diaphragm wall was modelled using the NULL command in *FLAC^{3D}*. The command APPLY NSTRESS was used to apply the normal hydrostatic bentonite pressure (i.e., the normal pressure was a function of the unit weight, 10.1 kN/m^3 , and the depth of the bentonite) on the excavated face, Figure 5.5.
2. At this stage the concrete was cast into the trench by increasing the lateral pressure inside the excavated zone from the bottom using the empirical bilinear wet concrete

pressure proposed by Ng (1992) and Lings *et al.* (1994), who compared the results given by the equation with a number of case histories for various sites and ground conditions. The bilinear envelope adopted for the construction process was as follows:

$$\sigma_h \text{ (kPa)} = \begin{cases} 24z \rightarrow z \leq 5.5m \\ 64 + 10.1z \rightarrow z \geq 5.5m \end{cases} \quad \text{Equation 5.1}$$

where z represents the depth below the head of the pile. As reported by Ng and Yan (1998) this equation suggests that lateral pressure exerted by concrete placed under bentonite in a bored pile wall follows a bilinear pressure envelope, in which full fluid concrete pressure applies only above a critical depth. Below this depth, the pressure increases with depth following the slope of the hydrostatic bentonite line. This proposed envelope takes account of the effects of concrete consolidation and set on the lateral pressure during concreting.

3. The hardening of the concrete was modelled by replacing the panel with elastic material elements and removing the applied bilinear concrete pressure. Again, the same procedure was used by Gourvenec and Powrie (1999) and Ng and Yan (1998).
4. This procedure is applied to the successive panel or panels depending on which construction sequence is modelled, Figure 5.2. It was chosen to use five different construction sequences to cover a range of diaphragm wall installation schemes.
5. As the procedure of wall installation is usually rapid, an undrained assumption has been made for this analysis following Ng and Yan (1998).

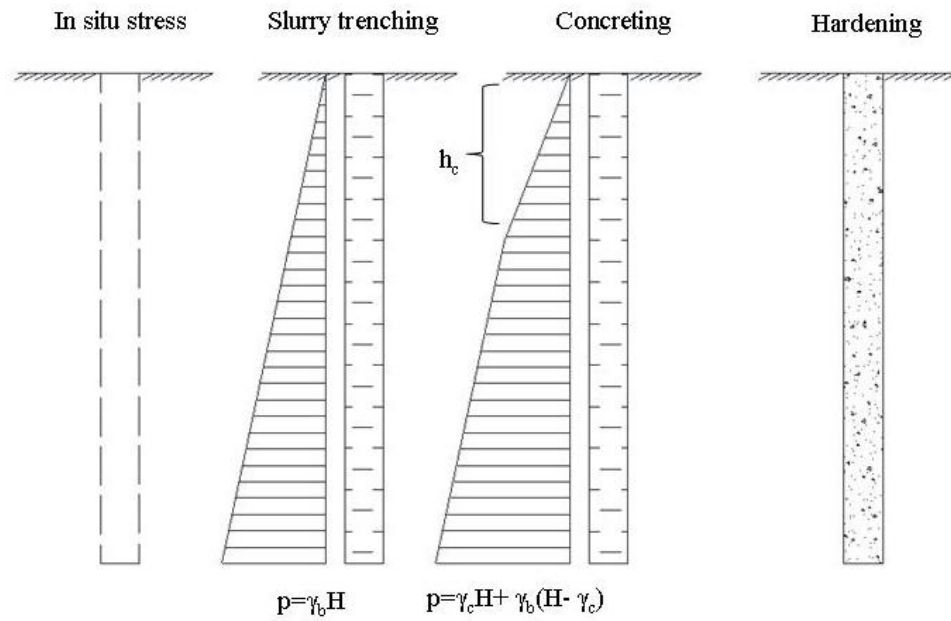


Figure 5.5. Sequence of construction stages. (a) In situ stress (b) Slurry trenching, (c) Concreting, (d) Hardening of concrete and (e) excavation in front of the wall.

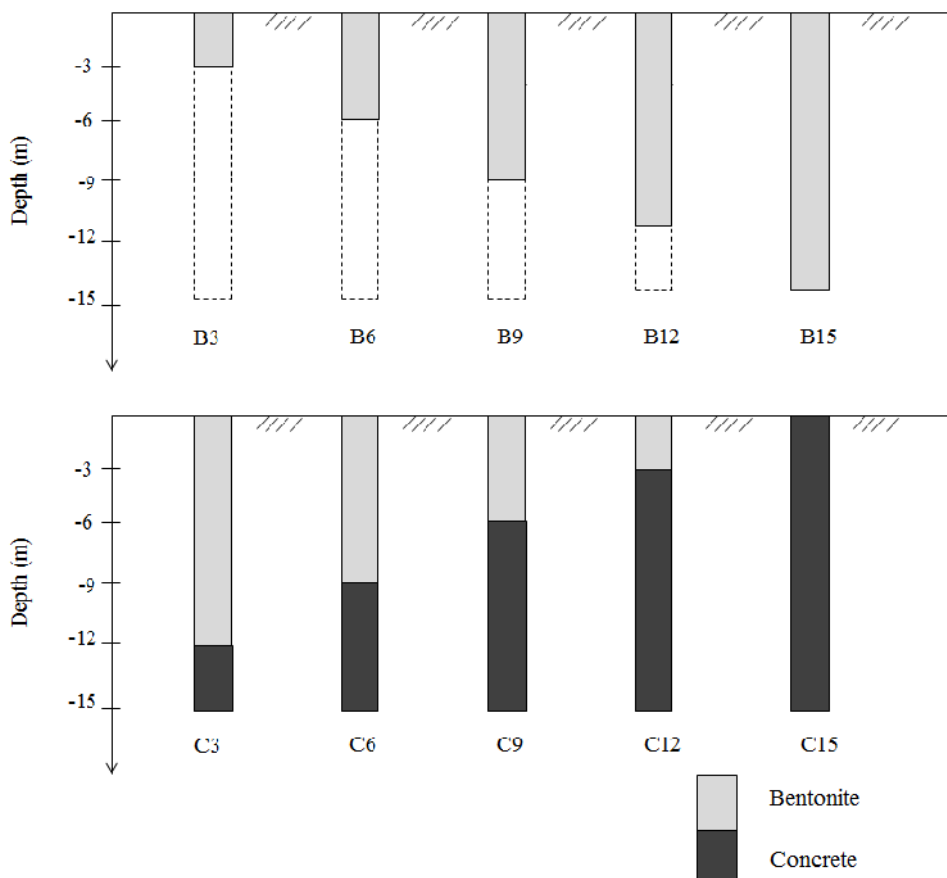


Figure 5.6. Modelling sequence for Construction Diaphragm Wall Panel.

5.3 Results and analysis

5.3.1 Stress distributions for a single panel excavation

In this section the stress changes during the construction of a single panel are presented and discussed. Figure 5.7 shows the notation adopted in this analysis to describe the 3D stress state. The total horizontal stresses behind the wall are redistributed laterally via the shear stresses component (τ_{xy}), and vertically via the shear stress component (τ_{zy}). Figure 5.8 shows the plan view of the diaphragm wall panels.

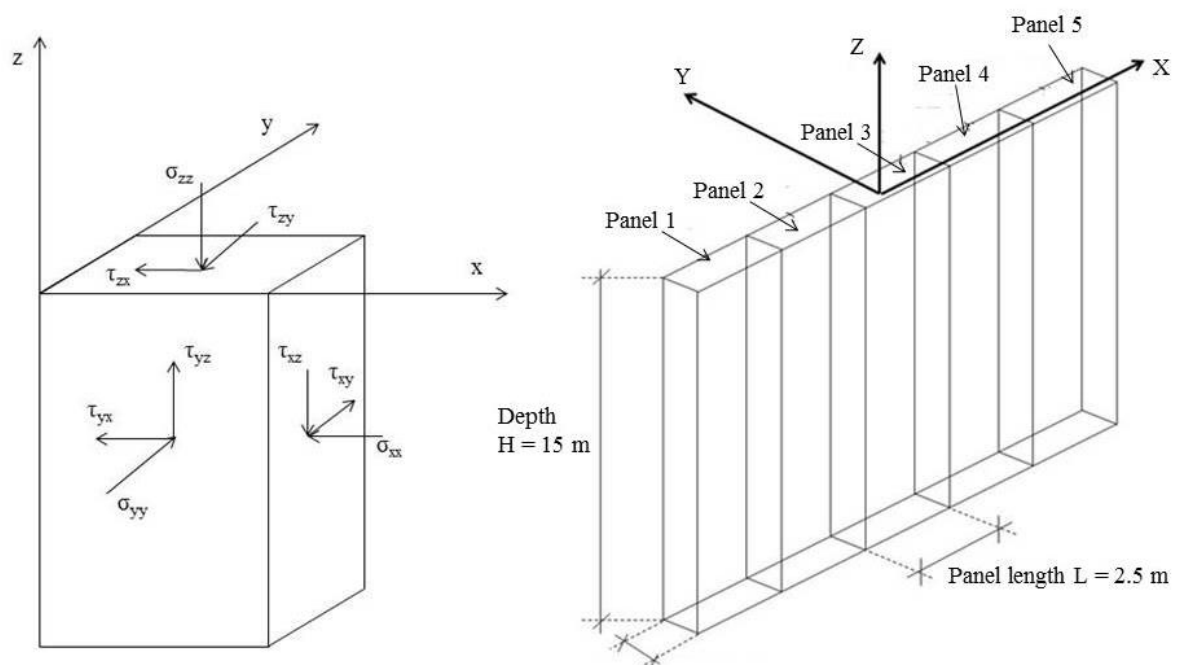


Figure 5.7. 3D Stress state.

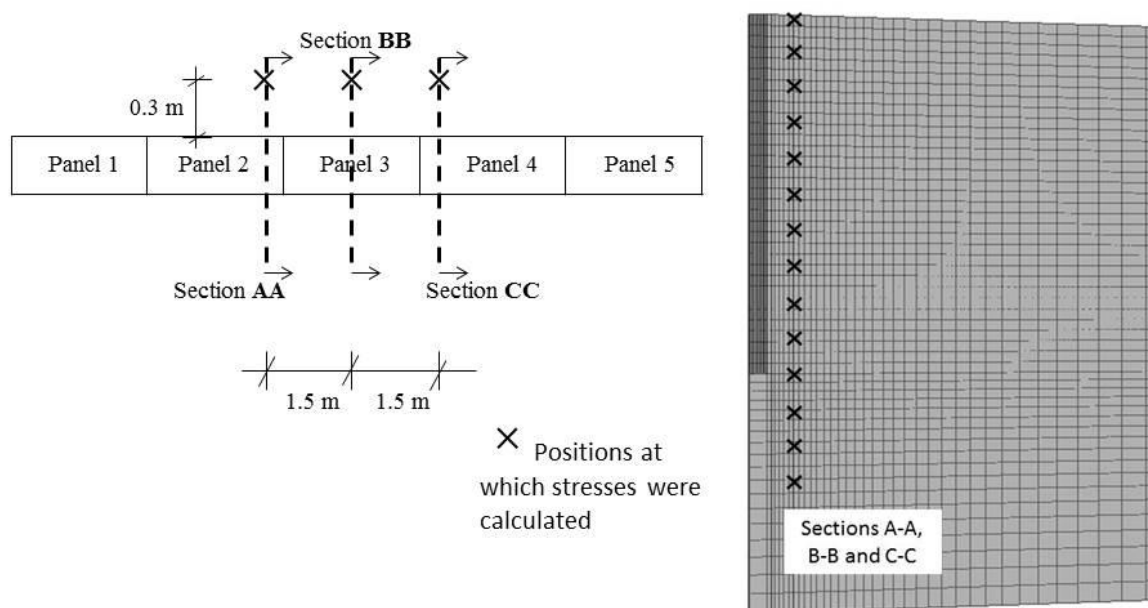


Figure 5.8. Plan view.

Figures 5.9 and 5.10 show the profiles of horizontal stress after the casting of the concrete during the construction of the panel 3, sequence 1, Figure 5.2. From Figure 5.9 and 5.10 it can be observed that the initial stresses reduce at section B-B and increase in the corners of the panel, sections A-A and C-C. The stress state does not change at distances along the wall of more than one and a half panel lengths from the centre of the panel installed. This means that the installation of a panel leads to a change in stress on the adjacent panel. However, the stresses in the soil at the centre area which is two panels away from installed panel do not change.

This is different from the finding provided by Ng and Yan (1998) where the construction of the adjacent panels has a minor influence on the stress distribution with depth on the middle section in the central panel. This is due to the large panel of 8m in length which limits the extent of the horizontal arching action. Instead, in this chapter, it was found that the installation of a panel of length 2.5 m influences the stresses at the middle of the adjacent panels, Figures 5.9 and 5.10.

Furthermore, Figures 5.9 and 5.10, show that the installation of a second group of panels does not lead to any further variation in the stress state in the soil on the section B-B. The increases in the stress near the edges of the panel seen in Figures 5.9 and 5.10 were also observed by

Gourvenec and Powrie (1999) and Ng and Yan (1998). Ng and Yan (1998) suggest that an increase in lateral stress of the order of 20% of the in situ value would be expected within $0.1 L$ of the edge of the panel, with a return to the in situ value within $0.15 L$ (where L is the length of the panel). These results are different from those found in Chapter 3 where an increase of the total horizontal stress near the edges of the pile installed was not seen. As discussed in Chapter 3, this is mainly the consequence of the different geometries.

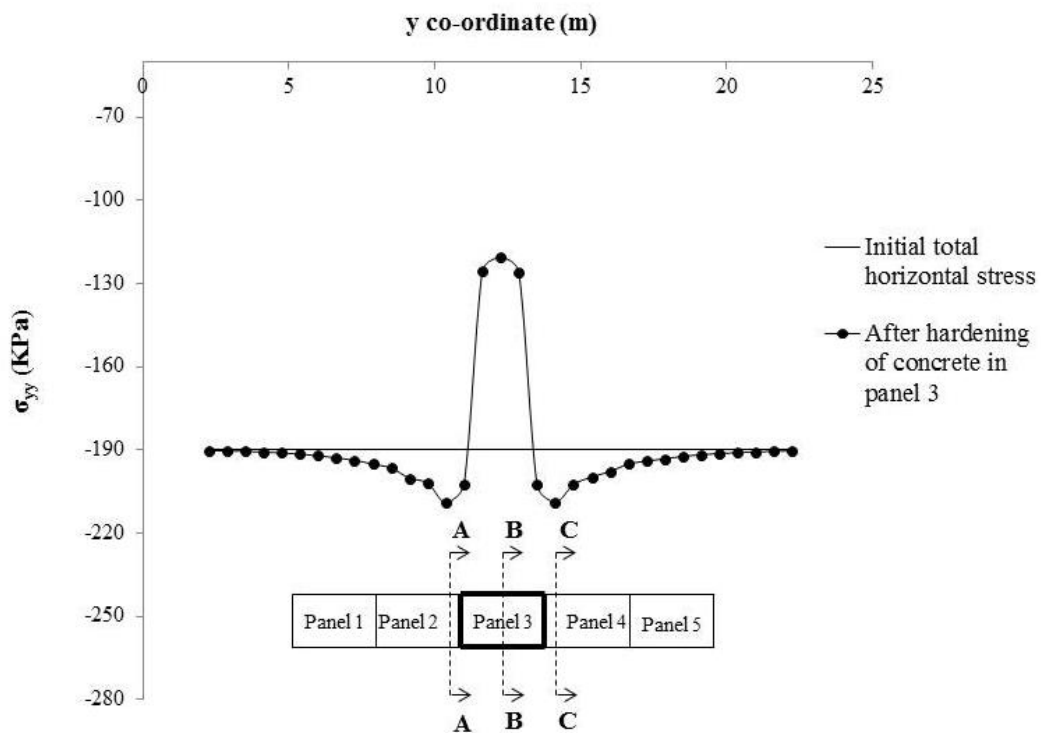


Figure 5.9. Distribution of total horizontal stresses (σ_{yy}) along the length of the wall after concreting of the central panel at a depth of 3.3 m.

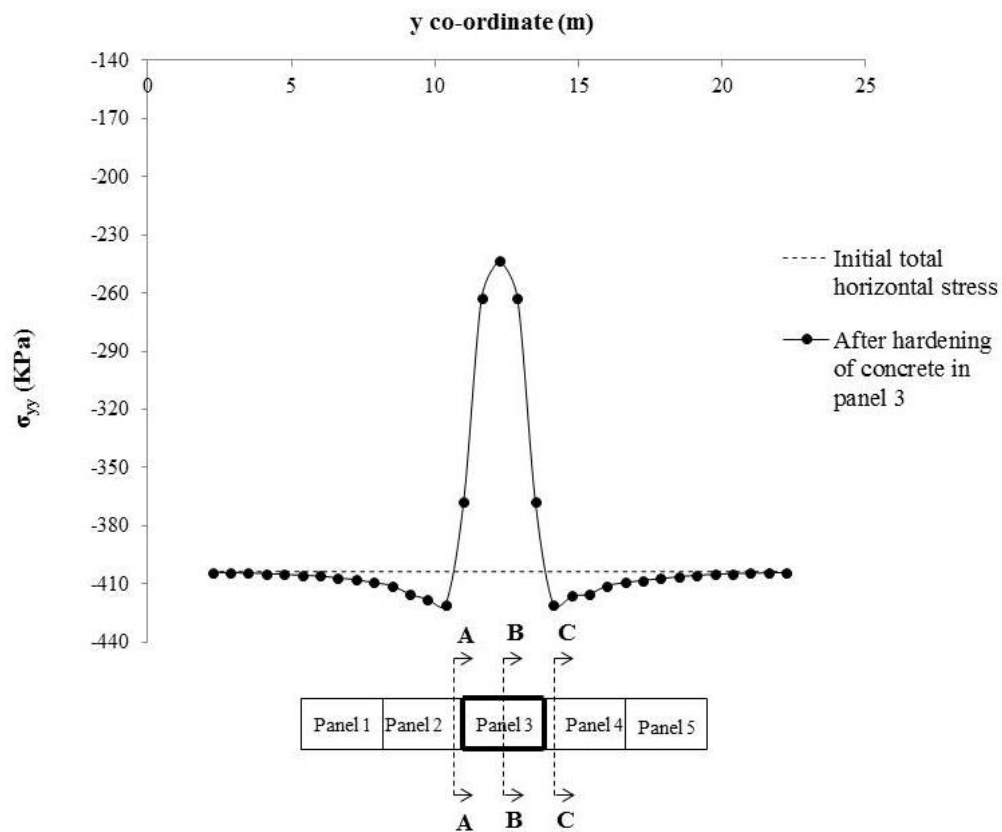


Figure 5.10. Distribution of total horizontal stresses (σ_{yy}) along the length of the wall after concreting of the central panel at a depth of 15.3 m.

Figure 5.11 shows the computed horizontal stress distribution at different construction stages at one location, section B-B in Figure 5.8, at a distance of 0.3 m behind the wall during the installation of the panel 3, sequence 1, Figure 5.2.

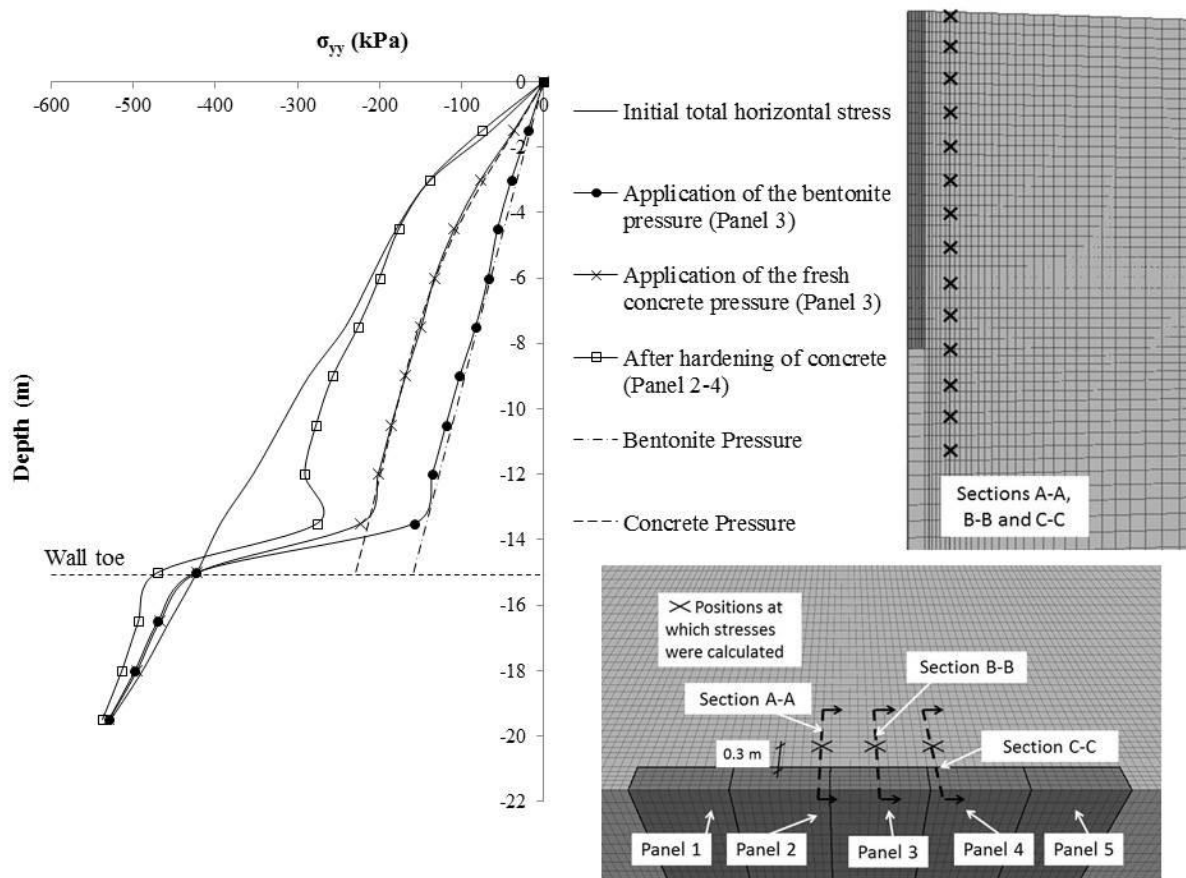


Figure 5.11. Variation with depth of the total horizontal stress (σ_{yy}) acting on section B-B, at a normal distance from the wall of 0.3 m.

Bentonite is used to provide temporary support to the excavation. As reported by Ng *et al.* (1995) and as shows in Figure 5.11, the initial horizontal stress (σ_{yy}) in the soil adjacent to the trench is reduced to the hydrostatic bentonite pressure. After the casting of the concrete, the horizontal stress increased and became equal to the bilinear wet concrete proposed by Ng (1992) and Lings *et al.* (1994), Figure 5.11.

Figure 5.11 shows a slight increase in the total horizontal stress at about 1 m beneath the toe of the panel after the installation of the first panel. The horizontal stress increased after each sequence of construction. Similar results were found by Ng and Yan (1998). As described by Ng and Yan (1998), if the stress reduction were solely attributed to downward vertical load transfer, the area of the stress reduction above the toe would equal to the area of the horizontal stress increase beneath the toe. However, this is not the case and some of the stress reduction

must be attributed to the horizontal shear stress component (τ_{xy}) as also explained by Ng and Yan (1998). The distribution of the shear stress (τ_{xy}) is presented and discussed later in this chapter.

An increase in the earth pressure coefficient behind the primary panel was also observed by Gourvenec and Powrie (1999). They concluded that the horizontal displacements along both the vertical and horizontal edges of the trench are restricted by end effects, and this kinematic restraint results in an increase in the lateral stresses on either side of and below the trench to above their *in situ* value. They did not report any correlation between the total horizontal stress changes and the shear stress variation in the soil close to the wall during panel installation.

Ng *et al.* (1995) found that after the panel had been installed the stresses above the toe of the wall had decreased, and the stresses beneath the toe increased by a roughly equivalent amount. These results are quite different from those found in this chapter and those calculated by Gourvenec and Powrie (1999) and Ng and Yan (1998). As a matter of fact, the analysis from Ng *et al.* (1995) was an approximate analysis with some limitations, as reported in Chapter 2. The difference between the true and the pseudo three-dimensional analyses is that the downward load transfer and the horizontal arching mechanisms were uncoupled in the pseudo three-dimensional analyses. Then, in the two-dimensional plane strain analysis by Ng *et al.* (1995) any reduction of the total normal horizontal stress above the toe of the wall will cause an equal amount of the stress increase below the toe of the wall.

Figure 5.12, shows the variation of the total horizontal stress in section A-A, Figure 5.8, during the installation of panel 3, sequence 1, and the final stress distribution of this installation sequence. The total horizontal stress during the application of the bentonite and fresh concrete pressure is higher than the initial total horizontal stress. Ng and Yan (1998) attributed the increase of the total horizontal stress near the edges of the panel to the redistribution of the horizontal stress via the shear stresses (τ_{xy}). A significant amount of the shear stress (τ_{xy}) develops in the area near the edge of the panel, due to the horizontal arching mechanism which redistributed the horizontal stresses from the centre to the edge of the panel. They did not investigate the shear stress variation after a subsequent panel installation.

Again, this mechanism was also explained by Gourvenec and Powrie (1999) as a result of the horizontal displacement along both the vertical and the horizontal edges of the trench being restricted by end effects, with this kinematic restraint resulting in an increase in the lateral stresses on either side of and below the trench to above their *in situ* values.

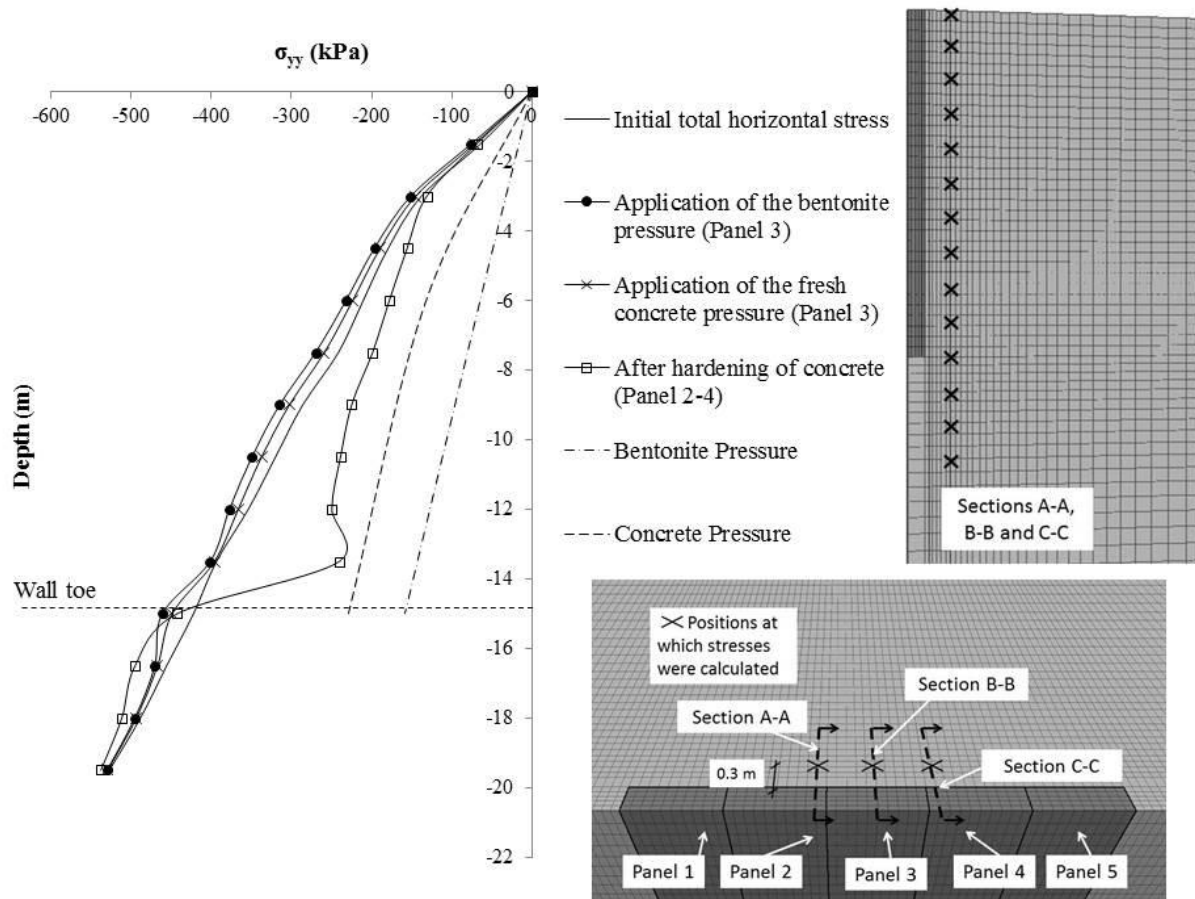


Figure 5.12. Variation with depth of the total horizontal stress (σ_{yy}) acting on section A-A, at a normal distance from the wall of 0.3 m.

5.3.2 Comparison of 3D installation effects for five different panel installation sequences

In this section the final computed stresses behind the central panel, Figure 5.4, on sections A-A, B-B and C-C, at the end of each of the different construction sequences modelled are presented.

Figure 5.13, 5.14 and 5.15 show the total horizontal stresses variation (σ_{yy}) at the sections A-A, B-B and C-C at a distance of 0.3 m behind the wall, Figure 5.8, after the five installation sequences that were investigated (sequence 1, 2, 3, 4 and 5, Figure 5.2). From the computed results shown in Figures 5.13, 5.14 and 5.15 it was found that the horizontal stress is not much affected by the installation sequence. In fact, similar results were calculated after each of the different construction sequences.

However, the horizontal stress (σ_{yy}) on section C-C, Figure 5.15, after construction sequence 4 is slightly different from those calculated in sequences 1, 2, 3 and 5. This is mainly the consequence of a small difference in the shear stress distribution (τ_{xy}) on section C-C during sequence 4 compared to the other sequences. Later in this chapter, the variations of the horizontal shear stress (τ_{xy}) for sequence 4 during each construction step are compared with those for the other sequences.

Figures 5.13, 5.14 and 5.15 show that the major horizontal stress relief for all the sequences modelled is concentrated above the toe of the wall and in the centre area of the soil behind the panel wall. Similar distributions of the total horizontal stresses were observed by Ng and Yan (1998). They found a significant reduction of the total normal horizontal stress above the toe of the central panel. They reported that shear stresses (τ_{xy}) and (τ_{zy}) are effectively zero at this section (the central section on the central panel of a diaphragm wall). However, slightly different results were found in this chapter; in fact, a minor increase of the shear stress (τ_{xy}) in the middle section of the central panel in sequence 4 was calculated. This is mainly because the installation in sequence 4 is not symmetric with respect the centre of the wall. In fact, it was found that for a non-symmetric sequence of panel installation (sequence 4) the shear stresses (τ_{xy}) increase slightly in the middle section in the central panel.

Decreases in the area above the toe of the wall were also observed by Ng *et al.* (1995). They carried out an analysis of the three-dimensional effects of diaphragm wall installation using two simplified plane analyses. They found that the stresses above the toe of the wall decreased and were similar to those measured at the end of wall installation at Lion Yard.

Ng and Yan (1998) calculated a large lateral stress reduction especially in the area above the toe of the wall after the installation of a single panel. In their paper they modelled only the installation of a single panel without considering the installation of successive panels.

Gourvenec and Powrie (1999) found that the installation of a group of panels had a significant effect on the final earth pressure. Slightly different results are found in Figure 5.13, 5.14 and 5.15 where the stress decrease is mainly concentrated above the toe of the wall. Gourvenec and Powrie (1999) calculated a significant earth pressure decrease at a distance 1 m behind the wall along the length of the entire panel, especially in the area close to the ground surface.

Reductions in total horizontal stress during the wall installation have been measured at various sites in the U.K.; Tedd *et al.* (1984) and Lings *et al.* (1991). Field data from two further sites are reported by Symons *et al.* (1992). They found that the decrease in the total lateral stresses at a depth of 10 to 12 m in the vicinity of the wall was similar to that observed at the Bell Common Tunnel. Carswell *et al.* (1993) monitored a contiguous bored pile retaining wall in an over-consolidated deposit immediately and after its construction as part of the A406 North Circular Road Improvement Scheme in Walthamstow. They reported that in general the large reduction occurred at the greater depths. Similar results were calculated and showed in Figure 5.13, 5.14 and 5.15. Large total horizontal stresses near the toe of a bored pile wall were also measured by Bennett *et al.* (1996). They found that the largest reductions of the total horizontal stresses were measured behind and in front of the wall respectively at 14.5 m depth.

The results plotted in Figures 5.13, 5.14 and 5.15 may be compared with those during the installation of a bored pile wall, Figure 4.21, 4.22. It can be seen that in the case of a bored pile wall the horizontal stress decreases are much concentrated in the area above the toe of the wall. For a diaphragm panel wall, the stress decreases are distributed along the entire depth of the wall. However, as in the case of bored pile wall, the stress decreases during diaphragm wall installation are mainly concentrated in the area about 2 m above the toe of the wall.

Furthermore, Figures 5.13, 5.14 and 5.15 show an increase in the total horizontal stress to a depth of 2.5 m below the toe of the wall. In contrast, for a bored pile wall, (Figures 4.21 and 4.22) the stresses behind the wall return to the initial values by approximately 1.5 m below the toe of the bored pile wall.

The lesser redistribution of the shear stress (τ_{xy}) below the toe of the bored pile wall compared with those calculated below the toe of the diaphragm wall could lead to a different redistribution of the total horizontal stress beneath the toe of the diaphragm wall compared with the bored pile. In fact, smaller horizontal stress changes were calculated after bored pile construction than for a diaphragm panel wall.

In general, comparing the results calculated by Gourvenec and Powrie (1999), Ng and Yan (1998) and by Chapters 3 and 4 with those calculated in this chapter, it was found that the construction of a bored pile wall lead to lower stress changes than installation of a diaphragm wall. Geometry effects could be the main reason for the differences between the stress changes calculated during the installation of a single pile and those found after the installation of a diaphragm wall.

Figure 5.14 shows the variation with depth of the total horizontal stress acting on section B-B (middle section in the central panel, Figure 5.8) for all the sequences investigated. The total horizontal stresses on sections A-A and C-C (Figures 5.13 and 5.15) are lower than those in the middle section B-B. This was also found by Gourvenec and Powrie (1999), who calculated an increase in the earth pressure coefficient behind the primary panel after the construction of each of the adjacent panels. They found also that the increase in the earth pressure coefficient was greater near the top of the panel.

Ng and Yan (1998) found no significant change in the stress distribution on the middle section behind the central panel following the installation of two adjacent panels. This is different from the results shown in Figures 5.13, 5.14 and 5.15, where the installation of the adjacent panels led to an increase in stress in the middle area of the central panel. This is mainly because Ng and Yan (1998) modelled panels of 8 m length, while in this chapter the panels were 2.5 m length. When the length of the panel is large (e.g. 8 m) the total horizontal stress changes at the

edges of the panel are not redistributed to the centre of the panel. This is because the large panel limits the stress redistribution via the shear stress (τ_{xy}) to the centre of the panel.

Figure 5.13, 5.14 and 5.15 show an increase of the total horizontal stress below the toe of the wall during panel installation. It was observed that the area of the stress decrease above the toe is larger compared to the area of the total horizontal stress increase behind the toe of the wall. This means that only a portion of the total horizontal stress decrease is redistributed via the shear stress (τ_{xy}) below the toe of the wall. The remaining part of the horizontal stress is redistributed via the shear stress (τ_{xy}) in the area close to the edges of the panel installed.

Ng and Yan (1998) found that the horizontal stress increased below the toe of the primary panel installed during the construction of the adjacent panels. They observed a small stress increase above and below the toe of the wall on the central panel due to the construction of the two adjacent panels. Similar results were found in Chapter 4 during the installation of a bored pile wall; as Figure 4.22 shows, a slight increase in total horizontal stress below the toe of the pile during the installation of the adjacent piles was calculated. The redistribution and increase of the shear stress (τ_{xy}) during wall installation is the main reason for the increase of the horizontal total stress below the toe of the wall during panel or pile installation. In fact, as shown later and as reported in Figure 4.24, the shear stress (τ_{xy}) increased during wall construction especially in the area below the toe of the wall.

The installation of a panel of 8 m length modelled by Ng and Yan (1998) led to a variation of the shear stress (τ_{xy}) for a depth of 3 m below the toe of the wall. Differently, the shear stress (τ_{xy}) which developed under the toe of the bored pile wall, as shown in Chapter 4, became zero only at a depth of 1 m below the toe of the wall. Similar results were found in this chapter; in fact, for a panel 2.5 m in length the shear stress (τ_{xy}) became minimal at a depth of 1.5 m below the toe of the wall. These results suggest that there is a correlation between the stress changes below the toe of the wall and the length of the panel installed. However, Gourvenec and Powrie (1999) did not find any significant variation in the total horizontal stresses below the toe of the wall with the length of panel installed.

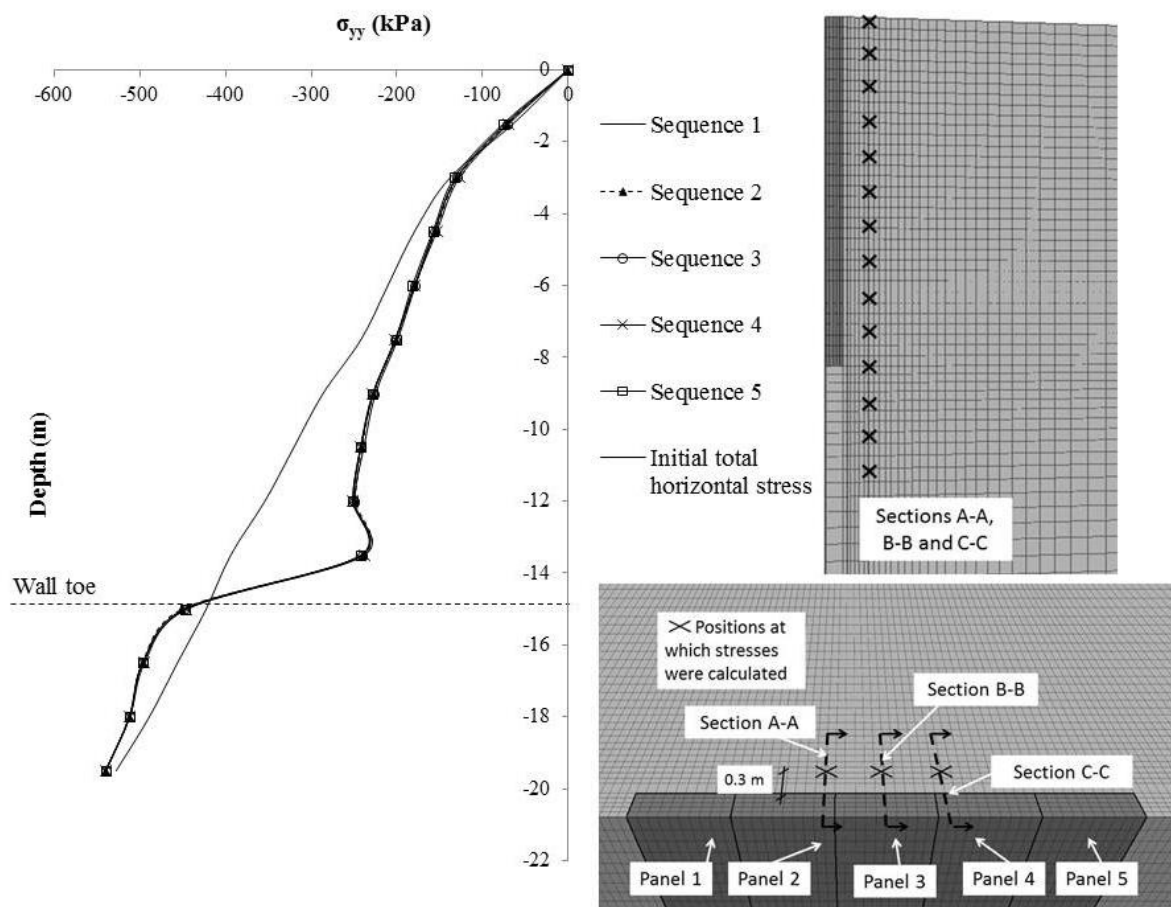


Figure 5.13. Variation with depth of the total horizontal stress (σ_{yy}) acting on section A-A, at a normal distance from the wall of 0.3 m. Sequences 1, 2, 3, 4 and 5.

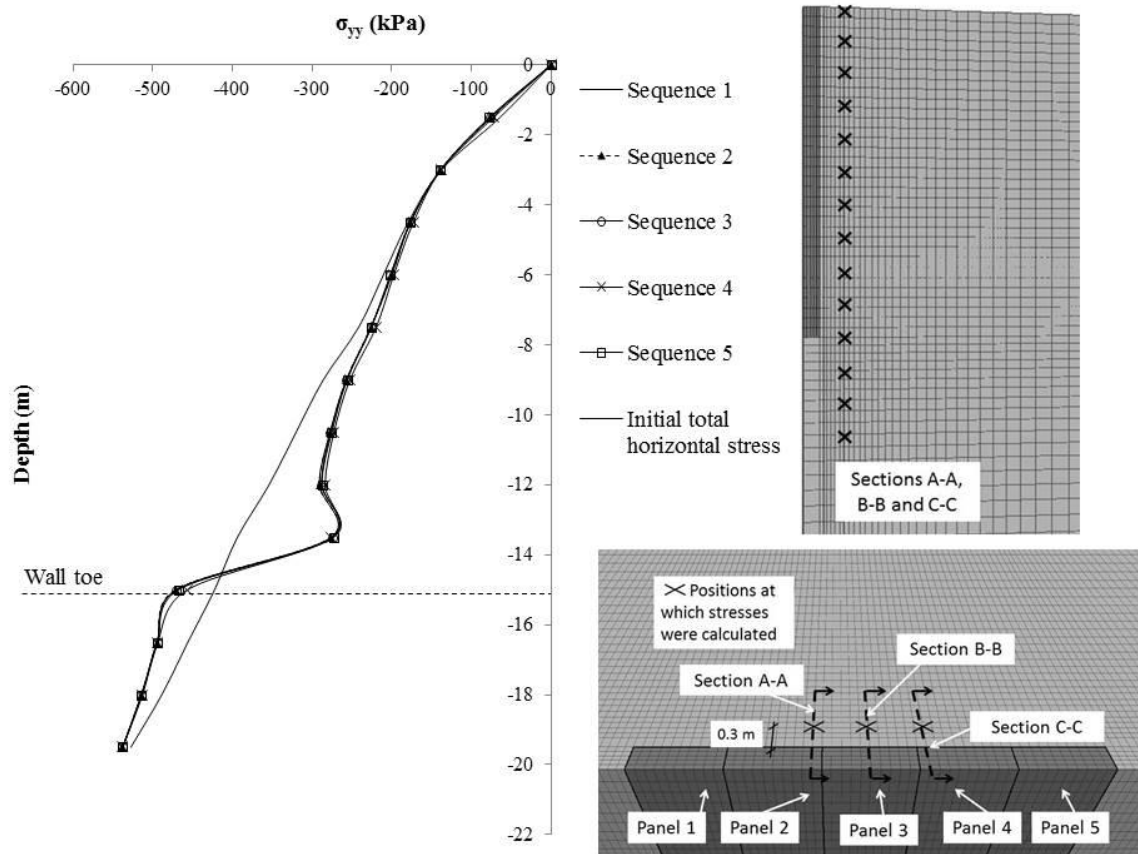


Figure 5.14. Variation with depth of the total horizontal stress (σ_{yy}) acting on section B-B, at a normal distance from the wall of 0.3 m. Sequences 1, 2, 3, 4 and 5.

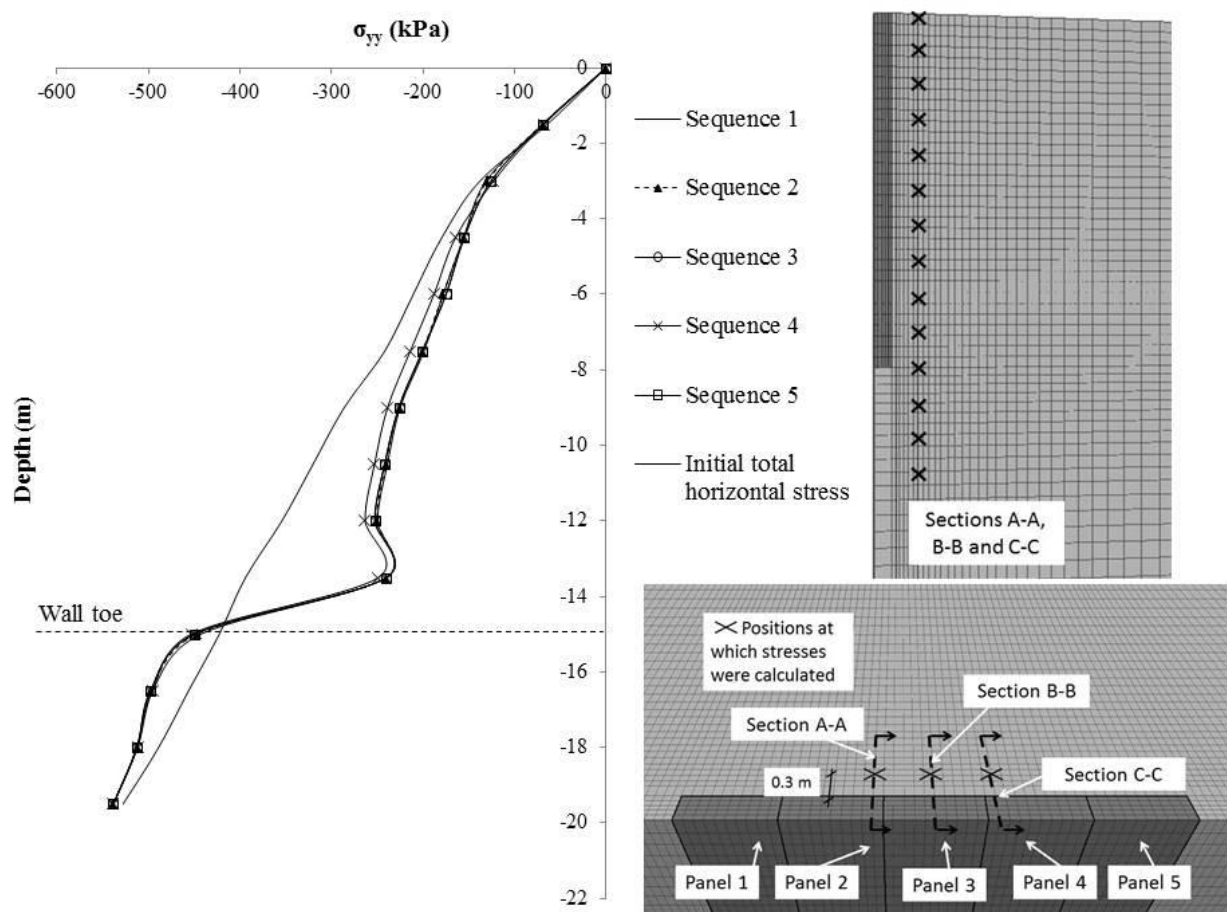


Figure 5.15. Variation with depth of the total horizontal stress (σ_{yy}) acting on section C-C, at a normal distance from the wall of 0.3 m. Sequences 1, 2, 3, 4 and 5.

5.3.3 Comparison of the vertical shear stress (τ_{zy}) after the five sequences of the diaphragm wall installation.

Figure 5.16, 5.17 and 5.18 show the calculated distributions of vertical shear stress (τ_{zy}) acting on section A-A in Figure 5.8, for each of the five sequences of diaphragm wall installation. The vertical shear stresses (τ_{zy}) in these areas do not change after any of the five construction sequences which were investigated. However, Figure 5.17, sequence 4, shows a slight decrease in the vertical shear stresses (τ_{zy}) in the area above the toe of the wall compared to the values calculated for the other sequences. The shear stress (τ_{zy}) variation for sequence 4 during each construction step is presented later in this chapter.

The distributions of vertical shear stress (τ_{zy}) are quite similar to those found by Ng and Yan (1998), while lower shear stresses were found in the zone from the surface to a depth close to the toe of the wall. The shear stress (τ_{zy}) increase in the area near the toe of the wall, and decrease under the toe of the wall. For a wall installation with panels of 2.5 m of length, the shear stress became zero at a depth of 1.5 m from the toe of the wall, Figures 5.16, 5.17 and 5.18. For a bored pile wall the shear stress became zero at a distance of 1 m below the toe of the wall. This means that the stress redistribution below the toe of the wall is a function of the length of the panel installed. When the length of the elements installed is low compared to the depth of the wall (e.g. a bored wall pile, Chapter 3 and 4), the total horizontal stress changes below the toe of the wall are minimal.

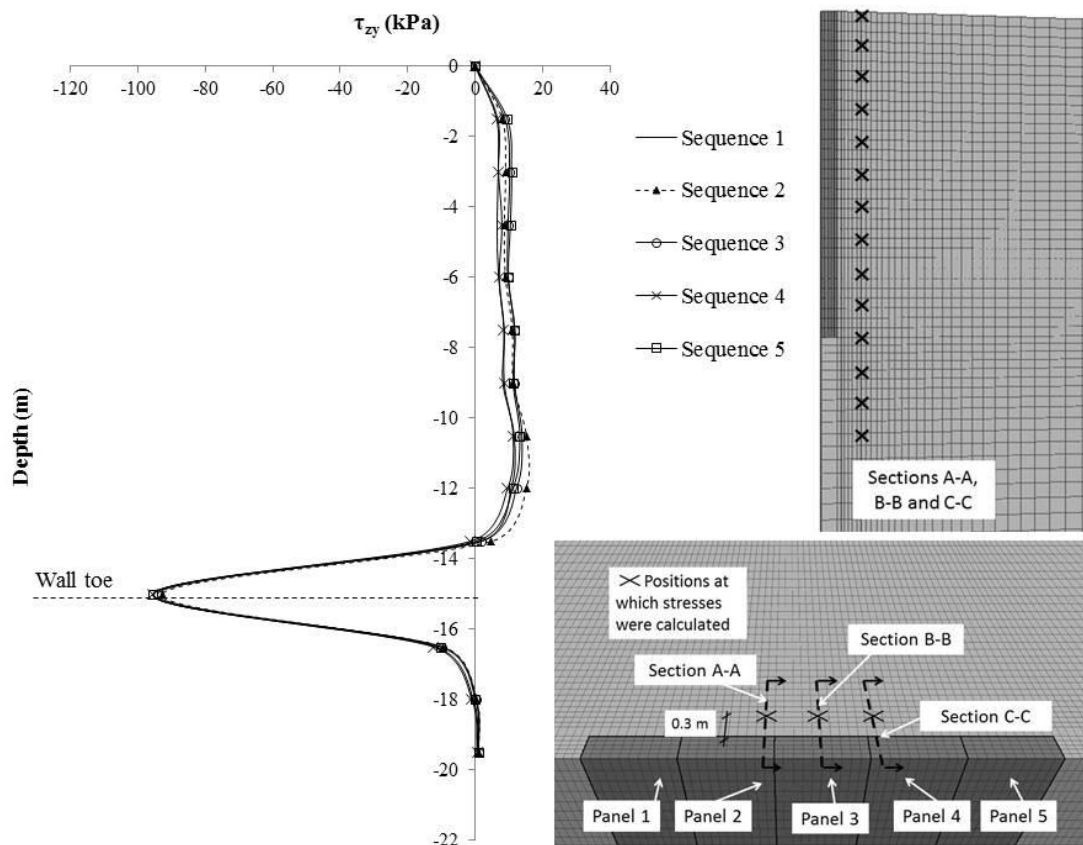


Figure 5.16. Variation with depth of the shear stress (τ_{zy}) acting on section A-A, at a normal distance from the wall of 0.3 m. Sequences 1, 2, 3, 4 and 5.

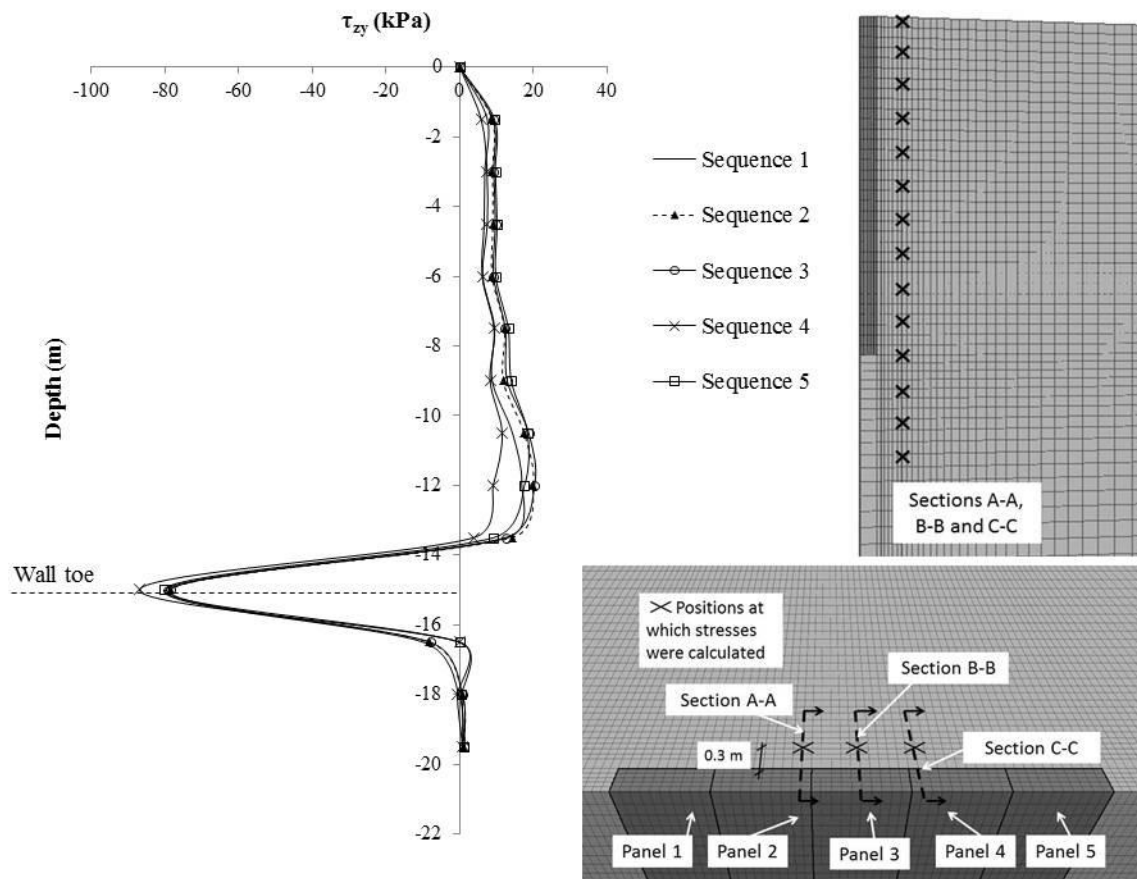


Figure 5.17. Variation with depth of the shear stress (τ_{zy}) acting on section B-B, at a normal distance from the wall of 0.3 m. Sequences 1, 2, 3, 4 and 5.

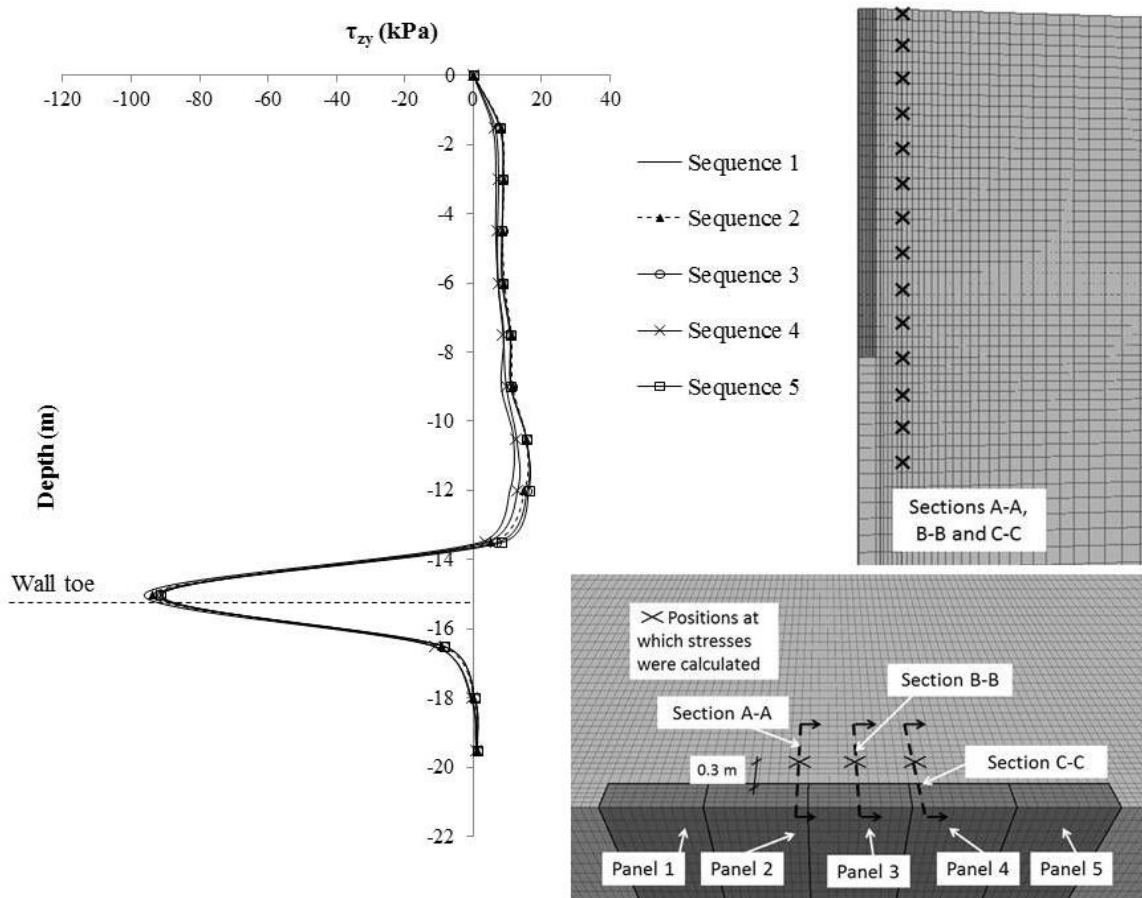


Figure 5.18. Variation with depth of the shear stress (τ_{zy}) acting on section C-C, at a normal distance from the wall of 0.3 m. Sequences 1, 2, 3, 4 and 5.

5.3.4 Comparison of the horizontal shear stress (τ_{xy}) after the five sequences of diaphragm wall installation

Figures 5.19, 5.20 and 5.21 show the computed distributions of horizontal shear stress (τ_{xy}) acting on section A-A, B-B and C-C, Figure 5.8, for each of the five sequences of diaphragm wall installation. The shear stress (τ_{xy}) is not much affected by the installation sequence. However, the shear stress (τ_{xy}) for sequence 4 was slightly different from those calculated for the other sequences (see Figure 5.20 and 5.21). The stress distribution during sequence 4 is discussed later in this Chapter.

The global distributions of horizontal shear stresses (τ_{xy}) are similar to those found by Ng and Yan (1998). The shear stresses are distributed along the entire depth of the wall with an

increase above the toe of the wall. For a diaphragm wall 8 m in length, Ng and Yan (1998) calculated that the maximum shear stress (τ_{xy}) was about 3 m above the toe of the wall with a magnitude of 100 kPa. Instead, for a wall panel 2.5 m in length, it was 20 kPa.

As expected, the variation in shear stress (τ_{xy}) with depth on section B-B is negligible during construction sequences 1 and 2, Figure 5.20. This is because of the symmetry of installation in respect of the section B-B. This implies that the directions of the two principal horizontal stresses are parallel and perpendicular to the centre of the panel 3 (section B-B). Again, from Figure 5.20 it can be noted that the distribution of the horizontal shear stress (τ_{xy}) on section B-B is non-linear after the sequences 3, 4 and 5. However, the magnitude of the horizontal shear stress (τ_{xy}) is minimal while the maximum value calculated was -5 kPa, as shown in Figure 5.20. The shear stress (τ_{xy}) is large for sequences in which the installation is non symmetric respect the centre of the wall.

Figure 5.21 shows the computed horizontal shear stress distribution on section C-C, Figure 5.8, 0.3 m behind the wall. These results are similar to those found in Figure 5.19. However, lower values of the horizontal shear stress were found in the area above the toe of the wall after sequence 4. Similar values of horizontal shear stress after construction sequences 1, 2, 3 and 5 were calculated, Figure 5.21.

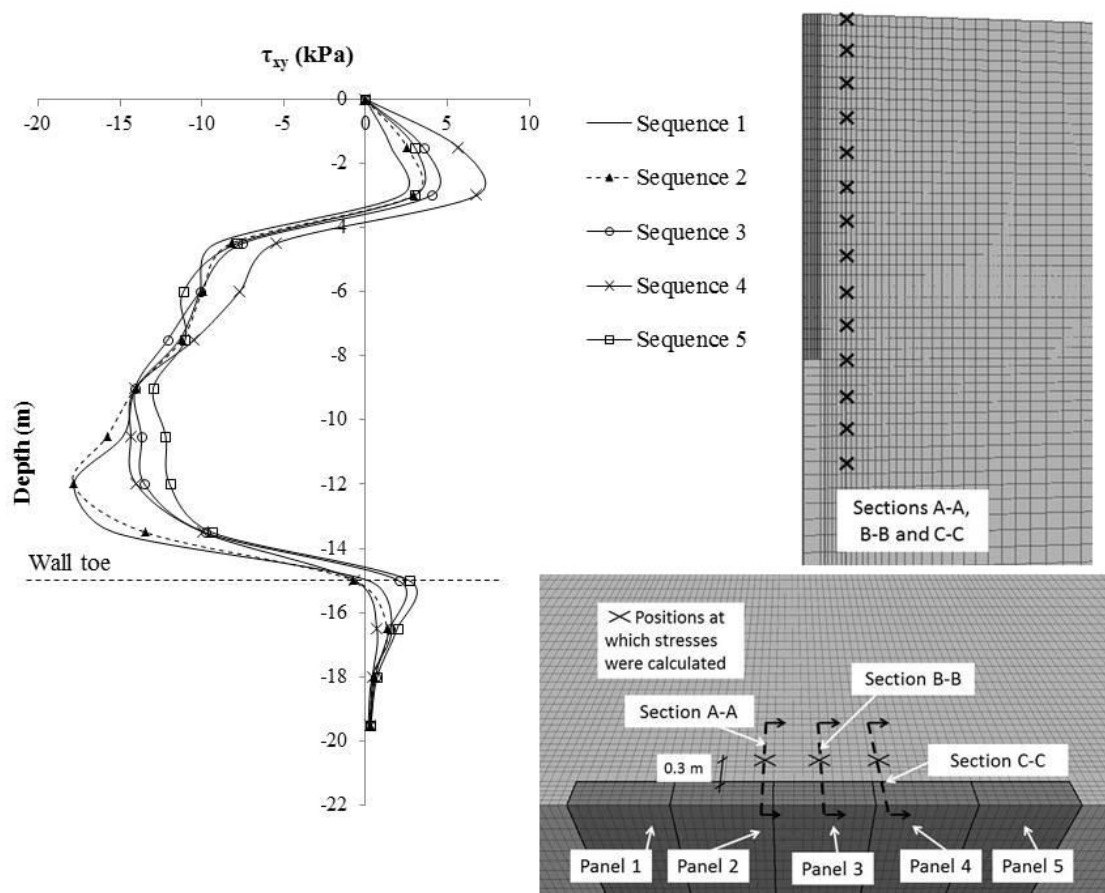


Figure 5.19. Variation with depth of the shear stress (τ_{xy}) acting on section A-A, at a normal distance from the wall of 0.3 m. Sequences 1, 2, 3, 4 and 5.

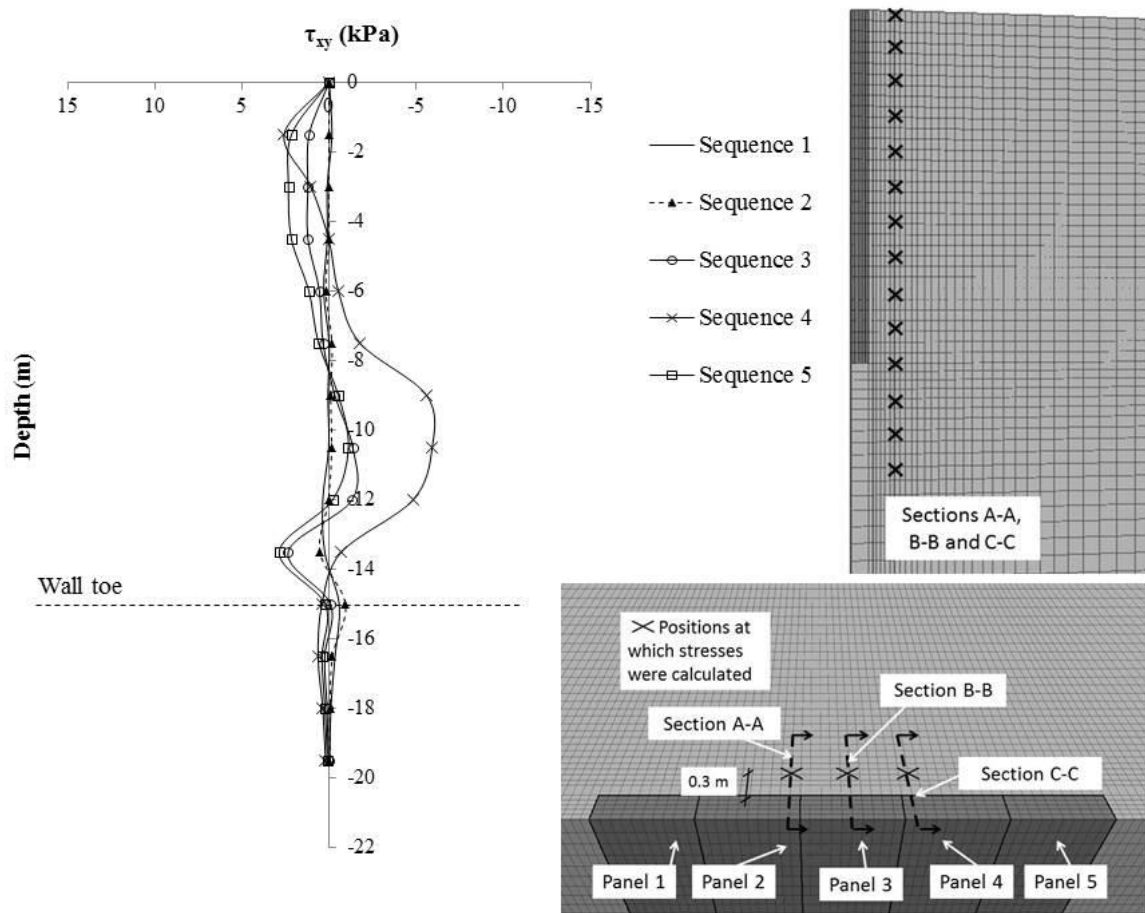


Figure 5.20. Variation with depth of the shear stress (τ_{xy}) acting on section B-B, at a normal distance from the wall of 0.3 (m). Sequences 1, 2, 3, 4 and 5.

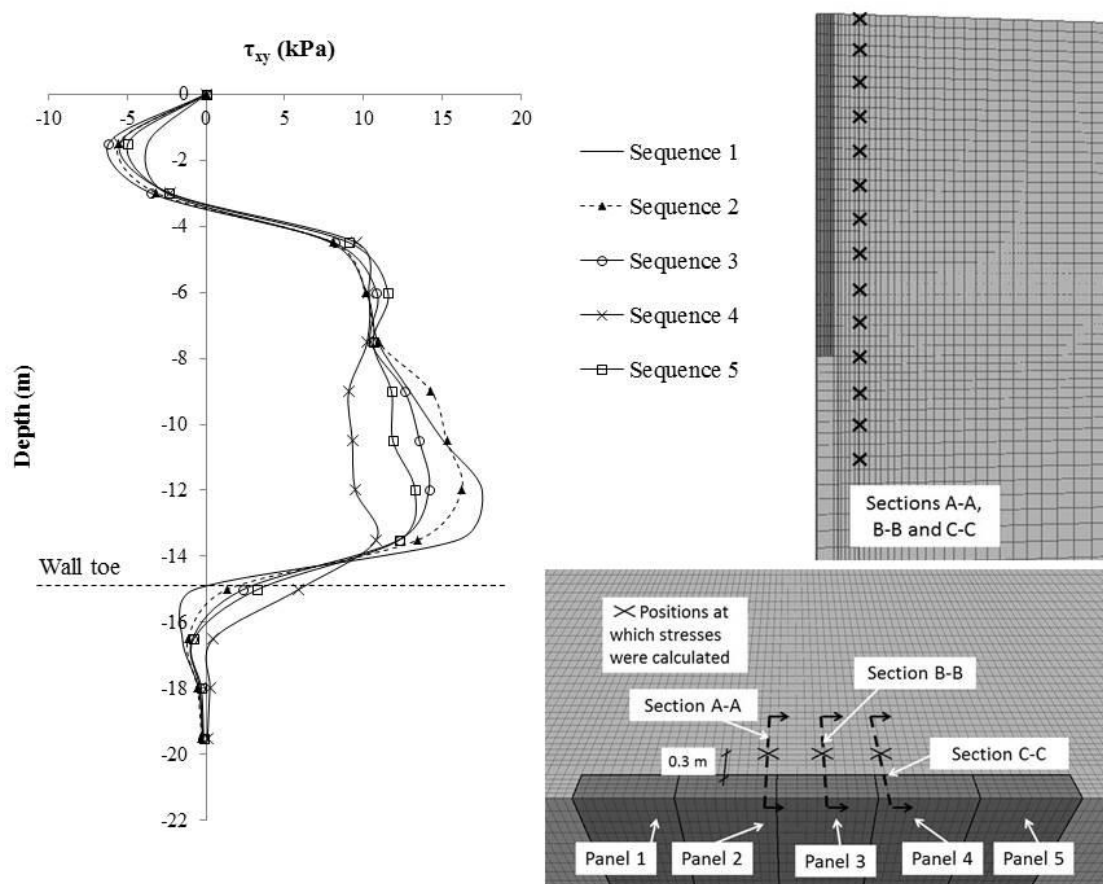


Figure 5.21. Variation with depth of the shear stress (τ_{xy}) acting on section C-C, at a normal distance from the wall of 0.3 m. Sequences 1, 2, 3, 4 and 5.

The same results were found after wall construction for the sequences 1, 2, 3 and 5, while a slightly different stress state was calculated during sequence 4. Then, it was chosen to investigate the stress change during the panel installation for sequences 1 and 4. The following paragraphs describe in details the stresses variation during diaphragm wall installation in sequences 1 and 2, Figure 5.2.

Total Horizontal stress distribution in sequence 1

Figure 5.22 shows the horizontal stress distributions during panel installation in sequence 1 in the region of the section A-A. After the excavation of panel 3, the horizontal stresses on section A-A do not change and remain similar to the initial values. In contrast, in section B-B at the centre of the panel, Figure 5.23, a significant decrease in total horizontal stress was calculated. This means that a small proportion of the total horizontal stress was redistributed from the

centre to the edge of the panel via the shear stress (τ_{xy}). This is also confirmed by the significant amount of shear stress developed in the soil in section A-A. The variations in shear stress (τ_{xy}) are presented later. Similarly, Ng and Yan (1998) found that after installation of a single panel, the total horizontal stresses at the edge of the panel did not change. They reported that this implies that a significant amount of shear stress (τ_{xy}) develops in the soil element at the edge of the panel. Similar results were also calculated at section C-C, Figure 5.24.

Gourvenec and Powrie (1999), found that the installation of a panel of length of 5 m led to a slight increase in the total horizontal stress below the toe of the wall. Similar results were found by Ng and Yan (1998).

The stress changes were minimal during the installation of a panel of 2.5 m length, Figure 5.24. Furthermore, in Chapter 4 it was shown that the construction of a single pile 1 m in diameter did not lead to significant total horizontal stress changes below the toe of the wall as shown in Figure 4.22. In fact on the central section B-B, the stress change under the pile remained similar to the initial stress. Again, there is a correspondence between the length of the panel installed and the increase in the horizontal stress below the toe of the wall.

The variation in the shear stress (τ_{zy}) during the installation of a single 8 m panel, under the toe of the wall, calculated by Ng and Yan (1998) is substantially different from that found after the installation of a single pile and after the construction of a panel with 2.5 m length. When the length of the panel increases (8 m panel length, Ng and Yan 1998) the shear stress (τ_{zy}) changes are large and go deeper than during the installation of a bored pile and a panel 2.5 m in length.

The installation of panels 1 and 5 (Figure 5.23) do not cause any changes in the horizontal stress on sections A-A, B-B and C-C. These panels are far from the section A-A and these construction stages do not lead to any stress state change in the zones of ground close to that section.

Significant horizontal stress relief was observed on section A-A during the excavation of panels 2 and 4, Figure 5.23. The stress decrease is concentrated near the toe of the wall. An increase

in the total horizontal stress was observed under the toe of the wall. Similar results were observed on section C-C, Figure 5.23. This is the consequence of symmetric panel installation with respect the centre of the wall.

In contrast, a significant increase in the total horizontal stress was calculated after the excavation of panels 2 and 4 on section B-B, Figure 5.24. This increase does not seem to have been due to the redistribution of shear stress (τ_{xy}) from the edges of the panel 3 to the section B-B. In fact, it is shown later that the shear stresses (τ_{xy}) are zero on section B-B, Figure 5.27, because the installation is symmetric in respect the centre of the wall and the directions of the major axis are perpendicular to the wall in the middle section. Thus, the total horizontal stress increase shown on section B-B is due to the redistribution of the horizontal stress via the shear stress (τ_{zy}). In fact, as shown later in this chapter, the shear stress (τ_{zy}) on section B-B increases during wall installation. This increase is mainly concentrated in the zone above the toe of the wall, after the installation of panel 2 and 4.

Gourvenec and Powrie (1999) did not report any increase below the toe of the wall. This could be due to the fact that they calculated the stress changes 1 m behind the wall. In this chapter and also from Ng and Yan (1998) the stress changes were calculated 0.3 m behind the wall.

Ng *et al.* (1999) found that the construction of the adjacent panel had only a minor influence on the stress distribution with depth on the middle section of the central panel because the large panel length limited the extent of the horizontal arching action. However, they calculated a small stress increase above and below the toe of the wall due to the construction of the two adjacent panels. The same result was found here; it can be seen in Figure 5.23 that the installation of successive panels led to an increase of the total horizontal stress below the toe of the wall.

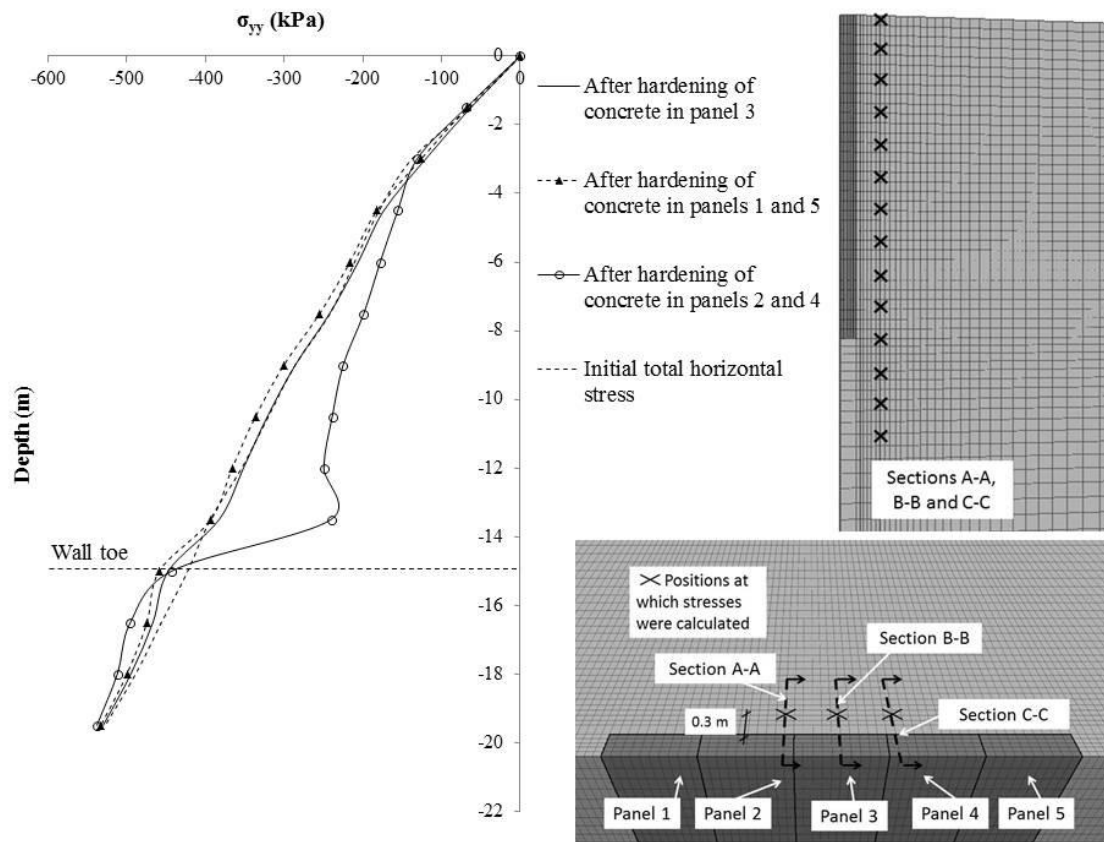


Figure 5.22. Variation with depth of the total horizontal stress (σ_{yy}) acting on section A-A, at a normal distance from the wall of 0.3 m. Sequence 1.

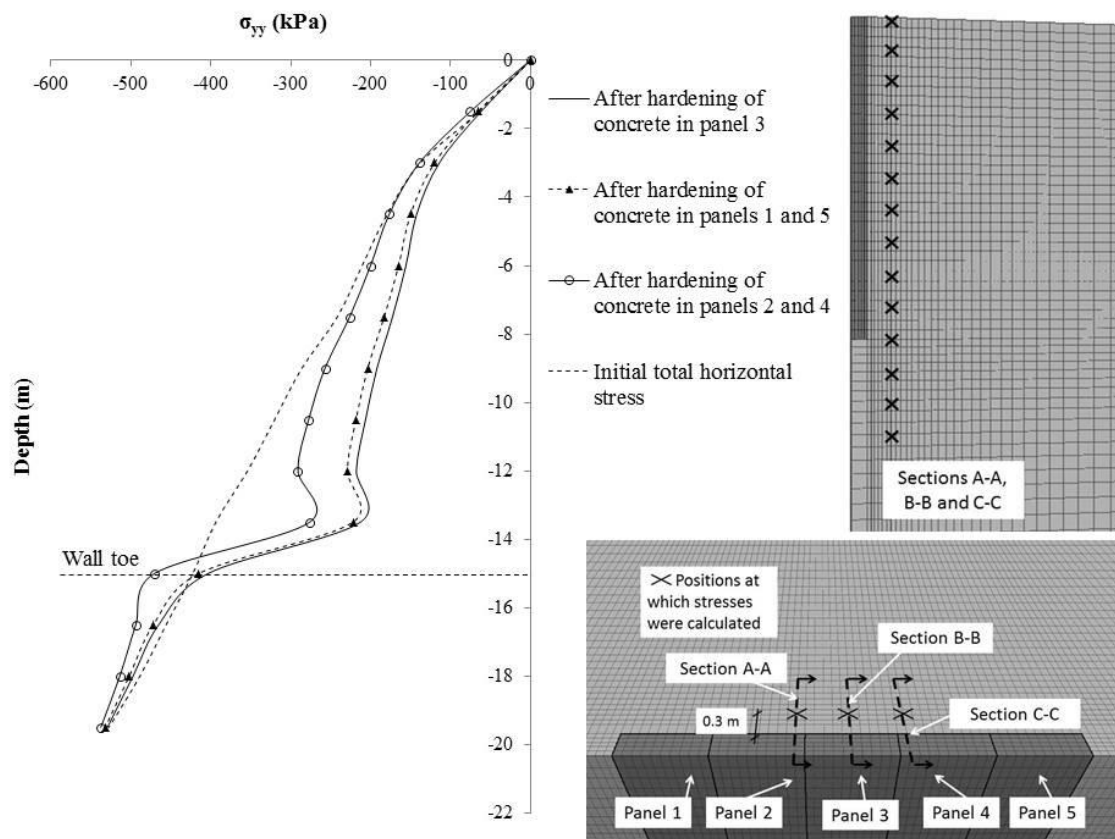


Figure 5.23. Variation with depth of the total horizontal stress (σ_{yy}) acting on section B-B, at a normal distance from the wall of 0.3 m. Sequence 1.

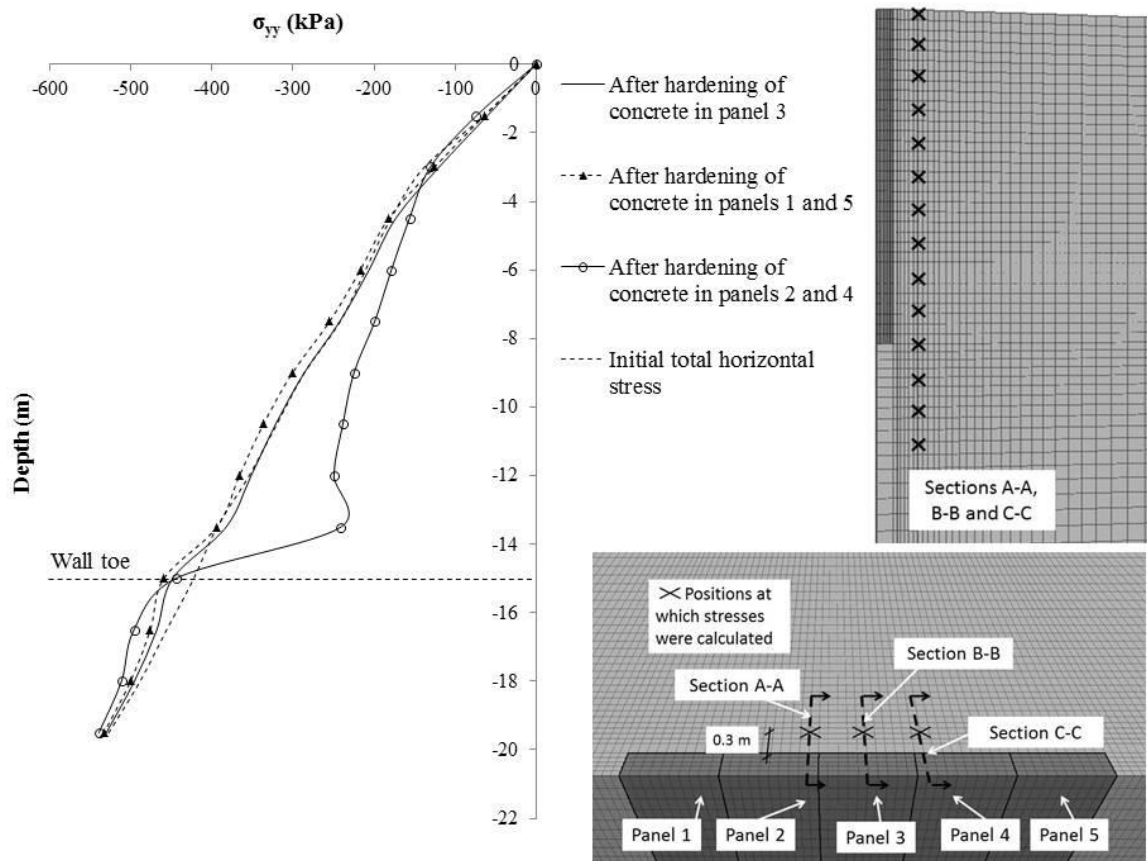


Figure 5.24. Variation with depth of the total horizontal stress (σ_{yy}) acting on section C-C, at a normal distance from the wall of 0.3 m. Sequence 1.

Horizontal shear stress distribution (τ_{xy}), sequence 1

Figure 5.25 shows the variation in the horizontal shear stress (τ_{xy}) acting on section A-A at a distance of 0.3 m behind the wall.

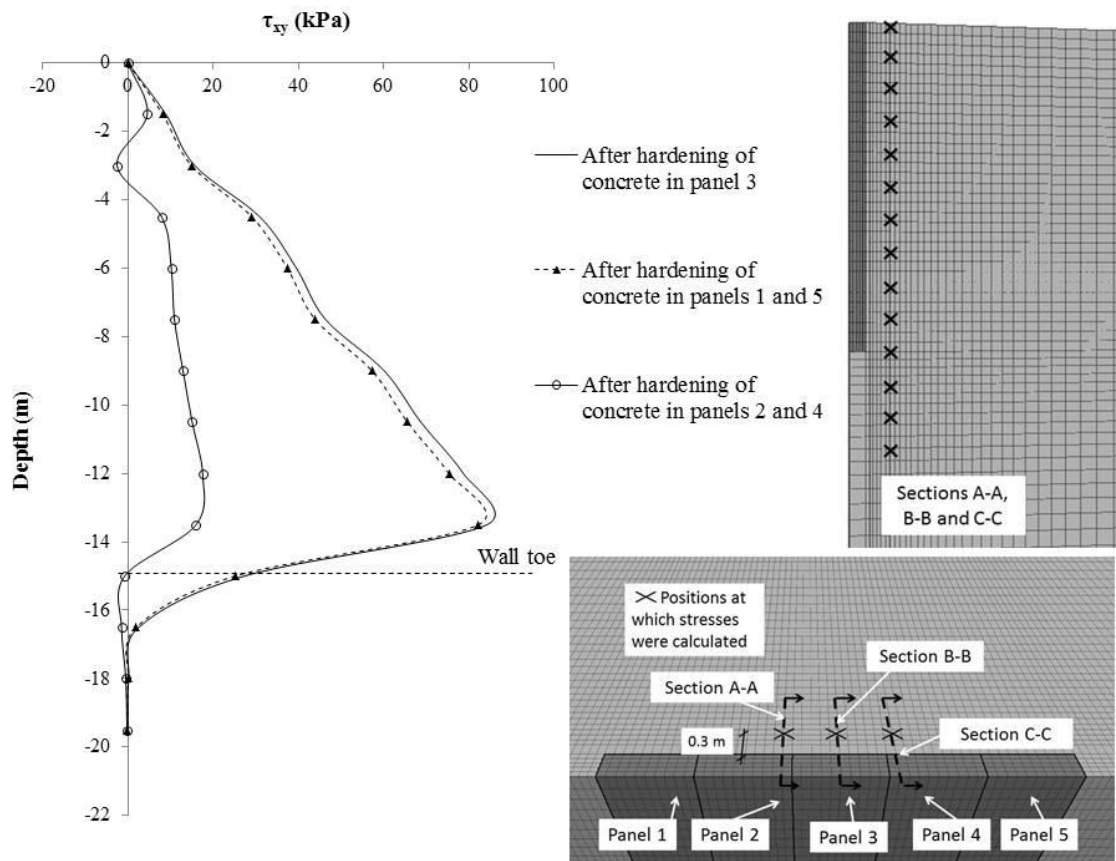


Figure 5.25. Variation with depth of the shear stress (τ_{xy}) acting on section A-A, at a normal distance from the wall of 0.3 m. Sequence 1.

After the excavation of the central panel, the horizontal shear stresses (τ_{xy}) increased. The largest shear stresses (τ_{xy}) are concentrated above the toe of the wall. After the excavation of panels 1 and 5, the horizontal shear stress (τ_{xy}) did not change. This was because these panels are quite far from the section A-A and their installation does not influence the shear stress at the section A-A. The installation of panels 2 and 4 led to a decrease of the horizontal shear stress as shown in Figure 5.25.

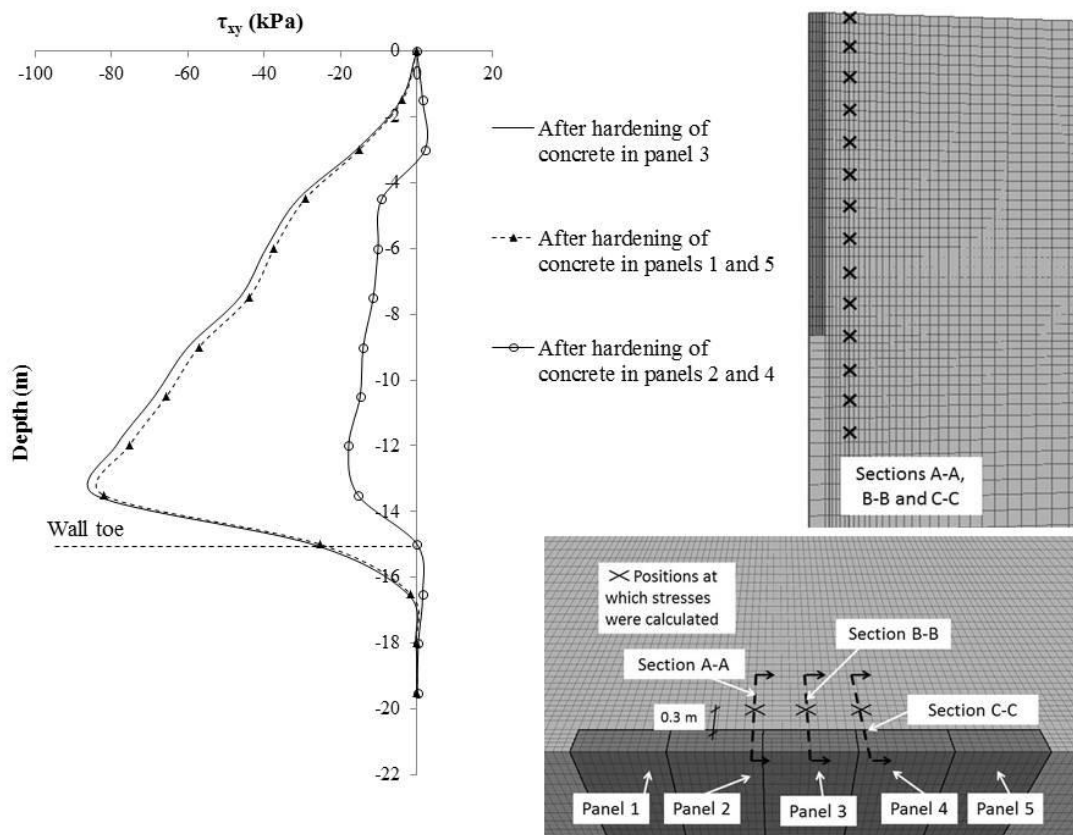


Figure 5.26. Variation with depth of the shear stress (τ_{xy}) acting on section C-C, at a normal distance from the wall of 0.3 m. Sequence 1.

As expected, the horizontal shear stresses (τ_{xy}) are small at section B-B, 0.3 m behind the wall, Figure 5.27, because the sequence of installation was symmetric with respect to the centre of the group of the panels. The direction of the major stress is perpendicular to the wall in the region of the section B-B.

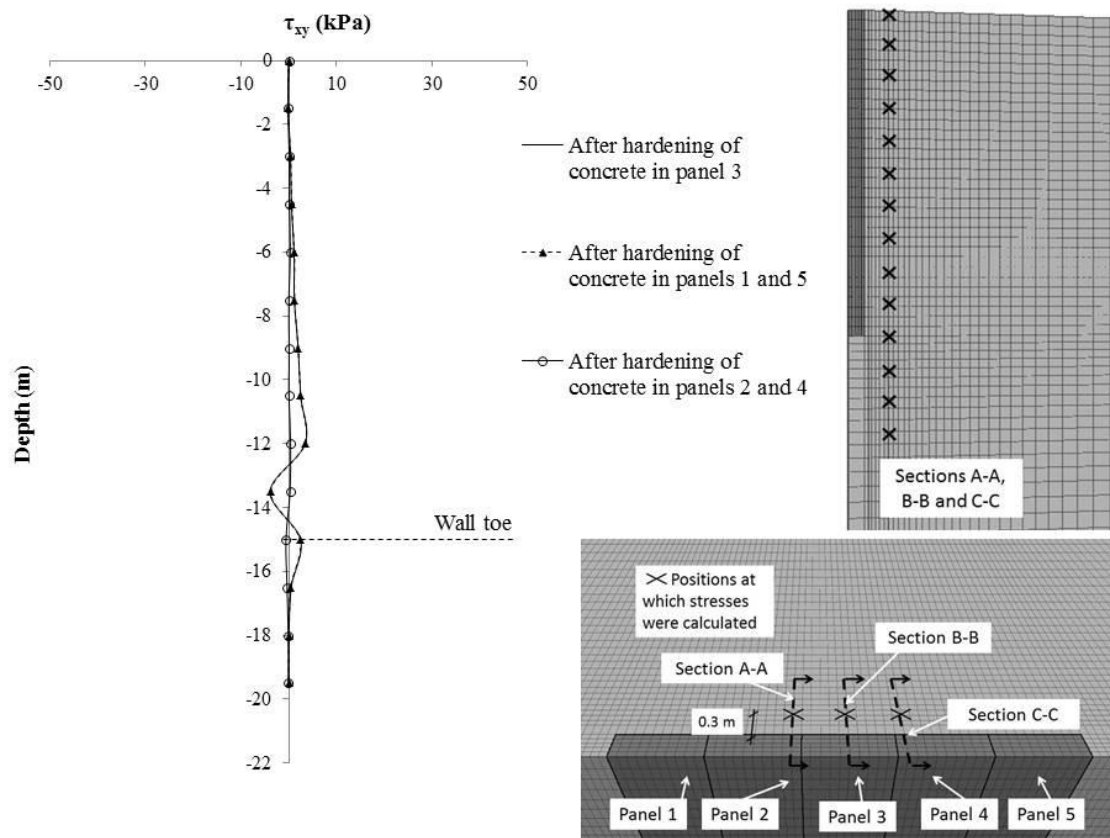


Figure 5.27. Variation with depth of the shear stress (τ_{xy}) acting on section B-B, at a normal distance from the wall of 0.3 m. Sequence 1.

Similar results were calculated by Ng and Yan (1998), who found the shear stresses τ_{yx} and τ_{zx} to be effectively zero at the central section of a group of installed panels

Vertical shear stress distribution (τ_{zy}), sequence 1

Figure 5.28 shows the vertical shear stress acting on section A-A after diaphragm wall installation sequence 1.

During the installation of the panels 1, 2, 4 and 5 the shear stress (τ_{zy}) increased below the toe of the wall. The increment of shear stress (τ_{zy}) below the toe of the wall led to an increase in the horizontal stress in this area as shown in Figure 5.2. Below the toe of the wall, the shear stress (τ_{xy}) remained small during the wall installation.

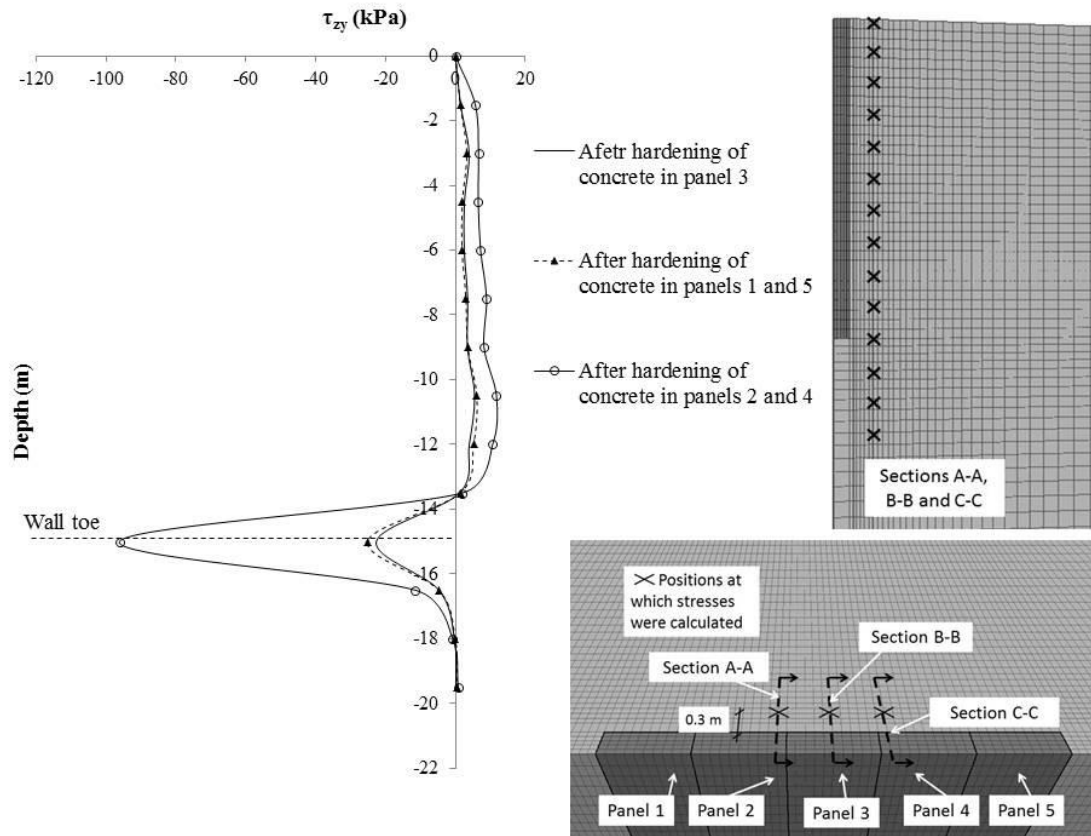


Figure 5.28. Variation with depth of the shear stress (τ_{zy}) acting on section A-A, at a normal distance from the wall of 0.3 m. Sequence 1.

After the installation of panels 3, the stresses increased slightly below the toe of the wall and remained constant behind the panel. During the installation of the panels 1 and 5 the vertical shear stresses did not change. As reported previously, these panels are far from the section A-A and their installation did not affect the stresses in that area. A significant increase in the shear stress (τ_{zy}) below the toe of the wall was calculated during the installation of the panels 2 and 4, Figure 5.28. These stresses reached values of approximately 100 kPa. Overall, the vertical shear stress distributions are similar to those found by Ng and Yan (1998). Similar results were found in section C-C, Figure 5.29, owing to the symmetry of the diaphragm wall installation with respect to the centre of the wall.

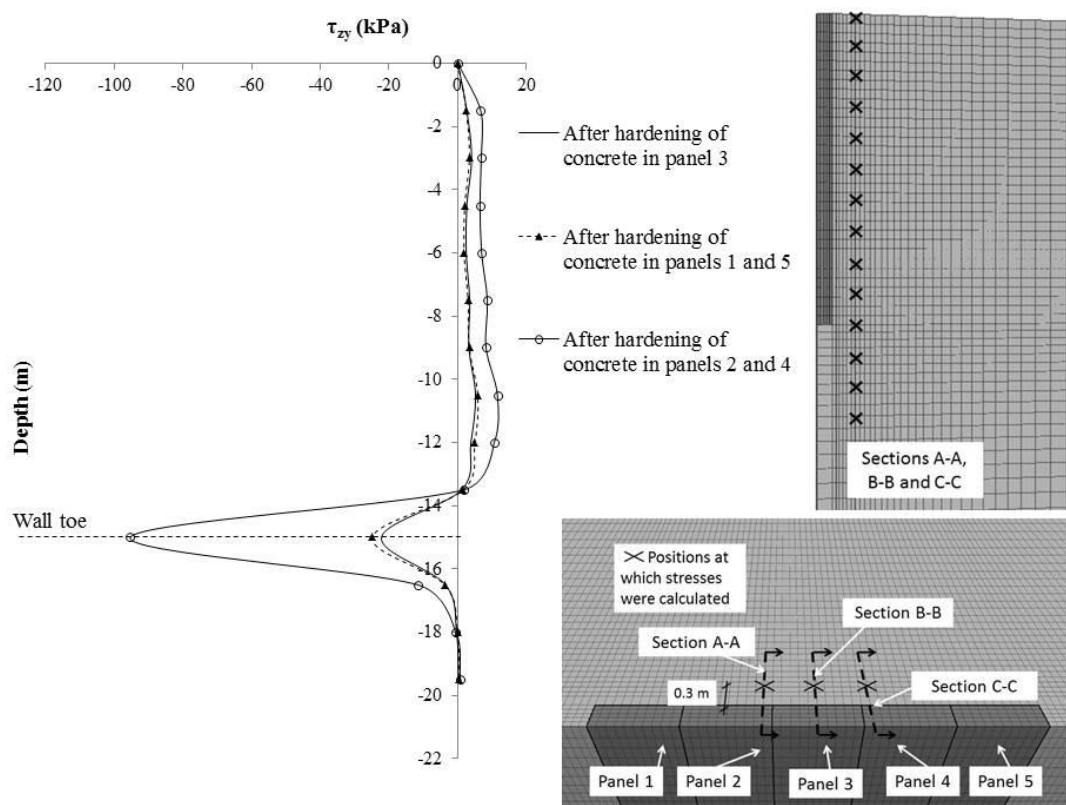


Figure 5.29. Variation with depth of the shear stress (τ_{zy}) acting on section C-C, at a normal distance from the wall of 0.3 m. Sequences 1.

Figure 5.30 shows the vertical shear stress after diaphragm wall installation in sequence 1. After the excavation of the panel 3, the vertical shear stress increases below the toe of the wall. During the subsequent installation of panels 1 and 5 the stress did not change. A slight increase in the vertical shear stress (τ_{zy}) was calculated after the subsequent installation of panels 2 and 4.

The horizontal stresses are redistributed vertically during wall construction with an increase of the stress occurring especially in the area above the toe of the central panel on section B-B (Figure 5.23). This horizontal stress increase is mainly due to the variation of the shear stress (τ_{zy}) in the area above the toe of the wall as shown in Figure 5.30. In Figure 5.30, the increase of the shear stress (τ_{zy}) was probably concentrated in the zone from 8 to 14 m depth. Similar results were also obtained by, Ng and Yan (1998).

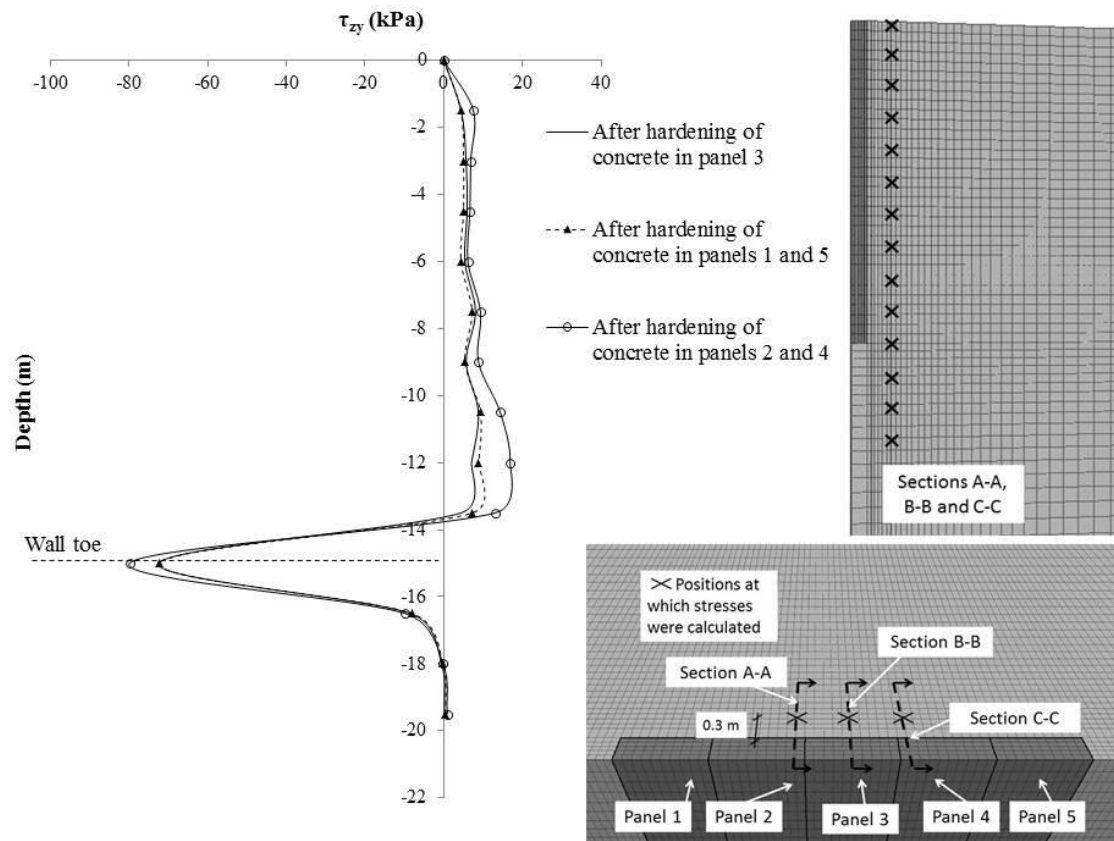


Figure 5.30. Variation of the shear stress (τ_{zy}) acting on section B-B, at a normal distance from the wall of 0.3 m. Sequence 1.

The following paragraphs describe in detail the stress variation during diaphragm wall installation in sequence 4.

Total Horizontal stress distribution, sequence 4

Figure 5.31 shows the variation of the total horizontal stress (σ_{yy}) acting on section A-A during the installation of panel 1. The total horizontal stress increases slightly on section A-A, because a smaller amount of the total horizontal stress is redistributed via the shear stress (τ_{xy}) from the soil close to the panel 1 to the section A-A. Figure 5.34 shows a minimal increase of the shear stress (τ_{xy}) on section A-A during the installation of the panel 1.

The installation of panel 1 did not cause any variation in the shear stress (τ_{zy}) on sections A-A, B-B and C-C, Figures 5.37, 5.38 and 5.39. The distribution of the shear stress (τ_{zy}) and (τ_{xy}) is also presented and discussed later.

The installation of panel 2 led to a slight decrease in the total horizontal stress on section A-A, Figure 5.31. In contrast, at section B-B the horizontal stress during the installation of the panel 2 increases slightly. Again, this was mainly due to the redistribution of the horizontal stress via the shear stress (τ_{xy}) on section B-B after the installation of panel 2, Figure 5.36. Thus, the installation of panel 2 leads to an increase in the shear stress (τ_{xy}) on section B-B, Figure 5.34. In this area (section B-B) in sequence 1, the shear stresses (τ_{xy}) were zero during all phases of construction because of the symmetry of the construction sequence with respect to the centre of the wall.

Figure 5.31 shows a slight increase in the total horizontal stress below the toe of the panel in section A-A during the installation of panel 2. Again, this is because the horizontal stresses were redistributed via the shear stress (τ_{zy}) below the toe of the wall as shown in Figure 5.37.

The construction of panel 3 led to a decrease in the total horizontal stress at section B-B, Figure 5.33, and a smaller decrease at section A-A, Figure 5.31. At section C-C, the total horizontal stress did not change during the installation of panel 3. The different total horizontal stress changes between sections A-A and C-C must be a consequence of the different patterns of shear stress (τ_{xy}) re-distribution for a non-symmetric installation sequence with respect to the central section of the panels.

After the excavation of panel 3, the shear stress (τ_{xy}) on section C-C increased while the shear stress on section A-A decreased, implying that the soil is sheared in two opposite directions.

The installation of panel 4 did not cause any change in the total horizontal stress on section A-A, Figure 5.31. In contrast, the total horizontal stress on section B-B, Figure 5.33, showed a slight increase due to the variation of the shear stress (τ_{xy}), Figure 5.36. The shear stress (τ_{zy}) on section B-B, Figure 5.39, remained constant during the installation of panel 4. Again, this

means that the horizontal total stress changes were mainly a consequence of the variation of the shear stress (τ_{xy}).

A large decrease in the total horizontal stress (σ_{yy}) at section B-B was calculated after the installation of panel 3, Figure 5.33. At this section these stresses did not change after the installation of panels 4 and 5. This means that the panels 4 and 5 were far enough from the section B-B for their installation not to influence the stresses changes at the section B-B.

Figure 5.32 shows the total horizontal stress changes at section C-C, Figure 5.8, during sequence 4. It was found that the horizontal stress did not change after the installation of panels 1, 2 and 3. A slight horizontal stress increase was found after the installation of panel 3. In contrast, a large decrease in the horizontal stresses was calculated after the installation of panel 4. The horizontal stress on section C-C did not change after the installation of panel 5. The stress relief was concentrated in the zone above the toe of the wall, while a slight stress increase was apparent behind the toe of the wall.

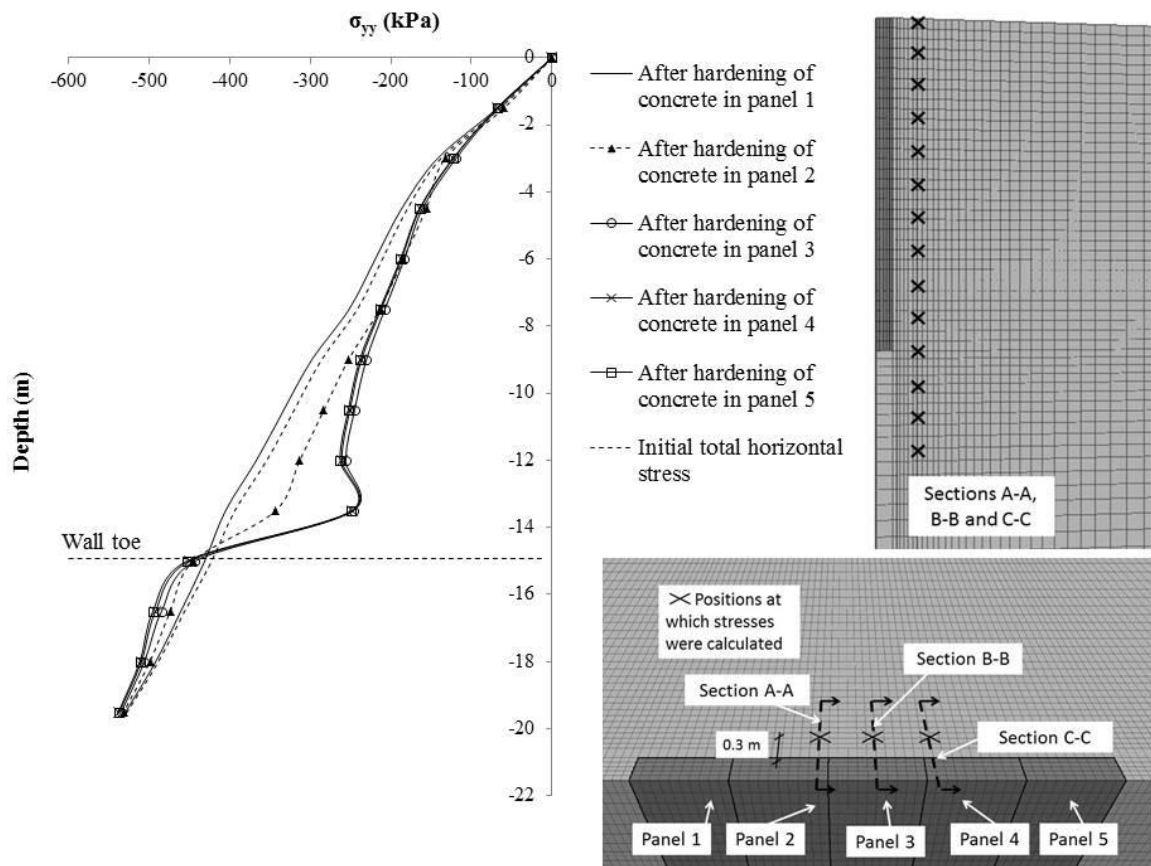


Figure 5.31 Variation with depth of the total horizontal stress (σ_{yy}) acting on section A-A, at a normal distance from the wall of 0.3 m. Sequence 1.

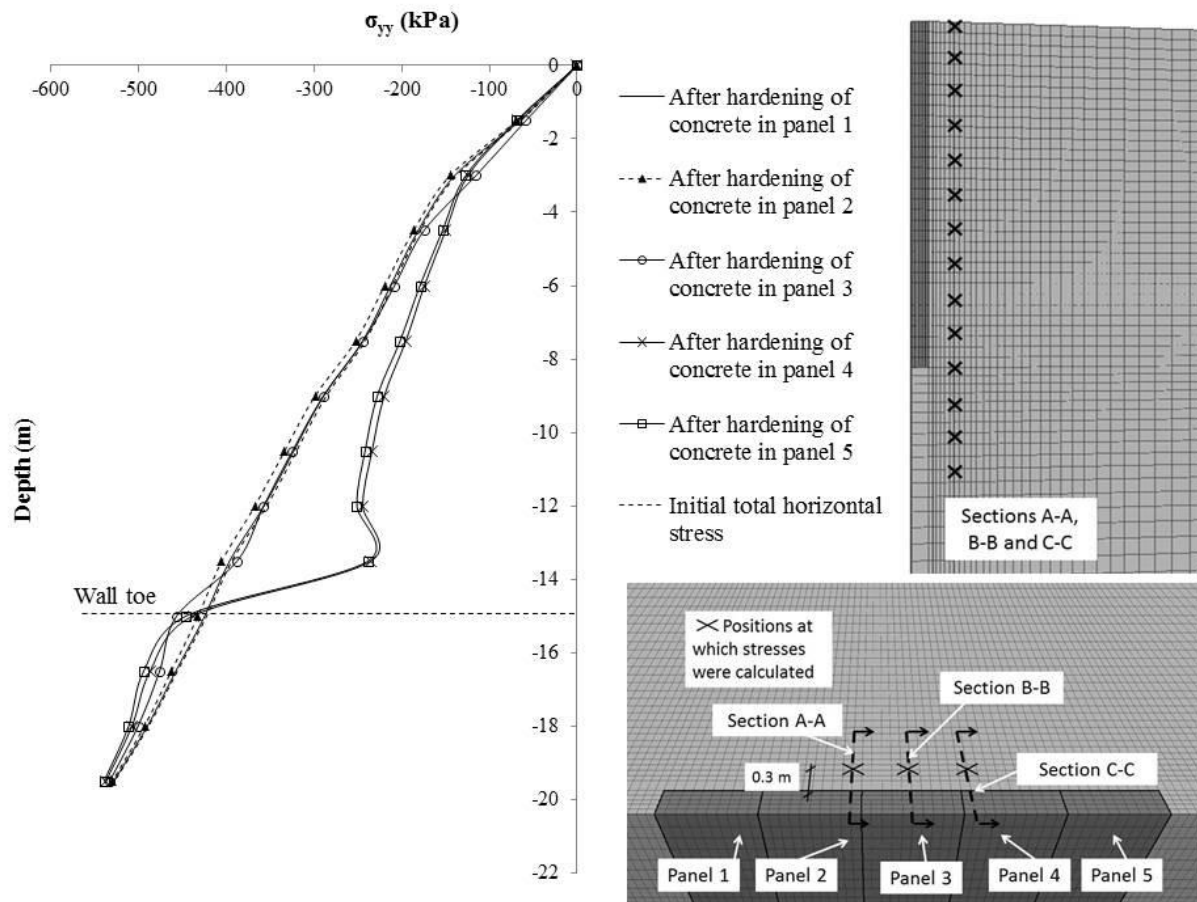


Figure 5.32. Variation with depth of the total horizontal stress (σ_{yy}) acting on section C-C, at a normal distance from the wall of 0.3 m. Sequence 4.

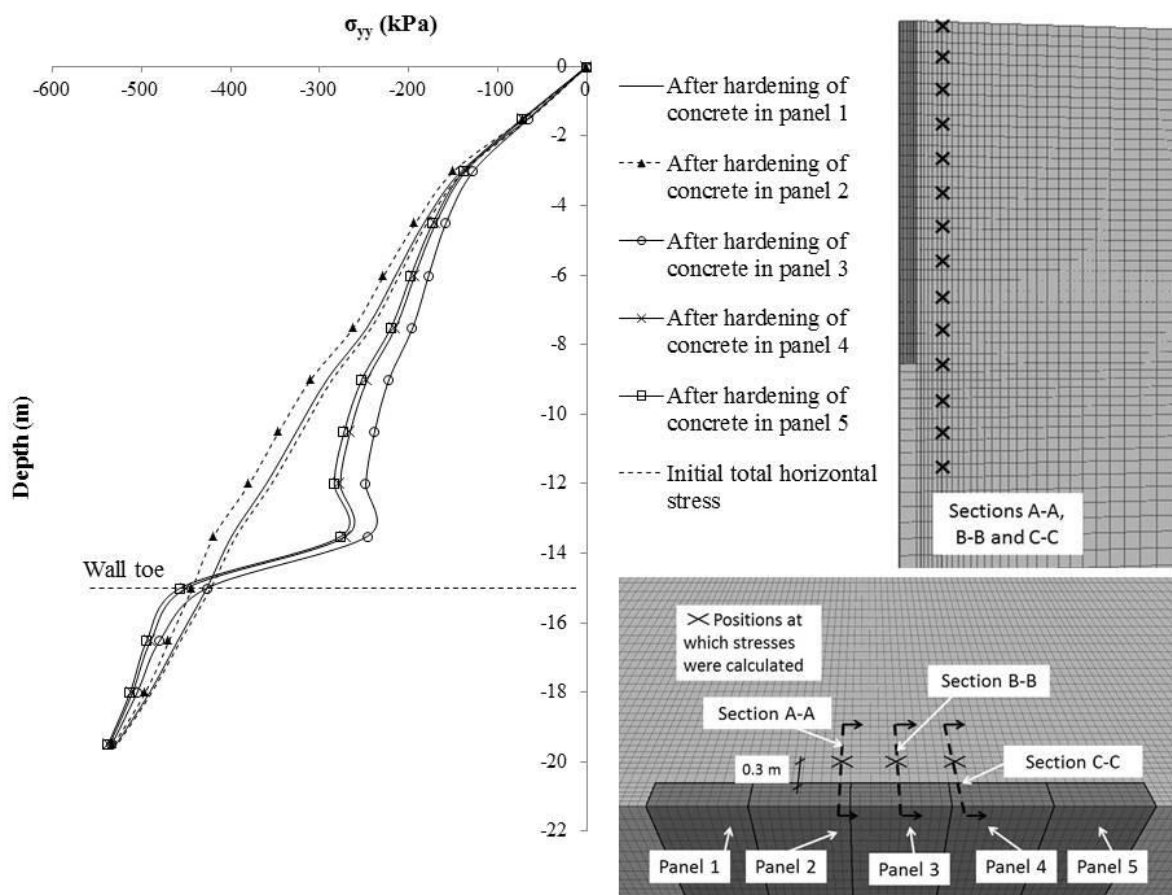


Figure 5.33. Variation with depth of the total horizontal stress (σ_{yy}) acting on section B-B, at a normal distance from the wall of 0.3 m. Sequence 4.

Horizontal shear stress distribution (τ_{xy}), sequence 4

Figure 5.34 shows the horizontal shear stress distributions (τ_{xy}) at section A-A during sequence 4, Figure 5.8.

As reported previously the installation of panel 1 did not cause any change in the shear stress (τ_{xy}) on section A-A. However, a large increase in the horizontal shear stress (τ_{xy}) was calculated after the excavation of panel 2. From Figure 5.34 it can be observed that these stresses became zero after the installation of the subsequent panel 3. During the installation of panel 3 the direction of the shear stresses (τ_{xy}) were opposite to those during the installation of panel 2. After that the shear stresses (τ_{xy}) on section A-A remained constant and small during the subsequent installation of the panels 3, 4 and 5, Figure 5.34.

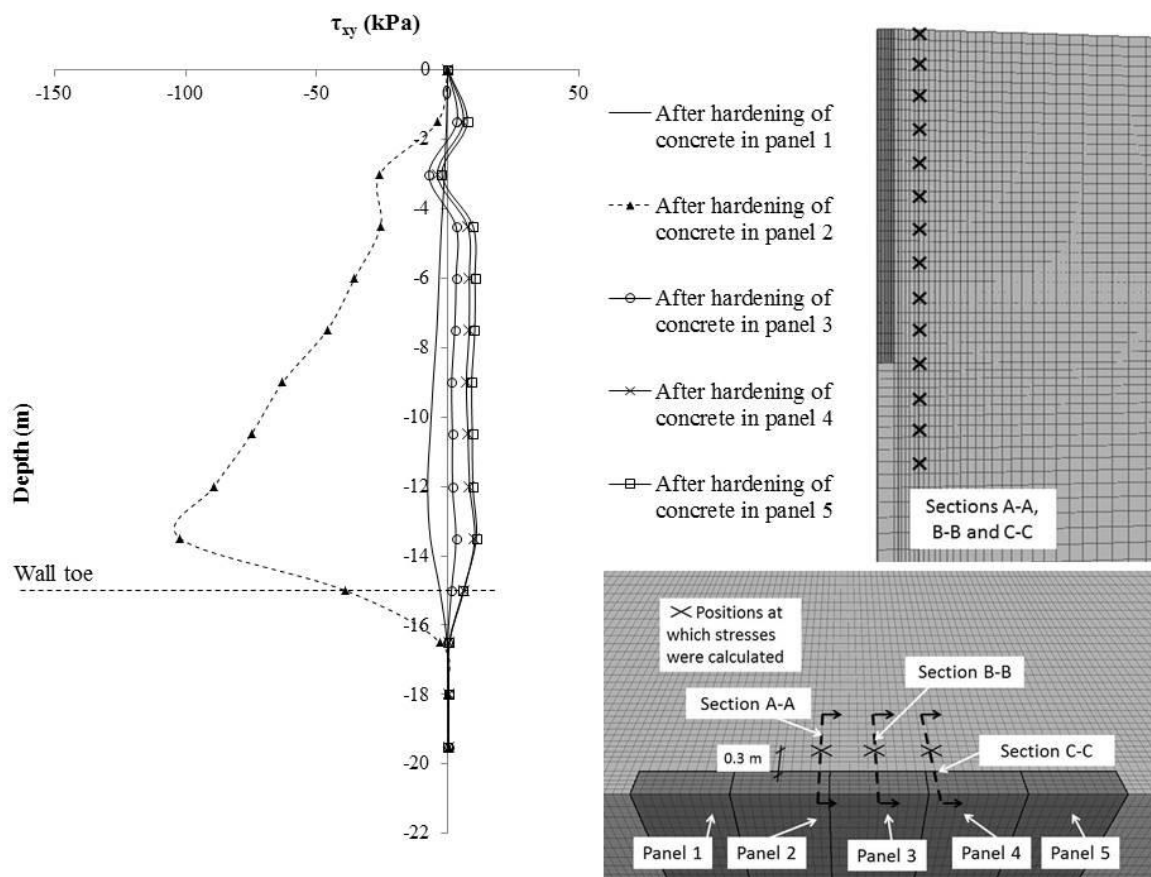


Figure 5.34. Variation with depth of the shear stress (τ_{xy}) acting on section A-A, at a normal distance from the wall of 0.3 m. Sequence 4.

Figure 5.35 shows the variation of the horizontal shear stress (τ_{xy}) with depth at section C-C. The horizontal shear stresses (τ_{xy}) remained small during the installation of panels 1 and 2. In contrast, a large increase in the horizontal shear stress occurred during the installation of panel 3. Again, a significant decrease in the horizontal shear stress (τ_{xy}) was apparent after the installation of panel 4.

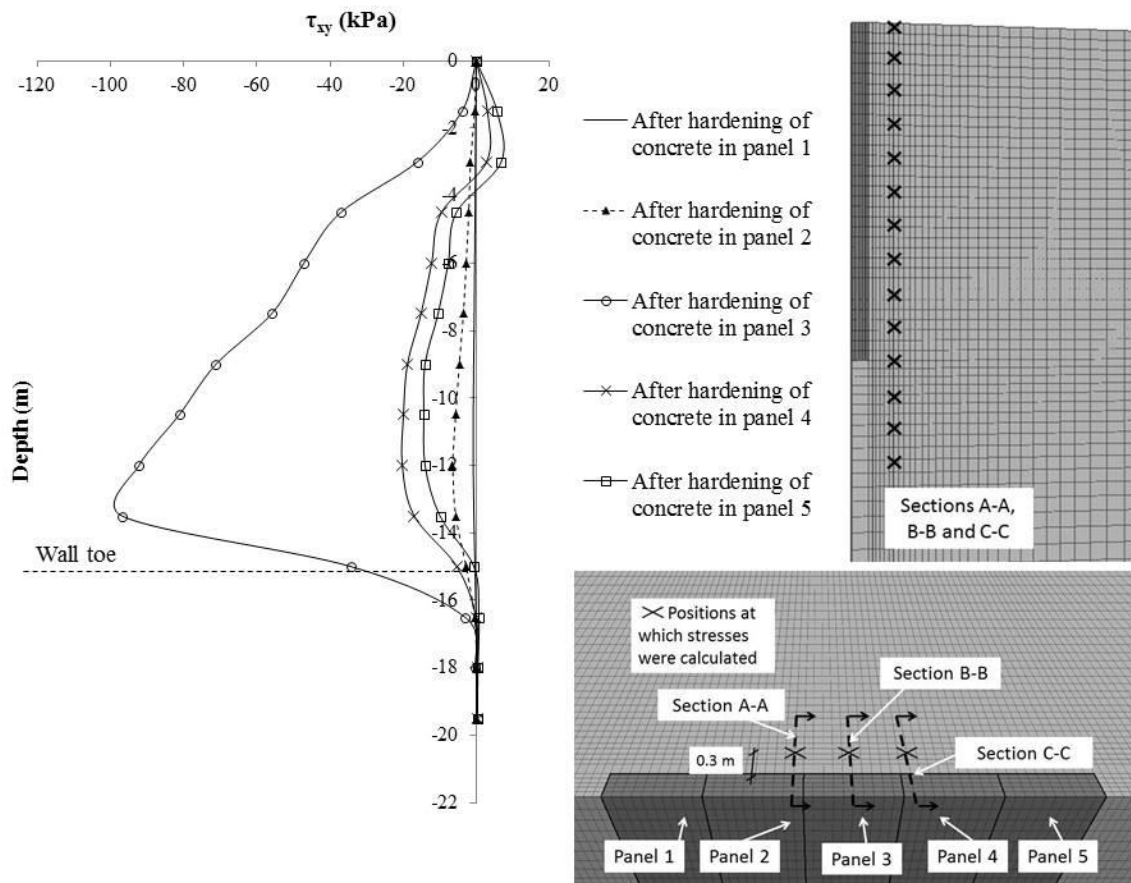


Figure 5.35. Variation with depth of the shear stress (τ_{xy}) acting on section C-C, at a normal distance from the wall of 0.3 m. Sequence 4.

Figure 5.36 shows the horizontal shear stress variations at section B-B, 0.3 m behind the wall, in sequence 4. It can be noted that the installation of panel 1 did not lead any variation of the horizontal shear stress (τ_{xy}). In contrast, the installation of panel 2 led to an increase in the shear stress (τ_{xy}) especially in the centre of the panel at section B-B. The shear stresses did not change after the installation of panel 3. However, a decrease in the shear stress (τ_{xy}) was calculated after the installation of panel 4. The installation of panel 5 did not result in any variation in those stresses. Overall, the horizontal shear stress changes at section B-B are slightly different from those found in sequence 1, in which the installation was symmetric with respect to the centre of the wall.

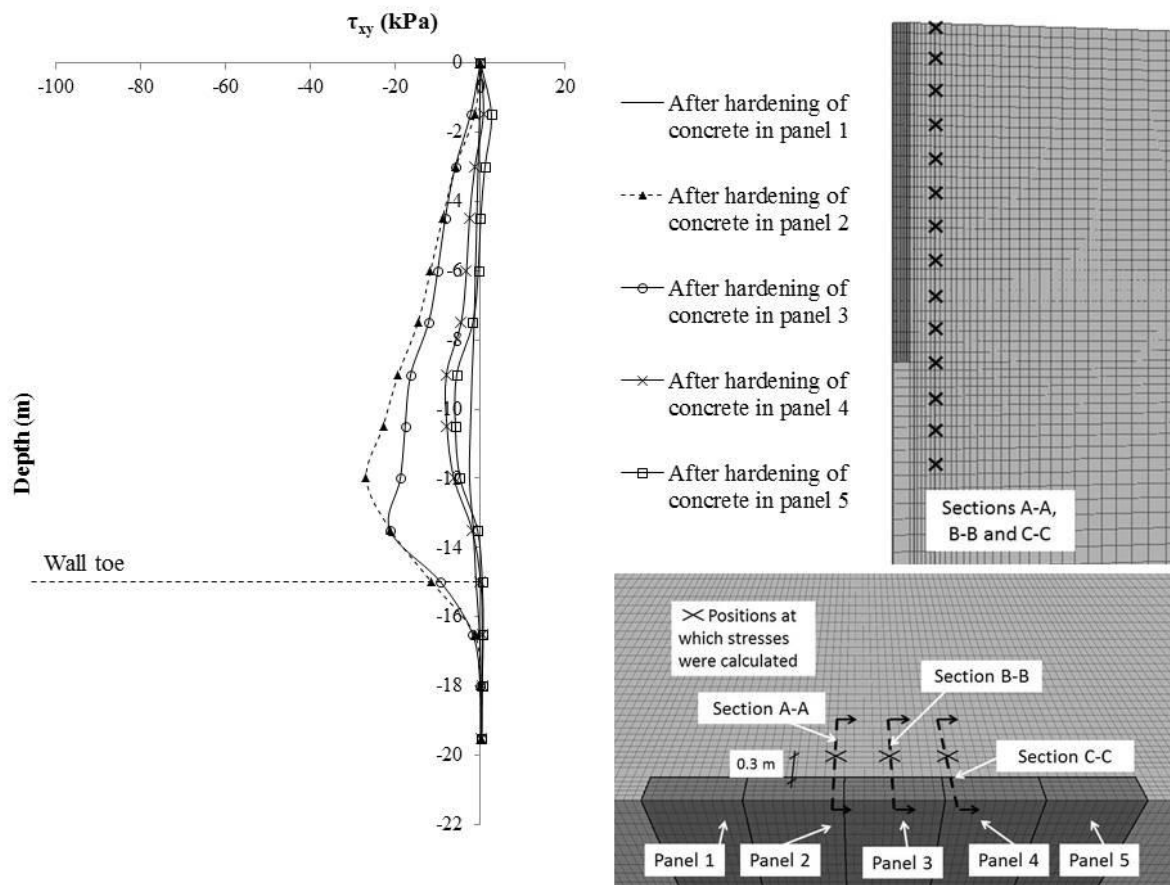


Figure 5.36. Variation with depth of the shear stress (τ_{xy}) acting on section B-B, at a normal distance from the wall of 0.3 m. Sequence 4.

Vertical shear stress distribution (τ_{xy}), sequence 4

Figure 5.37 shows the vertical shear stress (τ_{zy}) on section A-A, Figure 5.8, during the panel installation in sequence 4.

The vertical shear stresses remained zero during the construction of panel 1. An increase in these stresses below the toe of the wall occurred during the installation of panel 2. A further increase in the vertical shear stress, especially below the toe of the wall, occurred during the construction of panel 3. These stresses did not change during the subsequent phases of construction, panels 4 and 5.

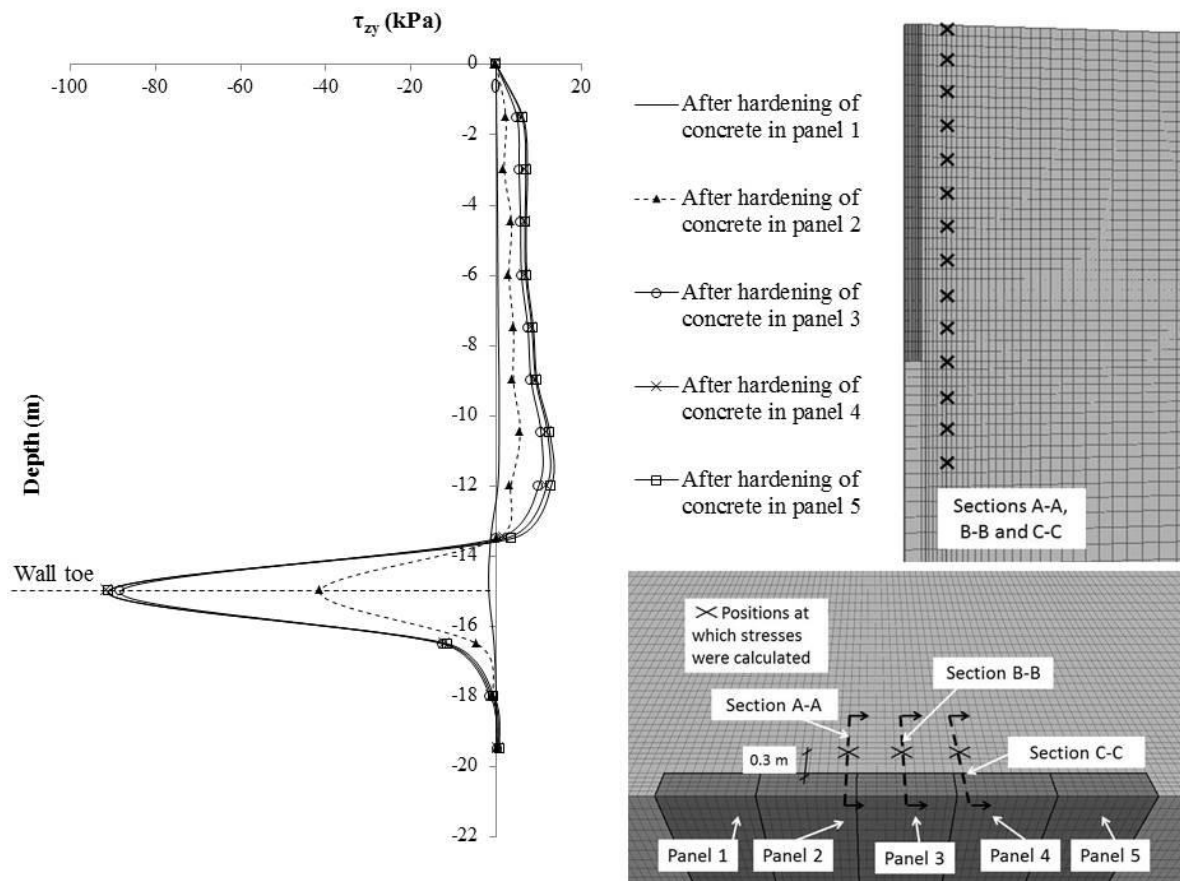


Figure 5.37. Variation with depth of the shear stress (τ_{zy}) acting on section A-A, at a normal distance from the wall of 0.3 m. Sequence 4.

From Figure 5.38 it can be noted that the vertical shear stresses (τ_{zy}) remained small during the installation of panels 1 and 2. A slight increase in the vertical shear stress (τ_{zy}) occurred beneath the toe of the wall during the excavation of panel 3.

Again, in Figure 5.38 a significant increase in the vertical shear stress occurred after the excavation of panel 4. The vertical shear stresses (τ_{zy}) were concentrated below the toe of the wall and remained almost constant from the head of the wall down to 12 m depth. Finally, the vertical shear stresses (τ_{zy}) did not change after the construction of panel 5, as can be seen in Figure 5.38.

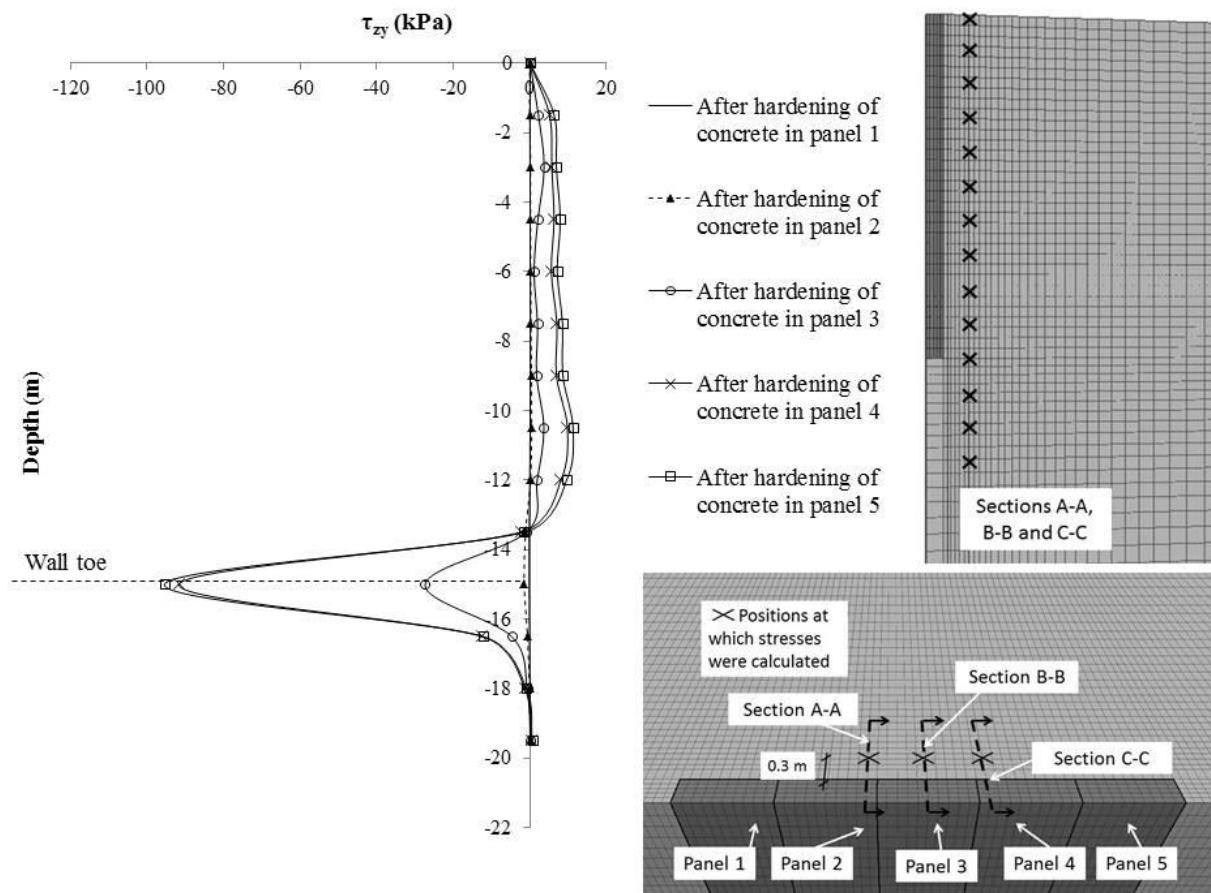


Figure 5.38. Variation with depth of the shear stress (τ_{zy}) acting on section C-C, at a normal distance from the wall of 0.3 m. Sequence 4.

Figure 5.39 shows that the vertical shear stresses did not change during the installation of panels 1 and 2 in the region of section B-B. However, significant increase below the toe of the wall occurred during the construction of panel 3. The vertical shear stresses (τ_{zy}) remained constant during the subsequent installation of panels 4 and 5.

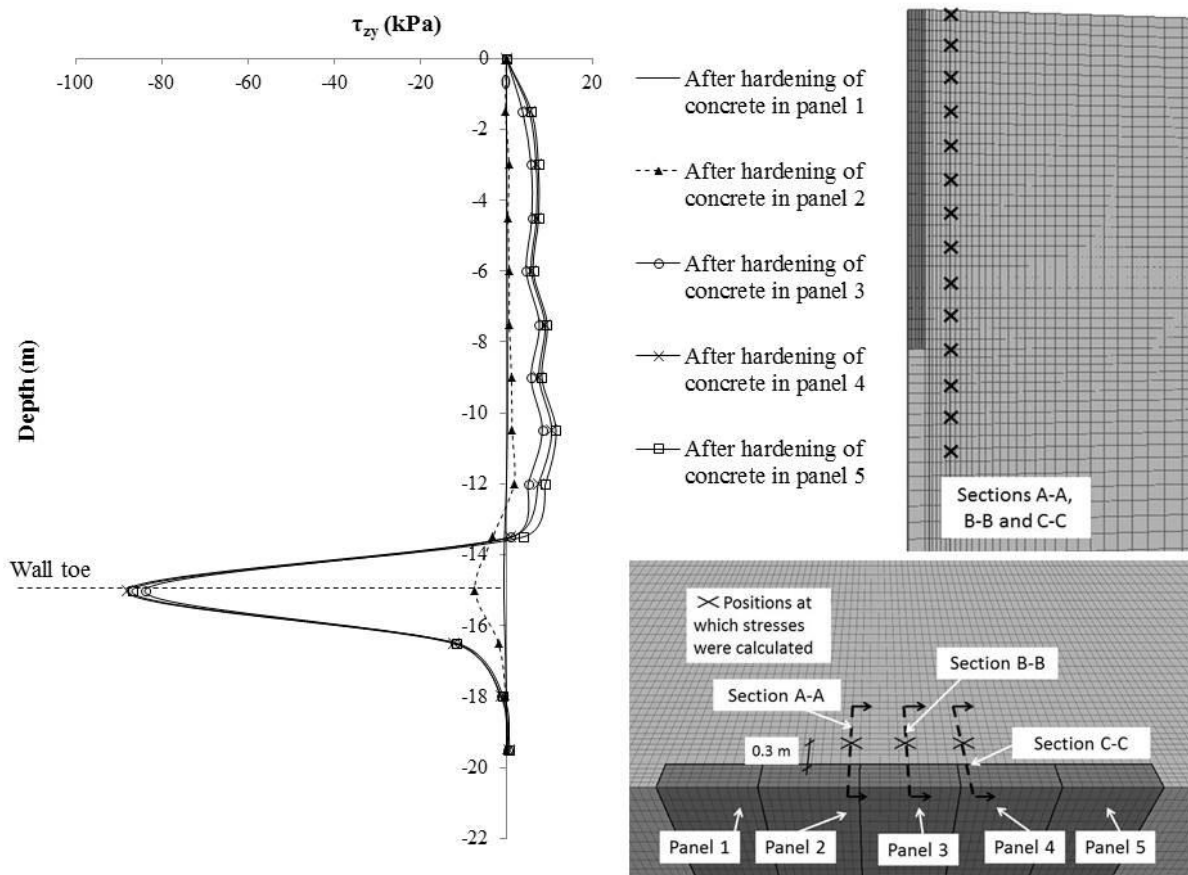


Figure 5.39. Variation with depth of the shear stress (τ_{zy}) acting on section B-B, at a normal distance from the wall of 0.3 m. Sequence 4.

5.3.5 Stress distribution behind the wall at 0.3, 5, 10, and 15 m far from the wall

Figure 5.40 shows the final total horizontal stress profiles 5 m from the centre of the wall for all of the investigated sequences.

Figure 5.40 shows that the stresses are equal during all the construction sequences. Overall, the total horizontal stress decreased over a zone extending from 6 m to 16 m below the top of the wall.

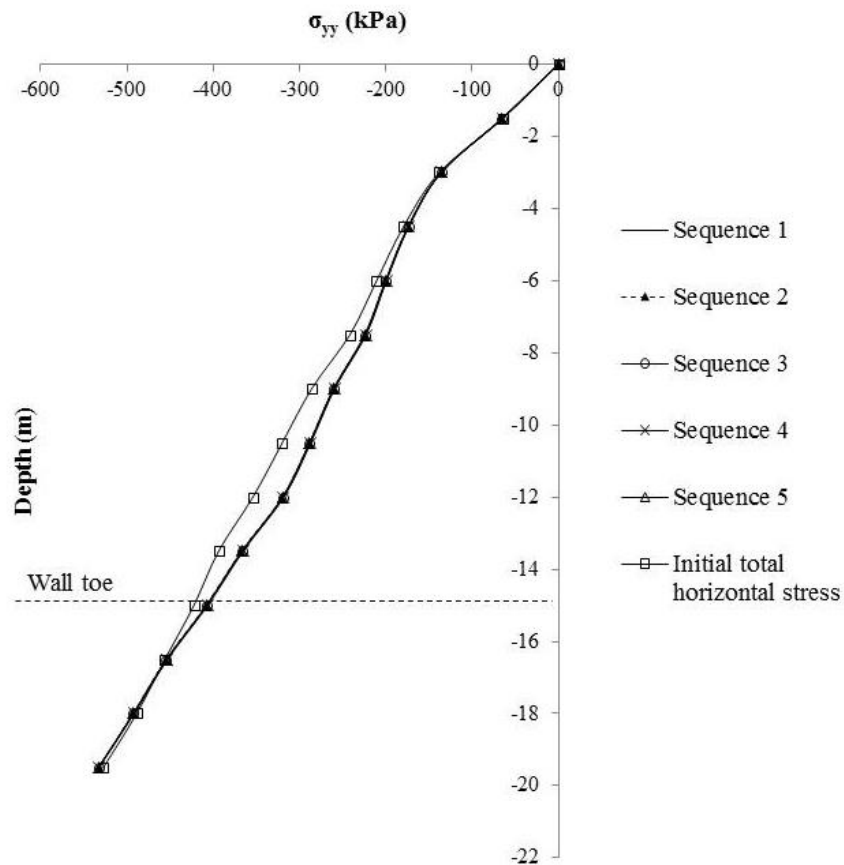


Figure 5.40. Total horizontal stress (σ_{yy}) profiles 5 m from the wall, normal to the centre of panel 3, for all installation sequences.

Figure 5.41 shows the horizontal stress change 10 m away from the wall at the centre of the diaphragm wall. A slight horizontal stress decrease in the zone from 8 to 14 m depth has occurred.

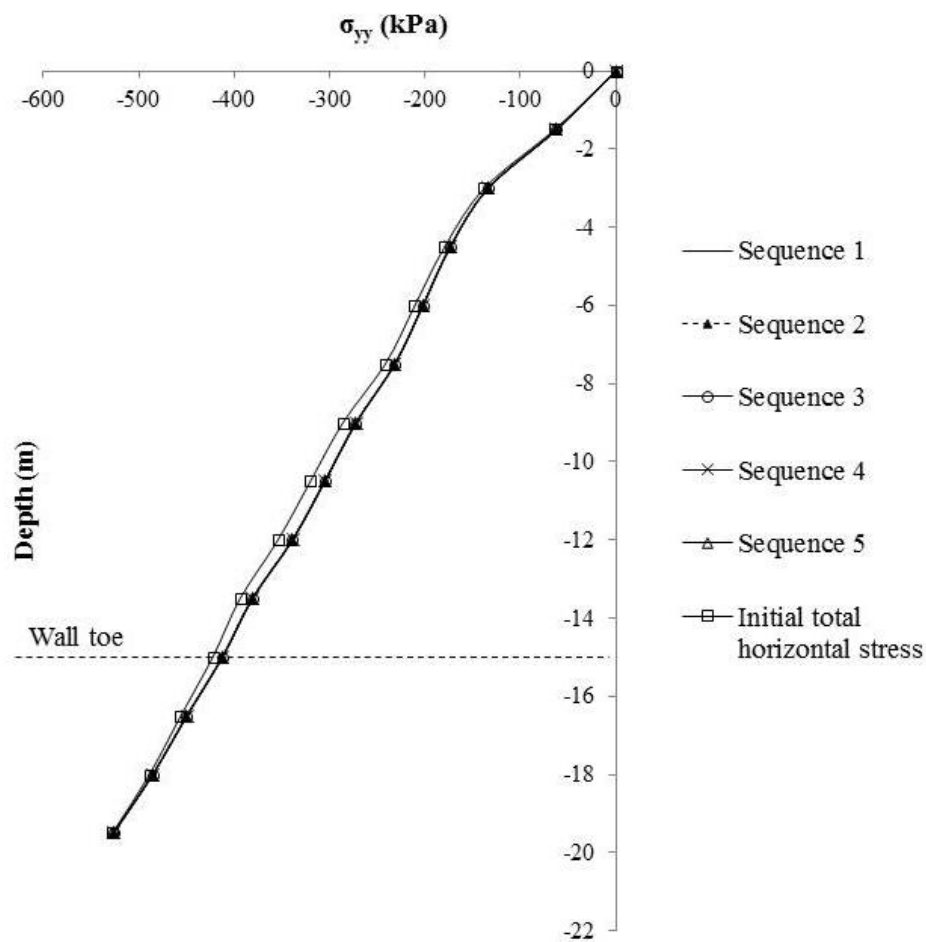


Figure 5.41. Total horizontal stress (σ_{yy}) profiles 10 m from the wall, normal to the centre of panel 3, for all installation sequences.

The horizontal stresses changes 15 m behind the wall were found to be negligible, Figure 5.42.

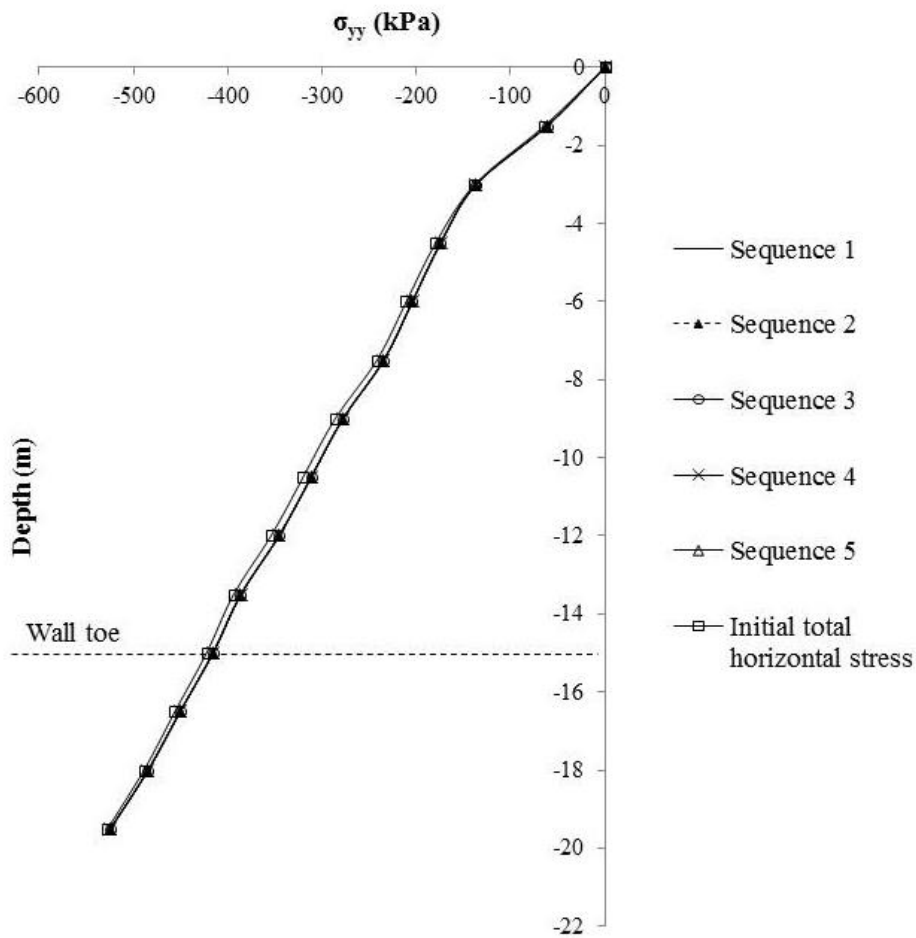


Figure 5.42. Total horizontal stress (σ_{yy}) profiles 15 m from the wall, normal to the centre of panel 3, for all installation sequences.

The total horizontal stress changes at various distances from the wall are not affected by the sequence of panel installation (Figures 5.41, 5.42 and 5.43).

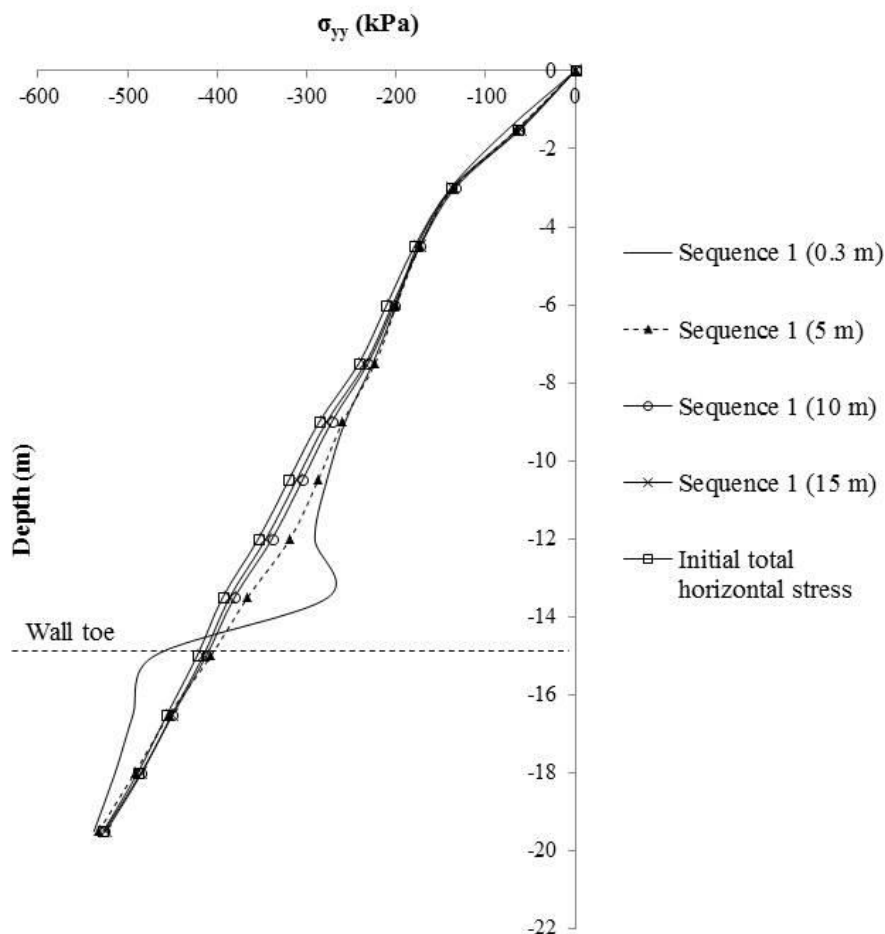


Figure 5.43. Total horizontal stress (σ_{yy}) profiles at various normal distances from the centre of panel 3 (sequence 1).

5.3.6 Horizontal displacement along the excavation after all the sequences modelled

Farmer and Attewell (1973) investigated the horizontal stress variation and the deformation of a diaphragm panel excavation supported by bentonite slurry. The trench excavation was 6.1 m long, 0.8 m wide and 15 m deep. They found that the maximum horizontal deformation occurred at about one-third of the panel depth below ground level. Beyond a distance of about two-fifths of the panel depth from the trench, the horizontal movements at the surface were negligible.

Powrie and Kantartzi (1996) reported that the deformation associated with a trench excavation of a finite length was less than for a plane strain excavation. Ground movements were found to depend on a number of factors, including the geometry (length/depth ratio) of the panel. This

was also found when comparing the displacement after a diaphragm wall installation with those calculated in Chapter 3 and 4 during the installation of a bored pile wall.

Ng and Yan (1998) found that the horizontal ground deformation was larger at the centre of the panel. They reported that the deformation at the centre was about 5 times larger than that at the edge of the panel.

Figure 5.45 shows the horizontal displacements behind the wall at sections A-A, B-B and C-C, after the installation of all panels in sequence 1. The horizontal displacements behind the wall at the edge of the central panel are bigger than the displacement at the middle section of the central panel.

Gourvenec and Powrie (1999) found that after the installation of the primary panel the displacements along the edges of the panel were very small. Displacements were larger along the centre line of the panel. They compared the horizontal displacement profile calculated along the centre of the panel with those calculated in the plane strain analysis, and found that the maximum displacement profile of the excavation boundary was up to three times smaller than in plane strain. From Figure 5.45 it was found that the horizontal displacement at the middle section became minor compare to those found at the edges of the central panel installed. Thus, the displacement at the edge of the panel could be large in comparison to those in the middle section of the panel, owing to the effects of the panels subsequently installed.

Gourvenec and Powrie (1999) found that the maximum horizontal displacement behind the panel wall was at the head of the wall. This is different from the results show in Figure 5.46, 5.47 and 5.48 where it was found that the maximum horizontal displacement was found above the toe of the wall. Similar results were also found by Ng and Yan (1998). Figure 5.44 shows the horizontal displacement calculated in this chapter compared to those calculated by Ng and Yan (1998) and Gourvenec and Powrie (1999). It can be noted that a similar trend of the horizontal displacements behind the wall were found between the results shown in this chapter and the results calculated by Ng and Yan (1998). The difference in the computed trend results calculated by Gourvenec and Powrie (1999) with those in this chapter and by Ng and Yan (1998) could be due to the fact that Gourvenec and Powrie (1999) used consolidation elements with smaller shear strength to avoid the need to assume that wall installation would be an

undrained event. Instead undrained soil parameters were assumed in this chapter and by Ng and Yan (1998).

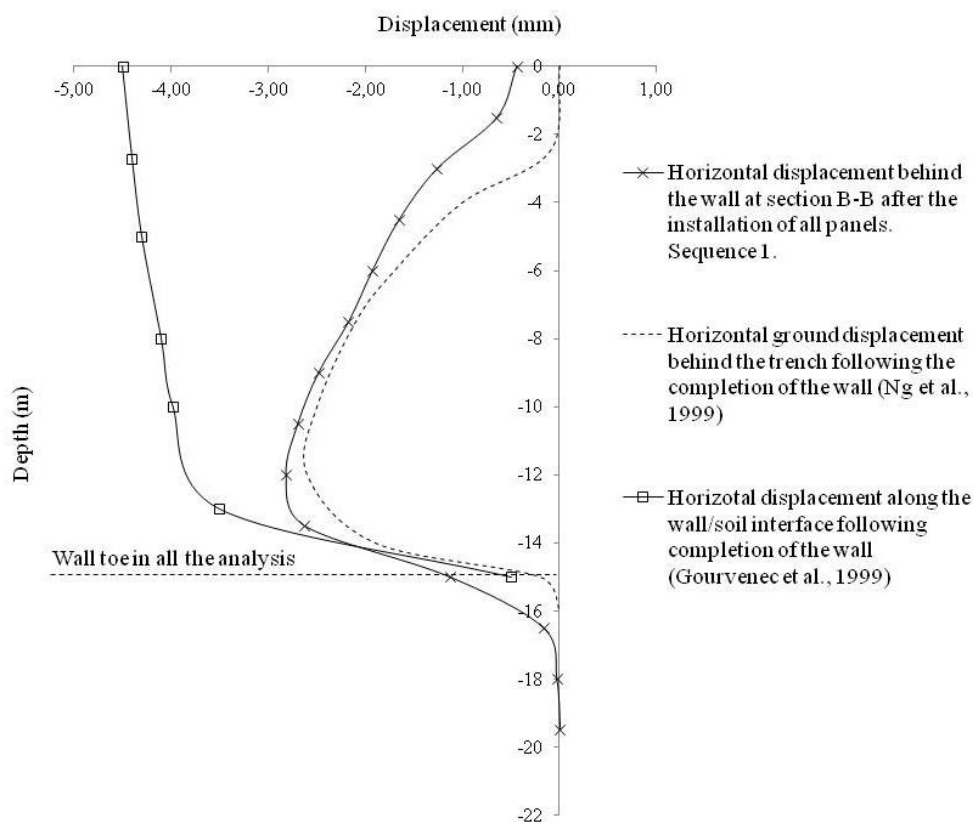


Figure 5.44. Comparison of the horizontal displacements behind the wall at sections B-B with those calculated by Ng and Yan (1998) and Gourvenec and Powrie (1999).

The horizontal displacement plotted in Chapters 3 and 4 may be compared with the calculated displacements in this chapter. Horizontal displacements below the toe of the wall became negligible 0.3 m below the toe of the wall for a bored pile wall, Figure 4.30. For a diagram wall panel the horizontal displacements below the toe became zero at a distance of 1.6 m below the toe of the wall. Gourvenec and Powrie (1999) do not show the displacement below the toe of the wall, but found that the displacement became zero at 1 m depth below the toe of the wall for a single panel installed. Again, the results suggest that as the length of the element installed increases, the depth of measurable horizontal displacement below the toe of the wall also increases.

It can be observed from Figures 5.46, 5.47 and 5.48 that the horizontal displacements 0.3 m behind the wall at sections A-A, B-B and C-C are the same after each of the five sequences that

were investigated. The horizontal ground deformation was largest above the toe of the wall. Furthermore, the horizontal ground displacements were non-linear with depth behind the panel.

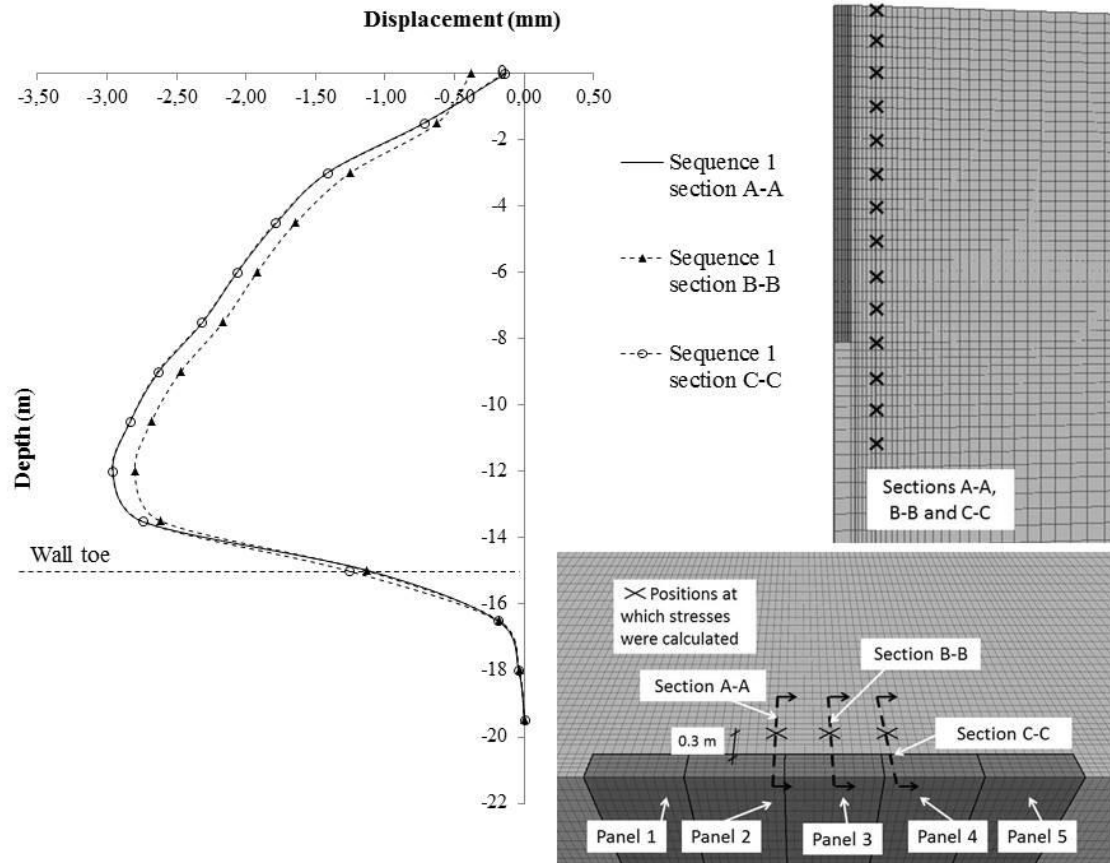


Figure 5.45. Horizontal displacements behind the wall at sections A-A, B-B and C-C, after the installation of all panels. Sequences 1.

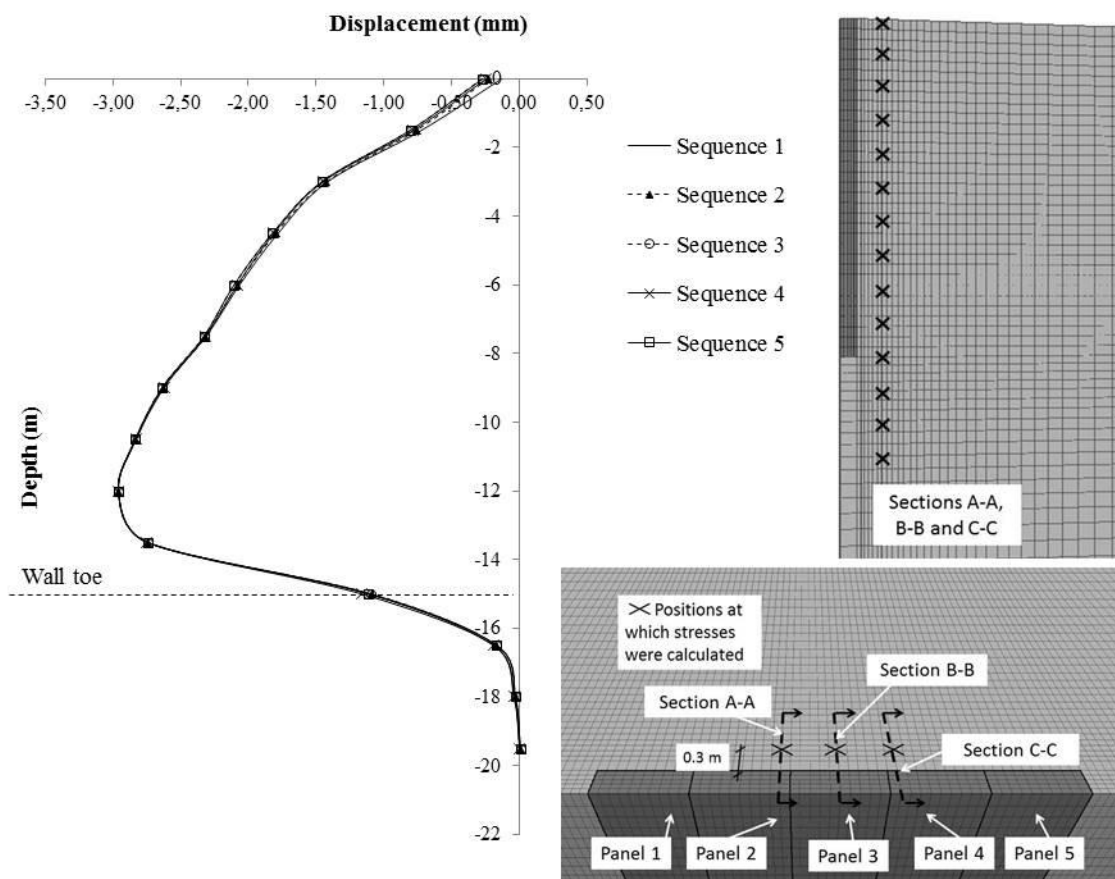


Figure 5.46. Horizontal displacements behind the wall at section A-A after the installation of all panels. Sequences 1, 2, 3, 4 and 5.

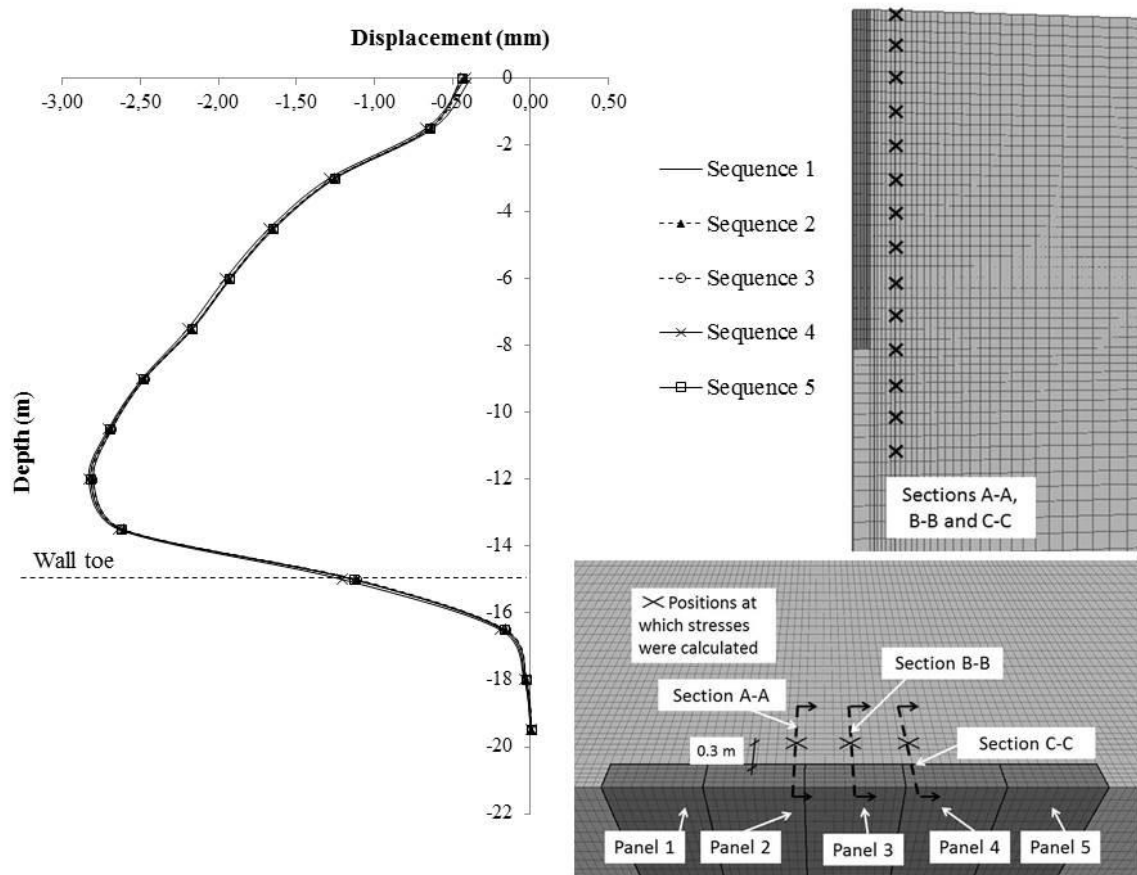


Figure 5.47. Horizontal displacements behind the wall at section B-B after the installation of all panels. Sequences 1, 2, 3, 4 and 5.

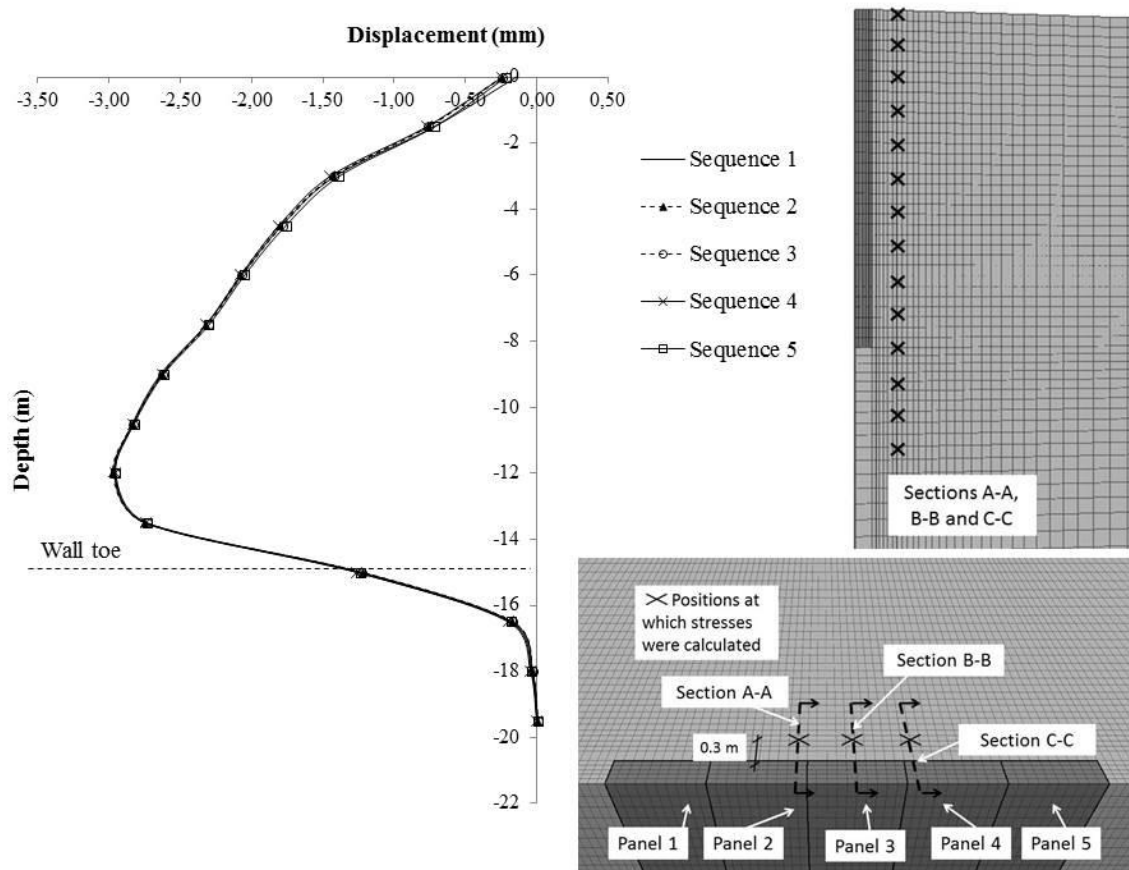


Figure 5.48. Horizontal displacements behind the wall at section C-C after the installation of all panels. Sequences 1, 2, 3, 4 and 5.

5.4 Summary

The installation of a sequence of diaphragm wall panels in the ground, involving in each case excavation under a bentonite support slurry followed by placing and subsequent hardening of the concrete, is in reality a complex three-dimensional event (Gourvenec and Powrie, 1999). In this chapter, the ground stress changes and displacements associated with five different sequences of diaphragm wall panel installation were investigated. The numerical simulations of diaphragm walls construction were carried out using a finite difference programme $FLAC^{3D}$ 4.0.

Analyses were carried out to compare the final stress variations for five different installation sequences of a group of five panels installed in an overconsolidated soil deposit. Then,

innovatively in this chapter, it was investigated whether a different sequence of panel installation could lead to a different pre-excavation stress distribution behind the wall.

- It was found that the maximum distance along the wall, at which the installation of a single panel has an effect, is approximately 7.5 m. An increase of the total horizontal stresses in the soil close to the edges of the panel was observed. This result was also observed by Gourvenec and Powrie (1999) and Ng and Yan (1998). This result confirms that the different geometry between a pile and panel leads to different stress changes in the soil during their installation.
- It was found that the construction of the adjacent panel influences the stress at the middle section of the central panel. This is different from the finding by Ng and Yan (1998), that the construction of the adjacent panel has only a minor influence on the stress distribution at the middle section in the central panel. This is mainly because the large panel length (8 m) used by Ng and Yan (1998), which limited the extent of the horizontal arching action. In this chapter, the modelled panel length was 2.5 m.
- It was found that the horizontal stress at the edges and the middle section of the centre panel is not much affected by the installation sequence. However, the horizontal stresses (σ_{yy}) after the construction in sequence 4 on section C-C (edge of the centre panel), was slightly different from those calculated in the other sequences. The non-symmetric process of panel installation on sequence 4 affected slightly the final stress distribution in the soil close to the edge of the central panel. For a non-symmetric installation (sequence 4), the value of the shear stress (τ_{xy}) on the edge of the central panel was slightly different than those found during the other construction sequences.
- The results reported in this chapter may be compared with those calculated for the installation of a bored pile wall, chapter 3 and 4. For a bored pile wall the horizontal stress decrease is more focussed above the toe of the wall. Instead, for a diaphragm panel wall, stress decreases are also computed on the entire depth of the wall. However, the stress decreases are mainly concentrated in the zone above the toe of the wall. Furthermore, it has been calculated that beneath the toe of the diaphragm wall the total horizontal stress became higher compare to the initial stress for a depth of approximately 2.5 m behind the toe of the wall. In contrast, for a bored pile wall it was calculated that the stress behind the wall fell to the initial stress values approximately 1.5 m below the toe. This is mainly due to the lower redistribution of the shear stress

(τ_{zy}) below the toe of the bored pile wall compared to those calculated below the toe of the diaphragm wall, which lead to a different redistribution of the total horizontal stresses beneath the toe of a diaphragm wall and a bored pile wall.

- Geometry effects are the main reason for the differences between the stress changes calculated during the installation of a single pile and those found after the installation of a diaphragm wall.
- The global distribution of the horizontal shear stresses (τ_{xy}) was similar to that found by Ng and Yan (1998). The shear stresses are distributed along the entire depth of the wall with an increase above the toe. For a diaphragm panel 8 m long, Ng and Yan (1998) calculated that the maximum shear stress (τ_{xy}) occurred at about 3 m above the toe of the wall with a magnitude of 100 kPa. For a wall with a 2.5 panel length, the equivalent shear stress was 20 kPa.
- Gourvenec and Powrie (1999), found that the installation of a panel 5 m long led to a slight increase in the total horizontal stress below the toe of the wall. Similar results were found by Ng and Yan (1998), who calculated an increase in the horizontal stress after the installation of a panel of 8 m length. In contrast, in this chapter, it was calculated that the stress changes are minimal during the installation of a panel of 2.5 m length. Furthermore, in Chapter 4, it was shown that the construction of a bored pile wall with 1 m of diameter of the piles does not lead to significant total horizontal stress changes below the toe of the wall.
- When the length of the panel increased (8 m panel length, Ng and Yan 1998) the shear stress (τ_{zy}) redistribution became larger and penetrated deeper when compared to the installation of a bored pile wall and a diaphragm panel wall of 2.5 m length.
- Comparing the results from this chapter to those found by Gourvenec and Powrie (1999), Ng and Yan (1998) and in Chapter 3 and 4, it can be concluded that the installation of a bored pile wall in overconsolidated deposit leads to a lower stress variation in the soil close to the wall than construction of a diaphragm wall. Thus, a smaller degree of damage to an adjacent building could be achieved.

CHAPTER 6

LONG TERM MONITORING

6.1 Introduction

One of the key uncertainties associated with the design of in situ embedded retaining walls in overconsolidated deposits concerns the long-term horizontal stress acting on the wall. This has been the subject of considerable research over the last few decades, including attempts to analyse walls already in service (Symons & Tedd, 1989; Carder & Symons, 1989; Symons & Carder, 1990).

There is some concern that the high horizontal stresses in an overconsolidated deposit may become re-established in the long-term, despite the reductions that occur during retaining wall installation and subsequent excavation in front of the wall. This would require the shear stresses maintaining the difference between the far field and near field horizontal stresses to break down (Clark, 2006). As pointed out by Simpson and Powrie (2001), it seems likely that if the horizontal shear stresses break down, particularly in the design lifetime of the wall, then

the vertical shear stresses necessary to produce a K_0 greater than 1 will not exist either. Therefore the long-term value of K_0 cannot be greater than 1. In contrast, the design Standard BD 42/00 (Highways Agency, 2000) requires that in situ retaining walls are designed to withstand a long term lateral earth pressure coefficient of up to 1.5. Report/CP/96 (Gaba *et al.*, 2002) states that for walls embedded in stiff overconsolidated clay, the long term total lateral earth pressure remains largely unchanged from that at the end of the construction period. At the serviceability limit state, Report/CP/96 (Gaba *et al.*, 2002) suggests that the greatest pressures and loads are likely to act on the structure during its design life in which any long term changes in pore water pressures are taken into account.

A better understanding of the changes in stress that occur on installation of an in situ retaining wall, during excavation in front of the wall and in the long-term, could result in better estimates of prop loads, wall bending moments and ground settlements, and lead to more economical designs.

In this chapter, long term field data from the instrumented section of in situ embedded retaining wall which forms part of the Channel Tunnel Rail Link at Ashford, Kent, are presented and discussed. Further high quality case records of long term bending moment data from a retaining wall at Coventry are presented and discussed. Innovatively, with respect to previous research in this area, the evolution of the lateral stresses around a wall in an overconsolidated deposit over a long period of 4700 days (13 years) is presented.

6.2 Total horizontal stress and pore water pressure measurements at the Ashford site

6.2.1 Geology

The geology of the site as described in Chapter 2, consists of 4 main soils, Hythe Beds, Upper Atherfield Clay, Lower Atherfield and Weald Clay. The Weald Clay is generally a freshwater deposit, although the upper region is believed to have been laid down in brackish waters. It is a generally stiff to very stiff, brown to grey clay, and in places it is thinly bedded with silt. The overlying Lower Greensand was deposited in marine conditions. The basal layer of the Lower Greensand is the Atherfield Clay, a deposit generally up to 15 m thick in the Ashford region (Clark, 2006). The boundary between the Weald Clay and the Atherfield Clay is

sharply defined by an undulose erosion surface which represents a slight unconformity; however the bottom metre of the lower Atherfield Clay is sometimes confused for the top of the Weald Clay. This band of clay differs distinctly from the underlying Weald Clay and often contains a number of large oysters (*Aetostreon* or *Exogyra*) in the lowest 0.5 m, forming a useful marker horizon (Roberts, 2003). The boundary is also often stained light brown. The Atherfield Clay is a stiff to very stiff, closely fissured fairly fossiliferous clay and consists of two distinct materials. The lower Atherfield Clay includes reddish brown or chocolatey-brown clay. The upper layer (upper Atherfield Clay) is closely to extremely closely bedded, greyish blue to brown, sandy and about 8 m thick. Humpage and Booth (2000) reported that the Atherfield Clay weathers to a brown mottled orange and red silty clay.

6.2.2 Instrumented section of the retaining wall at Ashford

As described in Chapter 3, the section of the Channel Tunnel Rail Link (CTRL) approximately 350 m northwest of Ashford International Station in Kent consists of a propped contiguous bored pile retaining wall formed from 21 m long, 1 m diameter piles spaced at 1.35 m centres, Figure 3.1. Figure 3.2 shows a cross-section of the instrumented section. The cutting width is approximately 12 m and the excavation depth 10 m. The walls are permanently supported at crest level by 1 m square reinforced concrete props spaced at 4.5 m centres and at formation level by a reinforced concrete base slab. A corbel was added to the retaining wall above the base slab at a later date to prevent slab uplift. Temporary tubular steel props were used during excavation to support the walls until the base slab had been constructed.

The instrumentation used at the Ashford site consisted of 17 vibrating-wire spade cells with integral vibrating-wire piezometers to measure the total horizontal stresses and pore water pressures near the retaining wall. A detailed description of the instrumentation and geotechnical properties at the instrumented section was given in Chapter 3.

6.3 Long term pore water pressure variation

Long term pore water pressure data were collected by Wiggan (2013). The pore pressure measurements were taken at various time intervals during the monitoring period, ranging

from 15 minutes to 1 hour. The distribution of the pore water pressure collected by Wiggan (2013) are presented and discussed in the following sections. These data are then compared with the long term total horizontal stresses monitored at the same site and elaborated in this thesis.

6.3.1 Pore water pressure variation behind the retaining wall

Figures 6.1, 6.2 and 6.3 show the pore water pressure distributions 1.275 m, 2.375 m and 3.475 m respectively behind the wall.

The variation of the pore water pressure behind the wall during the construction period is typical of the behaviour encountered in stiff soil. An initial decrease in pore water pressure was monitored during bored pile installation. This initial reduction in pore pressures was also observed by Symons and Carder (1993) and Gourvenec *et al.* (1999). Both attributed this variation to stress relief in the surrounding soil due to excavation of the piles during the installation process.

After this initial reduction an increase was observed especially at the spade cells 1.275 m behind the wall (Figure 6.1). This is possibly due to the placement of the support for the bore, in this instance a bentonite slurry mix, and later to the pressure exerted by the wet reinforced concrete for the piles (Gunn and Clayton, 1992).

From Figures 6.1, 6.2 and 6.3 it can be noted that further reductions in pore water pressure are caused by the dewatering and subsequent excavation of the soil in front of the retaining wall. As the concrete for the base slab was poured a slight increase in the pore water pressure was monitored especially at the spade cells 4 and 5 (Figure 6.1). The pore pressure variations, situated at corresponding depths and at distances of 2.375 m and 3.475 m behind the retaining wall, were consistent with those measured at a distance of 1.275 m behind the retaining wall.

As it is possible to see in Figure 6.1, the decrease in pore water pressure is more significant at spade cells closer to the soil surface. High suctions were measured at Spade Cells 1, 2 and 3. Conversely, the pore water pressure measured at Spade Cells 5, 4 and 10, at greatest depth, have attained steady state equilibrium conditions. The pore water pressures at these instruments have remained almost constant for 2500 days after construction. However, Figure

6.1 shows that the pore pressure at the instruments located closest to the ground surface and to the exposed face of the bored pile wall have continued to decrease.

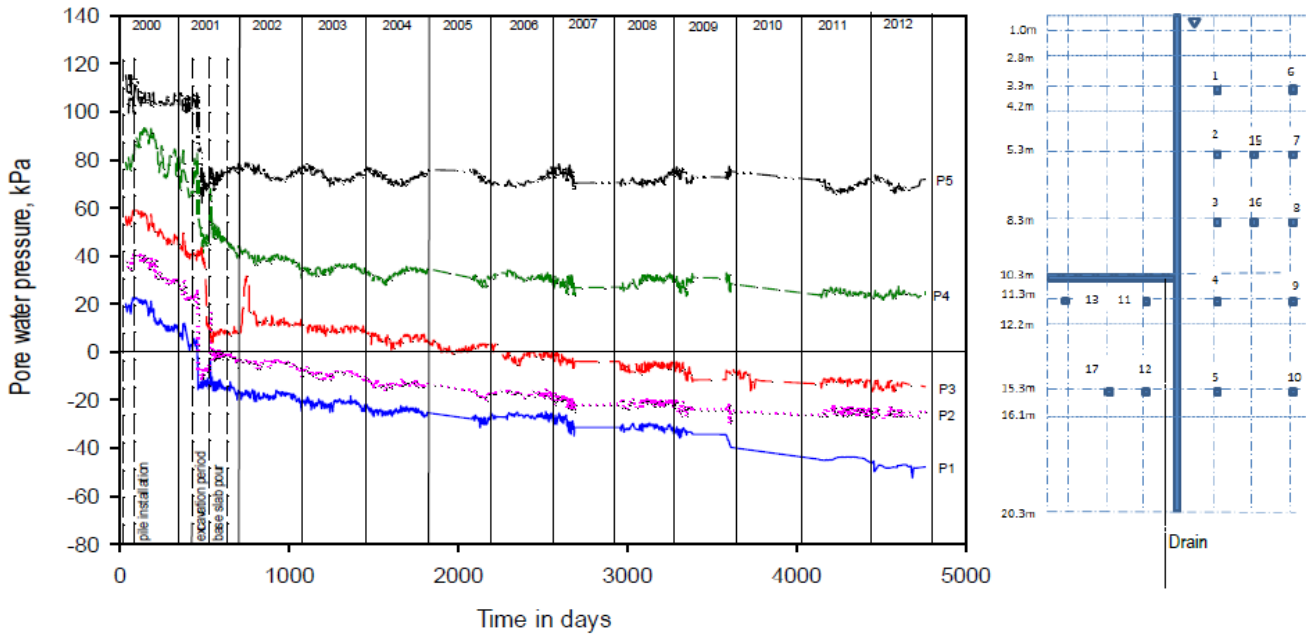


Figure 6.1. Pore water pressures measured before, during and over 13 years after wall installation (Spade Cells 1, 2, 3, 4 and 5) (Wiggan, 2013).

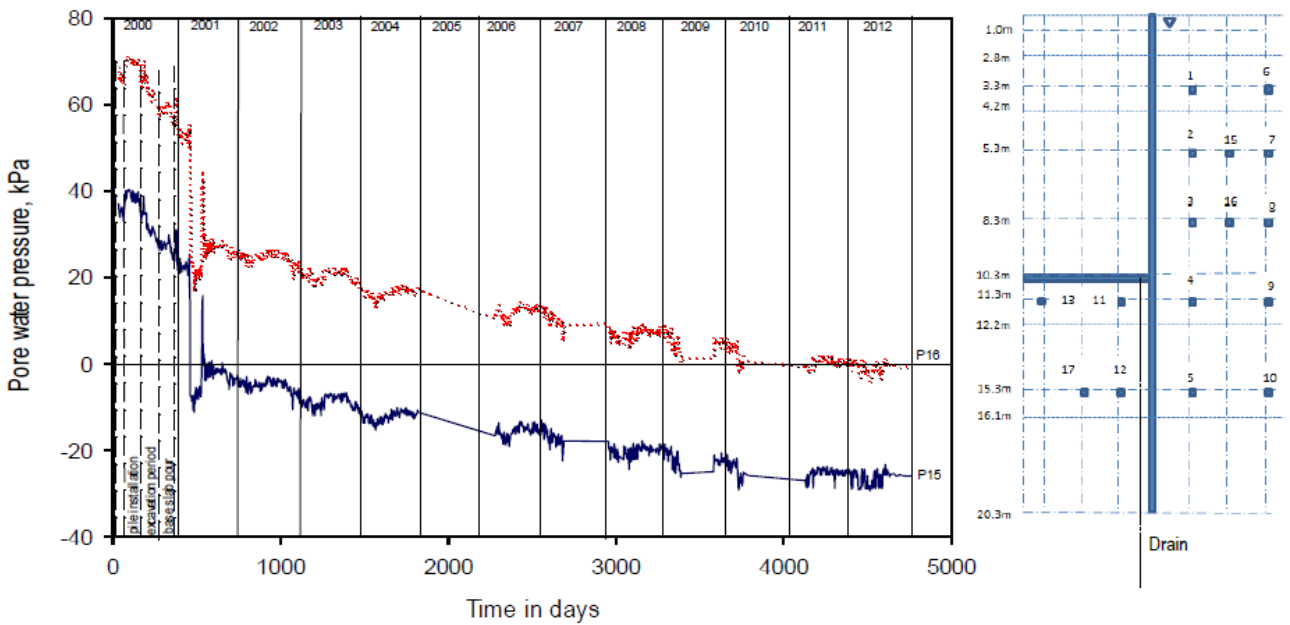


Figure 6.2. Pore water pressures measured before, during and over 13 years after wall installation (Spade Cells 15 and 16) (Wiggan, 2013).

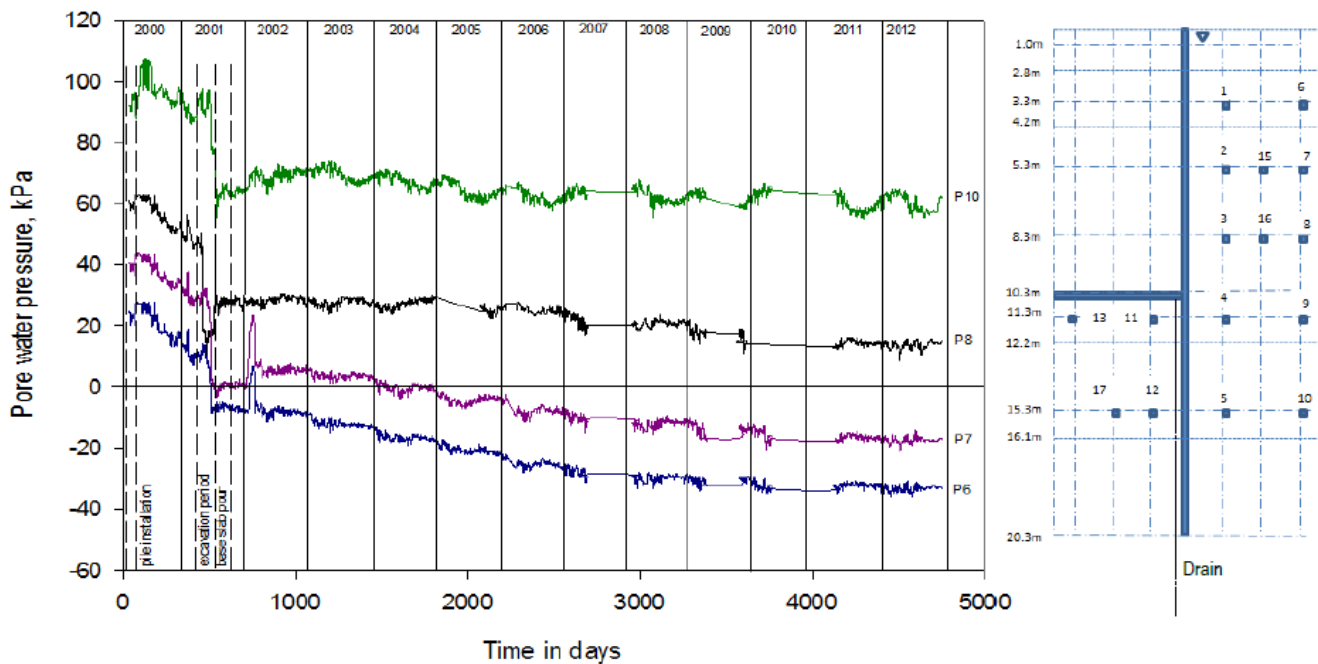


Figure 6.3. Pore water pressures measured before, during and over 13 years after wall installation (Spade Cells 6, 7, 8 and 10) (Wiggan, 2013).

Hubbard *et al.* (1984) monitored a retaining wall in overconsolidated London Clay at Bell Common. They showed that pore pressures behind the secant bored pile retaining wall followed a similar trend during construction. Installation effects were manifest as reduction in pore water pressures due to excavation of the bore followed by increased pressures during concreting. This was followed by a reduction in pressure due to the excavation of the soil in front of the retaining wall. Similarly, Figure 6.1 shows that the long term pore water pressure in the soil close to the wall formed of bored pile in overconsolidated clay deposit did not return to their pre-construction values, as reported by Wiggan (2013).

Figure 6.4 and 6.5 show the pore water pressure variation at two different distances behind the wall. Wiggan (2013) compared the pore water pressure profiles for the short, medium and long-term conditions corresponding to 100, 1100-2500 and 4600 days after construction of the retaining walls began.

Pore pressure profiles

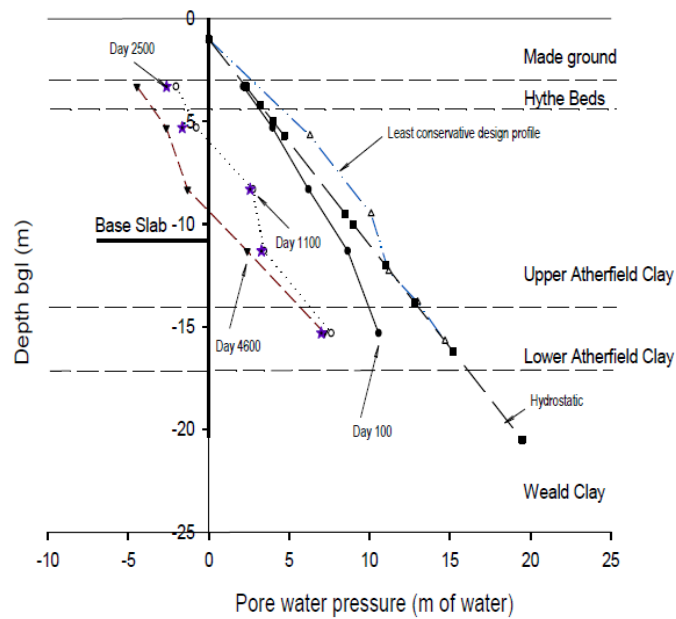


Figure 6.4. Pore water pressure profile taken at different times at a distance of 1.275 m behind the retaining wall (Wiggan, 2013).

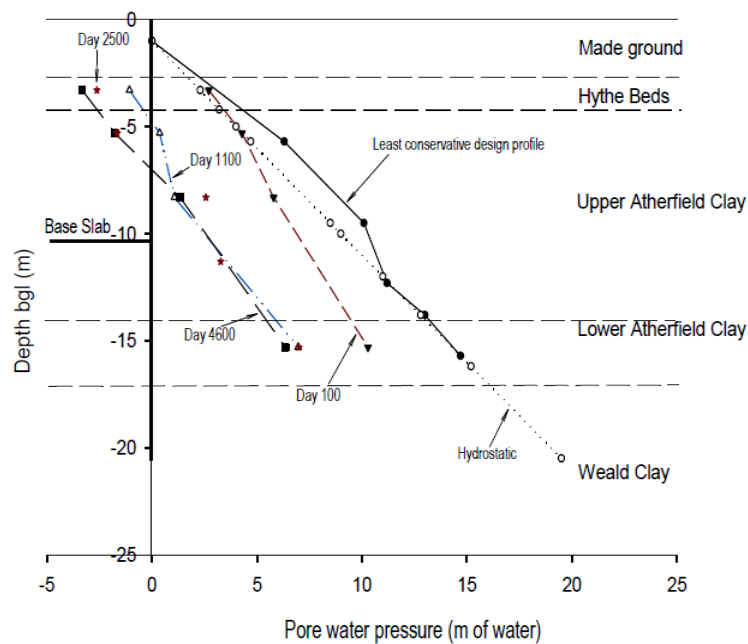


Figure 6.5. Pore water pressure profile 3.475 m behind the retaining wall (Wiggan, 2013).

The pore water pressure 100 days after the construction commenced showed some divergence from the hydrostatic profile particularly at greater depths (Figure 6.4). This could be due to underdrainage of the Atherfield Clay into the more permeable Weald Clay. Additionally, this period included the installation of the contiguous bored piles and so any changes in pore pressures could also be attributed, perhaps in part, to mechanical actions such as the installation drains (Wiggan, 2013). The shallow spade cell did not measure any changes during this initial period. This could also be due to the use of the casing resulting in less mechanically action and inducing less change on the pore pressure change on the spade cell close to the surface.

Figure 6.5 shows that after the completion of all the construction phases (1000 days) the pore water pressures had fallen significantly. Furthermore a substantial amount of suction at a depth of about 6 m is also apparent. After 4600 days the pore pressures measured were much less than at 2500 days. The pore water pressure decrease was concentrated at the surface level.

Pore pressures have continued to fall and the final equilibrium values, particularly those measured by the piezometers closer to the soil surface, are much less than assumed in the design and less than hydrostatic (Wiggan, 2013).

Figure 6.5 shows the pore water pressure profile at a different distance of 3.475 m behind the wall. The variation of pore water pressure is similar to that in Figure 6.4 at 1.275 m behind the wall. Pore water pressure equilibrium was achieved at generally higher values of pore water pressure than close to the wall. However, the presence of a region where high suction has developed is again evident (Figure 6.5).

6.3.2 Pore water pressure distribution in front of the retaining wall

Only four spade cells were positioned in front of the retaining wall. Additionally, the spade cell located at a distance of 2.375 m in front of the retaining wall and 15.3 m below the original ground level encountered intermittent disruptions that limited the amount of useful data obtained at that location. Furthermore, the data measured from spade cell 12 were generally inconsistent with those found from the other spade cells. For instance, although spade 12 was located at greater depth than spade cell 11, the initial pore water pressure was

much lower (Figure 6.6). Consideration was therefore given to the possibility to the instrument numbers having been swapped.

The changes in pore pressures at space cell 12, which were due to the installation of the piles, were inexplicably larger than those measured from the spade cell 11, which were similar to the values observed at other piezometers. This large change in pressure was unexpected due to the pile being bored, which causes less mechanical influence on pore pressures than a driven pile (Gunn and Clayton, 1992). Wiggan (2013) suggested that the apparent anomalous measured may have been due to spade cell 12 being located in the Weald Clay. Excavation of the soil in front of the retaining wall, as would be expected, produced significant falls in pore pressure for the two piezometers located below the excavated area. This is attributable to stress relief due to the removal of overburden. Subsequent construction of the base slab caused increased pore pressures similar to those observed behind the retaining wall.

From Figure 6.6 it can be observed that the pore water pressure at space cells 11 and 12 continued to decrease at a slower rate than at spade cell close to the surface behind the wall. However the pore water pressures continued to decrease in the long term.

A similar trend was measured at spade cell 13 (Figure 6.7), which showed an initial decrease in the pore water pressure mainly due to boring of the piles followed by an increase due to concreting (Figures 6.6).

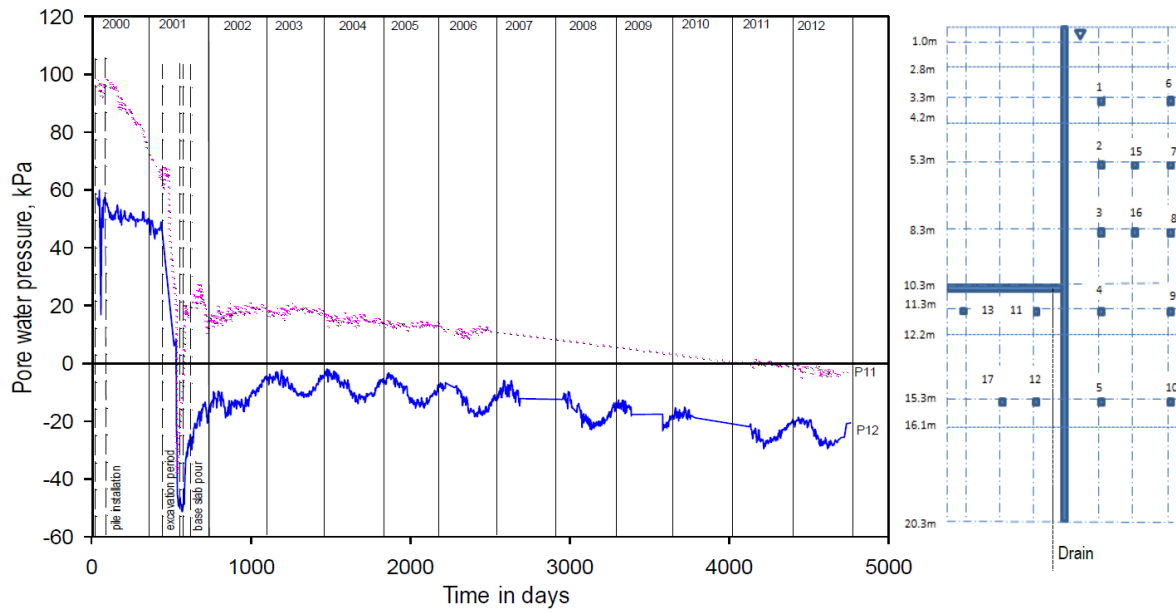


Figure 6.6. Long term pore water pressures 1.275 m in front of the retaining wall (Wiggan, 2013).

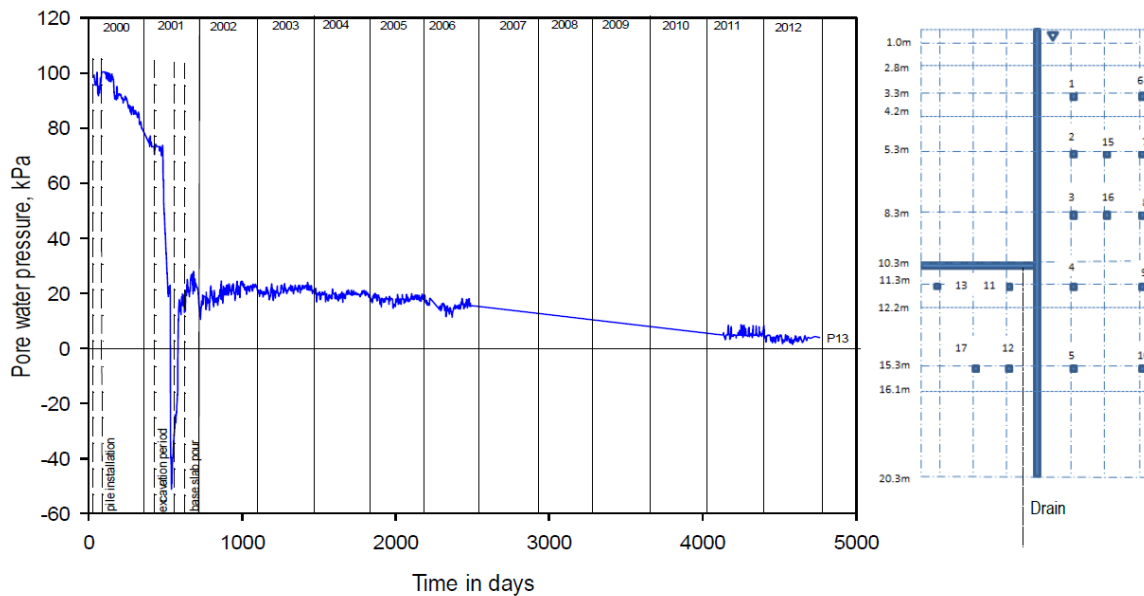


Figure 6.7. Long term pore water pressures 3.475 m in front of the retaining wall (Wiggan, 2013).

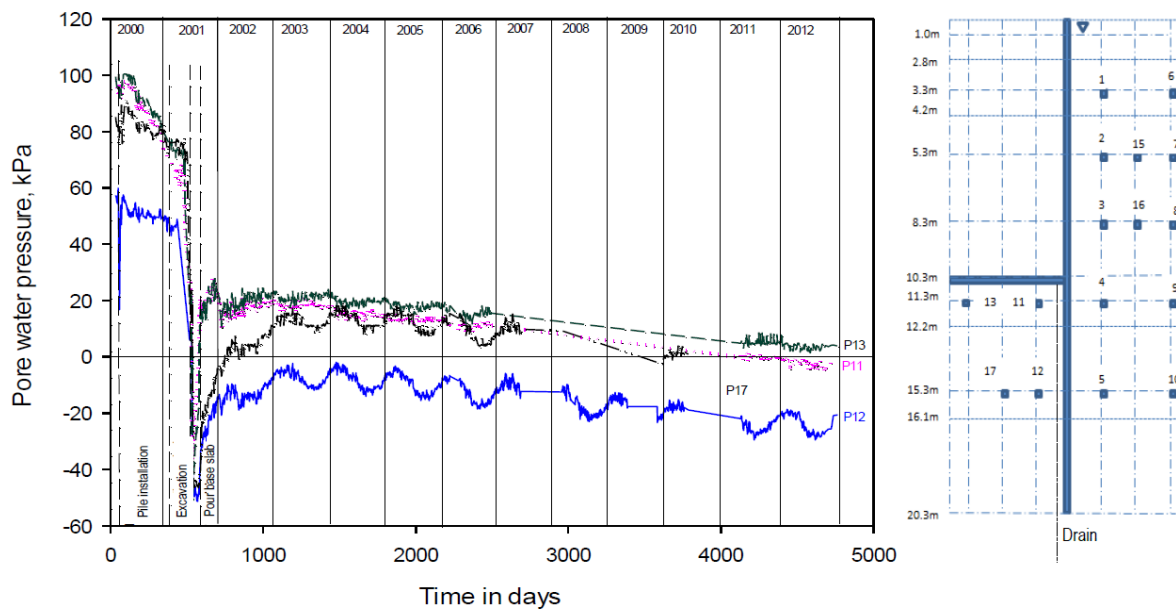


Figure 6.8. Long term pore water pressures in front of the retaining wall (Wiggan, 2013).

6.3.3 Pore pressure at various depth below ground level

The measured values of the pore water pressure from the spade cells at various distance in front of and behind the wall by Wiggan (2013) were compared to investigate whether the variation of hydraulic heads would give an indication of the flow behaviour around the wall. The following observations are then based on the general rule that groundwater flows from a region of high to one of low hydraulic head.

3.3 m below ground level

Figure 6.9 shows the variation of the pore water pressure at spade cells 1 and 6 located at a depth of 3.3 m below ground level. The decrease of the pore water pressure in the long term is greater at space cell 1, which is closer to the exposed face of the bored pile wall, than measured at spade cell 6. However, as also observed by Wiggan (2013), the variation in pore water pressure during the excavation of the soil in front of the walls and construction of the base slab was similar. Dewatering and excavation of the cutting resulted in the pore water pressure falling below zero in the areas of both spade cells 1 and 6. Additionally, it is also possible to observe from Figure 6.9 that long term equilibrium conditions have been achieved

by about 4000 days. However, the pore water pressure measured at spade cell 1 seemed to continue to decrease slightly after 4000 days.

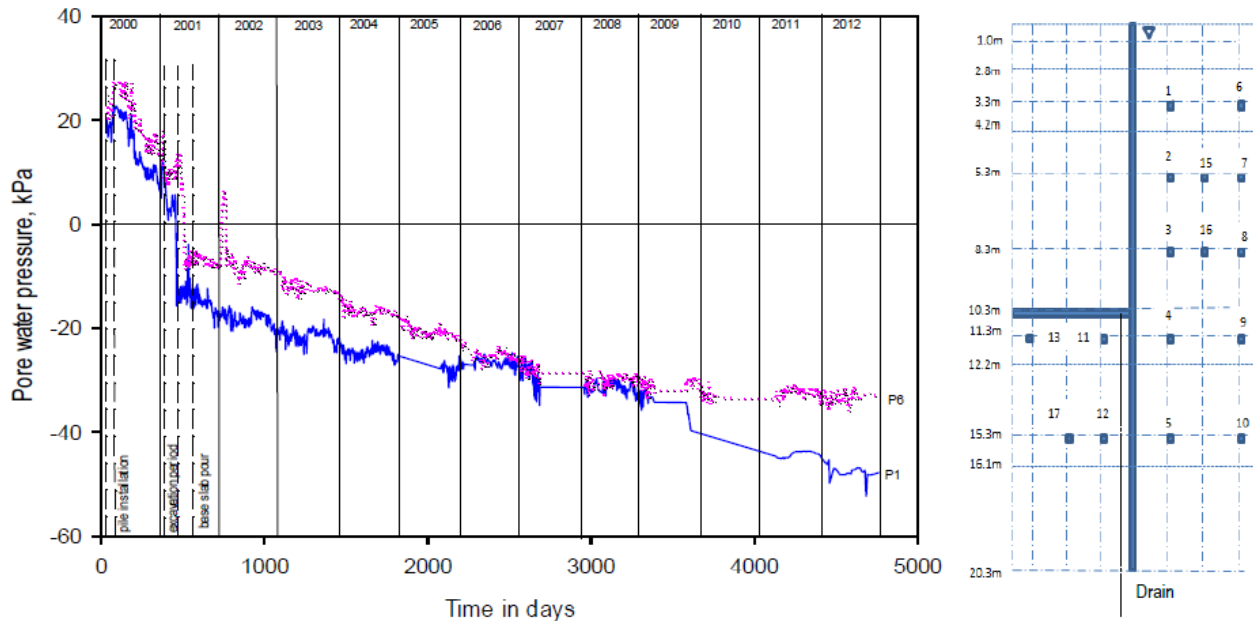


Figure 6.9. Long term pore water pressures at a depth of 3.3 m below ground level (Wiggan, 2013).

5.3 m below ground level

Figure 6.10 shows the pore water pressure changes at spade cells 2, 7 and 15, located at distances of 1.275 m, 3.475 m and 2.375 m behind the retaining wall and at a depth of 5.3 m. Figure 6.10 shows similar trends in pore water pressure variation during pile installation, excavation period and base slab poured for the data measured from the spade cells 7, 2 and 15. A large decrease in the pore water pressure occurred specifically during the excavation period. The long term pore water pressure continued to fall and all three spade cells measured relatively high suctions. From the data presented in Figure 6.10 it is evident that the long term pore water pressures reduce towards the retaining wall. The pore water pressure decreases are major in the area of the spade cell closer to the exposed face of the wall (spade cells 2 and 15). Figure 6.10 indicates that long term pore water pressure equilibrium is not reached at any of the spade cells.

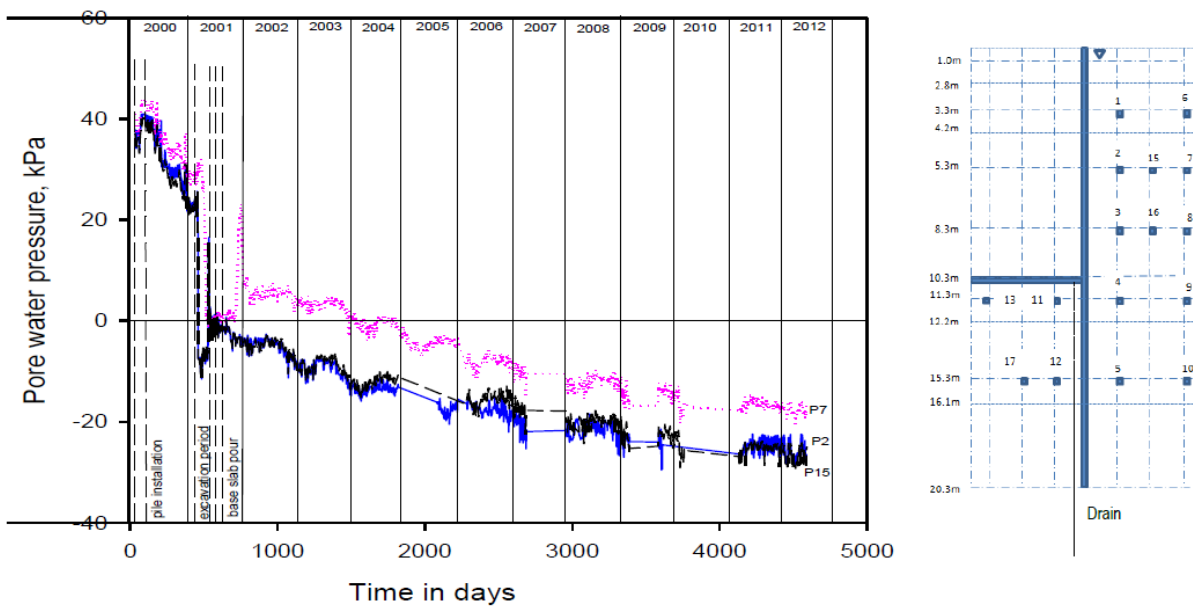


Figure 6.10. Long term pore water pressures measured at a depth of 3.3 m below ground level (Wiggan, 2013).

8.3 m below ground level

Figure 6.11 shows the pore water pressure changes at a depth of 8.3 m behind the retaining wall. The pore water pressure changes are well defined. The change in pore pressure is significant at spade cell 3, which is the closest to the exposed face of the cutting. However, the pore pressure changes during pile installation and the excavation period were identical. After construction of the base slab, the pore pressure continued to decrease and the long-term equilibrium condition was reached after 4000 days following the excavation of the cutting. From the measured data it can be observed that there is a reduction in the pore pressure towards the retaining wall. High suctions were recorded at the spade cell 3, which is the closest to the exposed face of the retaining wall.

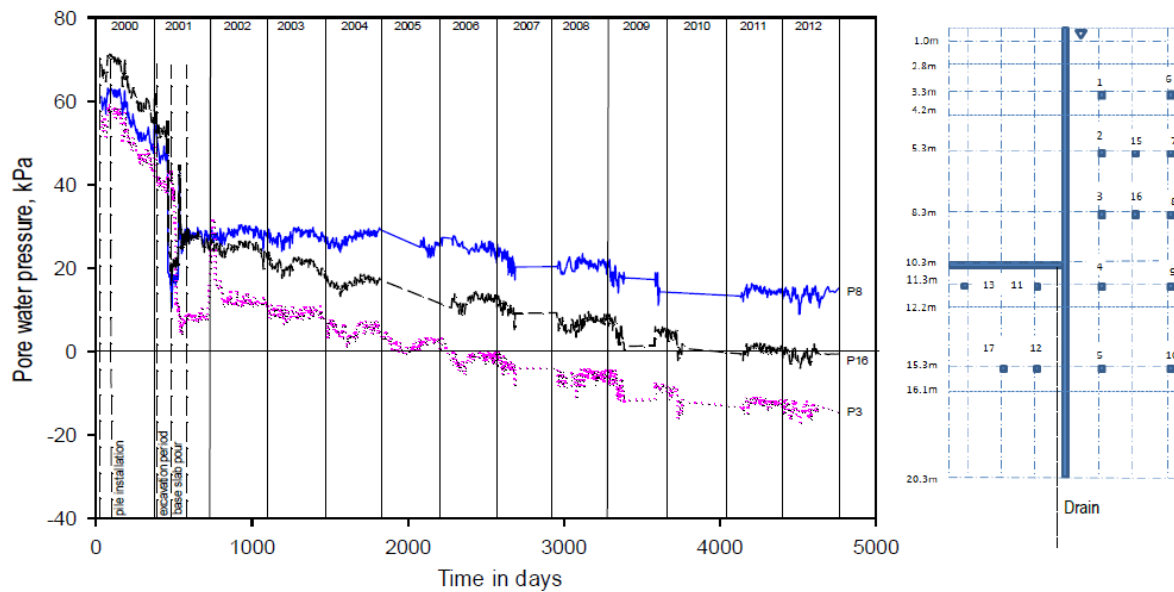


Figure 6.11. Long term pore water pressures at a depth of 8.3 m below ground level (Wiggin, 2013).

11.3 m below ground level

Spade cells 11 and 13 were located in front of the retaining wall while spade cells 4 and 9 were located behind the retaining wall. Spade cell 9 malfunctioned during the early stage of the work and the data from this instrument was not recorded. From Figure 6.12 it can be seen that the pore pressure variations during pile installation were similar at spade cells 13 and 11 although the values were slightly different for the spade cell 4.

As expected, the reduction in pore pressure during dewatering and excavation of the soil in front of the wall was large for spade cells 11 and 13, which are located just below the base slab. The pressure induced by the slab generated almost constant pore pressure for a period of 4 years at spade cells 11 and 13 after the pouring of the slab. In the long term, the pore pressures are still reducing at low rate. The pore water pressure measured at spade 11 became negative at about 4000 days from the excavation phases.

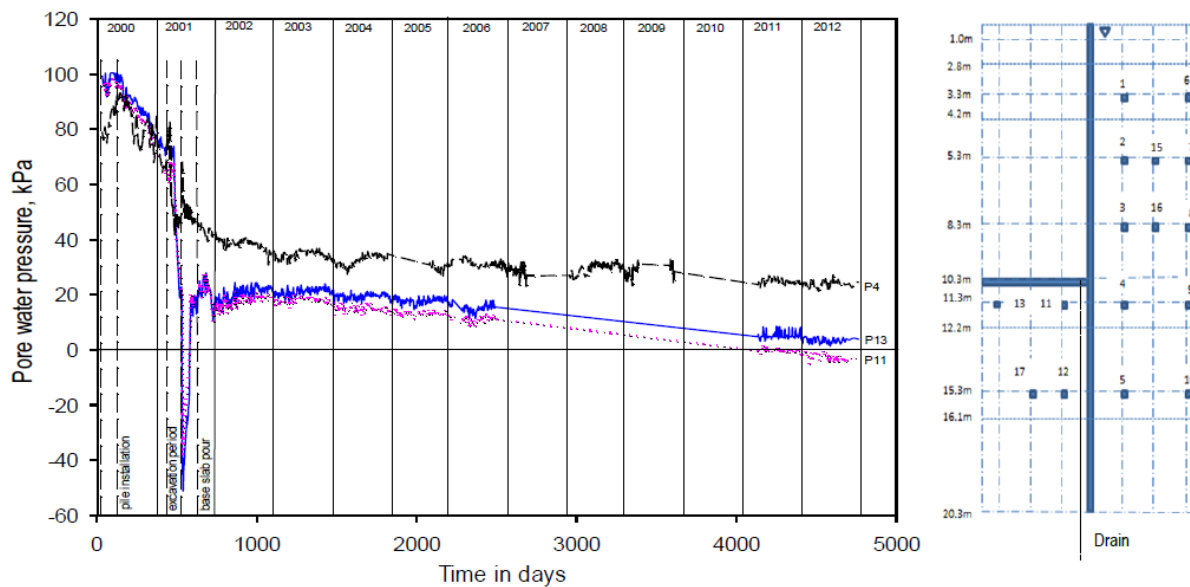


Figure 6.12. Long term pore water pressures measured at a depth of 11.3 m below ground level (Wiggan, 2013).

15.3 m below ground level

Identical pore water pressure changes were measured at spade cells 5, 10 and 17 during pile installation. However, unexpected large pore pressures were measured at spade cell 12. The installation of the piles caused an initial decrease followed by an increase in the pore water pressure at all the spade cells. The pore water pressures measured at spade cell 12 are unexpectedly lower than those measured at spade cell 17, while the pore pressures at spade cell 5 are similar to those at spade cell 10. As expected, the dewatering led to a large decrease in the pore water pressure on the spade cell close to the excavated side. From Figure 6.13 it can be observed that spade cell 17 stopped recording data during the year 2010, probably due to a malfunctioning of the instrument.

From the data reported in this section and previously, it is apparent that the long term pore water pressures decreased towards the wall. The measured pore water pressures were affected by the construction activities and the hydraulic condition around the wall, and varied according to the distance from the wall and the depth of the spade cells. Furthermore as shown by Wiggan (2013), spade cells at the same depth recorded similar variations in pore water pressure.

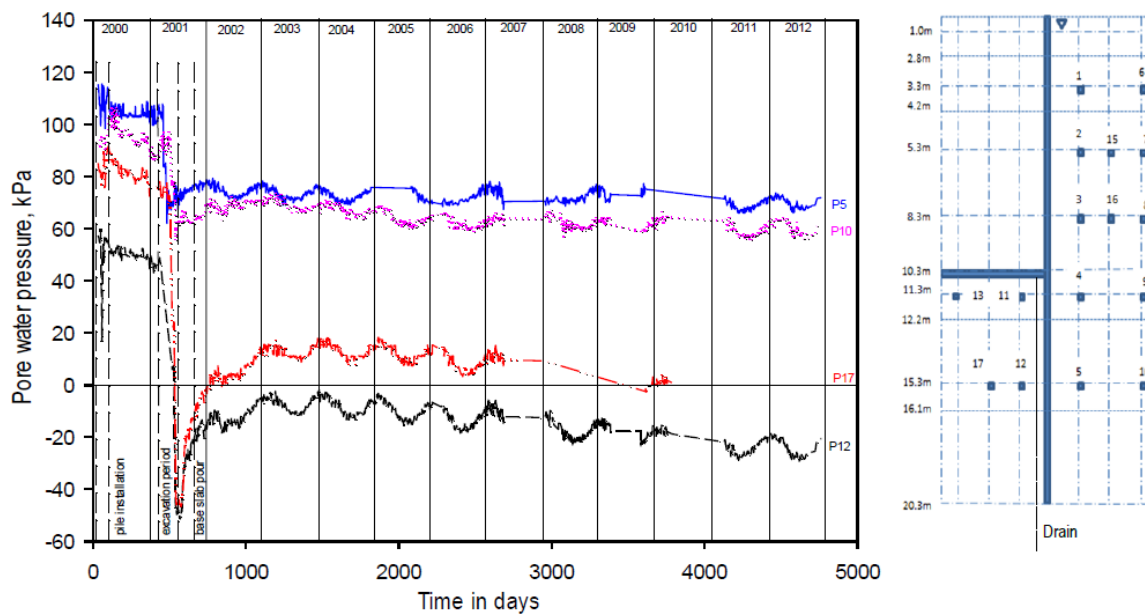


Figure 5.19: Pore water pressures measured at a depth of 15.3 m below ground level.

Figure 6.13. Long term pore water pressures measured at a depth of 15.3 m below ground level (Wiggan, 2013).

Hydraulic head distribution around the retaining wall

Wiggan (2013) analysed the variation in total head to determine how the flow regime developed during the period between installation of the retaining wall and the establishment of steady state long-term equilibrium conditions.

He found the existence of some amount of under-drainage of the less permeable Atherfield Clay by the Weald Clay. This is similar to underdrainage of London Clay to the more permeable Chalk layer inferred by Powrie et al. (1999) and Carder et al. (1999). The low permeability of the Atherfield Clays meant that undrained conditions persisted during construction (short-term), as Richards *et al.* (2007) demonstrated.

Furthermore, Wiggan (2013) showed that in the medium term (from 1100 to 1500 days after the pile installation) the installation of the wall and the excavation of the cutting significantly affected the flow regime. However, in the medium term, owing to the low permeability of the Atherfield Clay, he was unable to confirm definitively if the hydraulic regime around the contiguous pile retaining wall was fully established.

Wiggan (2013) also investigated the long term ground water flow regime (from 2100 to 4600 days after the installation of the wall). He reported that the groundwater flow was influenced by the presence of the contiguous pile retaining wall, with seepage from the back to the front of the retaining wall taking place through the pile gaps. After 4600 days the groundwater flow regime had mostly attained its long term equilibrium condition and flow behind the wall above the base slab level was dominated by seepage through the gaps between the contiguous piles.

6.3.4 Comparison between the total horizontal stress with the pore water pressure variation and impact of pile gaps on lateral loads on the retaining wall

The pore water pressures, u , presented by Wiggan (2013), were compared with the total horizontal stress, σ_h , that were measured and collected from the instrumented section at distances of 1.275 m and 3.475 m behind, and at a distance of 1.275 m in front of the retaining wall. Hence, this was to determine the correlation between changes in pore pressures and lateral stresses with respect to their *in situ* values.

The initial *in situ* horizontal total stresses, σ_{h0} , were obtained from a best-fit line through field data presented by Clark (2006). The horizontal stresses, σ_h , were normalized with respect to the *in situ*, (σ_h / σ_{h0}) and compared. Equation 6.1 shows the best fit line for, σ_{h0} , from Clark (2006).

$$\sigma_{h0} = 20.6z' + 0.8 \quad \text{Equation 6.1}$$

Equation 6.2 shows the initial *in situ* pore pressures, u_0 , that were also calculated from a best-fit line.

$$u_0 = 8.6z' - 10.5 \quad \text{Equation 6.2}$$

The pore water pressure data, which came from each spade cell, was normalised with respect to *in situ* pore water pressure, (u / u_0) .

Comparison between the pore water pressure data and the long term horizontal stresses at a distance of 1.275 m behind the retaining wall

Figure 6.14 shows a general decrease in the total horizontal stress measured at 1.275 m behind the retaining wall over the monitoring period. It can be observed that the long term stresses are less than the in situ values. An unexplained increase in normalised stresses at SC1 above those at the other spade cells was measured before the excavation period. This could be due to the effect of thermal expansion of the reinforced concrete props, which were positioned just above the position of SC1.

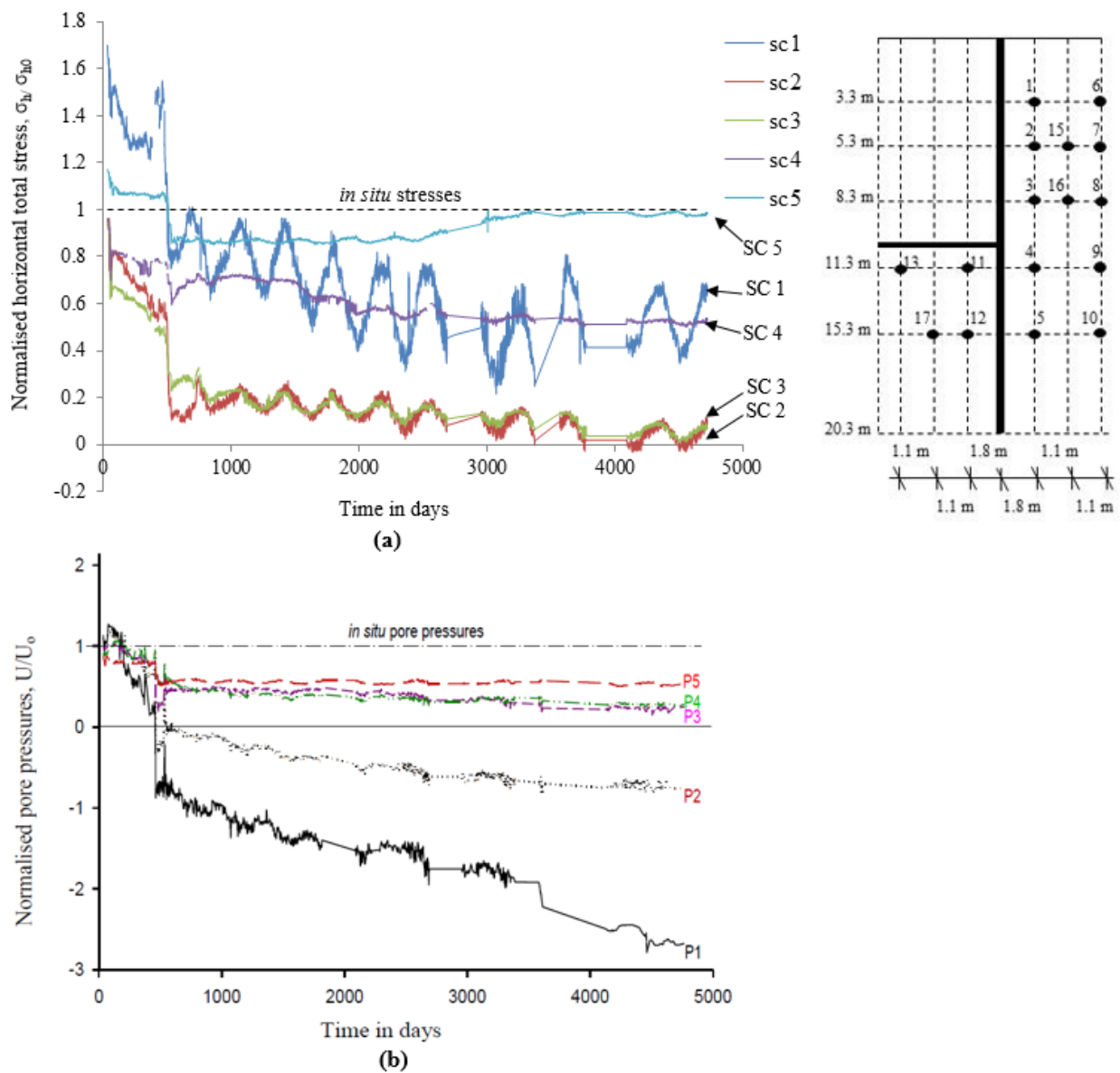


Figure 6.14. Normalised (a) horizontal total stresses and (b) pore water pressures 1.275 m behind the contiguous pile retaining wall.

From Figure 6.14 it can also be noted that the magnitudes of the normalised stress variations depend on the position of the spade cell. During pile installation the stress increases at spade cell 1, but in the long term the total horizontal stress on spade cell 1 is only 40% of the in situ values. The initial stress changes on spade cells 1 and 2 were within 10-20 % of the in situ values.

The long term stress measured at spade cells 3 and 2 dramatically decreased until reaching negative values. In the long term the stresses on space cells 2 and 3 were less than the 10% of their in situ values. At spade cell 5, an unexplained increase over the last 5 years was measured. However the total horizontal stress remained lower than the in situ values. From the measured data shown in Figure 6.14, it can be seen that overall the horizontal stress decreases are major at the spade cells closer to the soil surface. The pore water pressure data also confirms this trend. In fact the spade cell closest to the surface (spade cells 1) measured a high decrease of pore water pressure compare with those measured at spade cells 4 and 5. The pore pressures at spade cells 4 and 5 remained within 20 to 50% of their in situ values.

Comparison between the pore water pressure data and the long term horizontal stresses at a distance of 3.475 m behind the retaining wall

Figure 6.15 shows the long term horizontal total stress and pore water pressure 3.475 m behind the retaining wall. By comparing Figure 6.15 with Figure 6.14 it can be noted that the trend of the variation of the pore water pressure and total horizontal stress are similar. In the long term, an overall decrease of the total horizontal stress behind the retaining wall was measured.

The variation in total horizontal stress measured at spade cell 6 is similar to those measured at spade cell 1. However in the long term the normalized values of total horizontal stress measured at spade cells 6, 7 and 8 are within 20-50% of in situ values.

The normalized total horizontal stress at the location of spade cell 8 seems to be much lower than the expected value, especially compared to the values measured at spade cell 7. This could be due to a malfunctioning of spade cell 8. Overall, the normalized total horizontal stresses show a decrease of stress in the long term. A similar trend was also observed for the

pore water pressures, where spade cell 6 (located close to the soil surface) measured a decrease in the pore water pressure that was almost three times more than the in situ value. In contrast, the pore water pressure variation at the deeper spade cell 10 was about 50% of the in situ values.

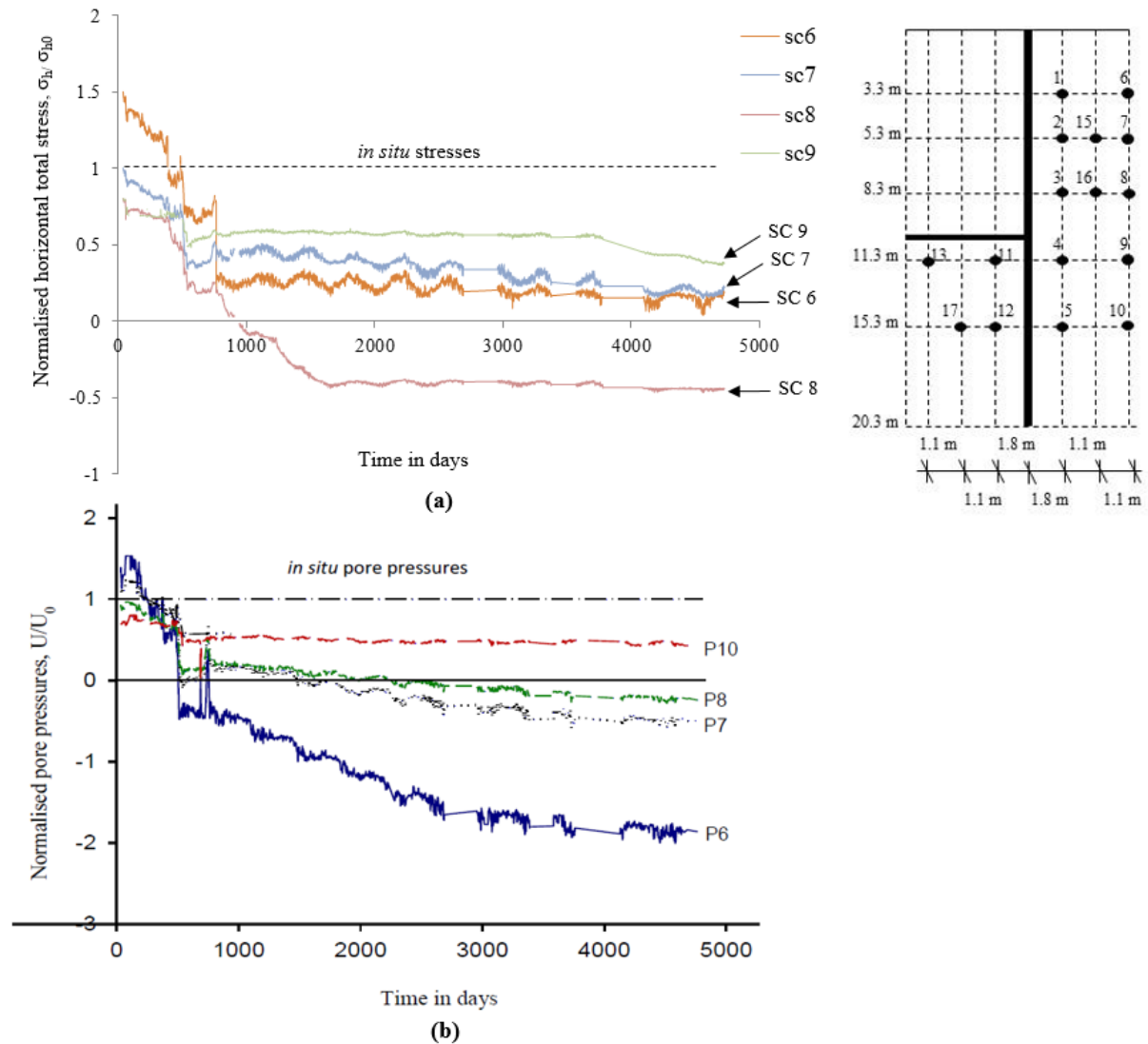


Figure 6.15. Normalised horizontal total stresses and pore water pressures 3.475 m behind the contiguous pile retaining wall.

Comparison between the pore water pressure data and the long term horizontal stresses at a distance of 3.475 m behind the retaining wall

As it would be expected, the total horizontal stresses in front of the wall are much less than the in situ values; this is due to the removal of the overburden. The long term total horizontal stress measured at spade cells 12 and 11 fell to 25 % and 40 % of their in situ values. The

trends between the long term total horizontal stress and pore water pressure are quite different from those reported in Figure 6.14 and 6.15. The long term pore water pressures are similar to the in situ values, while the long term total horizontal stresses are much less than the in situ values.

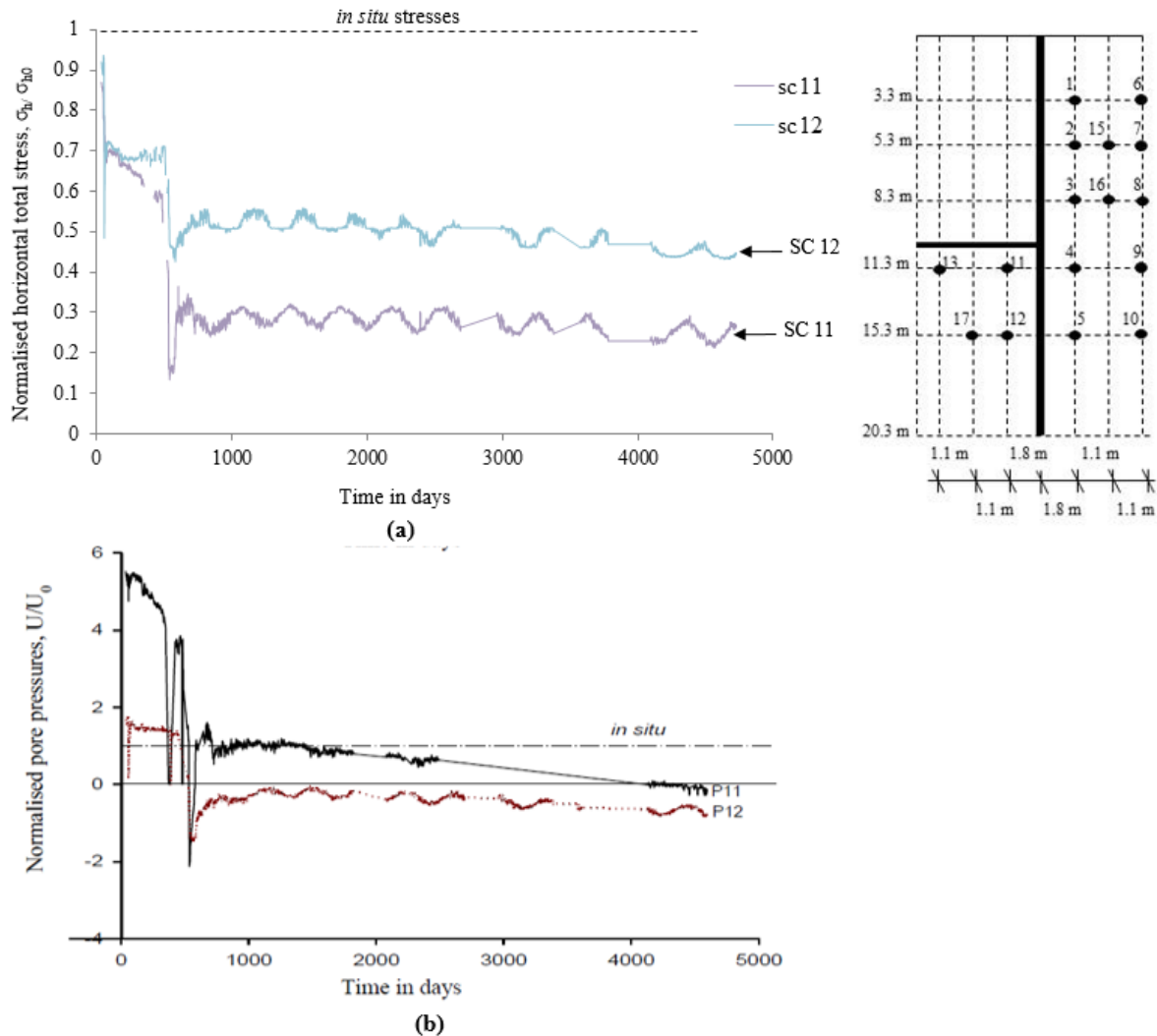


Figure 6.16. Normalised (a) horizontal total stresses and (b) pore water pressures 1.275 m in front of the contiguous pile retaining wall.

6.3.5 Comparison between the short and long term horizontal total stress and pore pressure

Figures 6.17, 6.18 and 6.19 show the long term and short term horizontal total stress and pore pressure changes at various distances behind the wall. The stress and pressure changes were calculated using Equations 6.3 and 6.4 respectively for the short term (ST) and long term (LT). The variations in pore water pressure are similar on all three figures (Figures 6.17, 6.18 and 6.19), where all figures show some evidence of proportionality between the pore water pressure changes and the total horizontal stress variations.

$$\Delta\sigma_h = \sigma_{ST} - \sigma_{LT} \quad \text{Equation 6.3}$$

$$\Delta u = u_{ST} - u_{LT} \quad \text{Equation 6.4}$$

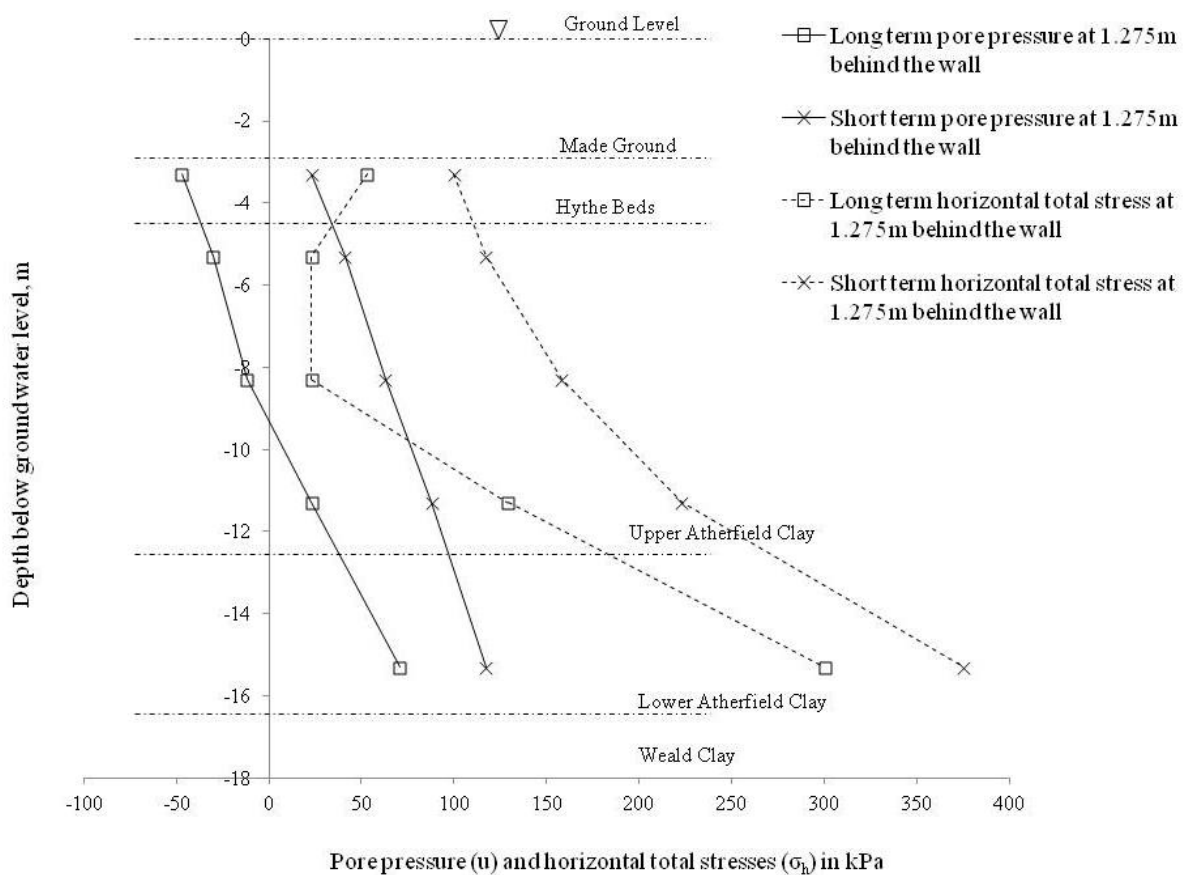


Figure 6.17. Comparison of the pore water pressure and horizontal stress profiles for short term and long term conditions at a distance of 1.275 m behind the retaining wall.

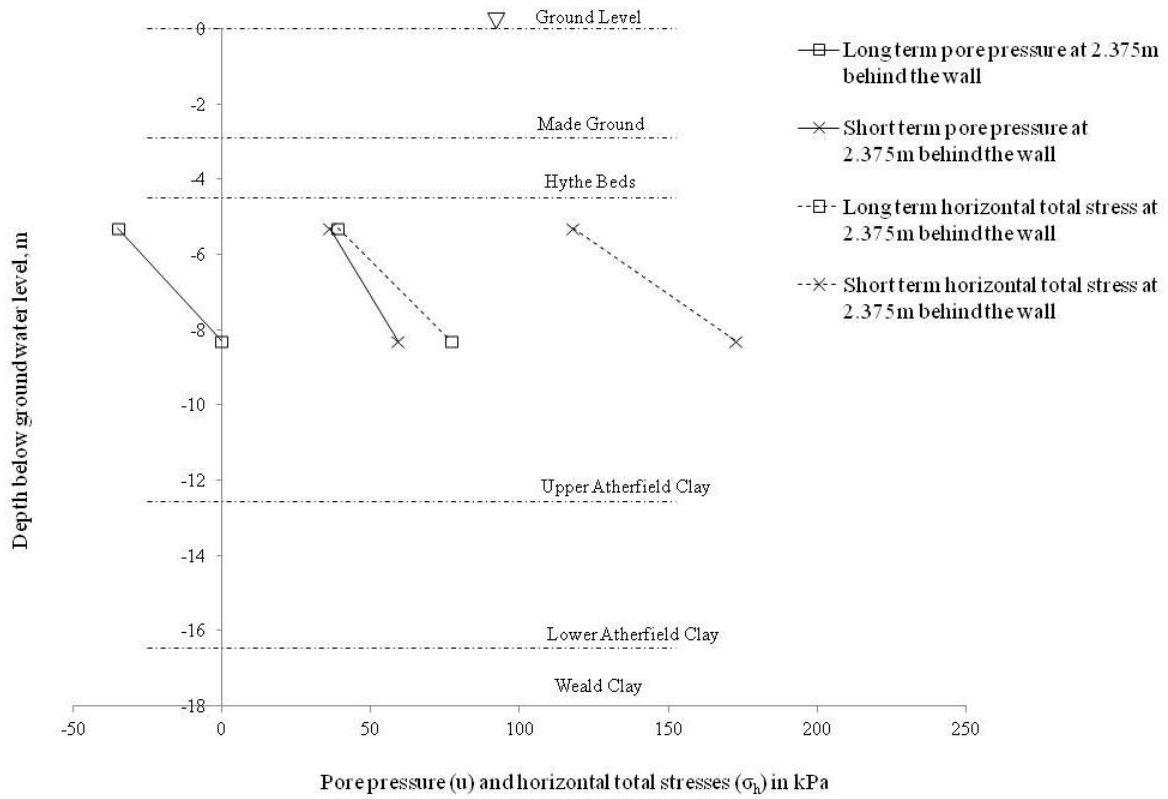


Figure 6.18. Comparison of the pore water pressure and horizontal stress profiles for short term and long term conditions at a distance of 2.375 m behind the retaining wall.

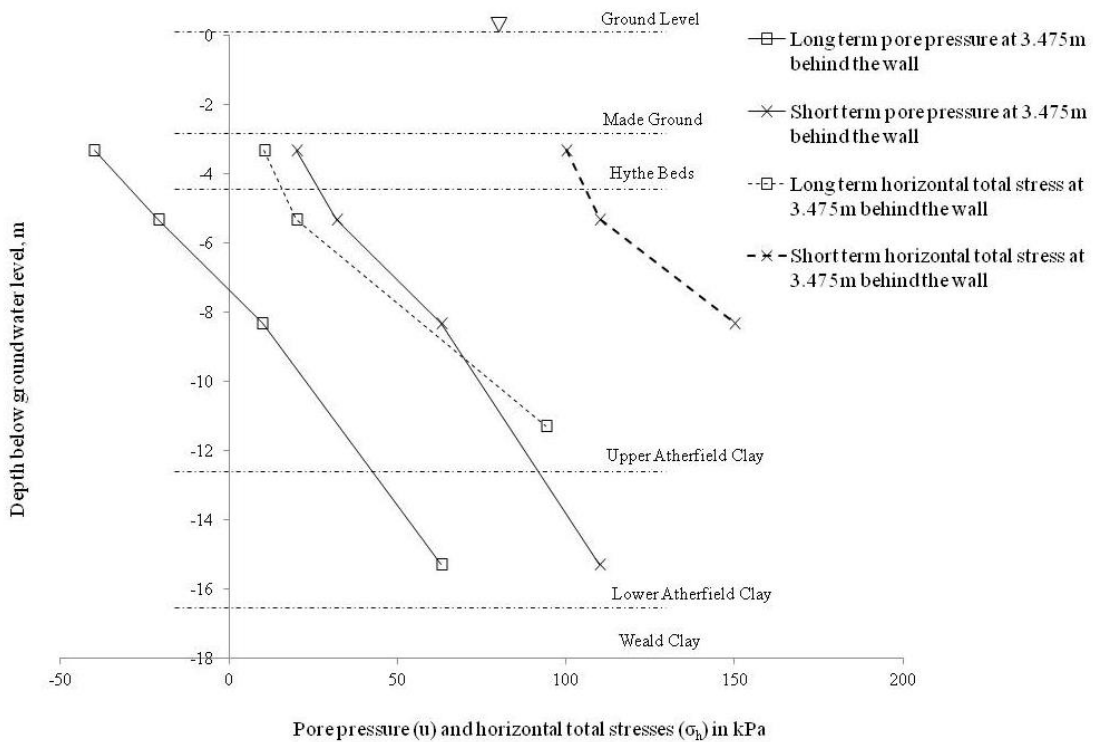


Figure 6.19. Comparison of the pore water pressure and horizontal stress profiles for short term and long term conditions at a distance of 3.475 m behind the retaining wall.

Comparison between the in situ and long term pore water pressure and total horizontal stress

Long term changes in the total horizontal stress and pore water pressure at distances of 1.275 and 3.475 m behind the wall are compared with the in situ values and in Figure 6.20. A large variation on the pore water pressure were measured especially in the soil close to the surface. The horizontal stress and pore pressure at a distance of 1.275 m were found to be similar to those at a distance of 3.475 m behind the wall. At greater depth, the changes in pore water pressure and changes in total horizontal stress became similar.

From Figure 6.20 it can be noted that the pore water pressure changes led to a variation in the total horizontal stress. Furthermore as discussed previously and as is reported later, there are other factors that contributed to the total horizontal stress variation such as the thermal expansion of the reinforced concrete props and base slab and the consequent movement of the retaining wall.

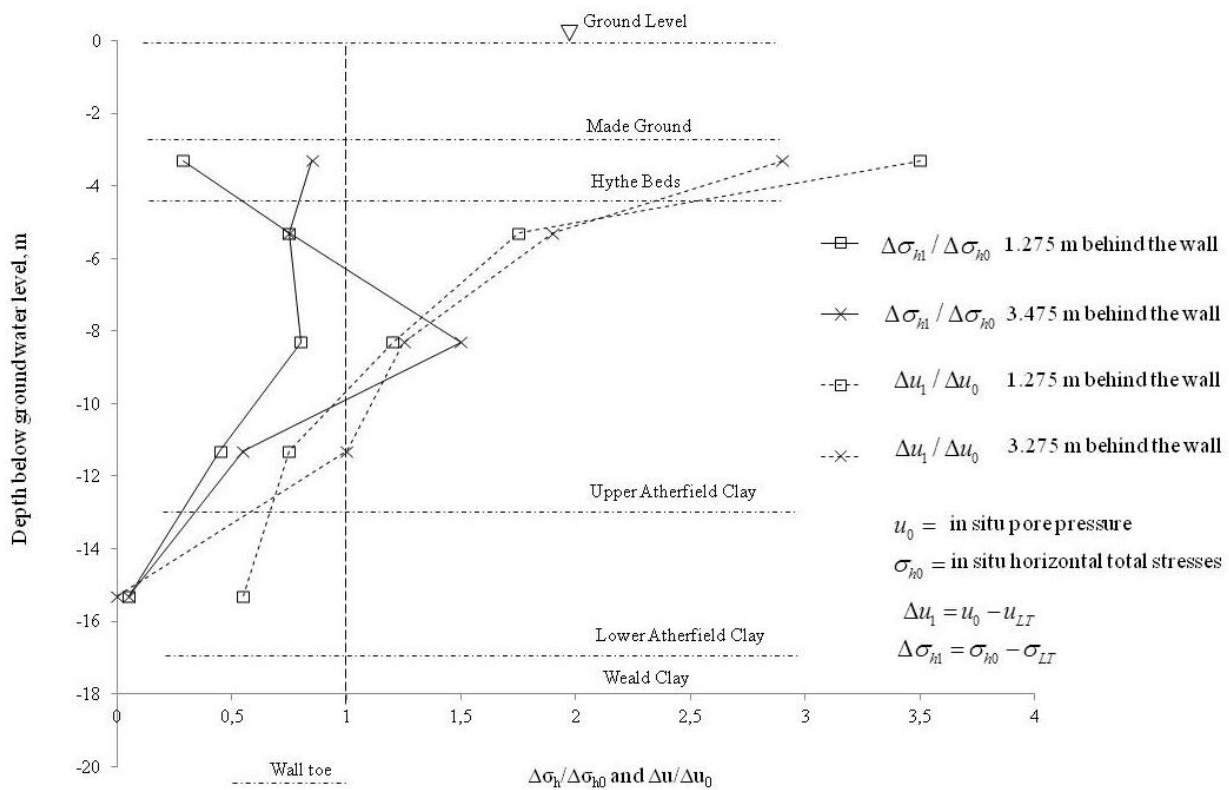


Figure 6.20. Changes in the total horizontal stresses ($\sigma_{h0} - \Delta\sigma_h$) and pore pressures ($u_0 - u$) normalised with respect to in situ values at distances of 1.275 m and 3.475 m behind the retaining wall.

6.3.6 Total horizontal stress measurements behind the retaining wall

The following sections show a continuance of the data recorded and interpreted by Clark (2006). The field data monitored by Clark, 2006, were recorded from November 1999 to December 2005. The horizontal stress and pore water pressure measured in the site at Ashford were then collected from December 2005 to January 2013.

Figure 6.21 shows the total horizontal stresses measured over the period from before pile installation to late 2012 by the spade cells 1.275 m behind the wall (Figure 3.2). An initial stress relief was measured during the pile installation. After this initial reduction an increase was observed, especially in the soil at spade cell 4. An immediate increase in pressure was then observed. This is possibly due to the placement of the support for the bore, in this instance a bentonite slurry mix, and later to the pressure exerted by the wet reinforced concrete for the piles (Gunn and Clayton, 1992).

It can be observed that further reductions in total horizontal stress are caused by the dewatering and subsequent excavation of the soil in front of the retaining wall.

Overall the installation of the contiguous pile retaining wall and the excavation of the cutting caused the main changes in the lateral stress state. The recorded stresses were smaller in winter and higher in summer for the spade cells 1.275 m behind the wall, with the highest readings occurring between approximately July and October.

From Figure 6.21 it can be noted that in the long term, 13 years after wall installation, a continuous slight decrease in horizontal stress has been recorded at spade cells 1, 2, 3 and 4 (Figure 3.2). These changes are mainly due to the effects of drainage through the secant piles wall; this is validated by Figure 6.14, where a clear decrease in the pore water pressure at spade cells 1, 2 and 3, during the period of 13 years after the wall construction is shown. The horizontal stress has remained almost constant for 4500 days after construction.

Overall, in the long term, the total horizontal stresses did not return to their pre-construction values. From spade cell 5 an unexplained increase over the last 5 years was measured. However, the total horizontal stress remains lower than the *in situ* value.

Figure 6.22 shows the total horizontal stress changes at spade cells 15 and 16. The installation of the contiguous piled retaining wall and excavation of the cutting caused the main changes in total horizontal stress. The values of total horizontal stress have remained almost constant in the long term. However a slight decrease of 10 kPa in the horizontal stress over the period of 11 years after the excavation of the cutting can be observed.

Figure 6.23 shows the total horizontal stress changes measured at spade cells 6, 7, 8 and 9. It can be noted that, in contrast to the other data collected the long term, the horizontal stresses measured at spade cell 8 were apparently negative; this was also reported by Clark (2006). This is most probably due to an error in the signal on spade cell 8. Apart from the data from spade cells 7 and 8, the main stress decreases are during the installation and excavation periods. In the long term, a slight decrease of a few kPa has occurred since the excavation of the cutting.

Total horizontal stresses measured at spade cells 6, 7 and 9 were found to be similar to those measured 1.275 m behind the wall.

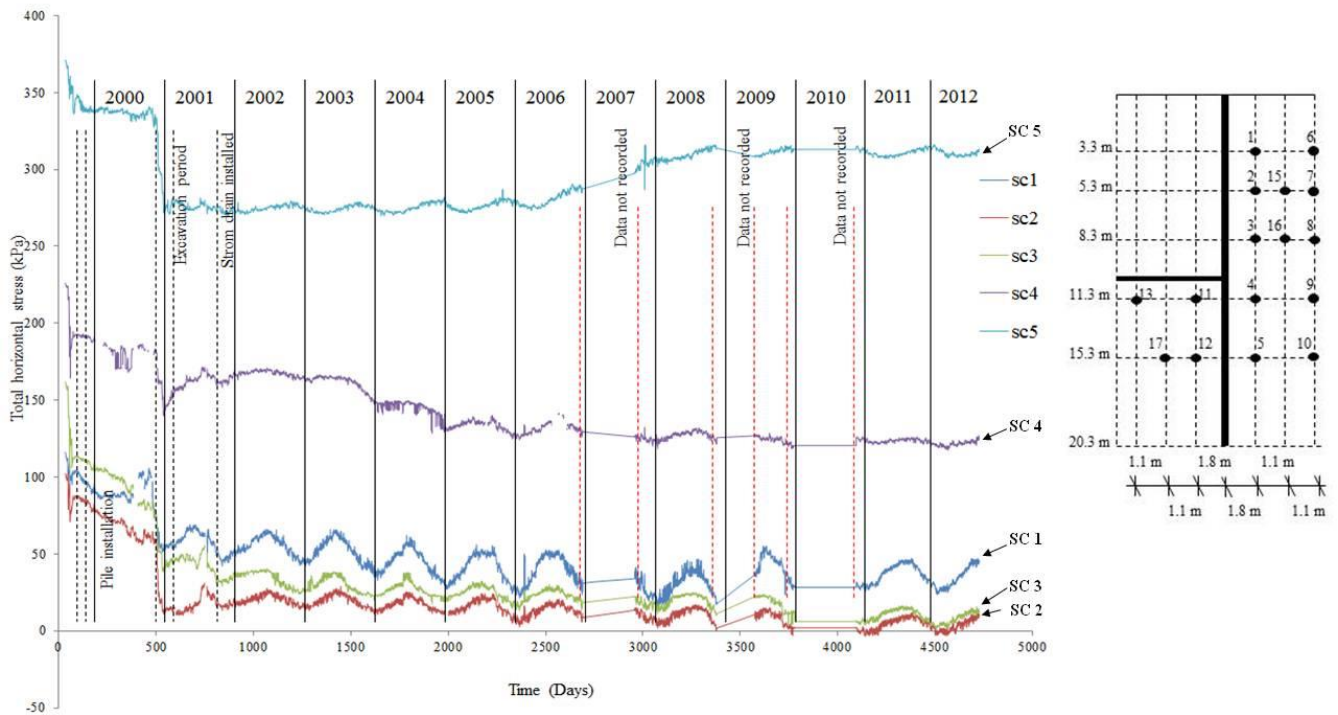


Figure 6.21. Total horizontal stress measured before, during and over 13 years after wall installation, (Spade Cells 1, 2, 3, 4, 5).

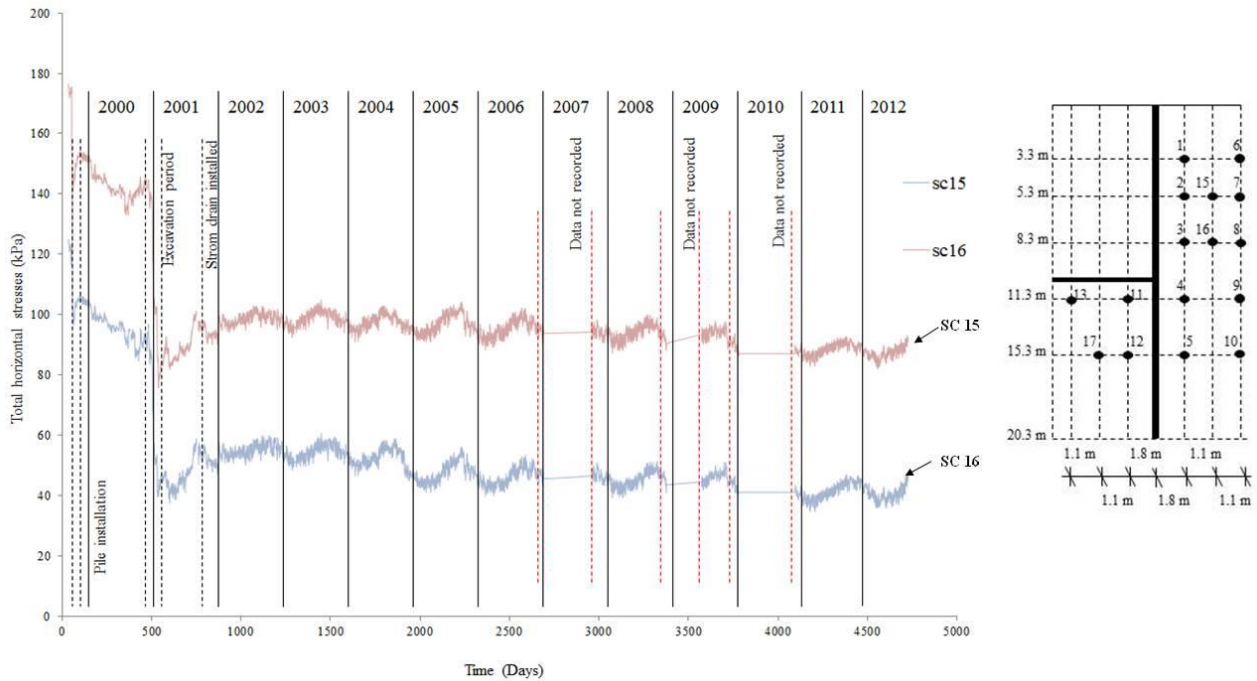


Figure 6.22. Total horizontal stresses measured before, during and over 13 years after wall installation (Spade Cells 15, 16).

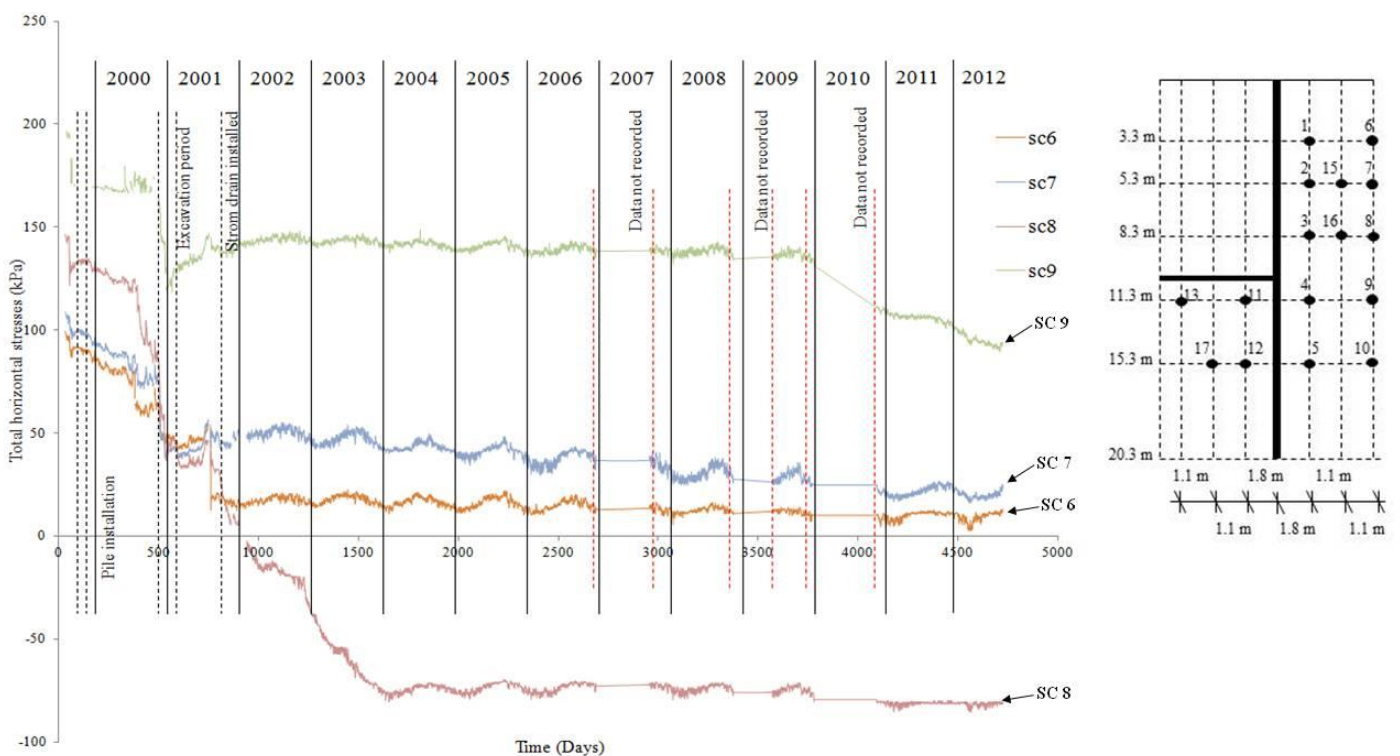


Figure 6.23. Total horizontal stress measured before, during and 13 years after wall installation. (Spade Cell 6, 7, 8, 9).

6.3.7 Total horizontal stress distribution in front of the retaining wall

Four spade cells were positioned in front of the retaining wall. An initial decrease in the total horizontal stress was measured during the piles installation and dewatering. As it was observed for the pore water pressures, the changes in the total horizontal stress at spade cell 12 were inexplicably larger than those measured at spade cell 11. It is possible that the higher initial total horizontal stress changes on spade cell 12 is due to the fact that this spade cell is located in the Weald Clay.

Figure 6.24 shows the long term horizontal stress changes in the area behind the wall measured at spade cells 11 and 12, Figure 3.2. Again, the main horizontal stress changes were observed during the period of excavation of the cutting. The subsequent construction of the base slab caused an increase in the total horizontal stress. Similar results were found for the pore water pressure changes, Figure 6.8. An approximately constant total horizontal stress in the long term was measured at both spade cells and 11 and 12.

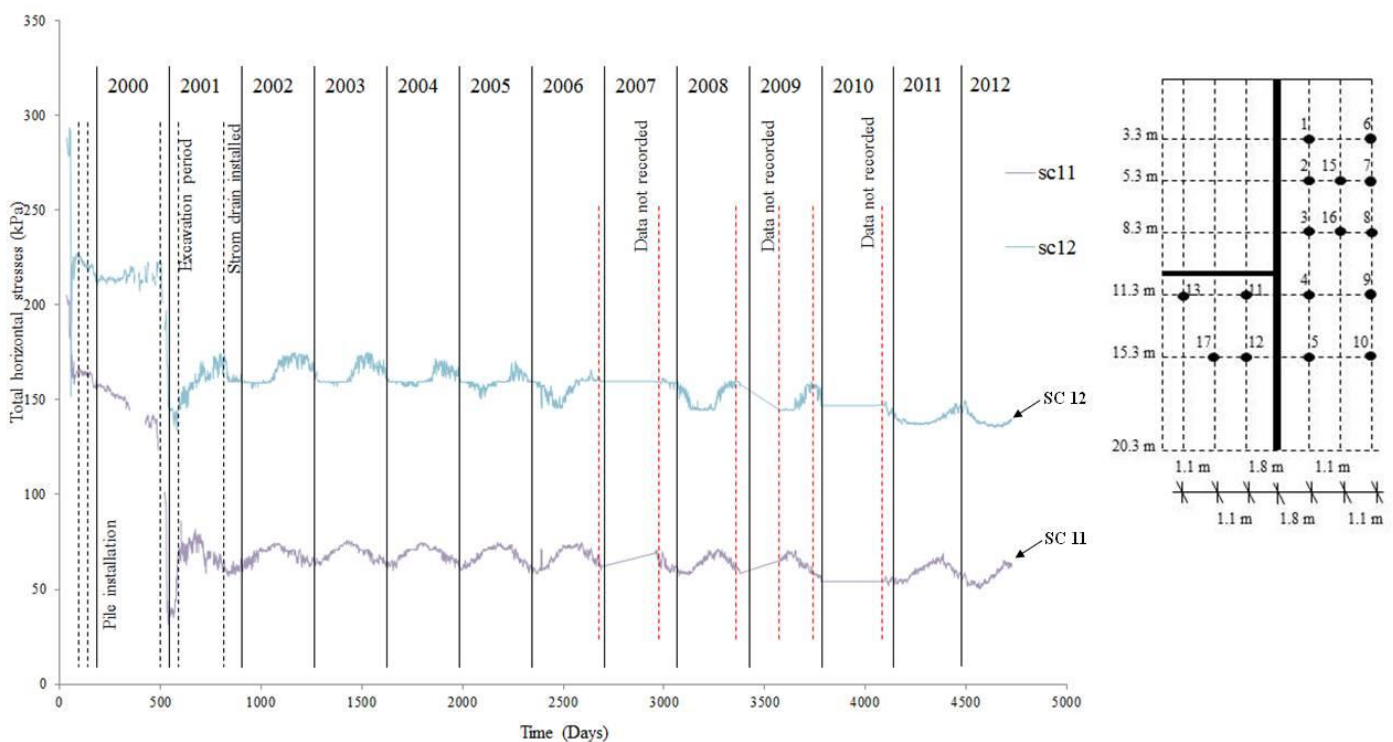


Figure 6.24. Total horizontal stresses measured before, during and over 13 years after wall installation (Spade Cells 11, 12).

Figure 6.25 shows the horizontal stress changes in the soil at spade cells 13 and 17. The total horizontal stress changes were similar to those measured at the spade cells 11 and 12. An initial decrease in the horizontal stress, which is due to boring of the piles, was followed by an increase due to concreting. The values of total stress seem to remain constant in the long term, as it was measured by spade cells 11 and 12.

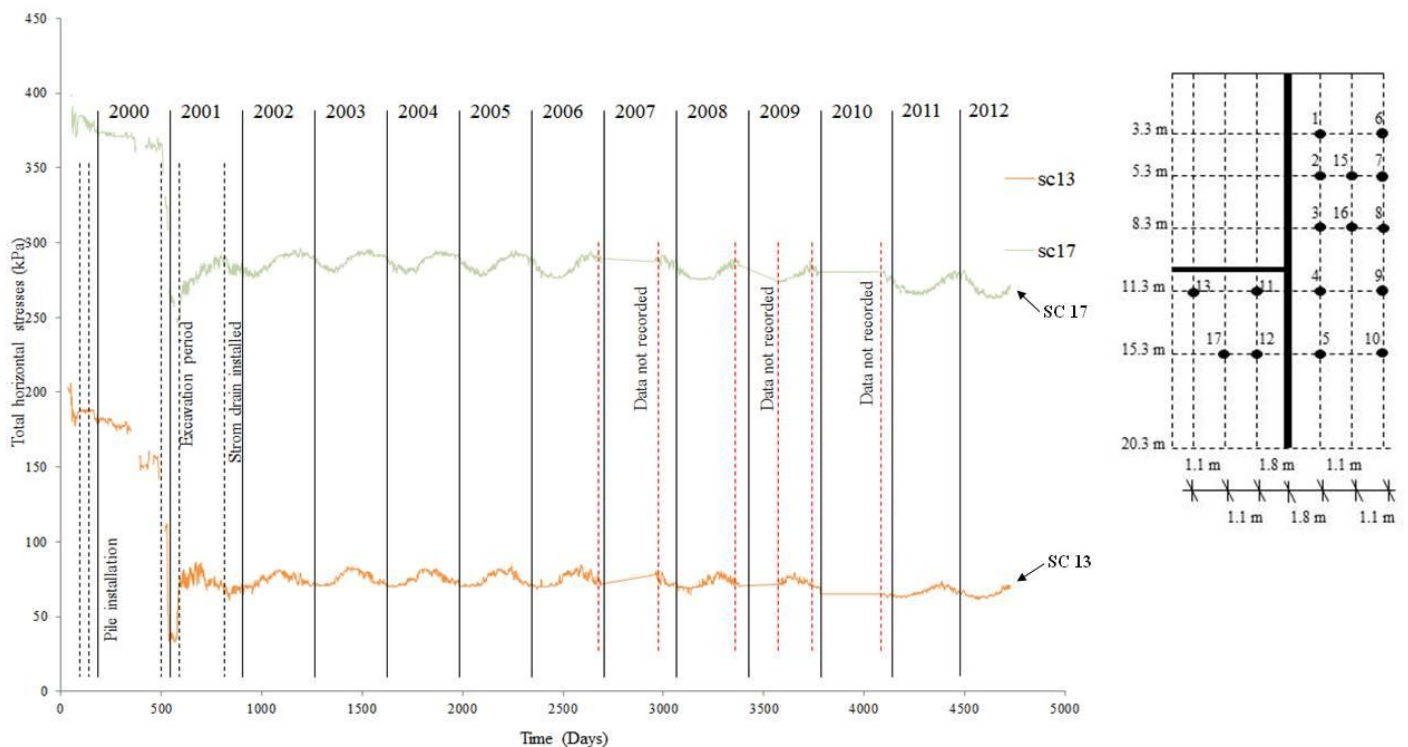


Figure 6.25. Total horizontal stresses measured before, during and over 13 years after wall installation (Spade Cells 13, 17).

6.3.8 Total horizontal stresses at various depth below ground level

3.3 m below the ground

Figure 6.26 shows the horizontal stress changes at spade cells 1 and 6 (Figure 3.2). The decrease of the total horizontal stress is larger at the spade cells closer to the exposed face of the bored pile than those measured from the spade cell 6. Similar results were found for the pore water pressure (Figure 6.3). The variation in total horizontal stress during the excavation

period was found to be greater in the soil close to spade cell 1 than at spade cell 6. However during dewatering, a major decrease in the horizontal stress on spade cell 6 was measured.

As it was observed for the pore water pressure, long term equilibrium conditions were achieved after about 4000 days. However, the total horizontal stress at spade cell 1 seemed to continue to decrease slightly after 4000 days from the excavation of the cutting.

It can be noted that the stresses measured in the soil close to spade cell 1 are lower during the winter period and increase during the summer. The horizontal stresses changes during each year are quite significant, with an average stress variation of 20 kPa. Furthermore, a significant decrease of the magnitude of the total horizontal stress cycles was observed in the long term. The total horizontal stress oscillation at spade cell 6 were not as marked as those at spade cell 1. However, as at spade cell 1, a gradual decrease in the total horizontal stress in the long term was measured from spade cell 6.

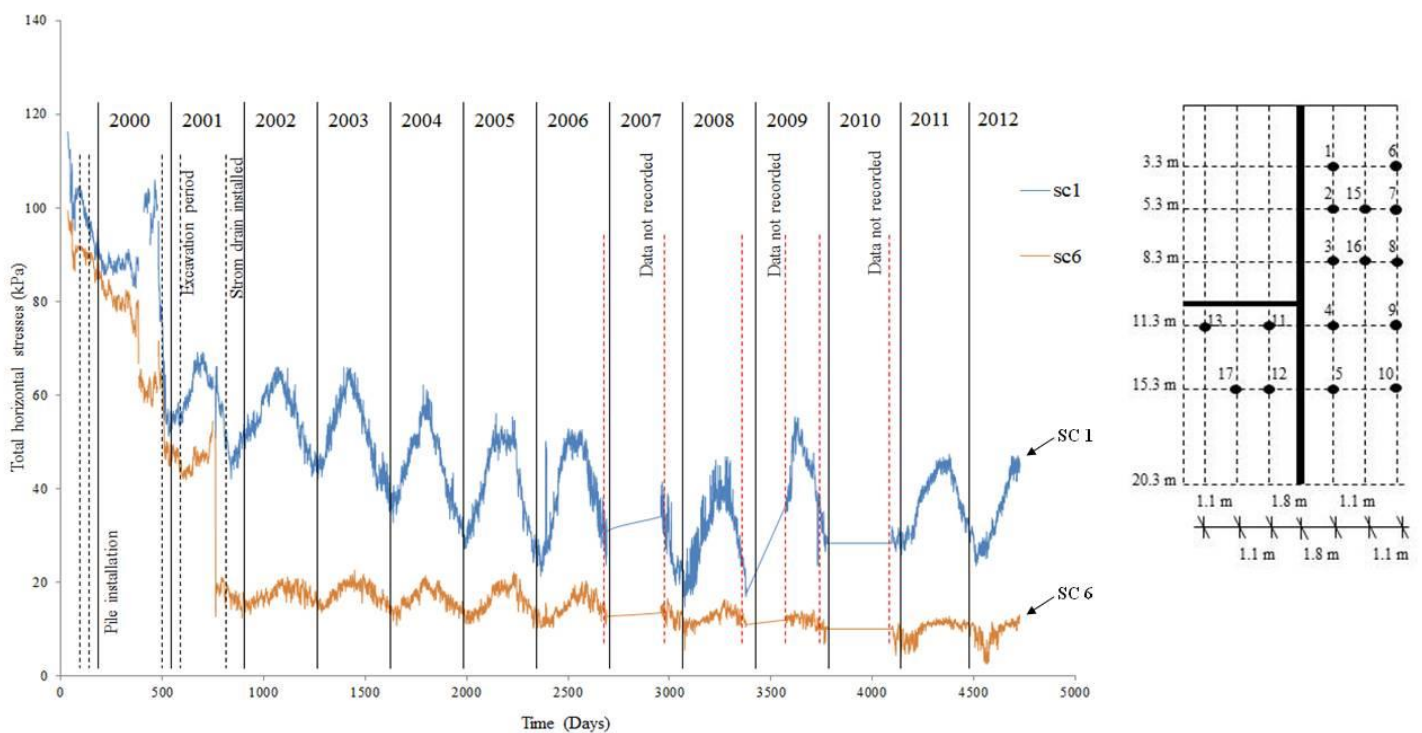


Figure 6.26. Total horizontal stresses measured before, during and over 13 years after wall installation (Spade Cells 1, 6).

5.3 m below ground level

Large decreases in the total horizontal stress were measured at spade cells 2, 7 and 15 during the excavation period. The long term total horizontal stresses continued to fall in the soil close to all the three spade cells. The total horizontal stress decreases are greatest in the area close to the exposed face of the wall. Long term total horizontal stress equilibrium is not reached in any of the spade cells.

Figure 6.27 indicates steady decrease in total horizontal stress at spade cells 2, 7 and 15. An average 20 kPa decrease in horizontal stress was observed at both spade cell 7 and 15. During the winter of 2012, the stress indicated by spade cell 2 became negative.

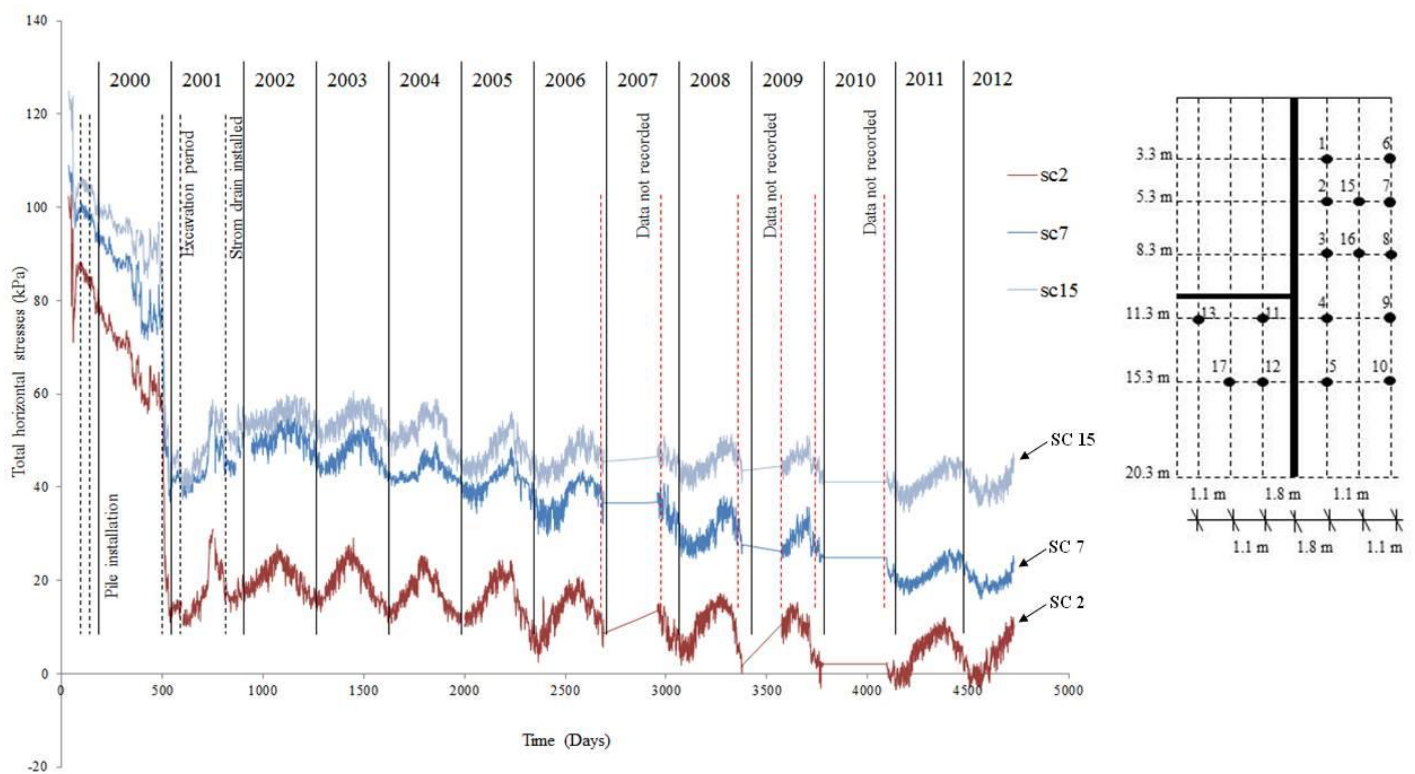


Figure 6.27. Total horizontal stress measured before, during and 13 years after wall installation. (Spade Cell 2, 7, 15).

8.3 m below ground level

Figure 6.28 shows the total horizontal stress changes at a depth of 8.3 m below ground level. The variation of the total horizontal stress is greatest at spade cell 3, which is closest to the

exposed face of the cutting. After the construction of the base slab, the total horizontal stress measured at spade cells 3 and 16 continued to decrease and long term equilibrium was reached at about 4000 days after the excavation of the cutting.

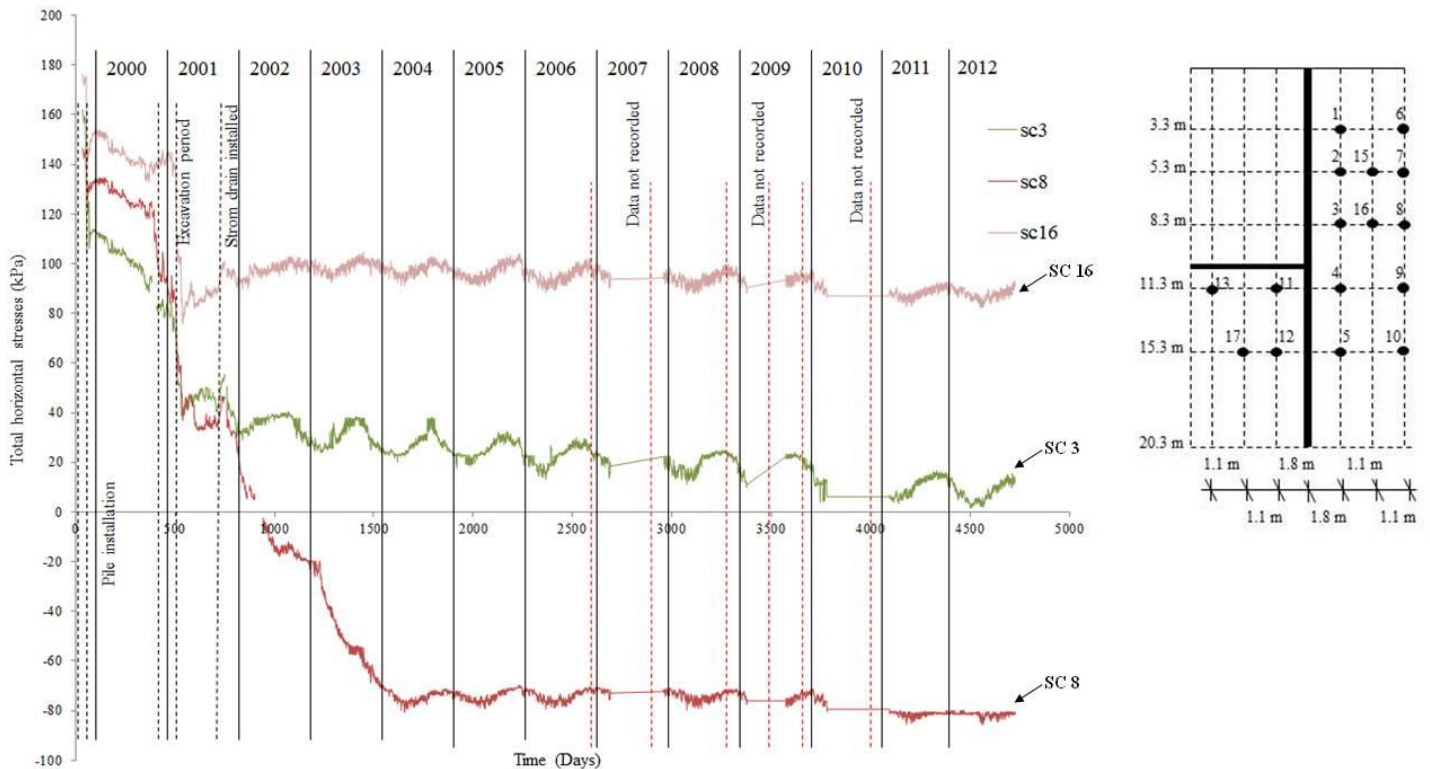


Figure 6.28. Total horizontal stresses measured before, during and over 13 years after wall installation (Spade Cells 3, 8, 16).

11.3 m below ground level

Spade cells 4 and 9 were located behind the retaining wall, while spade cells 11 and 13 were in front. As reported previously, spade cell 9 appeared to malfunction after 4000 days and in the long term measured an inexplicably large total horizontal stress decrease.

As expected, dewatering caused a large decrease in the total horizontal stress especially in the area of the soil close to spade cells 13 and 11 (Figure 6.29), in front of the wall and just below the base slab.

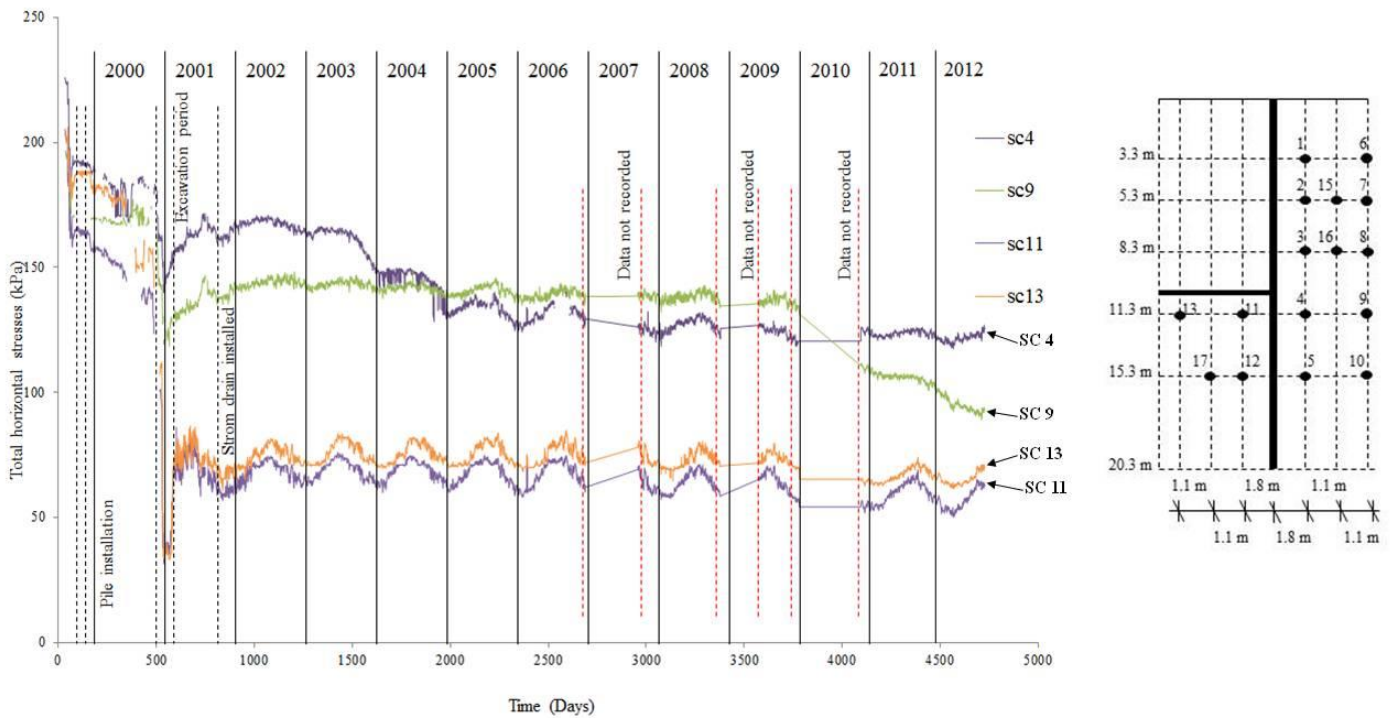


Figure 6.29. Total horizontal stresses measured before, during and over 13 years after wall installation (Spade Cells 4, 9, 11, 13).

15.3 m below ground level

Identical total horizontal stress changes were measured at spade cells 12 and 17 (Figure 6.30). As reported before, spade cell 5 measured an unexplained increase over the last 5 years. The installation of the bored piles caused an initial decrease in horizontal stress. The total horizontal stresses measured at spade cell 12 are unexpectedly lower than those measured at spade cells 5 and 17. This difference was also observed in the pore water pressure data. A decrease in horizontal total stress at all spade cells was measured during the excavation of the cutting. Additionally, the placement of the base slab led to a slight increase in the total horizontal stress at spade cells 17 and 12, in front of the wall.

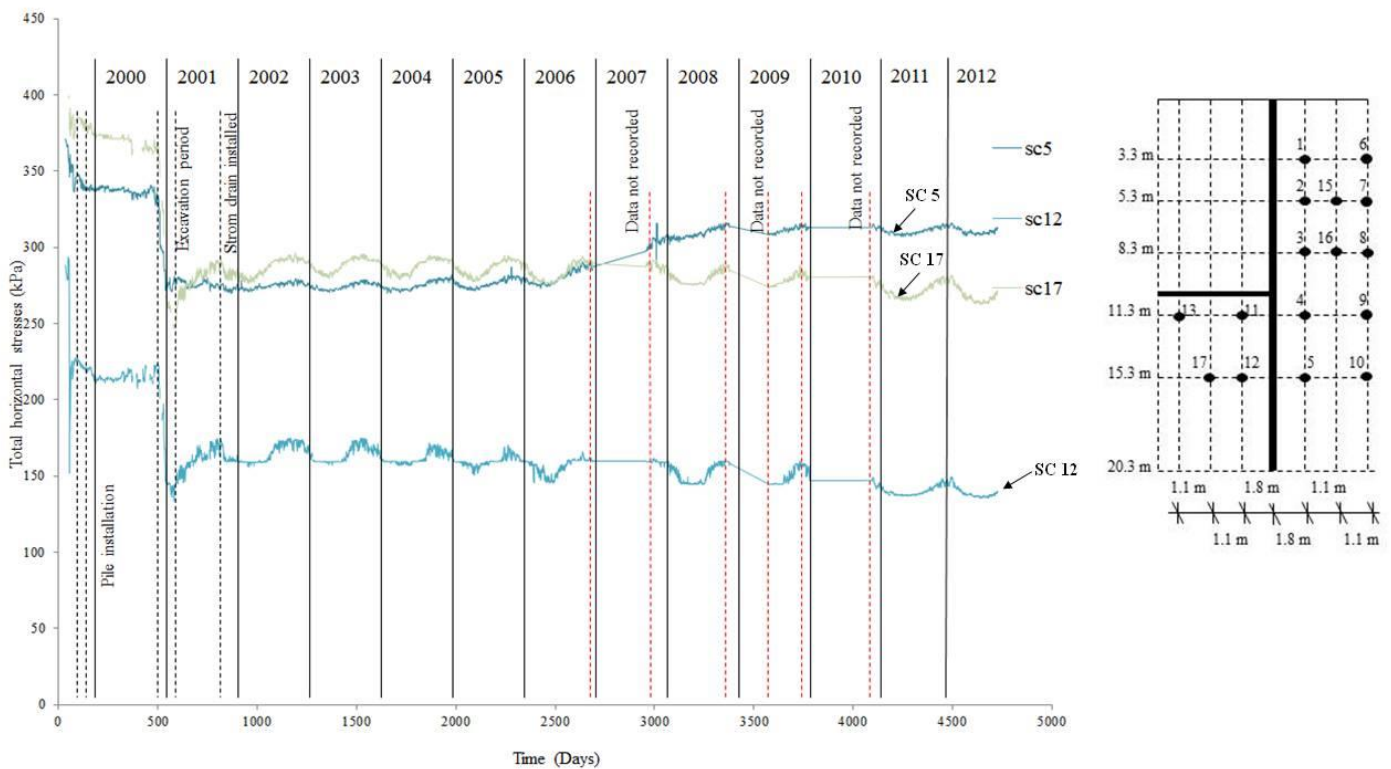


Figure 6.30. Total horizontal stresses measured before, during and over 13 years after wall installation (Spade Cells 5, 12, 17).

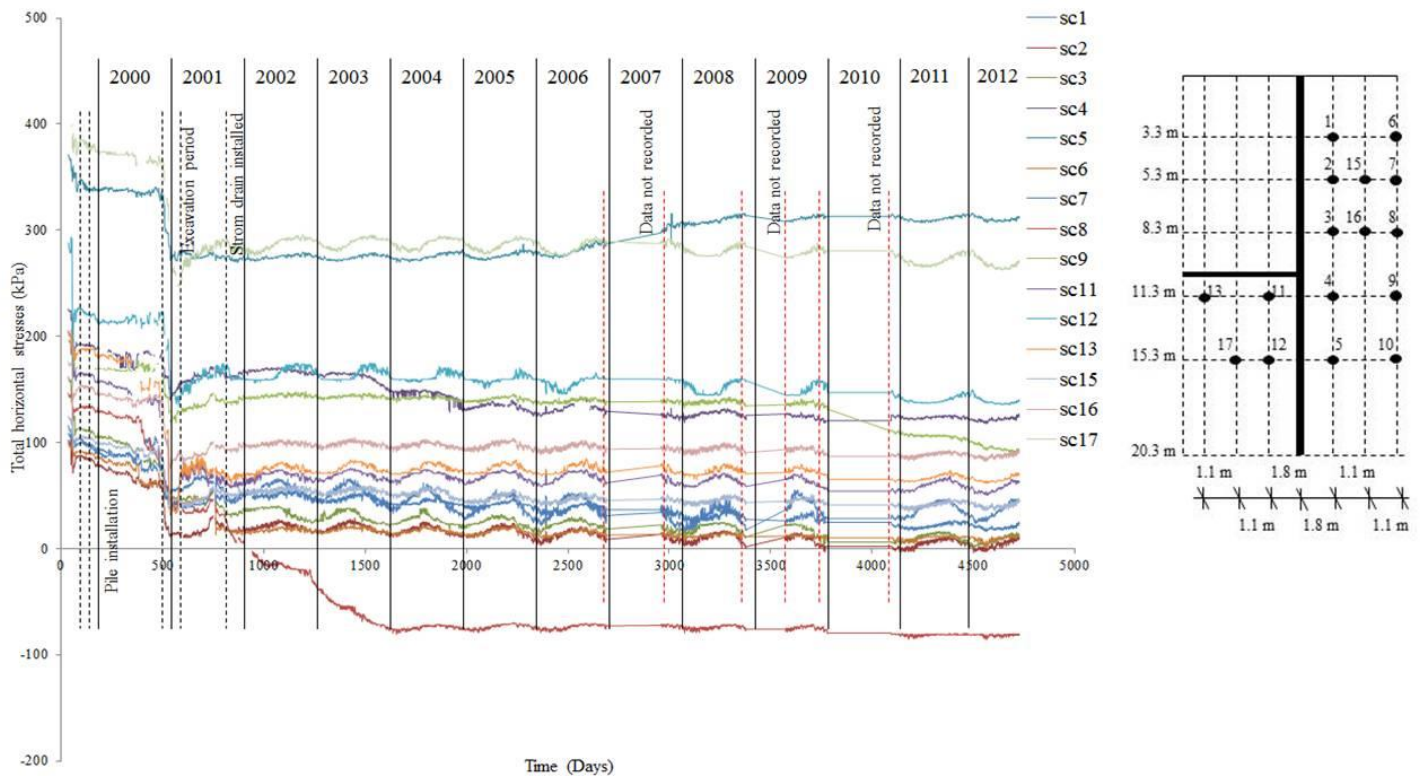


Figure 6.31. Total horizontal stresses measured before, during and over 13 years after wall installation (Spade Cells 1, 2, 3, 4, 5, 6, 7, 8, 9, 11, 12, 13, 15, 16, 17).

Figure 6.32 shows profiles of total horizontal stress behind the wall after wall installation, construction, excavation of the cutting and over a period of 12 years after the end of construction. The major horizontal stress changes occurred during pile installation and during excavation of the cutting. In the long term, the horizontal stresses behind the wall tended to decrease, especially in the area behind the wall from the surface down to 8 m depth. The total horizontal stresses became zero in the area from 5 m to 8 m depth behind the wall. From the pore water pressure data reported in previous sections it is apparent that the pore pressure decreased towards the wall. Then, in the long term, the through-wall seepage led to a decrease in the total horizontal stress behind the wall.

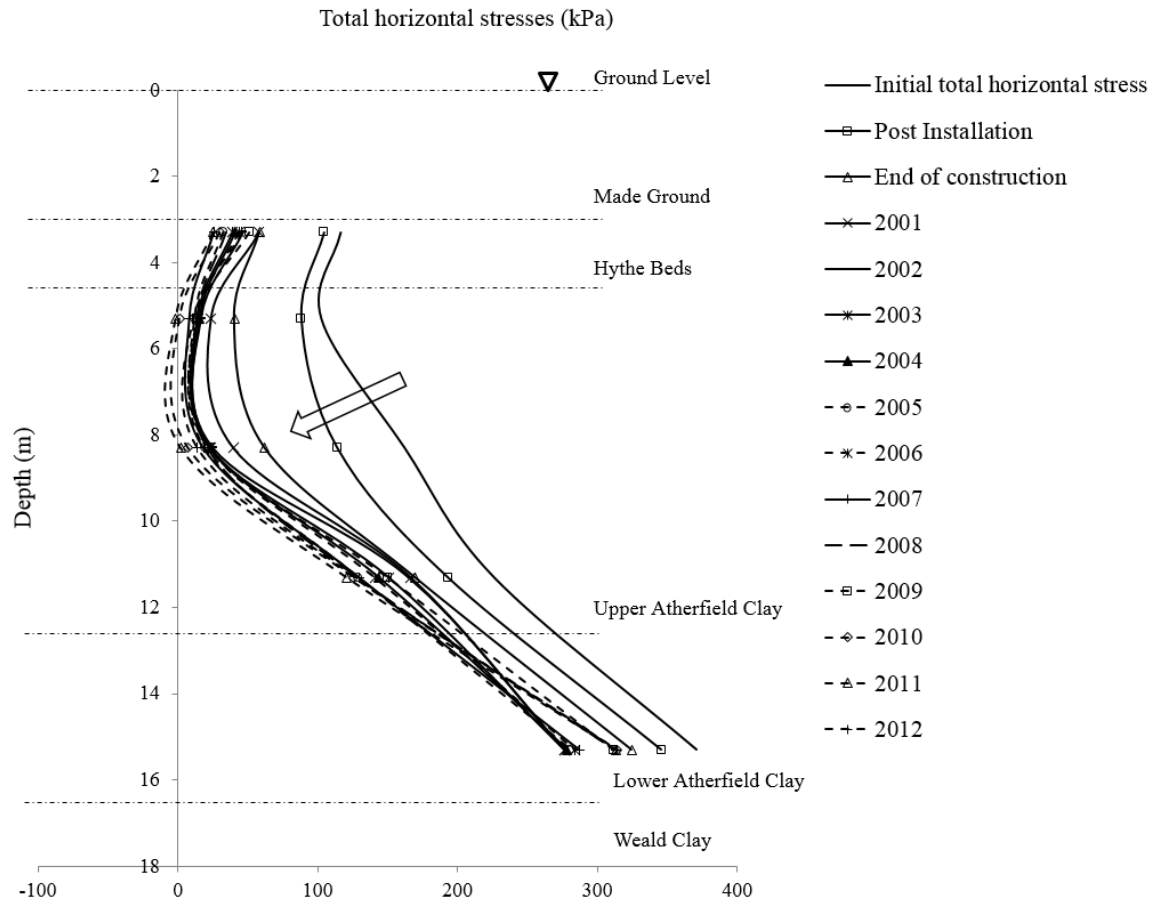


Figure 6.32. Total horizontal stresses behind the wall before and after wall installation, construction, excavation and long term (13 years).

6.4 Coventry long term data recording

6.4.1 Introduction

A case record of long term bending moment data from an embedded cantilever retaining wall with a stabilising base at Coventry, is reported in this section. These records are a continuation of the work done by Hayward (2000). Data from the instrumentations stopped being recorded in June 1999, in 2010 the signals from the instrumentations began to be recorded again. Hayward (2000) investigated embedded retaining walls that incorporate a stabilizing base projecting rigidly from the front of the wall at formation level. Results from these analyses are also presented and discussed by Richards *et al.* (2004).

6.4.2 The study site

The A444 Coventry North-South road links the M6 motorway north of Coventry, UK, with the A428 trunk road to the south. The section of stabilized base retaining wall at the Caludon Road overbridge, Figure 6.33, comprises 1 m diameter bored piles spaced at 1.1 m centres with an overall depth of 14 m and a retained height of 7.8 m. The centre of the 1m deep stabilising base extended 5 m into the excavation from the wall face. Its upper surface is 7.8 m below the top of the retaining wall, with the carriageway constructed on top.

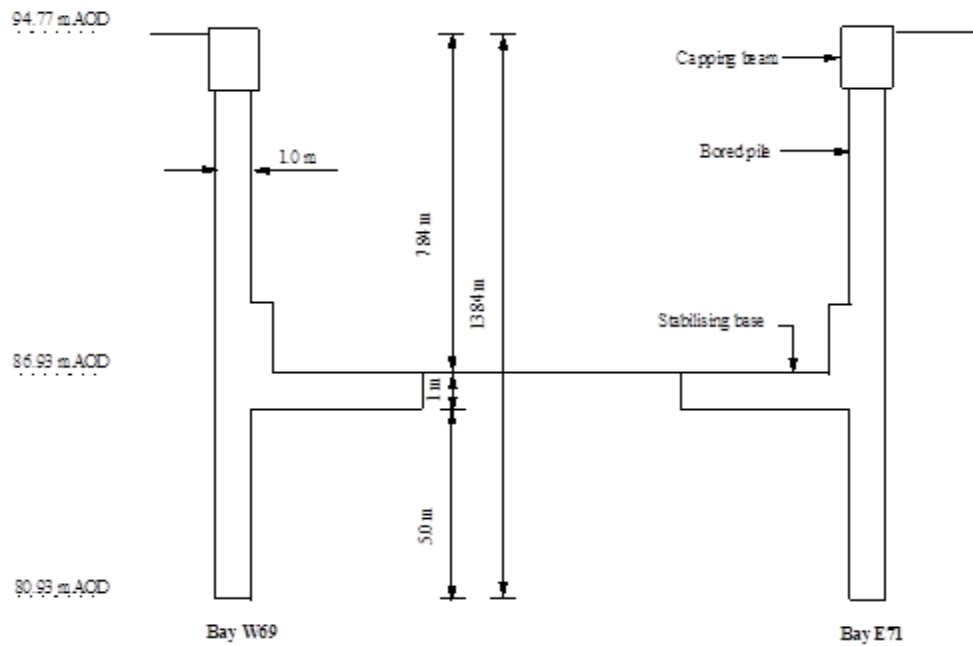


Figure 6.33. Cross section through monitored section of road (Hayward, 2000).

6.4.3 Ground conditions

A schematic cross section of the retaining wall, showing its geometry in relation to the site geology is shown in Figure 6.34.

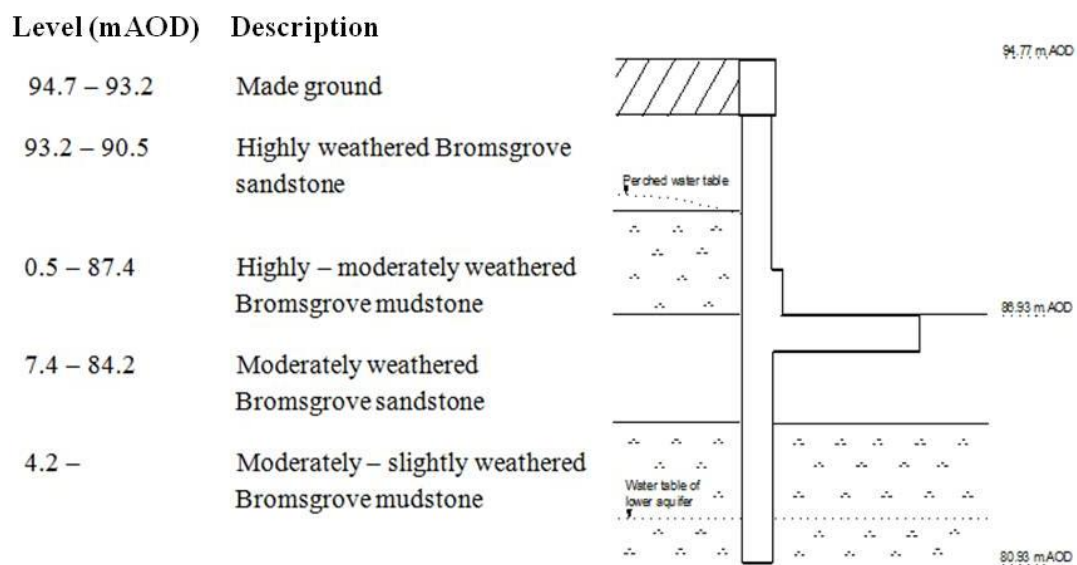


Figure 6.34. Ground condition at the instrumented cross section (Hayward, 2000).

Up to 1.5 m of made ground is underlain by the Bromsgrove Sandstone Formation, which consists of grey to buff sandstone interbedded with dark red-brown mudstone in layers typically 2-3 mm thick. The formation exhibits cyclic sedimentation, with the sandstone often passing upwards into mudstone. The strata at the top of the cutting were frequently highly weathered and extremely weak, while the lower material was typically slightly to moderately weathered, and weak (Hayward, 2000).

The principal stages of retaining wall construction at the instrumented section are summarised in Table 6.1. Self-boring pressuremeter and high pressure dilatometer tests were undertaken within the Bromsgrove formation as part of the original site investigation, from which the shear stiffness parameters were determined. To provide temporary support to the retaining walls, tubular steel props spanning the width of the cutting were installed at capping beam level at 5 m centres (Hayward, 2000). The props were pre-loaded to a nominal axial force of 1300kN, equivalent to 260 kN/m, during which the wall moved back into the retained ground by approximately 5 mm. The earth berms were then excavated to approximately final formation level.

Excavation for the stabilizing base slabs did not take place until immediately prior to their construction. The pile reinforcement cages incorporated a polystyrene void former, allowing couplers pre-fixed to the main pile reinforcement to be exposed following excavation to formation level. The steel reinforcement for the stabilizing base was connected to the main pile reinforcement using these couplers to form a rigid connection between the piles and the stabilizing base. On completion of the stabilizing bases, the temporary props were de-stressed and removed.

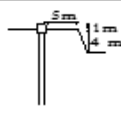
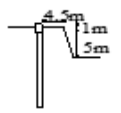
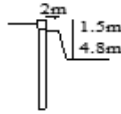
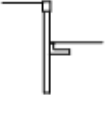
Stage	Description	Schematic	Date	Day
I	Installation of contiguous pile wall.		03/02/96	
II	First stage excavation.		14/05/96	0
III	Second stage excavation.		24/09/96	133
IV	Third stage excavation.		16/10/96	155
V	Temporary props installed and pre-loaded to 1300 kN.		22/11/96	192
VI	Earth berm removed.		25/11/96	195
VII	Excavation to stabilising base blinding level and construction of stabilising base.		11/12/96	211
VIII	Temporary props removed.		28/02/97	290
IX	Road opened to traffic		12/12/97	577

Table 6.1 Main stages of construction at the instrumented cross section (Hayward, 2000).

6.4.4 Instrumentation

Figure 6.35 shows the instrumentation used to monitor wall movements, wall and stabilising base bending moments, temporary prop loads and vertical pressures beneath the stabilising base. As reported previously, this work considers only the long term monitoring of the wall bending moments and vertical pressures beneath the toe of the stabilizing base.

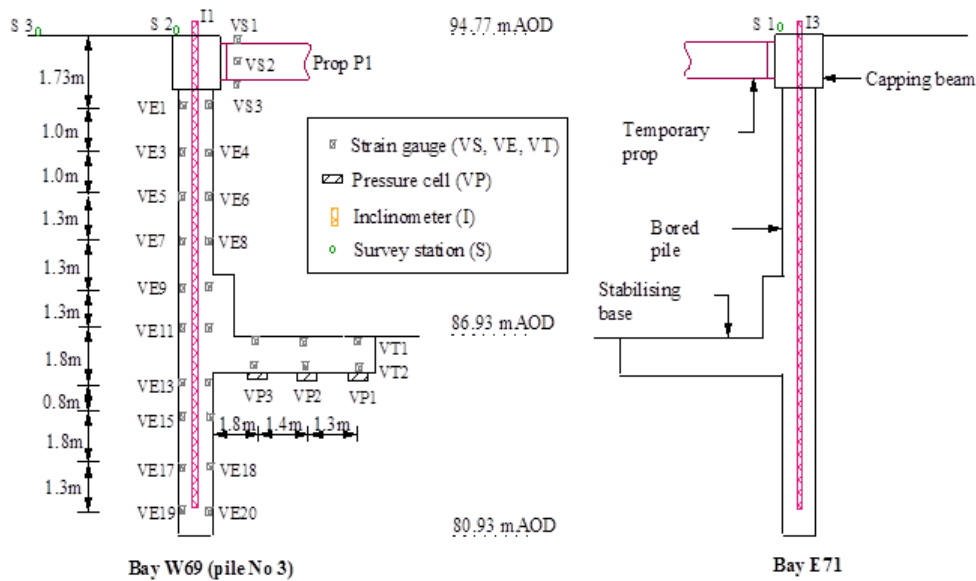


Figure 6.35. Cross section through monitored cross section, showing location of instrumentation (Hayward, 2000).

6.4.4.1 Wall bending moments and vertical stress beneath the stabilising base

Wall bending moments were measured at ten locations within each of the two of the piles that form the retaining wall in the instrumented section. At each measurement location, two vibrating wire embedment strain gauges were fixed within the reinforcement such that on placement of the reinforcement cage within the borehole, the gauges were positioned at the front and back of the pile on an axis perpendicular to the line of the retaining wall. Conventional engineers' beam theory was used by Hayward (2000) to deduce the bending moment (M) from the longitudinal bending strains ε_{front} and ε_{back} measured at each location.

$$M = \frac{EI}{y} \frac{(\varepsilon_{front} - \varepsilon_{back})}{2} \quad \text{Equation 6.4}$$

where EI is the composite bending stiffness of the pile and y is the distance from the gauge to the neutral axis of the pile. Similarly, following excavation to formation level and the connection of the main prop slab reinforcement bars into the pile, embedment strain gauges were connected to the slab reinforcement cage to measure bending strains ε_{top} , and ε_{bottom} .

Typical plots of wall bending moments against time recorded at ten different depths within the instrumented wall, Figure 6.35, are reported in Figures 6.36-6.45. The initial bending moments were recorded from 14/05/96 to 01/09/99; after that, the signal was interrupted until the 01/05/2011, when the data logger was reconnected.

Overall, constant values of bending moment were observed at each of the instrumented sections. The bending moments in the strain gauges at depths of 2.73 m, 6.33 m, 7.63 m, 9.43 m, 10.23 m, and 13.33 m from the head of the pile were almost constant in the long term. The bending moments recorded in the strain gauges at 6.33 m, 12.03 m, from the head of the pile were anomalous, display a rapid increase indicative of cracking in the concrete near these strain gauges.

The bending moment in Figure 6.36, 1.73 m depth from the head of the pile 3 and 5, shows a slight increase of the moment in the long term. In contrast, the bending moment at 5.03 m depth below the head of pile 5 shows a decrease in the long term. However, from the data collected it may be deduced that the long term trend of the bending moment remains substantially constant.

Figure 6.46 shows the variation in vertical total stress below the stabilising base. A gradual reduction in total vertical stress was measured at all of the pressure cells.

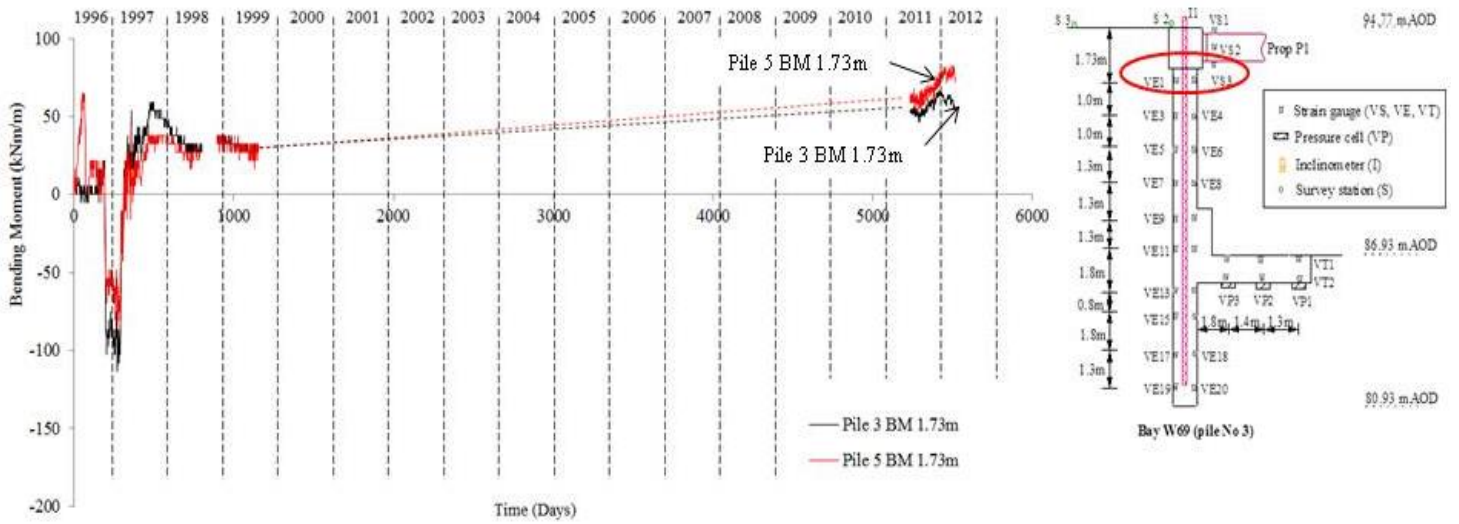


Figure 6.36. Development of wall bending moments at 1.73 m below top of wall.

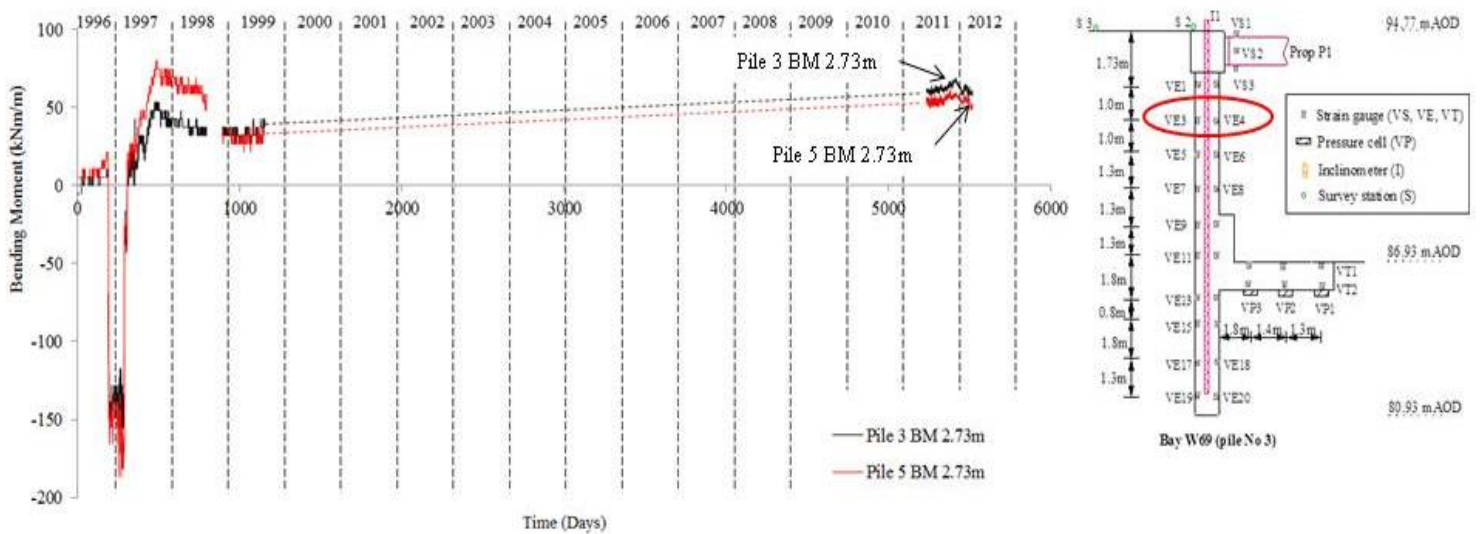


Figure 6.37. Development of wall bending moments at 2.73 m below top of wall.

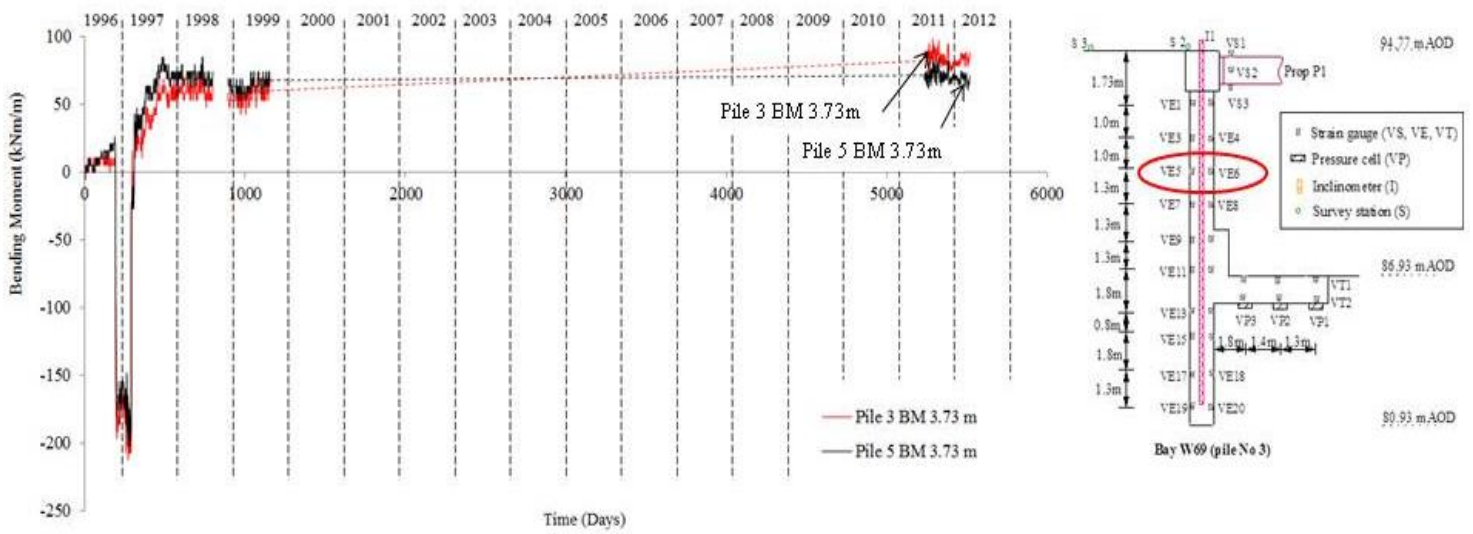


Figure 6.38. Development of wall bending moments at 3.73 m below top of wall.

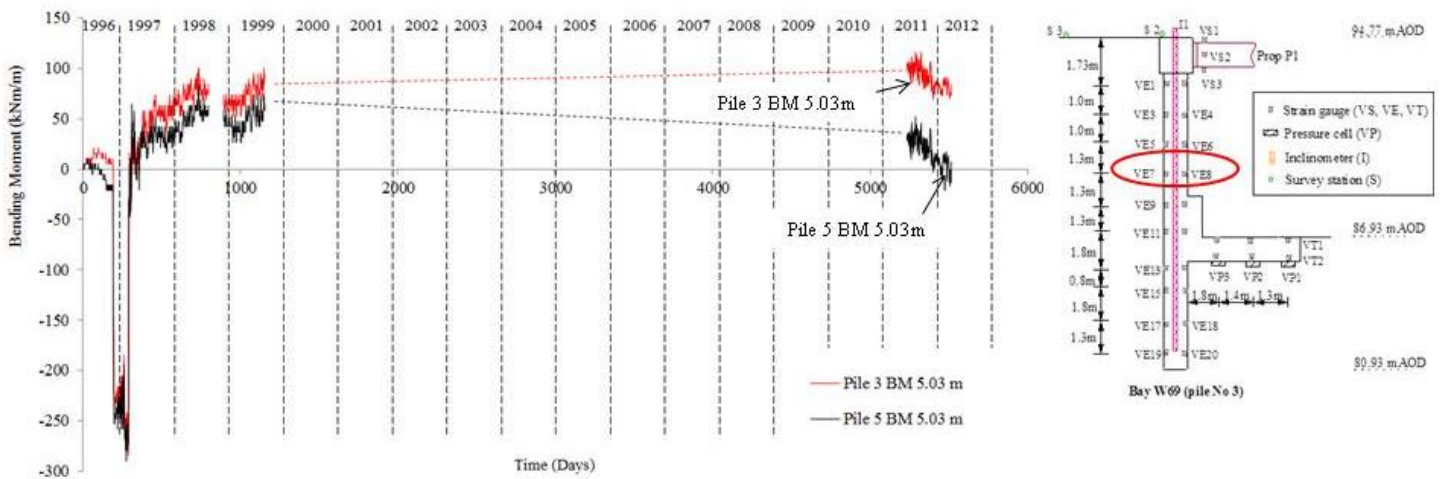


Figure 6.39. Development of wall bending moments at 5.03 m below top of wall.

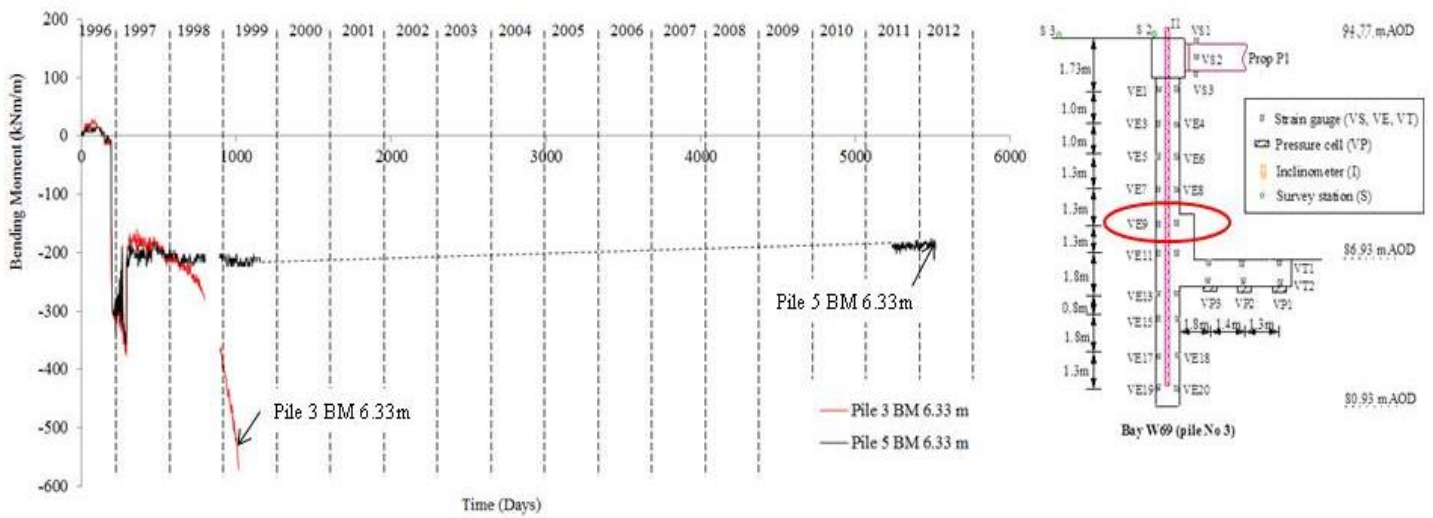


Figure 6.40. Development of wall bending moments at 6.33 m below top of wall.

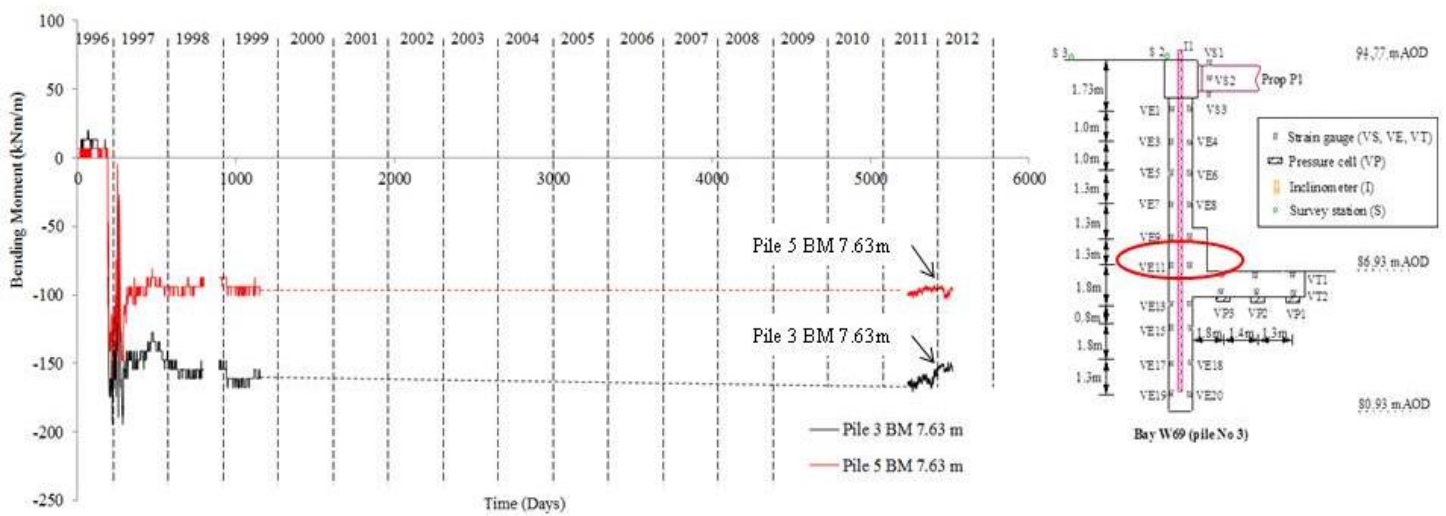


Figure 6.41. Development of wall bending moments at 7.63 m below top of wall.

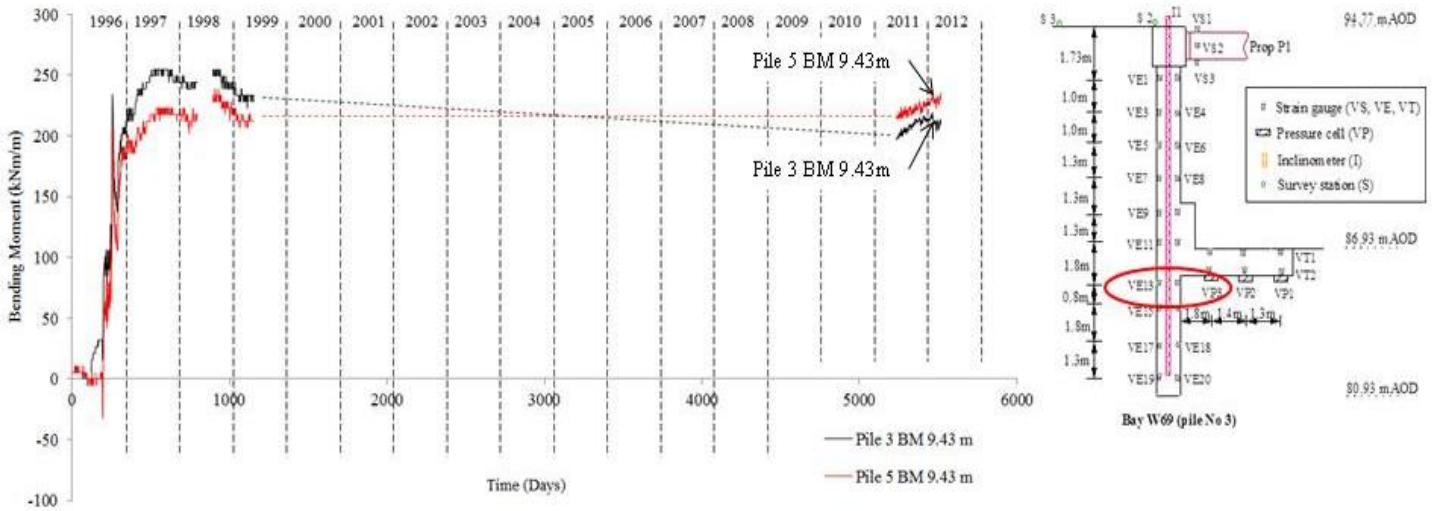


Figure 6.42. Development of wall bending moments at 9.43 m below top of wall.

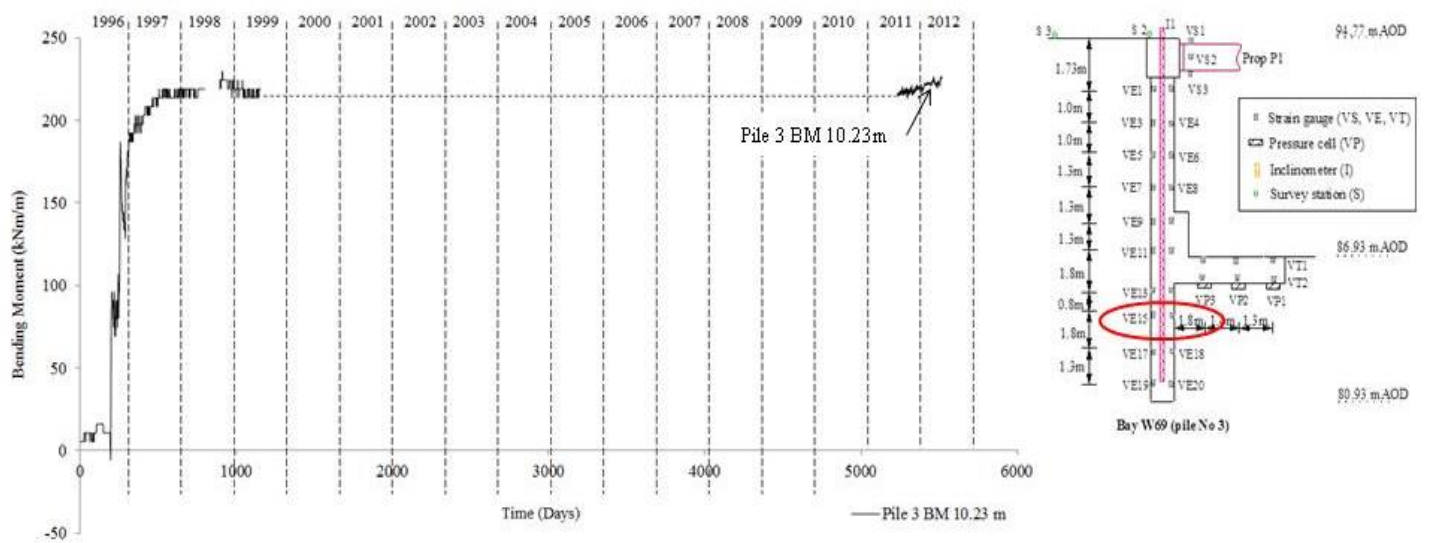


Figure 6.43. Development of wall bending moments at 10.23 m below top of wall.

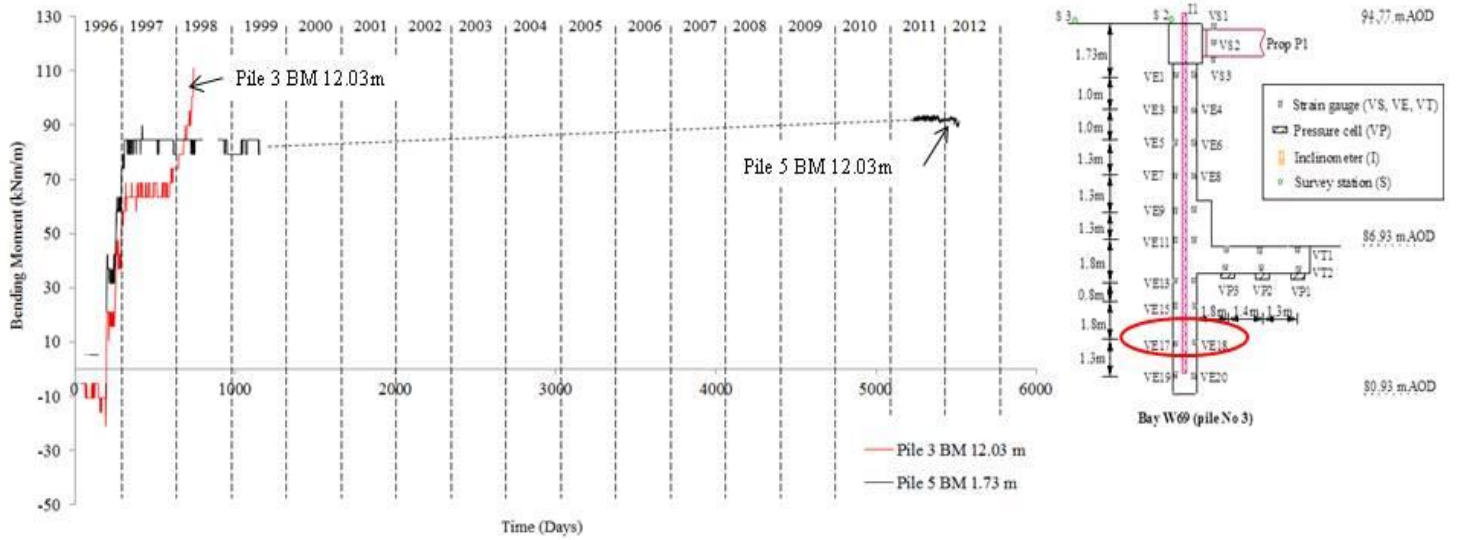


Figure 6.44. Development of wall bending moments at 12.03 m below top of wall.

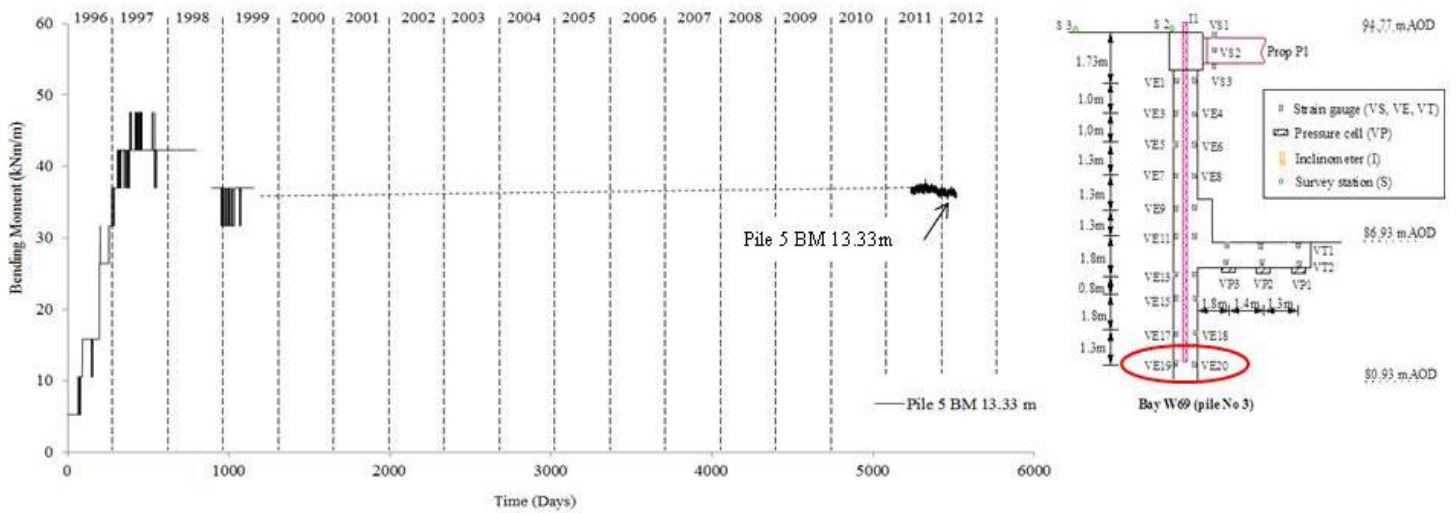


Figure 6.45. Development of wall bending moments at 13.33 m below top of wall.

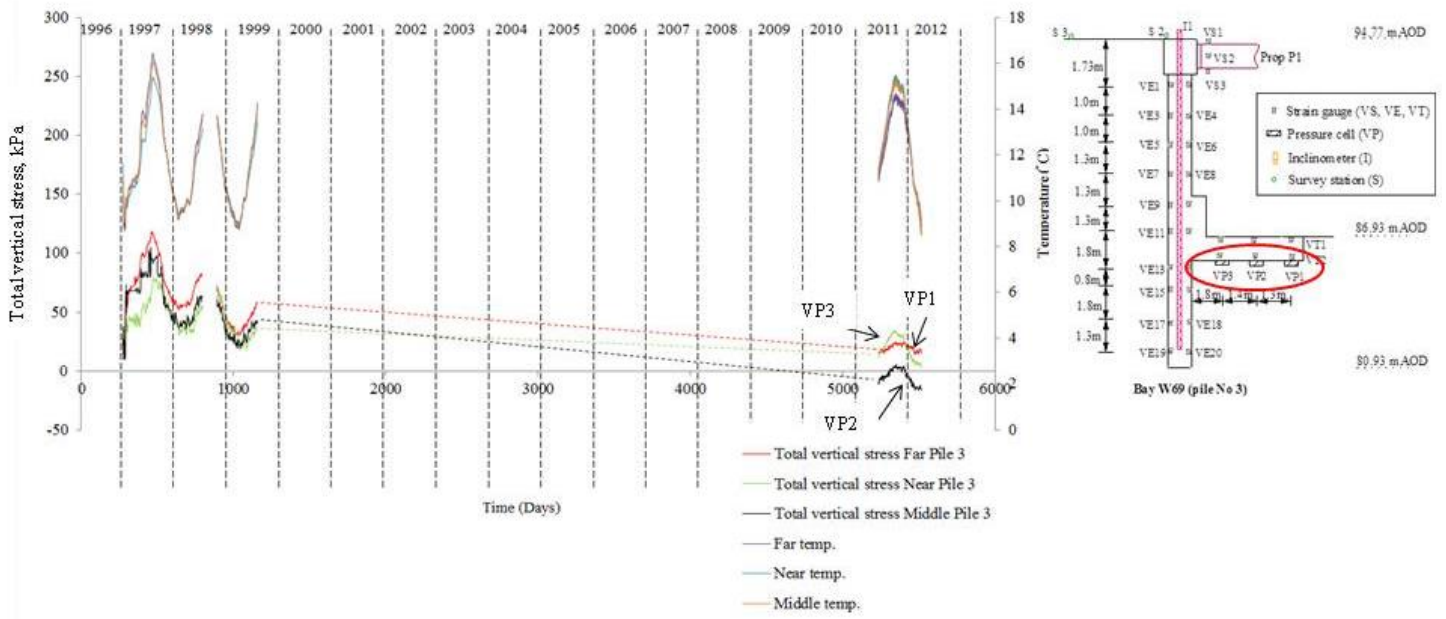


Figure 6.46. Stresses beneath the base adjacent to pile 3.

6.5 Summary

The following conclusions may be considered:

- The long-term spade cell measurements at the site in Ashford are showing generally a slight decrease of the total horizontal stress over the years following construction of the cutting, which are probably due to the drainage through the bored pile wall lowering the water pressures in day. From the data presented in this chapter it is evident that the pore water pressure reduces towards the retaining wall.
- The in situ total horizontal stresses did not re-establish during the 12 years after the excavation of the cutting.
- Overall constant values of the bending moment at the site in Coventry were observed in the long term, indicating no increase in lateral stress in a retaining wall in weak sandstones.
- Furthermore, the vertical stress beneath the stabilising base has decreased slightly in the long term. This is also consistent with there being no increase in total horizontal stresses behind the retaining wall over the long term.

CHAPTER 7

CONCLUSIONS AND FURTHER WORK

7.1 Conclusions

In the last few decades considerable effort has been spent on investigating the installation effects of diaphragm wall panels in overconsolidated deposits. In contrast, in the literature there is a relative lack of information on the installation effects of bored pile construction. In this thesis a comprehensive three-dimensional analysis has been presented to investigate the stress changes and consequent ground movements due to bored pile wall installation in an overconsolidated clay deposit.

A three-dimensional model was used to interpret and explain the real data of ground stress changes during bored pile wall installation in an overconsolidated deposit, in connection with the

Channel Tunnel Rail Link (CTRL; now HS1) at Ashford. Non-linear stress strain characteristics were also implemented in the model.

The thesis has presented a comprehensive analysis to investigate whether different sequences of diaphragm wall panel installation could lead to different initial stress redistributions behind the wall. In the literature, the limited research that has been carried out to quantify the three dimensional effects of diaphragm wall installation do not address this issue.

In this work, a continuation of the total horizontal stress and pore water pressure measurements that started one month prior to the installation of the contiguous bored pile wall at Ashford, Kent, has been presented. The evolution of the lateral stress around a wall in overconsolidated clay deposit over a long period of approximately 4700 days (13 years) since pile installation has been presented.

The major conclusions drawn from each chapter are summarised below.

Chapter 2

The sequence of diaphragm wall panel and bored pile construction in a stiff clay results in a complex soil behaviour that needs to be carefully investigated. This chapter has presented a review of the literature of the main research that previously addressed such issue.

The mechanisms of load transfer and ground deformation during the construction of a diaphragm wall have been investigated by many researches in the field (Farmer and Attewell, 1973; Lings *et al.*, 1991; Carder *et al.*, 1991; Ng and Yan, 1998). They observed in general a marked reduction in total lateral stress at the soil/wall interface due to diaphragm wall construction. However, relatively little research has been undertaken to investigate the mechanisms of load transfer and ground deformation during the construction of sequence of bored piles (Bennet *et al.*, 1996; Symons *et al.*, 1992; Carswell *et al.*, 1993). They reported that in general, a large reduction in the lateral stress behind the wall occurred only at depth.

Powrie *et al.* (1996) and Richards *et al.* (1998) investigated the effects of diaphragm wall installation using a centrifuge model. They found that ground movement depends on a number of factors, including the initial ground water level and the geometry (length/depth ratio) of the panel. Furthermore, Powrie *et al.* (1996) point out the importance of the three-dimensional effects in reducing the displacement at the centre-line of a single panel. Centrifuge model tests to investigate the effects of bored pile installation were not found in the literature.

As numerical modelling is much more economical than field monitoring, various research has been carried out using finite element and finite difference analysis to investigate the effects of diaphragm wall installation. Gunn *et al.* (1994) investigated the stress changes due to wall installation using a 2D finite element analyses. They found important lateral stress reductions during wall installation. Pantelidou (1994) calculated stress reductions during pile construction that did not exhibit any abrupt reduction on the lower part of the pile. She used 2D finite element analysis with an axi-symmetric condition to simulate the installation of a bored pile. Powrie and Batten (2000) investigated the effects of wall installation at Canada Water using an axisymmetric finite-element analysis to simulate the installation of a single pile. De Moor *et al.* (1994) presented an analysis of a plan (horizontal) section through a series of wall panels using 2D finite elements. Ng *et al.* (1995) used two simple perpendicular plane sections to investigate the three-dimensional effects of diaphragm wall installation.

Ng and Yan (1998) modelled the construction sequence of a typical diaphragm wall panel in stiff clay using a three-dimensional finite difference program. They attributed significant stress reduction at the centre and above the toe of the panel caused by the installation process to both downward load transfer and horizontal arching. At the edge of the panel, the horizontal arching mechanism appears to dominate, which limits substantial horizontal stress reductions and ground deformations. Gourvenec *et al.* (1999) carried out a series of 3D finite-difference analysis to investigate the impact of three-dimensional effects in lateral stress during the sequential installation of a number of diaphragm wall panels. From their analysis it was found that as the panel length increased, the degree of reduction in the earth pressure coefficient during installation of the primary panel also increased, while the increase in earth pressure coefficient during installation of the subsequent panel was reduced.

Chapter 3

This chapter described the use of a three-dimensional model to analyse, interpret and explain the real data of ground stress changes during bored pile wall installation in an overconsolidated clay deposit in connection with the Channel Tunnel Rail Link (CTRL; now HS1) at Ashford. Most previously publications analysed the three dimensional installation effects during construction of a diaphragm wall panel; innovatively in this Chapter an investigation of the changes in total stress associated with the installation of 21 bored piles excavated in eleven different construction steps was presented.

The following conclusions were made from the first analysis:

- The influence of pile installation became insignificant at a distance of $1.2 d$ along the line of the wall from the centre of the pile installed. The horizontal stress in the region of the edges of the pile installed does not change after pile construction.
- The horizontal stresses in the ground close to the edges of first pile installed did not change during the excavation of that pile. These results are different from those found by Gourvenec *et al.* (1999) and Ng and Yan (1998). The main reason is the different geometry between the panel (that was investigated by Gourvenec *et al.* (1999) and Ng and Yan (1998) and the pile. This led to different stress states following the wall construction.
- From the computed results minimal stress changes in the soil behind the pile, in the area from the head of the pile down to 15 m depth were calculated. Only a small total horizontal stress increase was observed below the pile installed. Again this was due to the difference in geometry between the panel and the pile.
- During the installation of a single pile it was calculated that the horizontal stress decreases were mainly concentrated above the toe of the pile. These results were quite different from those of Pantiledou, 1994. This is because she used a simplified 2D analysis with an assumption of axy-symmetric conditions, which cannot take into consideration the horizontal stress transfer below the toe of the wall via the horizontal and vertical shear stress.

- From the analysis, a small stress increase under the toe of the wall during bored pile construction was calculated. This was different from the results of Gourvenec *et al.* (1999) and Ng and Yan (1998) for the case of panel installation. Again this was mainly due to the geometry effects.
- A slight increase in the total horizontal stress behind the wall after the installation of the piles adjacent to the first pile installed was calculated. This was due to the three dimensional stress transfer mechanism in the soil close to the bored piles. Specifically this was attributed to the horizontal stress redistribution via the horizontal shear stress (τ_{xy}). Similar results were obtained by Bennet *et al.* (1996).
- Richards *et al.* (2006) compared the changes in stress measured due to the installation of a single pile with the values calculated using a simplified elastic analysis. They found that the reduction in stress due to pile installation measured by the instrumentation was generally larger than that calculated using the simple elastic analysis. Similar results were also found from the analyses presented in this Chapter.
- Reasonable correlations were found between the calculated stress change in the 3D model and the real data from the instrumented section of the bored pile wall at Ashford, Kent.
- It has been found that the stress change is relatively insensitive to K_0 .

Chapter 4

The aim of the finite difference programme described in this chapter was to simulate more realistically the effects of installing a bored pile wall in over-consolidated clay using a non-linear stress-strain soil model. Results were compared with real data of the ground stress changes during bored pile wall installation in an overconsolidated clay deposit in connection with the Channel Tunnel Rail Link (CTRL; now HS1) at Ashford. The results calculated from the non-linear stress-strain model were also compared with those from the linear stress-strain analysis.

The following conclusions were made:

- The computed profiles of total horizontal stress from the analysis were compared with those measured by the instrumentation at Ashford, Kent. The non-linear stress-strain characteristic gave overall slightly better results than the linear-stress-strain behaviour.

However both the analysis (non-linear and linear stress strain models) can capture the observed pattern of changes in stress.

- Both of the analyses (non-linear stress strain and linear stress-strain characteristics) gave better results than those found in Chapter 3. This was mainly due to the fact that in the previous model in Chapter 3 a constant value of Young's modulus, E , with depth, had been used.
- However, as in Chapter 3 where the Young's modulus, E , was constant with depth, the installation of a single pile did not affect the soil further than $1.2 d$ along the wall from the centre of the installed pile.
- Horizontal stress relief was mainly concentrated in the zone above the toe of the pile. Compared with the results in Chapter 3, a slight decrease in the total horizontal stress in the area from the head of the pile down to 14 m depth was calculated.
- At distances of 0.5 m and 1 m perpendicular to the wall the final stress state was similar to that calculated at 0.4 m from to the wall. At a distance of 4 m perpendicular to the wall the horizontal stress relief became minimal.
- Comparing the displacements calculated in Chapter 3 and Chapter 4 it was found that the differences in soil displacements were mainly due to the implementation of different values of Young's modulus. 23 mm of maximum horizontal displacement was calculated with the non-linear stress-strain relationship. This is substantially different from the results in Chapter 3, where the maximum horizontal displacement was 3.5 mm.
- In Gault Clay, Ng and Yan (1998) found that the horizontal ground deformation at the centre of the 8 m long panel installed was 5 times larger than that at the edge. In contrast, in Chapter 4, for a single pile installed, it was calculated that the horizontal displacement at the centre of the pile is less than twice that at the edges. Again this implies that the different geometries between a pile and a panel led to a different stress change and soil displacements in the ground close to the wall. A similar result was found by Gourvenec *et al.* (1999), who investigated the effect of panel aspect ratio on the response of the soil to panel installation.
- These results suggest that in a congested urban area, on a heavily overconsolidated soil, where disturbance to the adjoining ground must be kept to a minimum, a bored pile wall is a better solution than a diaphragm wall made up of panel. The results reported in this work show that the stress relief and ground displacement after installation of a bored pile

wall are lower than those calculated after diaphragm wall construction, reported in various researches.

Chapter 5

In this Chapter the ground stresses changes and displacements after different sequences of diaphragm wall panel installation were investigated. Several analyses were carried out to compare the final stress variations for five different installation sequences of a group of five panels installed in an overconsolidated soil deposit. Then, innovatively in this chapter, it was investigated whether the different sequences of panel installation could lead to significantly different pre-excavation stresses redistribution behind the wall.

The following conclusions were made:

- The maximum distance at which the installation of a single panel has an effect is approximately 7.5 m at depths of 3.3 m and 14 m, respectively, from the top of the wall. An increase in the total horizontal stresses in the soil close to the edges of the panel was calculated. This result was also obtained by Gourvenec and Powrie (1999) and Ng and Yan (1998), and again confirms that the different geometry between piles and panels leads to different stress changes in the soil during their installation.
- It was found that the construction of the adjacent panel influences the stress change at the middle section on the central panel.
- It was found that the horizontal stress at the edges and the middle section of the centre panel is not much affected by the installation sequence. However, the horizontal stresses (σ_{yy}) at one edge of the central panel during sequence 4 were slightly different from those calculated in the other sequences. The non-symmetric process of panel installation in sequence 4 has slightly affected the final stress distribution in the soil close to the edge of the central panel. For a non-symmetric installation (sequence 4), the value of the shear stress (τ_{xy}) on the edge of the central panel was slightly different from those calculated during the other construction sequences.
- The results calculated in Chapter 5 were compared with those in Chapter 3 and 4; it was found that for a bored pile wall, the horizontal stress decrease was much concentrated above the toe of the wall.

- In Chapter 5 it was calculated that beneath the toe of the diaphragm wall the total horizontal stress remained higher than the initial stress for a depth of approximately 2.5 m below the toe. In contrast, for a bored pile wall (Chapter 3 and 4) it was calculated that the stress below the toe of the wall fall to the initial values approximately 1.5 m below the toe of the bored pile wall. This is mainly due to the lower redistribution of shear stress (τ_{zy}) below the toe of the bored pile wall compared with those calculated below the toe of the diaphragm wall, which lead to a different redistributions of total horizontal stress in each cases. As reported previously, the geometry is the principal factor that led to a different stress redistribution during the installation of a bored pile wall than after a diaphragm wall construction.
- The global distribution of horizontal shear stresses (τ_{xy}) was similar to that found by Ng and Yan (1998). The shear stresses (τ_{xy}) was distributed along the entire depth of the wall with an increase above the toe of the wall. For a diaphragm wall panel of 8 m length, Ng and Yan (1998) calculated that the maximum shear stress (τ_{xy}) was about 3 m above the toe of the wall with a magnitude of 100 kPa. For a 2.5 m panel length it was 20 kPa.
- It was calculated that the stress changes below the toe of the wall are small during the installation of a panel of 2.5 m length. Furthermore, in Chapter 4 it was shown that the construction of a bored pile wall with piles 1 m in diameter does not lead to any important total horizontal stress changes below the toe of the wall. Comparing this result with those calculated by Gourvenec *et al.* (1999) and Ng *et al.* (1999) it was found that an increase of the length of the panel led to a direct increase in the total horizontal stress below the toe of the wall.
- The shear stresses (τ_{zy}) below the toe were minimal compared to those calculated for a panel of 8 m length (Ng *et al.*, 1999).
- The results reported in Chapter 5 seem to suggest that minimal damage of the adjacent building and safer construction could be achieved with the installation of a diaphragm wall made up of panels with a smaller length (2.5 m).

Chapter 6

There is some concern that the high horizontal stresses in an overconsolidated deposit may become re-established in the long-term, despite the reductions that occur during retaining wall installation and subsequent excavation in front of the wall.

In this chapter, long term field data from the instrumented section of in situ embedded retaining wall which forms part of the Channel Tunnel Rail Link at Ashford, Kent, were considered. Approximately 13 years of lateral stress monitoring around a wall in an overconsolidated deposit were presented and discussed. A further case record of the long term bending moment data from an embedded retaining wall at Coventry was also presented and discussed.

The following conclusions are reported:

- The long-term spade cell measurements at the site in Ashford show generally a slight decrease in the total horizontal stress over the years following construction of the cutting. These are probably due to drainage through the bored pile wall. From the data presented in this chapter it is evident that the pore water pressures reduce towards the retaining wall. The in situ total horizontal stresses did not re-establish during the 12 years after the excavation of the cutting.
- The long term bending moment from the site in Coventry indicate no increase in lateral stress in a retaining wall in weak sandstones.
- Furthermore, a continuing long term decrease in the vertical total stress beneath the stabilising base in the long term was measured.
- The results reported in this chapter suggest that the design of wall in overconsolidated deposits to current standards such as BD 42/00 (Highways Agency, 2000), which require that in situ retaining walls are design to withstand a long term lateral earth pressure coefficient of up to 1.5, will be overconservative.

7.2 Further work

This research has highlighted several areas of uncertainty. Suggestions for future work are as follows.

- Undrained conditions were implemented in the *FLAC^{3D}* models. It would be helpful to compare the results from the analyses in Chapter 3, 4 and 5 with those using geotechnical parameters representative of long term conditions to investigate the behaviour of piles in effective stress terms.
- It would be interesting to investigate the 3D installation effects of a bored pile wall in granular soils (non-clay).
- Data collected in this field study should be used for input and comparison of results from finite element analyses to better understand the long term performance of the walls.
- The properties of the Atherfield Clay are not well understood. Further studies will be helpful to better identify the geotechnical properties of this soil.
- More case studies on the impact of the long term hydraulic conditions to the stress state behind the wall are required.
- It will be helpful to investigate the stress variation behind the wall during bored pile installation, in which the width of the gaps between successive piles is varied.

LIST OF REFERENCES

- Alonso E.E. and Pineda J.A. (2006). Weathering and degradation of clay shales: experimental observations and models of degradation. *Vith South American Conference on Rock Mechanics*. pp. 249-296.
- Anders K. (2007). Effects of deep excavation in soft clay in the immediate surroundings. *PhD Thesis*. Chalmers University of Technology, Sweden.
- Andrew S. and Peter W. (1986). *Critical State Soil Mechanics*. Lecturers in Engineering at Cambridge University.
- Batten M., Powrie W., Boorma R. Leiper. (1999). Use of vibrating wire strain gauges to measure loads in tubular steel props supporting deep retaining walls. *Proc. Instn Civ. Engrs Geotech. Engng*.
- Benmebarek N. and Kastner R. (2006). Passive and active earth pressures in the presence of groundwater flow. *Geotechnique*. Vol. 56, pp. 149–158.
- Bennett S.N., Carder D.R. and Ryley M.D. (1996). Behaviour during construction of a propped secant pile wall in stiff clay at Hackney to M11 link. *Transport and road research laboratory*. Research Report 188.
- Bobet A. and Nam S.W. (2007). Stresses around pressure tunnels with semi-permeable liners. *Rock Mechanics and Rock Engineering*. Volume 40(3), pp 287-315.
- Bolton M. D. and Stewart D. I. The effect on propped diaphragm walls of rising groundwater in stiff clay. *Geotechnique*. Vol. 44, pp. 111-127.
- Bolton M. D., Britto A. M. and White T. P. (1989). Finite element analysis of a centrifuge model retaining wall embedded in overconsolidated clay. *Computers and Geotechnics*. Vol. 7, No. 9, pp. 289-318.
- Bolton M. D., Powrie W. and Stewart D. I. (1987). Effects on diaphragm walls of groundwater pressure rising in clays. *Groundwater effects in geotechnical engineering*. Balkema pp. 287-315.
- Britto A. M. and Gunn M. J. (1987). *Critical state soil mechanics via finite elements*. Ellis Horwood Limited, pp. 486.
- Burland J. B. (1997). Assessment of risk of damage to buildings due to tunnelling and excavation, *Earthquake Geotechnical Engineering*, Ishihara, Balkema, Rotterdam, pp. 1189-1201.
- Burland J. B. and Hancock R. J. R. (1977). Underground car park at the House of Commons: geotechnical aspects. *Struct Eng*. Vol. 55, pp. 87-100.

- Burland J. B. and Maswoswe J. (1982). Discussion on “In situ measurements of horizontal stress in overconsolidated clay using push-in spade-shaped pressure cells“. *Geotechnique* 32, No. 2, 285- 286.
- Burland J. B. Simpson B. and St. John H. D. (1979). Movements around excavation in London Clay. *Proceedings of 7th European Conference on Soil Mechanics and Foundation Engineering*, Brighton, Vol.1, pp.13-29.
- Carder D. R. (1995). Ground movements caused by different embedded retaining wall construction techniques. *Transport and road research laboratory*. Research report 172.
- Carder D. R. and Gent A. J. C. (1993). Behaviour during construction of a propped contiguous bored pile wall. *Transport and road research laboratory*. Research report 381.
- Carder D. R., Barker K. I. and Easton M. R. (1999). Performance during construction of a cut-and-cover tunnel founded in London Clay at Edmonton. *Transport and road research laboratory*. Research report 379.
- Carder D. R., Ryley M. D. and Symons I. F. (1991). Behaviour during construction of a propped diaphragm wall in stiff clay at the A406/A10 junction. *Transport and road research laboratory*. Research report 331.
- Carder D. R., Watson G. V. R., Chandler, J. and Powrie W. (1999). Long-term performance of an embedded retaining wall with a stabilizing base slab. *Proceedings of the ICE – Geotechnical Engineering*. No. 137, pp. 63-74.
- Carder D. R. and Darley P. (1998). The long term performance of embedded retaining walls. *Transport and road research laboratory*. Research report 381.
- Carswell I. G., Carder D. R. and Symons I. F. (1993). Long term performance of an anchored diaphragm wall embedded in stiff clay. *Transport and road research laboratory*. Research report 313.
- Clark J., Richards D. J. and Powrie W. (2004). Wall installation effects – preliminary findings from a field study at the CTRL. *Ashford. Proc. of the Skempton Memorial Conference*, London.
- Clark J. (2006). Performance of a propped retaining wall at the CTRL, Ashford. University of Southampton, School of Civil Engineering and the Environment, *PhD Thesis*, 276pp.
- Conti R., De Sanctis L. and Viggiani G. M. B. (2012). Numerical modelling of installation effects for diaphragm walls in sand. *Acta Geotechnica*. Vol. 7, pp. 219-237.
- Costa-Filho L. M. (1980). A laboratory investigation of the small strain behaviour of London clay. *PhD thesis*, University of London.
- Daramola O. (1978). The influence of stress history on the deformation of sand. *PhD thesis*. University of London.

- De Moor E. K. (1994). An analysis of bored pile/diaphragm wall installation effects. *Geotechnique*. Vol. 41, No. 4, pp. 499–514.
- Dimitrios K. and Peter W. (2006). Groundwater ingress to tunnels-The exact analytical solution. *Tunnelling and Underground Space Technology*. Vol. 22, No. 1, pp. 23–27.
- Farmer, I. W. and Attewell, P. B. (1973). Ground movements caused by a bentonite-supported excavation in London clay. *Geotechnique*, 23(4), 577-581.
- Fortuna S., Callisto L. and Rampello S. (2007). Small Strain Stiffness of a Soft Clay Along Stress Paths Typical of Excavations. *Solid Mechanics and Its Applications*. Vol. 146, No. 4, pp. 299–310.
- Gaba A., Simpson B. Powrie, W. and Beadman, D. R (2002). Embedded retaining walls: guidance for more economic design. *Construction Industry Research and Information Association*. Report/CP/96. CIRIA, London.
- Gallois R. W. (1965). British Regional Geology: The Wealden District, *Fourth ed.* HMSO for British Geological Survey, London.
- Gasparre A. Nishimura S. Minh N. A. and Jardine R. J. (2007). The stiffness of natural London Clay. *Geotechnique*. Vol. 57, No. 1, pp. 33–44.
- Glass P. R. and Powderham A. J. (1994). Application of the observational method at the Limehaose Link. *Geotechnique*. Vol. 44, No. 4, pp. 665–679.
- Gourvenec S. and Powrie W. (2000). Three-dimensional finite element analyses of embedded retaining walls supported by discontinuous earth berms. *Can. Geotech. J.* Vol. 37, pp. 1062–1077.
- Gourvenec S. M., Mair R. J., Bolton M. D. and Soga K. (2005). Ground conditions around an old tunnel in London Clay. *Proceedings of the ICE – Geotechnical Engineering*. Vol. 158, No. 1.
- Gourvenec S., Powrie W. and De Moor E. K. (2002). Three-dimensional effects in the construction of a long retaining wall. *Proceedings of the ICE – Geotechnical Engineering*. No. 3, pp. 163–173.
- Gourvenec, S. M. and Powrie, W. (1999). Three-dimensional finite-element analysis of diaphragm wall installation. *Geotechnique*. Vol. 49, No. 6, pp. 801–823.
- Gunn M. J. and Clayton C. R. (1992). Installation effects and their importance in the design of earth-retaining structures. *Geotechnique*. Vol. 42, No. 1, pp. 137–141.
- Gunn M. J., Satkunanathan A. and Clayton C. R. I. (1993). Finite element modelling of installation effects. *Retaining structures*, Thomas Telford Ltd., London, England, 46-55.
- Hayward T. (2000). Field studies, analysis and numerical modelling of retaining walls embedded in weak rock. *PhD thesis*. University of Southampton, Engineering and the Environment. 295pp.

- Higgins K. G, Potts D. M. and Symons, I. F. (1989). Comparison of predicted and measured performance of the retaining walls of the Bell Common tunnel. Report CR 124. Crowthorne: Transport and Road Research Laboratory.
- Highways Agency (2000). *Design Manual for Roads and Bridges. Part 2: Design of Embedded Retaining Walls and Bridge Abutments*, BD42/00 London: HMSO.
- His J.P. and Small J. C. (1992). Analysis of excavation in an elasto-plastic soil involving drawdown of the water table. *Computer and Geotechnics*. Vol. 13, pp. 1–19.
- Holmes G., Roscoe H. and Chodorowski A. (2005). Construction monitoring of cut and cover tunnels. *Geotechnical Engineering*. Vol. 158, pp. 187–196.
- Houlsby, G. T. (1991). How the dilatancy of soils affects their behaviour. *10th European Conference on Soil Mechanics and Foundation Engineering*, Florence, Italy, 28 May 1991. Volume 4., pp 1189-1202.
- Hubbard H. W., Potts D. M., Miller D. and Burland J. B. (1984). Design of the retaining walls for the M25 cut and cover tunnel at Bell Common. *Geotechnique*. Vol. 34, No. 4, pp. 495–512.
- Humpage A. J. and Booth K. A. (2000). *The Lower Greensand in the Mid-Kent and Ashford Contract Sectors of the Channel Tunnel Rail Link Construction Works*. British Geological Survey Commercial Report CR100/19.
- Itasca (2006). *Fast Lagrangian Analysis of Continua in 3 Dimensions, Version 3.1: Users Manual*, Itasca Consulting Group, Minneapolis, USA.
- Jardine R. J., Potts D. M., Fourie A. B. and Burland J. B. (1986). Studies of the influence of non-linear stress-strain characteristics in soil-structure interaction. *Geotechnique*, 36(3): 377–396.
- Jones B. D. (2007). Stresses in sprayed concrete tunnel junctions. *PhD Thesis*. University of Southampton.
- Kevin A. (1984). Three dimensional behavior of retaining wall systems. *PhD Thesis*. Louisiana State University and Agricultural and Mechanical College, Southern University.
- Lai C. H. (1993). Finite-element analysis of deep excavation in layered sandy and clayey soil deposit. *Geotechnical and Environmental Engineering*. Vol. 32, No. 2, pp. 204-214.
- Lei G. H. (2005). Yielding mechanisms in a rectangular trench. *Proceedings of the Institution of Civil Engineers*. Vol. 158, pp. 169–172.
- Lings M. L., Ng C.W. W. and Nash D. F. T. (1994). The lateral pressure of wet concrete in diaphragm wall panels cast under bentonite. *Proc. Instn Civ Engrs Geotech. Engng*. Vol. 107, pp. 163–172.

- Lings M.L., Nash D.F.T., Ng C.W.W. and Boyce M.D. (1991). Observed behaviour of a deep excavation in Gault Clay: a preliminary appraisal, *Proc. 10th European Conf. SMFE*, 467–470.
- Loveridge F. (2001). Evaluation of prop loads at Channel Tunnel Rail Link Contract 430-Ashford tunnels. *Cool Prize Ground Engineering*. 38–42.
- Mackinson C. (1988). Ground investigations: 1987 interpretative report A4/A46 Batheaston Swainswick bypass, vol. 3. Reading: Sir Alexander Gibb and Partners.
- Mesri G. (1971). Mechanisms controlling the permeability of clays. *Clay Sand Clayminerals*. Vol. 19, pp. 151–158.
- Michael L. (2001). Database for Retaining Wall and Ground Movements due to Deep Excavations. *Journal of Geotechnical and Geoenvironmental Engineering*. Vol. 127, No. 3, pp. 203–224.
- Neild S. A., Williams M. S. and McFadden P. D. (2005). Development of a Vibrating Wire Strain Gauge for Measuring Small Strains in Concrete Beams. Blackwell Publishing Ltd.
- Ng C. W. W, Lings M. L., Simpson B. (1995). An approximate analysis of the three-dimensional effects of diaphragm wall installation. *Geotechnique*. Vol. 45, No. 3, pp. 497–507.
- Ng C. W. W. and Lings L. (1996). Effects of modeling soil nonlinearity and wall installation on back-analysis of deep excavation in stiff clay. *Journal of Geotechnical Engineering*. Vol. 121, No. 10, pp. 687-695.
- Ng C. W. W. and Yan R. W. M. (1999). Three-dimensional modelling of a diaphragm wall construction sequence. *Geotechnique*. Vol. 49, No. 6, pp. 825-834.
- Ng C. W. W. and Yan R. (1998). Stress Transfer and Deformation Mechanisms around a Diaphragm Wall Panel. *Journal of Geotechnical and Geoenvironmental Engineering*. Vol. 124, No. 7., 638–648.
- Ng C.W.W., Bolton M.D. & Dasari G.R. (2000). The small strain stiffness of a carbonate stiff clay. *Geotechnique*. Vol. 50, No. 2, pp. 127-140.
- Ng. C.W.W., Hong Y., Liu G.B. and Liu T. (2012). Ground deformations and soil–structure interaction of a multi-propped excavation in Shanghai soft clays. *Géotechnique*. Vol. 62, No. 10, pp. 907-921.
- Ng. C. W. W., Lings, M. L., Simpson, B. and Nash, D. F. T. (1995). An approximate analysis of the three dimensional effects of diaphragm wall installation. *Geotechnique* 45, No. 3, 497-507.
- Ng. C.W.W. (1992). An Evaluation of Soil-Structure Interaction Associated with a Multi-propped Excavation. *Ph.D thesis*. University of Bristol, U.K.

- Ng. C. W. W. (1999). Stress paths in relation to deep excavations. *Journal of Geotechnical and Geoenvironmental Engineering*. Vol. 125, No. 5, pp. 687-695.
- Osman A. S. and Bolton M. D. (2006). Design of braced excavations to limit ground movements. *Geotechnical Engineering*. Vol. 159, pp. 167–175.
- Osman A. S. and Bolton M. D. (2004). A new design method for retaining walls in clay. *Can. Geotech. J.* Vol. 41, pp. 451–466.
- Ou C. Y., Chiou D. C. and Wu T. S. (1996). Three-dimensional finite element analysis of deep excavations. *Journal of Geotechnical Engineering*. Vol. 122, No.5, May.
- Ou C. Y., Liao, J. T. and Cheng, W. L. (2000). Building response and ground movements induced by a deep excavation. *Geotechnique*. Vol. 50, No. 3, pp. 209-220.
- Ou C. Y., Liao J. T. and Lin H. D. (1998). Performance of Diaphragm Wall Constructed Using Top-Down Method. *Journal of Geotechnical and Geoenvironmental Engineering*. 01/1998; 124(9).
- Paik K. H. and Salgado R. (2003). Estimation of active earth pressure against rigid retaining walls considering arching effects. *Geotechnique*. Vol. 53, No. 7, pp. 643-653.
- Pantelidou H. (1994). Changes in soil stiffness associated with diaphragm walling. *PhD Thesis*. University of London Queen Mary and Westfield College.
- Poh T. Y. and Wong I. H. (1998). Effects of construction of diaphragm wall panels on adjacent ground: field trial. *Journal of geotechnical and geoenvironmental engineering*. Vol. 124, No. 8, pp. 749-756.
- Powrie W. and Daly M. P. (2007). Centrifuge modelling of embedded retaining walls with stabilising bases. *Geotechnique*. Vol. 57, No. 6, pp. 485–497.
- Powrie W. and Kantartzi C. (1996). Ground response during diaphragm wall installation in clay: centrifuge model test. *Geotechnique*. Vol. 46, No. 4, pp. 725-739.
- Powrie W. and Li E. S. F. (1991) Finite element analysis of an in situ wall propped at formation level. *Geotechnique*. Vol. 41, No. 4, pp. 499–514.
- Powrie W. (2004) *Soil Mechanics: Concepts and Applications*, Second Edition.
- Bicocchi N. (2010). Interpretation of strain gauge data from reinforced concrete structures in the ground. *Transfer Thesis*. Southampton University.
- Powrie W. (2008). Contributions to Geotechnique 1948-2008: Groundwater. Contributions to Geotechnique 1948-2008: Groundwater. *Geotechnique*. Vol. 58, No. 5, pp. 435-439.
- Powrie W. and Batten M. (2000). Comparison of measured and calculated temporary prop loads at Canada water station. *Geotechnique*. Vol. 50, No. 2, pp. 127-140.

- Powrie W. and Kantartzi C. (1996). Ground response during diaphragm wall installation in clay: centrifuge model tests. *Geotechnique*. Vol. 46, No. 4, pp. 725-739.
- Powrie W. and Chandler R. J. (1998). The influence of a stabilizing platform on the performance of an embedded retaining wall. *Geotechnique*, 48, (3), 403-409.
- Powrie W. and Li E. S. F. (1991). Finite element analyses of an in situ wall propped at formation level. *Geotechnique*, 41(4), 499-514.
- Powrie W., Chandler R. J., Carder, D. R. and Watson, G. V. R. (1999). Back-analysis of an embedded retaining wall with a stabilizing base slab. *Proceedings of the ICE - Geotechnical Engineering*, 137, (2), 75-86.
- Finno R. J. and Harahap I. S. (1991). Finite Element Analyses of HDR-4 Excavation. *Journal of Geotechnical Engineering*. Vol. 117, No. 1, pp. 1590-1609.
- Finno R. J. and Calvello M. (2005). Supported Excavations: Observational Method and Inverse Modeling. *Journal of Geotechnical and Geoenvironmental Engineering*. Vol. 131, No. 7, pp. 826-836.
- Richards D. J., Clark J. and Powrie W. (2006). Installation effects of a bored pile wall in overconsolidated clay. *Geotechnique*. Vol. 56, No. 6, pp. 411-425.
- Richards D. J., Clark J. and Powrie W. (2007). Pore water pressure and horizontal stress change measured during construction bored pile multi-propped retaining wall in Lower Cretaceous clays. *Geotechnique*. Vol. 57, No. 2, pp. 485-497.
- Richards D. J., Clark J., Powrie W. and Heyman G. (2005). An evaluation of total horizontal stress measurements using push-in pressure cells in an overconsolidated clay deposit. *Proc. 16th Int. Conf. Soil Mech. Grnd Engng*, Japan.
- Richards D. J., Clark J., Powrie W. and Heymann G. (2007). Performance of push-in pressure cells in overconsolidated clay. *Proceedings of the Institution of Civil Engineers-Geotechnical Engineering*, 160, (1) 31-41.
- Richards D. J., Clayton C. R. I., Powrie W. and Hayward T. (2004). Geotechnical analysis of a retaining wall in weak rock. *Proceedings of the Institution of Civil Engineers: Geotechnical Engineering*, 157, (1), 13-26.
- Richards D. J., Powrie W. and Page J. R. T. (1998). Investigation of retaining wall installation and performance using centrifuge modelling techniques. *Proc. ICE, Geotech. Eng.*, 131, (3) 163-170.
- Richards D. J., Powrie W., Roscoe H. and Clark J. (2007). Pore water pressure and horizontal stress changes measured during construction of a contiguous bored pile multi-propped retaining wall in Lower Cretaceous clays. *Geotechnique*, 57, (2) 197-205.
- Roberts T. O. L., Roscoe H., Powrie W. and Butcher D. J. E. (2007). Controlling clay pore pressures for cut-and-cover tunnelling. *Proceedings of the ICE - Geotechnical Engineering*. Vol. 160, No. 4, pp. 227-236.

Roberts M. (2003). *Private communication*.

Ryley M. D. and Carder D. R. (1995). The performance of push-in spade cells installed in stiff clay. *Geotechnique*. 45(3): 533-539.

Schafer R. and Triantafyllidis T. (2004). Modelling of earth and water pressure development during diaphragm wall construction in soft clay. *Int. J. Numerical Anal. Meth. Geomech.* Vol. 28, pp. 1305–1326.

Schaferny R. and Triantafyllidis Th. (2004). Modelling of earth and water pressure development during diaphragm wall construction in soft clay. *Int. J. Numer. Anal. Meth. Geomech.* pp. 1305–1326.

Scott J. M., Pound C. and Shanghavi H. B. Heathrow Airside Road Tunnel: wall design and observed performance. *Proceedings of the International Conference on Underground Construction*, London, 2003, pp. 281–292.

Scott B., Kim B. J., and Salgado R. (2003) Assessment of Current Load Factors for Use in Geotechnical Load and Resistance Factor Design, *Journal of Geotechnical and Geoenvironmental Engineering*, ASCE, Vol.129, No.4, pp.287-295.

Scott J. M., Pound C. and Shanghavi H. B. (2003). Heathrow Airside Road Tunnel – wall design and observed performance. *Proc. Int. Conf. Underground Construction*. pp.281-292.

Scott J. M., Pound C. and Shanghavi H. B. (2003). Heathrow Airside Road Tunnel – wall design and observed performance. *Proc. Int. Conf. Underground Construction*. pp.281-292.

Shin J. H., Addenbrooke T. I. and Potts D. M. (2002). A numerical study of the effect of groundwater movement on long-term tunnel behaviour. *Geotechnique*. Vol. 52, No. 6, pp. 391–403.

Shirlaw J.N. (1993). Pore pressure around tunnel in clay: Discussion. Golder. *Canadian Geotechnical Journal*. Vol. 30, No. 6, pp. 1044–1046.

Sidney L. (2010). Ground movements due to excavation in clay: physical and analytical models. *PhD thesis*. University of Cambridge.

Simpson B. and Powrie W. (2001). Embedded retaining walls: theory, practice and design. *15th International Conference on Soil Mechanics and Geotechnical Engineering, Soil Mechanics and Engineering*, 2505-2524.

Skempton A. W. (1961). Horizontal stresses in an over-consolidated Eocene clay. *Proc. 5th ICSMFE*, Vol. 1 351-357.

Skempton A. W. and Weeks, A. G. (1976). The Quaternary history of the Lower Greensand escarpment and Weald Clay vale near Sevenoaks, Kent, *Philosophical Transactions Royal Society Series A*, 283, 493-526.

- Smith P. R., Jardine R.J. and Hight D.W. (1992). The yielding of Bothkennar clay. *Geotechnique* 42: 257-274.
- Smith R. E., Jahangir M. A., and Rinker W.C. (2006). Selection of Design Strengths for Overconsolidated Clays and Clay Shales. *40th Symposium on Engineering Geology and Geotechnical Engineering*, Utah State University, Logan, UT, May 24-26.
- Stallebrass S. E. and Taylor R. N. (1997). The development and evaluation of a constitutive model for the prediction of ground movements in overconsolidated clay, *Geotechnique*. 47, No. 2: 235–253.
- Standing J. R., Farina M. and Potts D. M. (1998). The prediction of tunnelling induced building settlements – A case study. *Tunnels and metropolises World tunnel congress, Tunnels and metropolises*. pp. 1053–1058.
- Symons I. F. and Carder D. R. (1993) Stress changes in stiff clay caused by the installation of embedded retaining walls Proc. *Conf. Retaining Structures*, Cambridge, 1992, Thomas Telford, London, 227-236.
- Symons I. F. (1983). Assessing the stability of a propped, in situ retaining wall in overconsolidated clay. *Proc. Insti Civ. Engrs*. Vol. 75, pp. 617–633.
- Symons I. F. and Carder D. R. (1990). Long term behaviour of embedded retaining walls in over-consolidated clay. *Geotechnical Instrumentation in Practice*, TTL, London, pp. 227-236.
- Symons I. F. and Carder D. R. (1992). Field measurements on embedded retaining walls. *Geotechnique* 42(1): 117-126.
- Symons I. F. and Carder D. R. (1993). Stress changes in stiff clay caused by the installation of embedded retaining walls. *Retaining structures*. Thomas Telford, London.
- Symons I. F. and Tedd P. (1989). Behaviour of a propped embedded retaining wall at Bell Common Tunnel in the longer term. *Geotechnique*. 34(4): 701-710.
- Tan Y. and Wei B. (2012). Observed Behaviors of a Long and Deep Excavation Constructed by Cut-and-Cover Technique in Shanghai Soft Clay. *J. Geotech. Geoenviron*. Vol. 138, No. 1, pp. 69–88.
- Tedd P. and Charles J. A. (1983). Evaluation of push-in pressure cell results in stiff clay. *Proceedings of International Symposium on In-Situ Testing*, Paris, 2, 579-584.
- Tedd P. and Charles J. A. (1985). The strength of London Clay in relation to the design of embedded retaining walls. *Geotechnique*. Vol. 35, No. 2, pp. 199–204.
- Tedd P., Chard B. M., Charles J. A. and Symons I. F. (1984). Behaviour of a propped embedded retaining wall in stiff clay at Bell Common Tunnel. *Geotechnique*. Vol. 34, No. 4, pp. 513–532.
- Tedd P. and Charles J. A. (1981). In situ measurements of horizontal stress in overconsolidated clay using push-in spade-shaped pressure cells. *Geotechnique* 31, No. 4, 554-558.

Tedd P., Chard B. M., Charles J. A. and Symons I. F. (1984). Behaviour of a propped embedded retaining wall in stiff clay at Bell Common. *Geotechnique* 34(4): 513-532.

Terzaghi K., and Peck R. B. (1967) *Soil Mechanics in Engineering Practice*, Second Edition: John Wiley & Sons, New York, 729 p.

Tsui Y. and Cheng Y. M. (1989). A fundamental study of braced excavation construction. *Computer and Geotechnics*. Vol. 8, pp. 39–64.

White D. J., Take W. A., Bolton M. D. (2001) Measuring soil deformation in geotechnical models using digital images and PIV analysis. *10th International Conference on Computer Methods and Advances in Geomechanics*. pp. 997–1002.

Wiggan C. (2013). Long-term pore water pressure changes around subsurface structures. *PhD thesis*. University of Southampton, Engineering and the Environment. 295pp.

Wongsaroj J., Soga K. and Mair R. J. (2007). Modelling of long-term ground response to tunnelling under St James's Park, London. *Geotechnique*. Vol. 57, No. 1, pp. 75–90.

Arai Y., Kusakabe O., Murata O. and Konishi S. (2008). A numerical study on ground displacement and stress during and after the installation of deep circular diaphragm walls and soil excavation. *Computers and Geotechnics*. Vol. 35, pp. 791–807.

Yong K.Y., Lee F.H. and S.L. Lee. (1989). Elasto-Plastic consolidation analysis for strutted excavation in clay. *Computer and Geotechnics*. Vol. 8, pp. 311–328.

Youssef M. A. and Abdolreza O. (2011). Three-dimensional inverse analyses of a deep excavation in Chicago clays. *Int. J. Numer. Anal. Meth. Geomech.* Vol. 35, pp. 1059–1075.

Youssef M. A. H., and Andrew J. W. (2002). Mechanisms of Load Transfer and Arching for Braced Excavations in Clay. *Journal of Geotechnical and Geoenvironmental Engineering*. Vol. 128, No. 3, pp. 187–197.

Youssef M.A. H. and Camilo M. (2008). Central Artery/Tunnel Project Excavation Induced Ground Deformations. *Journal of Geotechnical and Geoenvironmental Engineering*. Vol. 139, No. 9.

Zdravkovic L., Potts D. M. and St John H. D. (2005). Modelling of a 3D excavation in finite element analysis. *Geotechnique*. Vol. 55, No. 7, pp. 497–513.